The role of surface modified TiO$_2$ nanoparticles for application in ^{68}Ge/^{68}Ga generator systems and the use of molecular imprinted polymers for ^{68}Ge breakthrough control

A Dissertation Submitted in Fulfilment of the Requirements
for the degree
DOCTOR OF PHILOSOPHY DEGREE

to
The Faculty of Chemical Sciences
In Chemistry, UWC
September, 2021

Student: Sizwe Buwa

Student Number: 3280464

1st Supervisor: Prof. Leslie Petrik

2nd Supervisor: Dr. Mlungisi Nkosi

Abstract

Titanium dioxide (TiO_2) has potential as an adsorbent within the $^{68}Ge/^{68}Ga$ generator context. To function effectively, three basic requirements are required: optimum ^{68}Ga elution efficiency, stability and removal of the ^{68}Ge breakthrough. After analysis of the ^{68}Ga elution efficiency and the ^{68}Ge breakthrough, two models are proposed, namely; surface modification and molecular imprinted polymer, to address factors influencing ^{68}Ga elution efficiency and minimize ^{68}Ge breakthrough.

The surface modifiers that were investigated are 3-aminopolypropyltriethoxy silane (3-APTES), 3-mercaptopropyltrimethoxy silane (3-MPTMS), bis(3-aminopropyl)amine (BAPA) and 2-chloro-4,6-dimethoxy-1,3,5-triazine silane (CDMT). For a surface modifier to perform successfully, factors such as the stability, dispersibility and hydrophilicity were to be enhanced while clustering and agglomeration were to be avoided. The characterisation showed that 3-APTES modification offers benefits such as higher sorption capacity, adequate selectivity, increased radiation and chemical stability on prolonged use and greater efficiency for the improvement of performance of the $^{68}Ge/^{68}Ga$ generators.

Moreover, the use of MIPs demonstrated that the ^{68}Ge breakthrough was minimised to 0.001 %. Similarly, the ^{68}Ge breakthrough increased to 0.01 when NMIPs were used. Quality control parameters (pH, eluate volume,) were within the required levels. All findings are deemed significant and are likely to be considered for future $^{68}Ge/^{68}Ga$ generator systems. Consistent result were obtained for a period of up six months, with deviations that were considered insignificant. At no stage during this period did the ^{68}Ge breakthrough measurement show any signs of deterioration and this was considered a success. In comparison, deterioration was shown after three months before surface modification of the TiO_2 nanoparticles. An improvement efficiency of 45% was

I

realised as the ^{68}Ga efficiency was increased from 55 to above 90% for the unmodified and modified TiO$_2$ nanoparticles, respectively.

Dedications

This work is

Dedicated to my late parents, my mother, Mrs. Ntombizini Buwa and

my Father, Mr. Zibuzile Buwa

UNIVERSITY *of the*
WESTERN CAPE

III

Key Words

In the context of this research study, the following terms will be defined to have the following meanings:

^{68}Ga Efficiency   refers to the fraction of ^{68}Ga (daughter radionuclide) passed through the column in relation to the amount of the ^{68}Ge adsorbed on the column.

^{68}Ga Elution   refers to the continuous separation of the ^{68}Ga by means of acidic solution from a ^{68}Ge parent radionuclide. The decay of ^{68}Ga obtained in the eluate is measured using a High Purity Germanium (HPGe) detector, for quantification of the most intensive 511 keV line, following positron decay of ^{68}Ga.

^{68}Ga Radionuclide   refers to radiopharmaceuticals that are compounds of biomedical interest, which have attached radionuclides (^{68}Ga) as labels that allow us to quantify specific physiological processes.

^{68}Ge Breakthrough   refers to the fractions of ^{68}Ge (parent radionuclide) passed through the cation exchange micro-chromatography column along with the desired ^{68}Ga radionuclide

^{68}Ge/^{68}Ga generator   any system incorporating a fixed parent radionuclide from which a daughter product (^{68}Ga) is to be obtained by elution or any other method used in a radiopharmaceutical. In a radionuclide generator, both mother (^{68}Ge) and daughter (^{68}Ga) radionuclides are to be considered active ingredients.

Activity   The rate of radioactive transformations (radioactive decays) in a given source or sample (i.e. the intensity of the radioactive source or sample

Adsorption hysteresis   the deviation of the contact angle from its theoretical value due to physical phenomena such as microscopic surface defects and roughness.

Adsorption Isotherm   describes the equilibrium of the adsorption of a material at a surface at constant temperature. Is obtained by measuring the amount of gas

adsorbed across a wide range of relative pressures at a constant temperature (typically liquid N_2, 77K). Conversely desorption Isotherms are achieved by measuring gas removed as pressure is reduced. Adsorption isotherms are often used as empirical models, which do not make statements about the underlying mechanisms and measured variables

Adsorption   refers to the attraction of molecules to the surface of a nanoparticle

BET   The method of Brunnauer, Emmett, and Teller is employed to determine surface area on a model of adsorption which incorporates multilayer coverage

BJH   the method of Barrett, Joyner, and Halenda is a procedure for calculating pore size distributions from experimental isotherms using the Kelvin model of pore filling. It applies only to the mesopore and small macropore size range

Bombardment   acceleration of particle such as protons, deuterons and alpha particle by a cyclotron and directed towards a target material such as Zn or Ga

Calibration   the reference time used by the radiopharmacist to indicate when the isotope may be injected into a patient

Chemisorption   the binding of a species to a surface by chemical bonding forces

Cyclotron   a highly sophisticated machine used for the acceleration of charged particles such as protons, deuterons and alpha particles

De Boer t-Plot is commonly used to determine the external surface area and micropore volume of microporous materials. It is based on standard isotherms and thickness curves which describe the statistical thickness of the film of adsorptive on a nonporous reference surface

Half-life   the average time interval required for one-half of any quantity of identical radioactive atoms to undergo radioactive decay (i.e. the time interval required for the activity of a source of any single radioactive substance to decrease to one-half)

Isotope	one of two or more atomic species of an element having identical number of protons in the nucleus, but different number of neutrons. Thus, while chemically indistinguishable, they differ in mass and radioactive behaviour.
Langmuir	provides a means of determining surface area based on a monolayer coverage of the solid surface by the adsorptive
Molecular Imprinted Polymers	is a technique to design artificial receptors with predetermined selectivity and specificity for a given analyte.
Monomer	a molecule of any of a class of compounds, mostly organic, that can react with other molecules to form very large molecules, or polymers.
Nanotechnology	is the branch of technology that deals with dimensions and tolerances of less than 100 nanometres, especially the manipulation of individual atoms and molecules.
Photocatalysis	is a type of catalysis that results in the modification of the rate of a photoreaction - a chemical reaction that involves the absorption of light by one or more reacting species - by adding substances (catalysts) that participate in the chemical reaction without being consumed.
Physisorption	is a process in which the electronic structure of the atom or molecule is barely perturbed upon adsorption.
Positron Emission Tomography (PET)	Is a nuclear medicine functional imaging technique that is used to observe metabolic processes in the body as an aid to the diagnosis of disease. The system detects pairs of gamma rays emitted indirectly by a positron-emitting radionuclide.
Radiation	is the emission or propagation of energy through matter or space by electromagnetic disturbances which display both wave-like and particle-like behaviour.
Radioactivity	is the emission of radiation from the spontaneous disintegration (decay) of an unstable radionuclide.
Radiochemical purity	an Amount of radioisotope found in a known chemical form
Radionuclidic purity	the ratio of the activity of the desired radioisotope in relation to the total activity present in the sample

Radiopharmaceutical refers to a medicine that contains one or more radioactive isotopes

Single Photon Emission Computed Tomography (SPECT) is the use of radioactive materials to assess the physiological properties of organ systems. Typical examples include blood flow, glucose metabolism or protein aggregates.

Surface Modification   is the act of modifying the surface of a material by bringing physical, chemical or biological characteristics different from the ones originally found on the surface of a material.

Acknowledgements

I would like to thank Prof. Leslie Petrik for her never-tiring support and guidance throughout this work. Her constant positivity, help, suggestions and support went a long way in making this work a success. Thank you for encouraging me and for the support for me to excel. I would also like to thank Dr. Mlungisi Nkosi for providing me with the opportunity to work in this research and for his encouragement, support, and supervision at all levels.

A big thank you to the UWC Chemistry division staff for all my laboratory work, without your assistance this work would never have been fulfilled. Word of appreciation also goes out to UCT Engineering department staff, for never getting tired for my instrumentation and technical work. To all of the staff at the iThemba LABS, Nuclear medicine department, I would like to express deep thanks for their help and support, technical and otherwise, whenever needed. Thanks to CPUT staff and student, for their support when I was gathering information on my titanium dioxide analysis.

 Thanks as well to my fellow graduate and undergraduate students for providing support apart from academia. I am grateful to my family for never questioning my career choice.

Last but not the least; I would like to acknowledge the financial support from National Research Foundation and the following departments for laboratory work and time:

(a) **National Research Foundation**

(b) Material Research Department – **iThemba LABS**

(c) Nuclear Medicine Department – **iThemba LABS**

(d) ENS unit, department of Chemistry – **University of the Western Cape**

Table of Contents

XI

XIII

UNIVERSITY *of the*

WESTERN CAPE

List of Tables

List of Figures

XVIII

List of Abbreviations

3-APTES   3-aminopolypropylethoxy silane

3-MPTMS   3-mercaptopropyltrimethoxy silane

ABCHC   1, 1' – azobis (cyclohexanecarbonitrile)

BAPA   bis(3-aminopropyl)amine

BET   Brunnauer Emmett Teller

CDMT   2-chloro-4,6-dimethoxy-1,3,5-triazine

DOTA   1, 4, 7, 10-tetraazacyclododecane-N, N', N'', N''' – tetra acetic acid

EDMA   ethylene glycol dimethacrylate

FWHM   full width half maximum

HPGe   high purity germanium detector

HRSEM   high resolution scanning electron microscopy

HRTEM   high resolution transmission electron microscopy

IEC   ion-exchange chromatography

LET   linear energy transfer

MAA   methacrylic acid

MIPs   molecular imprinting polymers

MW   molecular weight

NOTA   1, 4, 7-triazacyclononane-N, N', N''-triacetic acid

PET   positron emission tomography

SCA   silane coupling agent

SPECT   single photon emission computed tomography

TEOS   tetraethylorthosilicate

XRD   x-ray diffractions

List of Units

µA/h	micro amp per hour
µm	micro metre
A	ampere
Bq	Becquerel
Ci	curie
cm³	centimetre cubed
eV	electron volts
eV	mega electron volt
g	gram
g/mol	gram per mole
keV	kilo electron volt
L	litre
M	molarity
m²/g	square metre per gram
mg	milligram
min	minute
mm	millimetre
nm	nanometres
ºC	degree Celsius
s	second
W	watt
β	beta
θ	theta
λ	lambda
ϒ	gamma-ray

CHAPTER I

INTRODUCTION

1.1   An Introduction

New imaging procedures in the nuclear medicine industry combine Positron Emission Tomography with computed X-ray tomography (CT) scans to give co-registration of the two images (PET-CT), enabling 30% better diagnosis than with a traditional gamma-camera alone (Crowe, 2003; Wechalekar et al., 2005; Delbeke & Martin, 2004). It is a very powerful and significant tool which provides unique information on a wide variety of diseases from dementia to cardiovascular disease and cancer (oncology). Positioning of the radiation source within the body makes the fundamental difference between nuclear medicine imaging and other imaging techniques such as X-rays. Gamma-ray imaging by either method described provides a view of the position and concentration of the radioisotope within the body. Organ malfunction can be indicated if the radioisotope is either partially taken up in the organ (cold spot), or taken up in excess (hot spot). If a series of images is taken over a period of time, an unusual pattern or rate of isotope movement could indicate malfunction in the organ (Christian & Waterstram-Rich, 2007; Schöder & Yeung, 2004).

Positron Emission Tomography (PET) is a type of molecular imaging where an unstable radioisotope from a radiopharmaceutical or biomarker emits a positron, which loses energy through collisions with surrounding atoms and molecules. For example, a positron-emitting radioisotope is introduced into a body, usually by injection, and accumulates in the target tissue. As it decays it emits a positron, which promptly combines with a nearby electron resulting in the simultaneous emission of two identifiable gamma-rays in opposite directions. These are detected by a PET camera and give very precise indication of their origin (Townsend, 2008; Karp et al., 2008; Watson et al., 2005). PET's most important clinical role is in oncology, with fluorine-18 (^{18}F) as the radioisotope, since it has proven to be the most accurate non-invasive method of detecting and

evaluating most cancers (Guillet et al., 2005). It is also often used in cardiac and brain imaging. Other prominent cyclotron produced PET radioisotopes include gallium-68 (^{68}Ga), rubidium-82 (^{82}Rb), oxygen-15 (^{15}O), nitrogen-13 (^{13}N) and carbon-11 (^{11}C) (Beyer et al., 2005; Grosu et al., 2005; Townsend, 2004).

Schubiger and colleagues (2007) presented an interpretation of Positron Emission Tomography (PET) chemistry as a driving force behind Molecular Imaging, a term that has become very popular in nuclear medicine. Simply put, molecular imaging means an image which reveals information about molecules. Price and Green (2011) refer to this definition as a process where imaging reveal processes, state and type of disease and what could be done with this information to help patients. ^{68}Ga is one of the early radionuclides applied to PET imaging, as stated by Rösch & Baum (2011). On the other hand, ^{68}Ga labelled DOTA-conjugate peptides are a particular type of radiopharmaceutical where ^{68}Ge/^{68}Ga generator plays a significant role. Combined with theory, radiochemistry and clinical diagnosis, ^{68}Ge/^{68}Ga generators provide researchers with ^{68}Ga labelled radiopharmaceuticals for molecular imaging, as well as means for further research work in this area. According to Dash and Chakravarty (2019) much of the growth in PET studies is attributed to an increasing number of ^{68}Ge/^{68}Ga generators taking a centre stage in imaging technology.

Although the concept of ^{68}Ge/^{68}Ga generators has been around for almost six decades (Roesch, 2012; Roesch & Riss, 2010; Eppard et al., 2014; Decristoforo, 2012), the technique remains obscure, because understanding of adsorbents such as titanium dioxide (TiO_2) and their potential for the benefit of the generators is still a concern (Rösch & Baum 2011). Dash and Chakravarty (2017) states unequivocally that adsorbents play a significant part of ^{68}Ge/^{68}Ga generator performance. To the researchers, the task and indeed challenge is to pursue a comprehensive understanding of adsorbent modification, which would typically encompass understanding such as thermal stability, improved mechanical properties, anticorrosive properties and durability, to aspects involving ^{68}Ga efficiency and ^{68}Ge breakthrough. Given this challenge, the question thus arises as to what conditions are necessary to ensure the successful modification of such adsorbents, and ultimately formulate a firm theoretical structure for the support.

Despite this challenge, the TiO_2 is basically an adsorbent like any other within a generator context. Consequently, it is important that the generator is treated under the afore-mentioned conditions if the elutions are to be successful. Radiation safety, legal requirements and labelling of medical tracers are critical to the success of any $^{68}Ge/^{68}Ga$ generator (Waterstra-Rich & Gilmore, 2016). A summary of the $^{68}Ge/Ga$ generator properties is presented in Appendix C. This being the case, the serious labelling and quality control parameters are as relevant to TiO_2 as they are to any other adsorbent. A table of Quality Control Parameters as stipulated by IAEA (2001) can be viewed on Appendix B. To function effectively, certain basic factors are required to exist in the metal oxide technology; the extent to which these factors are present increases the chances of a successful adsorbent outcome. The principal objectives of this study is to identify these task-based factors influencing the efficiency of TiO_2 metal oxide; to propose a conceptual model based on these factors and to subject the model to empirical testing.

A number of studies in the generator context have examined various existing adsorbents for their impact on $^{68}Ge/^{68}Ga$ generators (Chakravarty et al., 2011). Consequently, numerous general models for effective generator functioning have been proposed by, amongst others, Decristoforo et al., (2012); De Blois (2011); Velikyan (2015); Breeman et al., (2004). These models are useful for highlighting the necessary factors to be considered when nanoparticles are configured. Although these models differ in many aspects, such as type of adsorbent, eluent concentration and volume, they all look to address similar parameters but offer little common ground in strategies between different adsorbents.

After a careful analysis of various theoretical models, thermal stability, improved mechanical properties, anticorrosive properties and durability, two research areas are proposed for this study, namely, (1) surface modification, (2) $^{68}Ge/^{68}Ga$ generator and (3) molecular imprinted polymer technology. In addition, each research area comprises a number of underlying components. These two areas reflect the necessary criteria and essential requirements for effective theoretical and practical issues for that particular technology. The surface modification model, which proposes that nanoparticles may be modified under certain conditions, is the most important framework used to explain the way in which TiO_2 nanoparticles were able to be configured to enable effective adsorbency outcomes (Pan et al., 2013).

According to Aardaneh and Van der Walt (2006) criteria such the type, concentration and volume of eluent, recovery yield of ^{68}Ga, stability of ion-exchangers towards radiation, chemical contaminants, and ^{68}Ge breakthrough have been studied. This being the case, most ^{68}Ge/^{68}Ga generators face the challenge of meeting all necessary requirements. In their research, Aardaneh and Van der Walt (2006) together with Chakravarty and colleagues (2011), found that when generators function, the potential for failing one of the quality control measures is high. Given this unique challenge, the question thus arises as to what conditions are necessary to ensure the successful adsorption of ^{68}Ge followed by desorption of ^{68}Ga while maintaining satisfactory quality control measures.

The term surface modification is not widely recognised, even by researchers that investigated advantages and disadvantages of each of the generator systems that exist. The method is increasingly acknowledged as of great value for titanium dioxide (TiO$_2$) research, presenting a bottom-up approach to issues of thermal stability, improved mechanical properties, anticorrosive properties and durability. By investigating fabrication and modification methods, useful information about the modified TiO$_2$ surfaces can be developed and could be potentially exploited for ^{68}Ge/^{68}Ga generator system adsorbents. This approach fits within the discourse of sustainable surface chemistry, which promotes an integrated approach to problems of compatibility with the TiO$_2$ nanoparticles. Medical applications of short-lived isotopes emphasise that metal oxide adsorbents should comprise of the following properties, such as i.) be stable against radiation, ii.) be insoluble and non-toxic, iii) have good mechanical properties and iv.) possess very strong binding of the parent radionuclide. This last point plays an important role in this thesis.

The use of surface modification for tailoring the properties of inorganic sorbents has been the subject of increasing interest in recent years (Neouze & Schubert, 2008; Pan et al., 2013). The researchers, also, add that adoption of surface modification has a great potential to promote catalysis, coatings and chemical sensing for many other scientific applications. Alteration of the particle surface charge can be used to decrease particle aggregation, as well as to tune the attraction between the substrate and the particles. While inorganic nanoparticles with high surface activity agglomerate due to high ratio of surface area to volume (Pan et al. 2013), surface chemical modification with organic molecules can eliminate clustering, and may result in increased

4

dispersibility and stability of the nanoparticles. In addition, surface modification promotes the hydrophobic nature and enhances low surface energy when silane coupling agents are used, which in turn enhances stability.

Throughout the development of nanomaterials, it has emerged that surface modification can play an important part in improving TiO_2 inorganic nanoparticles, owing to properties such as superior wetting behaviour, mechanical strength, thermal stability, corrosion stability and antimicrobial activities (Wang and Hong, 2011). According to the literature (Shen et al., 2008), the controlled exploitation of surface chemistry can provide desirable functionalities to the TiO_2 nanomaterials. Additionally, this can lead to further investigations in developing new nanotechnology solutions by combining surface modification methods and adsorption properties. By introducing surface modification methods, it is also hypothesised that nanoparticles are able to escape some of the issues associated with traditional ^{68}Ga efficacies and [68]Ge breakthrough. This approach is central to this work as it explores the possible benefits that controlled surface area modification of metal oxides may provide.

The [68]Ge/^{68}Ga generator is a useful source of positron emitting radionuclides for institutions without a cyclotron on site. The long half-life of the parent radionuclide [68]Ge ($T_{1/2}$= 270.8 days) grants ^{68}Ga availability for long periods of time. Furthermore, the ^{68}Ga decay characteristics (89% β+, 1.92 MeV maximum energy) and its short half-life ($T_{1/2}$= 68 min) are suitable for PET application in a clinical setting. The expansion of surface modification of nanomaterials instigates a closer look at the issues surrounding generator adsorbents. Adsorbents, such as TiO_2, Al_2O_3 and SnO_2, represent controversial but fascinating issues in generator performance. There is an ongoing debate on some issues related to the adsorbents used as generators. The biggest debate relates to the steps necessary before the ^{68}Ga product is ready for use. Medical radiation restricts time of processing whilst on the other hand demands high standards at all times. When this is not the case, there is an uncertainty over that particular method of production. Thus, surface modification is of particular significance, because modified nanomaterials have received a growing interest due to physical uniqueness and chemical properties. The enhanced properties are expected to open new avenues to different technological, environmental and biological applications of these nanomaterials.

To sum up, many advances have been made in surface modification technology during the past few years, assisted by research, to provide a better understanding of the physical and chemical properties of the nanoparticles. The fields of research have included the factors affecting aggregation, improved stability, ion leakages, enhanced compatibility of nanoparticles with solid matrices and selectivity toward specific targets. The advanced knowledge acquired in each of these fields has contributed to the present realisation of surface modification with capabilities to achieve specific applications. Thus, if surface modification can be adopted on a large scale, the method has the potential to transform the existing production means towards coordination chemistry which may satisfy existing challenges. This study considers how the surface modification method offers the advantages being sought, namely, anticorrosion and durability. The method of choice for the production of the $^{68}Ge/^{68}Ga$ generators should be ascertained from various potential options.

1.2   Problem Statement

$^{68}Ge/^{68}Ga$ generators are medical radiation sources with long life cycles: including the production phase, evaluation phase, transportation phase, use phase and the disposal phase. All these stages should be controlled at all times. The most complex parts of the life cycles are the production and disposal phases. The main issues associated with the production of $^{68}Ge/^{68}Ga$ generators are the ^{68}Ga efficacies and the ^{68}Ge breakthroughs and the effect this may have on generator performance as well as the environment per se. ^{68}Ga efficiency, which considers the amount of the ^{68}Ga isotope produced compared to the ^{68}Ge radionuclide loaded initially, looks at the overall generator performance. During the use phase, usually more challenges are encountered by the end user (Zhernosekov et al., 2007). During the last two decades of the past century, the figures provided by elutions of the generators have been in decline due to instabilities of the adsorbents (Kopecky et al., 1973; Kopecky and Mudrova 1974; Loć h et al., 1982; Bao and Song, 1996; Nakayama et al., 2003). In addition, rising global environmental and clinical concerns slowed down production of the $^{68}Ge/^{68}Ga$ generators. Overcoming such challenges has attracted new opportunities for the use of ^{68}Ga to promote and expand clinical research and routine positron emission tomography (PET).

On the other hand, ^{68}Ge breakthrough, which considers the amount of ^{68}Ge isotope co-eluted with the ^{68}Ga radioisotope, is a measure of the toxicity levels found in these generators. Unmonitored

^{68}Ge (1/2 life = 279 days) levels in the product, caused by weak adsorption properties of the metal oxide have negative effects on health, which in turn has legal consequences. The effect of increased ^{68}Ge breakthrough poses significant challenges during the lifespan of the generator. This will lead to contamination of the product, reduced labelling quality through the effects of impurities and long lived radioisotopes mixed into ^{68}Ga radionuclide (Zhernosekov et. al., 2007). At the same time, the environment is also affected as increased ^{68}Ge radioisotope content leads to contamination of the environment by a long-lived radiation active isotope. This means that metal oxides that suffer as a result of weak ^{68}Ge adsorption properties pose great challenges. It is, therefore, an area that needs serious addressing because of the problems associated with lack of stability and corrosion of the metal oxide.

A big challenge in addressing the performance of the metal oxide is to develop an appropriate shape, size and pore volume of the relevant nanoparticle in order to undertake improvement where it is needed and create an adsorbent that is successful in the long-term. Roesch (2012) warns that non-radioactive metals such as ^{68}Zn^{+2} (which are generated on the generator as a decay product of ^{68}Ga), Fe^{+3} as a general chemical impurity, and ^{68}Ge^{+4} as a breakthrough impurity may represent metals competing with ^{68}Ga^{+3} for coordinative labelling of radiopharmaceutical precursors. Concerning solid phase based ion-exchange chromatographic ^{68}Ge/^{68}Ga radionuclide generators; some improvements may be within the resin material itself, in order to decrease the release of ^{68}Ge over time during generator use. Recent publications hint at the potential of sophisticated nanoparticles, such as Zr^{+4} and Ce^{+4}-systems, classified as nano-composites (Chakravarty et al., 2010 & 2011). The rational is to guarantee the effective adsorption of ^{68}Ge, the effective release of ^{68}Ga, chemical stability and radiation resistance.

From the literature, it is clear that there is no single definitive set of surface modifications, nor has an international consensus been reached as to which modifications are essential for producing successful and adaptive adsorbents. Whilst the Russian model is more realistic, focusing on a traditional set of parameters that are key to the generator production, other countries are yet to develop a more flexible and holistic surface modification approach, taking into account dominant characteristics as well as basic production regulations. As noted by Razbash et al., (2005), the focus of the Russian model appears to be more consistent with changes to the medical applications (e.g.,

the shift towards small eluent volume, the need to be less complicated, less ^{68}Ge breakthrough) than the other models found in other countries. However, the method of surface modification by the Eckert & Ziegler (Russia) is proprietary protected by trade secret.

Surface modification has now gained a reputation in the field of nanomaterials science as a routine technique for enhancing compatibility of nanoparticles with matrices. This will be discussed in more detail in chapter 2 under the heading "Surface Modification Methods". Prior to the 1980s, there was little interest in the area of inorganic matrices and organic resins as adsorbents, with most researchers directing technology away from clinical relevance. However, with the massive developments of the new classes of ^{99}mTc, ^{68}Ga imaging and ^{18}F-labelled diagnostics, it was recognised that there was a need for a precise control of the metal oxide surface chemistry in order to be compatible and selective toward specific targets. To date, most researchers have employed a 'mish mash' of approaches, when dealing with safety, legality and labelling of medical tracers, providing an abundance of information that, in some cases, is not valid and/or applicable for the given purposes (Rösch and Baum, 2011).

Therefore, this work aims to study how surface modification of the adsorbent governs parameters such as ^{68}Ga elution efficiency and minimise ^{68}Ge breakthrough in the medical radioisotope sector. With these critical factors identified, recommendations will then follow as to how the surface modification method together with its critical features could change the nanoparticle performance and adsorption properties in order to improve adsorption capacities. The majority of the literature reviewed is all written in hindsight and based on information once the process has already been considered and optimised by researchers. The benefit of adopting surface modification is in order to further develop several aspects of generator design and performance including labelling chemistry and clinical application. The main findings from this research project will be presented as suggestions for future improvements.

1.3 Research Goals, Objectives, Central Questions and Research Approach

1.3.1 Research Goals

The overall research goal is to explore the potential that surface modified TiO_2 might provide for $^{68}Ge/^{68}Ga$ generator sorbents produced, by assessing how to achieve precise control of its surface chemistry. A range of surface modification methods will be studied with the purpose of seeing how the surface properties of the nanoparticles can be improved and thereby to achieve specific performance. The results of the research will hopefully contribute to further development of the $^{68}Ge/^{68}Ga$ generator system in order to overcome challenges in production and use phases.

1.3.2 Objectives

The objective of this study is to explore how the surface properties of TiO_2 nanoparticles can be modified by particle surface treatment using silicon compounds that react with inorganic solid substrates to change the surface properties of those solids. The choice of TiO_2 as metal oxide stems from the fact that it exhibits interesting material properties, such as corrosion resistance, mechanical and thermal stability. By changing the particle surface properties, and consequently, the particle interactions, one can control dispersion stability and aggregate size (Kamiya & Iijima, 2010). These observations provide an interesting starting point, considering treatment with amino-organosilane that can be used to functionalise nanoparticles (Vrancken, 1995).

There are two research objectives:

- ✓ The primary aim of the research is to define surface modification of TiO_2 as a rather new concept as part of radioisotope production in the field of sustainable $^{68}Ge/^{68}Ga$ generators; finding evidence for its development in the field and analysing its impacts in a working example.
- ✓ The secondary research aim is to synthesize and characterize particles of molecularly imprinted polymers (MIP), with the idea of selectively retaining ^{68}Ge, to make sure that all relevant aspects are addressed and also monitor the process of implementation to ensure success.

In addition, the ^{68}Ga efficacies and ^{68}Ge breakthroughs of unmodified compared to modified TiO$_2$ will be examined to generate and evaluate empirical data.

The following hypothesis have been formulated to test the impact of surface modification on the success of a TiO$_2$ based ^{68}Ge/^{68}Ga generator:

- There is a positive relationship between surface modification and the perceived success of the TiO$_2$ based ^{68}Ge/^{68}Ga generators.

- There is a positive relationship between molecular imprinted polymers and the ^{68}Ge breakthrough performance of the TiO$_2$ based ^{68}Ge/^{68}Ga generators.

1.3.3 Central Questions

As a consequence, in order to understand the effectiveness of surface modification, research on the science about the surface of TiO$_2$ is crucial. One of the early examples is Diebold's (2002) work on TiO$_2$. His work investigated and demonstrated motivating principles for designing different types of adsorption mechanisms at TiO$_2$ oxide surfaces. At the heart of these mechanisms is the use of silane coupling agents (SCA), as the means for their synthesis and functionalisation. Its related topics will be covered in more detail later in this study. By establishing improved mechanical and surface properties through various surface modification methods, research could formulate and recommend steps to help improve the TiO$_2$ nanoparticles in their preparations as generator adsorbents. The central question was whether surface modification of nanoparticles was the way forward for the transformation of TiO$_2$ properties to achieve specific applications for the ^{68}Ge/^{68}Ga generators in the PET imaging industry. Further matters to be examined during this phase of the research were as follows:

a. What is the best ^{68}Ga separation technique for adoption when surface modification was used to alter the chemistry of the TiO$_2$ surfaces?

b. How this method can be best operationalised in the experimental environment created for observations?

c. When applied, tested and observed, does the method meet the requirements for good theory?

d. How the adsorbent can be improved, given the test results and what recommendations flow from the insight observed?

The overarching research question will be:

How could surface modification of the titanium dioxide (TiO_2) properties responsible for the production of the $^{68}Ge/^{68}Gas$ generator increase capacity to adsorb and desorb ^{68}Ge and ^{68}Ga radionuclides, respectively?

The following sub-questions were compiled to further analyse the impact that modification of the TiO_2 metal oxide will have upon the adoption of TiO_2 as an adsorbent:

✓ To what extent does the modification of the TiO_2 nanoparticles influence adsorption development of a $^{68}Ge/^{68}Ga$ generator?

✓ What are the crucial features of the modification method and its benefits?

✓ What is the likelihood that impurities may find their way into the final product?

✓ When applied, tested and observed, does the proposed surface modification model meet the requirements of a good ^{68}Ga generator application?

Building on these questions, the study realises a gap where surface modification of nanoparticles as well as Molecular Imprinted Polymer processes seems poorly covered and understood in the literature surrounding $^{68}Ge/^{68}Ga$ generators. The literature heavily focuses on the chemical and mechanical design of the nuclear reactions (Razbash et al., 2005; Naidoo et al., 2002), including the $^{68}Ge/^{68}Ga$ generator chemistry (Brownell & Sweet, 1953; Seaman at al., 1954; Brucer et al., 1953; Shealy et al., 1964), ion-exchange and anion exchange resins (Schumacher & Maier-Borst, 1981; Neirinckx & Davis, 1980; Nakayama et al., 2003; McElvany et al., 1984;] Loc´h et al., 1980), impact of impurities on ^{68}Ga eluates (Breeman & Verbruggen, 2007; Decristoforo et al., 2005; Meyer et al., 2006; Velikyan et al., 2004), but little research seems to have been done on the surface chemistry of the nanoparticles and complete ^{68}Ge retention. Taking as an example Roesch and Riss journal from 2010, they introduced new developments in ^{68}Ga Radiopharmaceutical Chemistry, but only elaborate on the nuclear reactions, chemical separations and impact caused by impurities. A conformational quote can be found in their article: "The $^{68}Ge/^{68}Ga$ radionuclide generator systems available today are not necessarily optimally designed for direct application for making a diagnostic

product for clinical and routine use in humans. The eluate from the commercial generator still contains measurable activities of long-lived ^{68}Ge" (Roesch and Riss, 2010). For the purpose of this research project, the main work that was used as a basis for the research method was the work of Marie-Alexander Neouze and Ulrich Schubert (Neouze & Schubert, 2008). Their framework emphasises the role that surface modification and functionalisation plays in the choice of metal oxide nanoparticles. The aim was to provide a solution for the conflicting results about the characteristics of adsorbent on the performance of ^{68}Ge/^{68}Ga generators. These authors set out a structured overview of research approach and research strategies and how they fit together. In this study, the approach and strategies that were used are threefold;

Schematic of the Experimental Flow
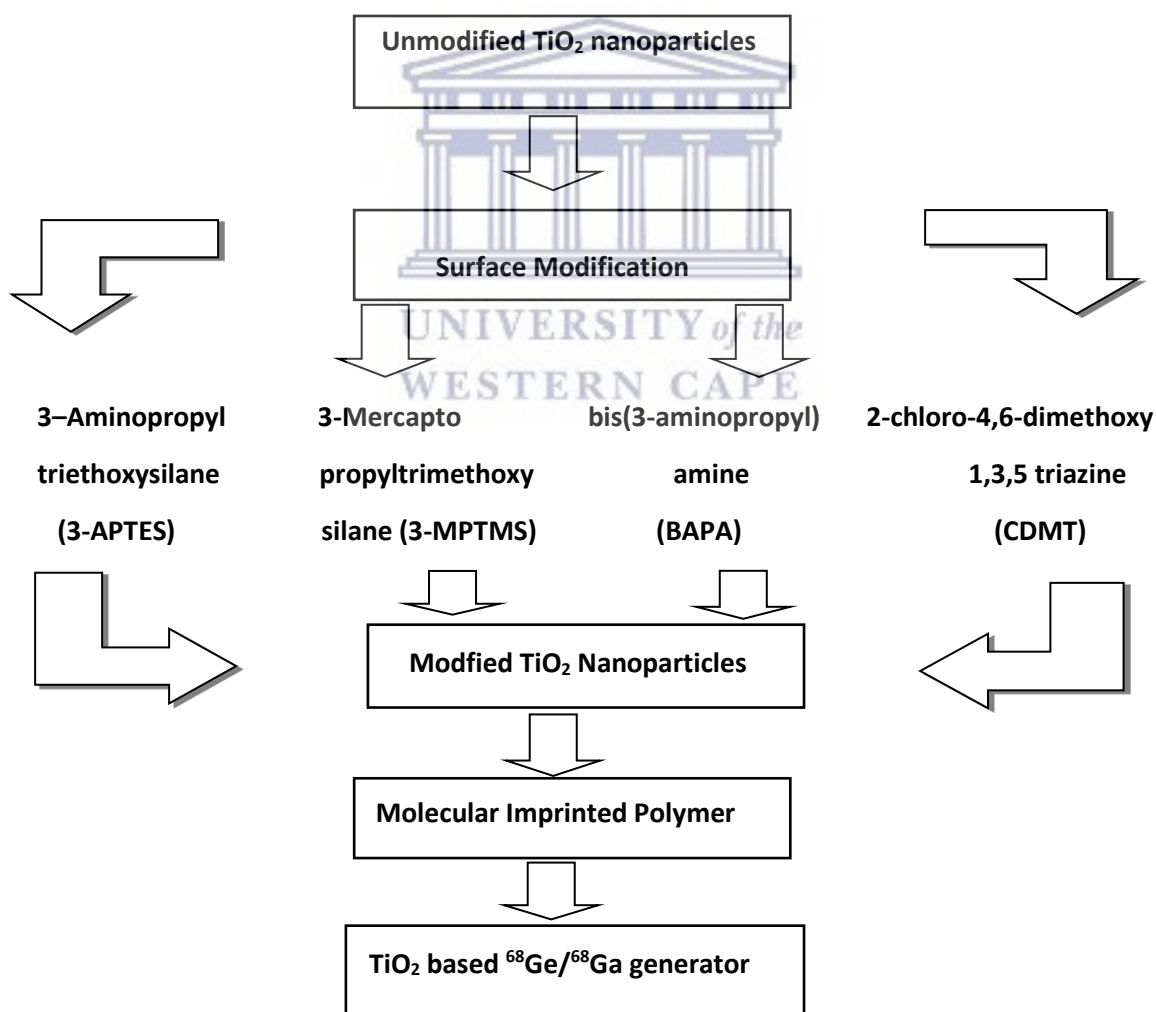
First, an initial exploratory study was conducted; in order to first develop a rough description on the performance of TiO_2 as an adsorbent and then provide a more detailed account of the areas of the various important topics related to ^{68}Ge/^{68}Ga generators. This stage corresponded with the logics of the introduction research strategy (Romero and Morcilo, 2017).

Second, a somewhat more applied approach was undertaken, conducting surface modification and functionalisation of the TiO_2 metal oxide with relevant organic ligands. The purpose was to come up with some suggestions for how these organic ligands can be used to introduce functionalities of the TiO_2 nanoparticles.

Thirdly, as mentioned under the introduction section 1.3.2, when the objectives of the study were listed, conceptual and methodological problems about the ^{68}Ge breakthrough still exist and are well documented (Romero and Marcilo, 2017; Roesch and Riss, 2010).

1.3.4 Research Approach

The research approach included evaluating supplied TiO_2 followed by annealing or by suitable surface modification methods (self-assembled monolayers, surface modifications based on organic reactions, surface modifications based on polymerisation, surface modifications with inorganic layers etc.). This was followed by the selective separation of the parent (^{68}Ge) and daughter (^{68}Ga). Preliminary experiments were used to obtain information about the role that annealing or surface modification plays in the production and optimisation of ^{68}Ge/^{68}Ga generators process. Then this was allowed by using various characterisation methods that seemed most appropriate for gathering information on the properties of the TiO_2 metal oxide and to test whether the modification improved the performance of these generators. It was desirable to chemically modify TiO_2 nanoparticles in such a manner for the modifier to impart:

    (a) Good stability – assist in alleviating instability problems associated with pH and temperature
    (b) Improve surface chemical properties - to address challenges of low efficiency
    (c) Permit a safe and reliable method – low ^{68}Ge breakthrough and very limited metallic impurities.

Based on the literature reviewed of an ideal ^{68}Ge/^{68}Ga generator system, the requirements were derived for efficient separation of the daughter and parent elements due to their different chemical properties, effective shielding of the generator, traceability of the process, reliability and robustness of the performance.

1.4   Focus and Limitations

1.4.1   Focus

It was hypothesised that the rutile and anatase form of titanium dioxide might be suitable starting points of research, to study whether their surface modification might be the solution to the challenges associated with the production, handling and use of the ^{68}Ge/^{68}Ga generators. In order to assess the potential of the surface modification method it was necessary to do a thorough assessment of the concept of a radionuclide generator and the demand for a relatively inexpensive supply of the ^{68}Ga radioisotope. Comparing the results between the two phases of TiO_2 nanoparticles could potentially give insight into areas of concern, such as the ^{68}Ga efficiencies and ^{68}Ge breakthroughs, and lead to considerations for further developments. In previous studies, anatase was found to be more suitable for the production of the ^{68}Ge/^{68}Ga generators when compared to the rutile, except that the method did not involve surface modification. In addition, in contrast to the SnO_2 method, ^{68}Ge loaded TiO_2 often gets eluted with a less concentrated acid, which implies less processing steps.

In one study by Roesch and Riss (2010), five critical areas of improvement were highlighted as important for the ^{68}Ge/^{68}Ga generators. Impurities, large eluate volumes, ^{68}Ge breakthrough, labelling yields and specific activities were all listed as areas looking for further improvements towards medically approved systems. All of these elements are mentioned in various research studies from a ^{68}Ge/^{68}Ga generators perspective. Some are only mentioned "in passing", while other topics are given a lot of space in the literature. The majority of surface modification presented in research is touched upon during the coming literature review. The overview does however create a structured idea of what some consider as being important elements of ^{68}Ge/^{68}Ga generators. (Roesch & Riss, 2010; Breeman & Verbruggen, 2007). It also emphasizes the need for the metal oxide to be able to contribute strategically as well as operationally. Thus, supporting the wide range of topics covered in the coming literature review.

An interesting aspect from the literature's point of view is to realise that the eluate from the commercial generators still contain measurable activities of long-lived ^{68}Ge. Based on the requirements, the study suggests Molecular imprinted Polymers with the idea of adapting to the proposed model. The main reason is that finding a best metal oxide match for ^{68}Ge/^{68}Ga generators might be an exhausting exercise, as properties among them differ fundamentally. Hence, a more promising strategy is to perform a 'safe' match on the design. An increasing number of studies show that having MIPs as an adapted prototype is very valuable for the proposed generator design. By addressing ^{68}Ge in the eluate during the elution step, but not showing any activity with the system, acts as a good starting point for this research, but the focus will be somewhat wider than this.

Reflecting on findings from the literature it is relevant to add that research of this nature is important for the future of radioisotope developments. The research is conducted to gain insight into the points raised regarding the gaps in knowledge about the role that surface modification can play in addressing ^{68}Ge/^{68}Ga generator challenges.

1.4.2 Limitations

A number of limitations have to be taken into account regarding the methodology of this research. Due to time constraints it was only possible to research the most available TiO_2 nanoparticles, anatase and rutile purchased from local suppliers. Moreover, both metal oxides are relatively easily accessible when buying from South Africa, where iThemba LABS is based. This was beneficial in terms of logistics and, indirectly, finances. This, to a large extent, defined the scale of this research. In order to narrow down the focus of the research it was decided to study the main two parameters (^{68}Ga efficiency and ^{68}Ge breakthrough) when evaluating modified TiO_2 as a generator model. A key construct in this research is to measure the value which surface chemistry may provide as a model for testing the research hypothesis by meeting requirements of a good generator as set out by the nuclear regulatory organisations.

1.5   Thesis Outline

This thesis is divided into five main chapters:

Chapter 1 – Introduction: This chapter provides an introduction to the background and problems of generator systems. It highlights the challenges and provides questions of the research leading up to this thesis.

Chapter 2 – Literature Review: This chapter is divided sub-chapters, each discussing a specific topic related to the research. Apart from this, each section first introduces the background of the related topic and then discusses how the contributions address the limitations of the current method. Each section is then concluded with a short summary of the challenges of that particular method and possible avenues for future work. The chapter is concluded by a summary based on the literature review and consideration will be given to the different approaches for increasing capacity and further improvements.

Chapter 3 – Methodology: This chapter represents the experimental part of this thesis where the various experimental protocols are detailed.

Chapter 4 – Results and Discussion: This chapter sets out the characterisation of feedstock and their modifications by providing results and discussions of the experiments pursued under this objective. The chapter will briefly discuss the characterisation results for each method pursued and thereafter conclude by highlighting challenges encountered and opportunities for further research.

- **The effect of surface modification on $^{68}Ge/^{68}Ga$ generator capacity**: This subsection will investigate how surface modification behaves in a generator model, as this behaviour may have a strong influence on which method is appropriate and where the preparations can be ideally placed. The study was undertaken mainly to evaluate the effectiveness of surface character changes on the basis of dispersion, morphology, adsorption capacity of the functionalised titania. The study by Siwínska-Stefánska (2012) found significant evidence that TiO_2 material was able to be

functionalised with selected silane coupling agents (SCA). Based on the results, recommendations will be derived for designing content as well as interactions and where such method should be optimally placed.

- **The effect of molecular imprinted polymers:** One of the major drawbacks plaguing ^{68}Ge/^{68}Ga generators is the ^{68}Ge breakthrough leakage to the final product, i.e. ^{68}Ge contamination. This subsection presents an approach that considers both information about the method of surface modification and the behaviour leading to what is known as ^{68}Ge breakthrough. In conjunction with breakthrough, comparisons between the modified and unmodified TiO_2 nanoparticles are presented.

Chapter 5 – Conclusion, limitations and Recommendations: This chapter first looks at suitable and easy to understand interaction method before more closely investigating factors that influence the technique to interact. As before, based on the findings, recommendations will be designed here and these can be used to build concrete evidence to more effectively communicate the proposed research methods. In the final chapter, the conclusion and a summary of the contributions will be presented in this thesis. Also, novelty and potential areas for future work will be identified.

Appendices - This chapter looks at suitable and easy-to-understand supporting documents to assist investigating factors that influence ^{68}Ge/^{68}Ga generator applications. Based on an observational studies, this work was able to align its findings with the agreed and legislated parameters in the field of nuclear medicine. The chapter introduces image-based figures, tables and documented information that can be used to build up ^{68}Ge/^{68}Ga generator in the nuclear imaging applications.

CHAPTER II

LITERATURE REVIEW

2.1   Titanium Dioxide (TiO$_2$): Origin, Properties and Applications

2.1.1   Origin

Titanium dioxide occurs in nature as the well-known minerals rutile, anatase and brookite (Figure 2.1). Additionally, it also appears as two high pressure forms, a monoclinic baddeleyite-like form and an orthorhombic α-PbO$_2$-like form, both found at the Ries crater in Bavaria (Legrini et al., 1993; Linsebigler et al., 1995). Rutile is the most abundant phase and contains around 98% titanium dioxide in the ore. The meta-stable anatase and brookite phases convert irreversibly to the equilibrium rutile phase upon heating above temperatures in the range 600–800 °C (Hanaor & Sorrel (2011); Bourikas et al., 2014; Elgh and Palmqvist, 2014; Fischer et al., 2017). Many methods such as the sol-gel process (Karami, 2010), hydrothermal methods (Andersonn et al., 2002), solvo thermal methods (Nam et al., 2013) and emulsion precipitation (Deosorla and Vallaurie, 2009) have been developed for the synthesis of titanium dioxide nanoparticles. Cho and Lee (2015) write that composite materials as the Titanium Dioxide (TiO$_2$) find their applications in a variety of industries – pharmaceuticals, food and agriculture, ceramics, electrical, automobile, electronics, cosmetics and so on. For dry particles coating processes, Cho and Lee (2015) further states that material with relatively large particle size are mechanically coated with small particles in order to create new functionality or to improve the initial characteristics.

O_2
Ti
(a)   (b)   (c
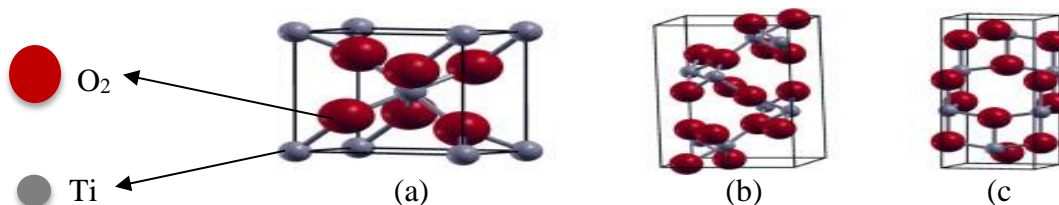
Figure 2.1: TiO$_2$ structures: (a) Rutile (b) Brookite and (c) Anatase

(SOURCE: Reyes-Coronado et al., 2008)

Anatase, as a meta-stable phase, is chemically and optically active, thus is suitable as a catalyst and as a support (Ding et al., 1997), while rutile, the thermodynamically stable polymorph, has the highest refractive index and ultraviolet absorption, and is widely used as white pigment (Zhao et al., 1998). It has been extensively demonstrated that the physicochemical properties of TiO_2 are strongly dependent on its crystal structure and morphology as well as grain size (Cozzoli et al., 2003). The expanding data base has made rutile TiO_2 a very popular model system for metal oxides. Furthermore, titania nanoparticles possess high available surface area, which are beneficial for aqueous photocatalytic reactions (Tachikawa et al., 2007). The most popular commercial form of TiO_2 is called Degussa P25. It contains almost 80% anatase and 20% rutile (Ohno et al., 2001).

Awareness is mounting that metal oxide adsorbents having high adsorption capacity for radioisotopes may soon become strategic raw materials for the development of radioisotope generators. The present recognition of the significance of TiO_2 has led to increasing interest in its intrinsic properties and particularly performance related properties. This interest indicates the need for thorough research into the development of adsorption performance to solve the problems encountered in the radioisotope generator field.

2.1.2   Properties

Due to its high diffraction index, strong light scattering and incident-light reflection capability, TiO_2 in rutile phase is mostly used as white pigment (Mandzy et al., 2005). Thus such properties earned TiO_2 the standard pigment status which is found in white dispersion paints with high hiding power. Since light scattering does not occur in nanoscale particles, the white titanium dioxide pigments used are almost exclusively rutile particles with grain sizes in the micrometre range. These white pigments are not only found in paints and dyes but also in varnishes, plastics, paper, and textiles. TiO_2 pigments used in plastics constitute the fastest growing market. It is in particular due to the packaging industry's strong demand that the consumption of titanium dioxide pigments is on the increase (Dufton, 1998).

Interestingly within the context of this research, Khataee and Mansoori (2011) portray different anatase to rutile ratios of ultra-fine TiO_2 powder as having large specific surface area, an excellent

property for a wide variety of adsorption applications. As a supplement to the background information to this work, Park et al., (2013) write that transformation of reactants adsorbed on the surface of TiO_2 photocatalysts are governed by three mechanisms: photo-generation, migration and trapping of charge carriers. However, designating research trajectories as problem-solving activities within surface modification is still a significant obstacles and has remained unexplored in the discourse of TiO_2 technology. With these critical factors identified, recommendations were then made as to how surface modification could change surface chemistry of the TiO_2 nanoparticles in order to improve their adsorption capacities.

2.1.3   Applications

Recently Matsunaga and his colleagues realised that the use of titanium dioxide (TiO_2) in applications for adsorption relied on its crystal structure and grain size to ensure that the material can resist bacterial activities (Matsunaga et al., 2016). When TiO_2 was used in water based paints, its specific properties which resulted from adsorption and reactions on the TiO_2 surface were observed in the presence of binders and amines. Warson and Finch (2001) published lessons learnt from a study of TiO_2 as a pigment and provided useful information for consideration for effectiveness and usability. They realised that surface treatment of titanium dioxide has the effect of vastly increasing the surface area even though the apparent particle size is substantially unchanged.

Although three crystalline phases of titanium dioxide exist, namely, anatase, rutile and brookite, anatase was the first powder to be used as crystalline solids by Harkins and Jura (1944); its technological interest explained why for a long time it was favoured as a non-porous adsorbent (Rouquerol et al., 2014). One of the most prominent discoveries at that time with rutile, when interacted with water vapour, was that molecular water could be removed by evacuation at 325 °C, leaving the surface partially hydroxylated. In later years, this explained why the dehydrated surface of rutile can interact specifically with a wide range of polar molecules, a notion strongly supported by Rouquerol and colleagues (2014).

Khataee and Mansoori (2011) reported on the challenges of recovering pure TiO_2 powders from water when used in aqueous systems. This was after they identified that ultra-fine TiO_2 powders

have large surface area but due to their easy agglomeration into larger particles, an adverse effect on their performance was observed. His advice was that dispersing TiO_2 particles in layered clay provided the solution to such a problem. Herrmann and colleagues (1986) looked at the production processes of TiO_2 as a powder. They reported that such processes require drying. However ultra-fine particles wetted with a solvent usually undergo intensive aggregation as the drying proceeds.

Though many research papers provide useful lessons learned or recommendations based on their findings, most previous work focused on rather specific applications (surface coatings, dielectric applications, pigments and photocatalysis), and draw conclusions only from findings of their deployment(s). To overcome these limitations, this section of literature review will cover a comprehensive literature review, identifying research questions, research approaches, and methods used in $^{68}Ge/^{68}Ga$ generator research, relating to the use of TiO_2.

2.1.4   Water Adsorption on TiO_2 Nanoparticles

The decision of which phase of TiO_2 may be used strongly depends on whether it is applicable to separate ^{68}Ge from ^{68}Ga only. This is usually a technical question. A comprehensive overview of how the parent and the daughter radionuclide follow the separation mechanism for a successful generator system can be found in section 2.2.1. Understanding how water adsorptions upon the TiO_2 nanoparticles takes place was essential for the proposed model of the ^{68}Ge generator. An often occurring question is how the water binds to the surface and how the potential energy of the surfaces will shape adsorption behaviour in order to be able to draw well-founded conclusions. The water molecule may produce vastly different results in different experiments and with different sizes of adsorbents. In rutile, for example, Bandura and colleagues (2004) demonstrated how the water molecule adsorbed differently when compared to anatase. But because the adsorption reaction can only proceed if water is present, attention was paid to water adsorption on the ^{68}Ge adsorption reaction and the influence of surface-bound-state water also known as hydrophilicity.

There have been several studies of this kind that looked at modification of surface chemistry as the most direct way to influence adsorption properties of nanoparticles (Albini and Fasani, 2013; Zheng, et al., 2009; Laskowski and Ralston, 2015). In particular, Wang et al. (1999) observed that in aqueous media, the surface of TiO_2 undergoes a conversion from the hydrophobic to the

hydrophilic state by adsorbing hydroxyl groups from the dissociation of water molecules and by forming hydrogen bonds with the OH groups of undissociated water molecules. Related studies by Isimjan and colleagues (2012) were able to support this notion by showing that the removal of the hydroxyl group was easier from anatase than rutile. The difference in reactivity between anatase and rutile can be ascribed to the higher adsorption capability of the OH for rutile. Similarly, the knowledge acquired in this field of research has contributed to the present realisation that the activity of anatase is observed to be higher than that of rutile. Nosaka and Nosaka (2016) write that the difference of the reaction paths, that is, OH release for anatase and dimer (Ti-O-O-Ti) formation for rutile, which may be caused by the difference of the Ti–Ti distance at the surface.
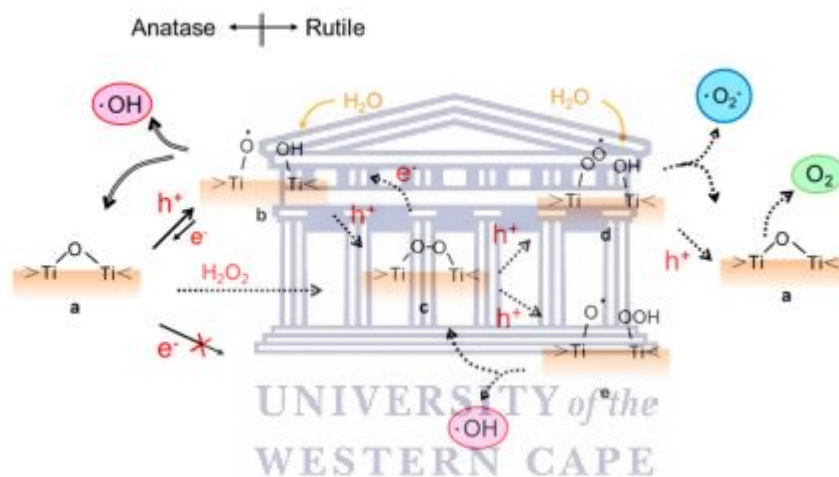
Figure 2.2: Illustration of photocatalytic on anatase (top) and rutile (bottom)

exerted by OH group in solution.

(SOURCE: Nosaka and Nosaka (2016))

From the results of the previous studies, it was evident and important to pursue the anatase phase rather than the rutile phase for the separation envisaged. A set of principles and concrete ideas could be formed as to how the anatase could be applied. The review has revealed a set of interesting effects, related to the morphology, particle size and composition, and provided an understanding of the impact of these parameters upon a ^{68}Ge/^{68}Ga generator system. It is envisioned that the prior arts and their implications will be useful for the future design of the ^{68}Ge model. This dissertation aimed to adhere to the above guidelines in order to establish observations of confirmable models related to the TiO_2 nanoparticles as adsorbents.

2.2   Theory of radioisotopes

The introduction of radioisotopes by scientists and physicians in the medicinal sector was regarded by scientists as the most useful research since the invention of the microscope in the 17th century. Radioisotopes differ from other isotopes of an element for the reason that their nuclei are unstable because they emit radioactive particles which usually result in the formation of another element (IAEA, 2001). On the other hand, isotopes differ from ordinary atoms by having an alternate (often greater) number of neutrons. Stable atoms persist indefinitely with this extra nuclear baggage, and can be identified on account of their increased atomic mass. By contrast, radioisotopes can be detected when they decay to another- usually stable- form, by emitting at least one of the three kinds of radiation. A list of radioisotopes produced at iThemba LABS is presented in Appendix A. Alpha particles (each made up of two protons and 2 neutrons) do not go far, and cannot pass paper. Beta particles (high energy electrons or positrons) are more penetrating, but can be stopped by wood. Gamma rays have high energy and travel the longest distance in air; they are stopped only by dense materials such as lead or concrete. An example of how isotopes are produced is given in Figure 2.3, along with the energies emitted for their stability status.

Biochemist used radioisotopes to reveal the sequence of chemical reactions in metabolism. Molecular biologists labelled nucleic acids with radioisotopes to follow the replication and expressions of genes. Physiologists tracked the movement and activity of hormones using radioisotopes. Ecologists used phosphorus-32, a radioisotope of phosphorus, to trace nutrient cycling through the living and non-living parts of aquatic and terrestrial landscapes. As labels, radioisotopes could be used to follow compounds through separation techniques (centrifugal, electrophoresis, chromatography) or through biological processes, such as the synthesis of proteins. In a book by Angela Creager (2013) it was concluded that radioisotopes were key ingredients for episteme of understanding life in molecular terms.
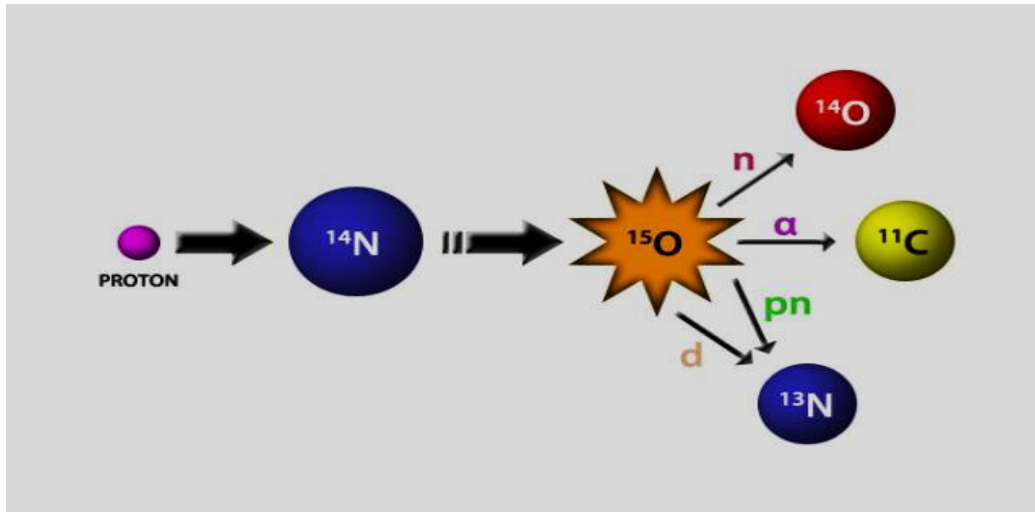
n=neutron; α=alpha; pn= protons & neutrons and d = deuterium

Figure 2.3: Schematic diagram of a stable nucleus (N-14) is bombarded with a proton and results in an

unstable O-15, that subsequently results in three stable atoms (O-14,

C-11 or N-13)

(SOURCE:https://www.simply.science/images/content/physics/modern_physics/nucleus/C oncept_map/Isobars_Isotopes_Isotones.html)

The use of radionuclides in the physical and biological sciences can be broken down into three general categories: imaging, radiotherapy and radiotracers (Velikyan et al., 2008). Imaging can be further divided into Positron Emission Tomography (PET) and Single Photon Emission Tomography (SPECT) (Rösch & Baum, 2011). This section of imaging modality explores the potential of radioactive tracers and special types of camera to look at organs in the body. Figure 2.4 illustrates the principle behind Positron Emission Tomography (PET) and Single Photon Emission Tomography (SPECT. The idea of a radioisotope used in therapy is based on the desire to link a radionuclide that has a high linear energy transfer (LET) associated with its decay products, such as Auger electrons, beta particles or alpha particles, to a biologically active molecule that can be directed to a tumour site (Rösch & Baum, 2011; Fani et al., 2008). The main difference between SPECT and PET scans is the type of radiotracers used. These topics are beyond the scope of this work and will not be described here. But because of the rapidly spreading use of PET and PET/CT (computed tomography), the number of positron emitting radiotracers such as ^{64}Cu and ^{68}Ga is expanding rapidly, and generator adsorbent technology needs to be understood by a much larger group of

scientists. Generator systems offer a solution to centres where there are no readily available sources of short lived PET radioisotopes and for specific applications, including radiotherapy.
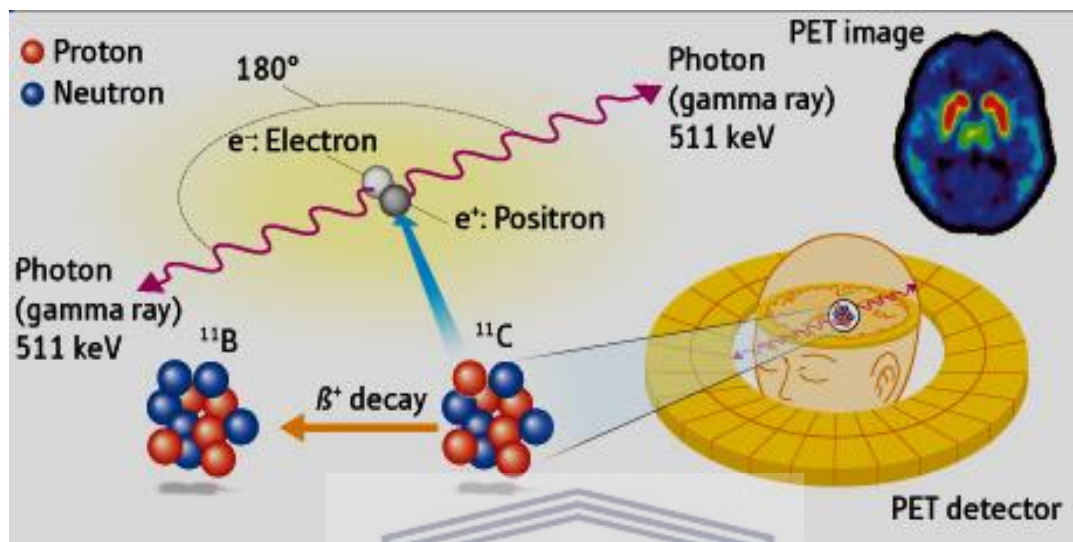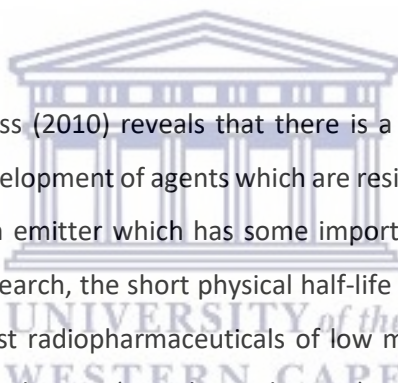
Figure 2.4: Principle of PET Imaging (SOURCE: Tout et al., 2016)

Indeed, the drive towards imaging improvement using radioisotopes cannot be overstated, given the verdict by Gründer and Wong (2003) that there are many challenges facing chemists in the preparation of PET tracers using short-lived isotopes. The half-life of an isotope refers to how long it takes for it to become fifty percent less active. A knowledge of the PET tracers half-life is important because, as Kara Duncan (1998) puts it, the nuclei must be active long enough to treat the condition, but a short enough half-life is required so that healthy cells and organs are not damaged by the radiation given off by the radioisotope due to decaying. The use of PET tracers with short half-lives ensure that radiation exist for the shortest time possible in human bodies.

2.2.1   The $^{68}Ga^{+3}$ Radionuclide

Waterstra-Rich and Gilmore (2016) described a generator system as a design constructed on the principle of the decay-growth relationship between a parent radionuclide with longer half-life that produces, by disintegration, a daughter radionuclide with shorter half-life. They explained that the parent and daughter radionuclides must have sufficiently different chemical properties in order to be separated (Figure 2.5). The daughter radionuclide is then used either directly or to label different

molecules to produce radiopharmaceutical molecules. The main advantage of the generator systems is that they can serve as top-of-the-bench sources of short-lived radionuclide in places located far from the site of a cyclotron or nuclear reactor facilities. The daughter radionuclide should be obtained by a simple elution process with high yield and chemical and radiochemical purity. The generator must be properly shielded to allow its transportation as well as manipulation. ^{68}Ge becomes strongly adsorbed to an ion exchange and because it is busy decaying to ^{68}Ga in the process, this gets eluted and collected for studies. The proper choice of sorbent or rather combination of sorbent/eluent is of extreme importance since it would control the efficiency of the generator operation. The sorbent is the most essential part to which the mother radionuclide is adsorbed on in the column. So, to understand the challenges and leverage such insight for research benefit requires a number of recognised techniques for surface treatment to produce effects that are long lasting and efficient; notions that Mike Sathekge and colleagues (2015) still continues to promote.

Research done by Roesch and Riss (2010) reveals that there is a well-established coordination chemistry of Ga^{3+} which allows development of agents which are resistant to in vivo trans-chelation of $^{68}Ga^{3+}$. Gallium-68 is a positron emitter which has some important advantages besides being available from a generator. In research, the short physical half-life of 68 min which is compatible with the pharmacokinetics of most radiopharmaceuticals of low molecular weight is one of the main determinants for wide-scale adoption (Maecke et al., 2005). A summary of quality standards prescribed for safe use of radiopharmaceuticals for humans is presented in Appendix E. Related to this is the research studies such as antibody fragments, peptides, aptamers, oligonucleotides and others (Roivainen et al., 2012; Smith-Jones et al., 1994; Maecke et al., 1993), that have found applications as a result of the $^{68}Ga^{+3}$ radionuclide. According to Deutsch (1993), the key to $^{68}Ga^{+3}$ success lies in the fact that gallium-68 decays by beta emission and by orbital electron capture. It has a short half-life (67.71 minutes), compatible with the pharmacokinetics of most low-molecular-weight radiopharmaceuticals and has convenient characteristics for PET imaging. This is beneficial to the research community because it allows imaging of rapid cells production such as proliferation, apoptosis and angiogenesis. In addition, inflammation, infections, myocardial and pulmonary perfusions can be targeted (Velikyan, 2015; Barnejee and Pomper, 2013; Zimmerman, 2013). The literature finds that the maximum positron energy is 1,899 keV (the average energy per

disintegration is 740 keV). Researchers often favour this characteristic because high energy positrons imply deeper tissue penetration since energy is deposited when it travels through human tissue.
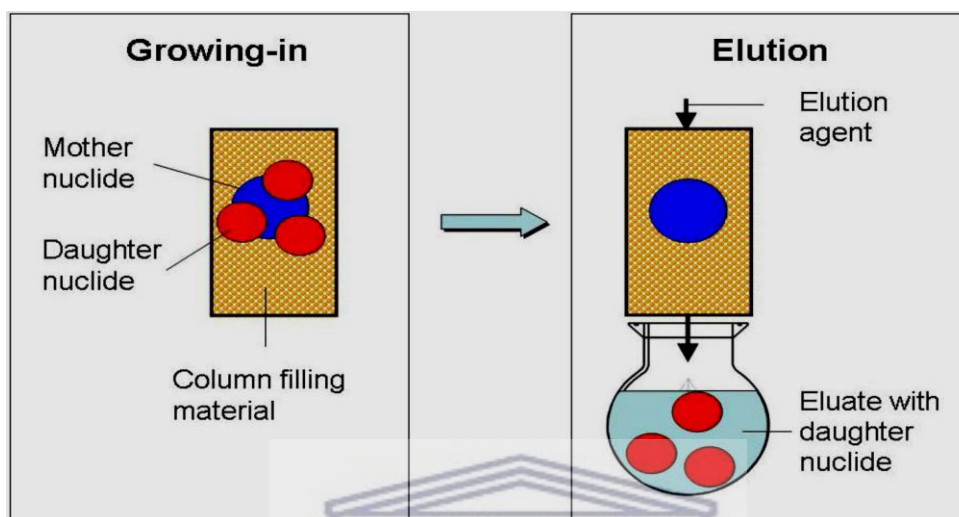
Figure 2.5: Schematic diagram of a ^{68}Ge/^{68}Ga generator principle
(SOURCE: Bjørnstad et al., 2013)

Another issue relevant in this context is related to the parent isotope ^{68}Ge (half-life = 271 days, which allows routine manufacture and shipment). Various studies reported in the literature demonstrated that ^{68}Ge is produced using natural gallium (60.1% ^{69}Ga, 39.9% ^{71}Ga) as target material for proton bombardment at energies >11.5 MeV, the threshold energy for ^{69}Ga (p, 2n) ^{68}Ge. Working with a gallium (Ga) target, however, is challenging due to its low melting point (39 °C) and corrosivity towards most metals. Niobium, however, does not react with liquid gallium at temperature <400 °C. For this reason, large-scale production of ^{68}Ge is carried out by irradiating water-cooled targets made of gallium encapsulated in niobium containers. The relatively long half-life of the parent radionuclide ^{68}Ge ensures the cost-effective availability of ^{68}Ga within the PET facility for long periods of time. It is found that in general the chemical properties of Ge(IV) and Ga(III) are sufficiently different and this leads to several different methods of efficient separation, as explained in detail in section 2.2.2. What is exceedingly relevant to the successful adoption of generators is the potential to develop a range of cold, freeze-dried kits which can be reconstituted and labelled, and requested at any time.

The topic will further go into the $^{68}Ga^{3+}$ chemistry in section 2.2.3 in order to review the aspects that make the $^{68}Ga^{+3}$ radionuclide more attractive. This overview of interaction models shows that no comprehensive model exists. Interaction is strongly depending on a number of different aspects, e.g., the supported interaction techniques, the content, the audience, and the envisioned type of interaction.

As mentioned before, generator based PET isotopes such as the ^{68}Ga are possible without an expensive on site cyclotron, generally leading to cost efficiencies (Schubiger et al., 2007; Rösch & Baum, 2011; Baum & Rösch, 2013), which is an important advantage. However, Waterstra-Rich and Gilmore (2016) maintain that there is a large and growing gap between radiation safety, legal requirements and labelling of medical tracers. With their focus on the nuclear medicine and PET/CT, they were able to deduce that the presence of trace metals, large volume of elution and high acid concentration required further attention. This is particularly so because quality control of the eluted ^{68}Ga is an important issue and cannot be left unattended. The field also requires further insight into the development of analytical techniques that measure ppm levels of ^{68}Ge in ^{68}Ga.

2.2.2   Separation of ^{68}Ga from ^{68}Ge

The literature review of the Masters work (Buwa, 2015) presented a short overview of how various chromatographic techniques were successfully used for achieving a desired separation of $^{68}Ga^{+3}$ and $^{68}Ge^{+4}$ ion species and how such models contributed to the therapeutic radionuclide generator production systems. According to a book edited by Strasheim and Steele (1978) chromatographic separation methods are emphasised because of their ability to achieve clean separations on complicated samples. The literature presented at least four closely related separation techniques which were:

2.2.2.1 Column extraction chromatography

In this technique a column is packed with a solid support that holds an organic stationary phase. In the sorption step, an aqueous sample is added to the column and the various solutes are distributed between the organic and the aqueous phases. Then the column is eluted with an aqueous solution

so that the inorganic solutes move down the column at different rates and are seprated this way. In Figure 2.6, a schematic diagram of a column extraction chromatography is shown. Sometimes the phases are reversed so that the aqueous phase stationary and elution is performed with an organic phase (Ni et al., 2009).
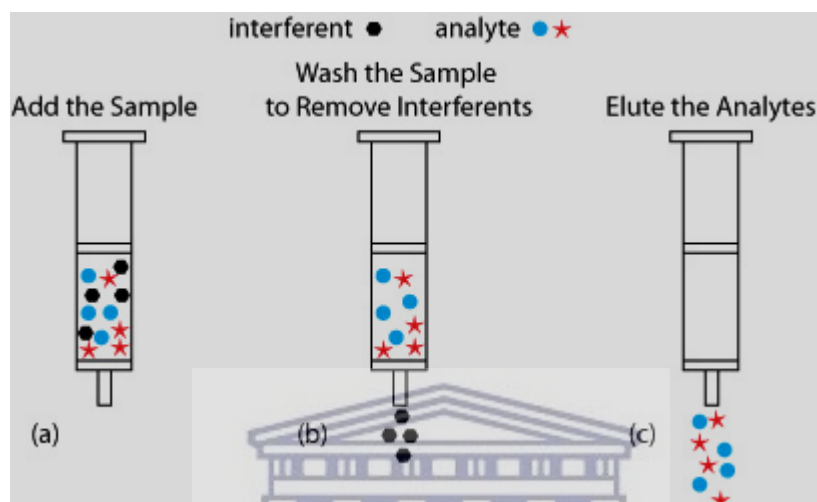
Figure 2.6:   Schematic diagram of a Column extraction chromatography
with its solid support that holds an organic stationary phase
(SOURCE: Harvey et al., 1991)

Manipulation of the technique is minimal and the scope of possible separation is quite large. One disadvantage of this technique is that there is often some bleeding or dissolving of the organic phase from the solid support. Presaturation of the eluent with organic solvent helps to prevent such.

2.2.2.2 The solvent extraction technique

A compound can be separated from impurities in a solution by extracting the compound from the original (or first) solvent into a second solvent. For the process to be selective, the compound must be more soluble in the second solvent than in the first solvent, and the impurities must be insoluble in the second solvent. Additionally, the two selected solvents must be immiscible, or not soluble in one another, so that they produce two separate solvent layers. After dissolving the mixture in the first solvent, the solution is added to a second solvent. The two layers are vigorously mixed to

maximize the surface area between them. This mixing facilitates the transfer of a dissolved compound from one solvent layer to another (Richter et al., 1996). Once the transfer process is complete, the layers are again allowed to form, as shown in Figure 2.7. Separation of the two layers then completes the separation of the desired compound from the impurities.
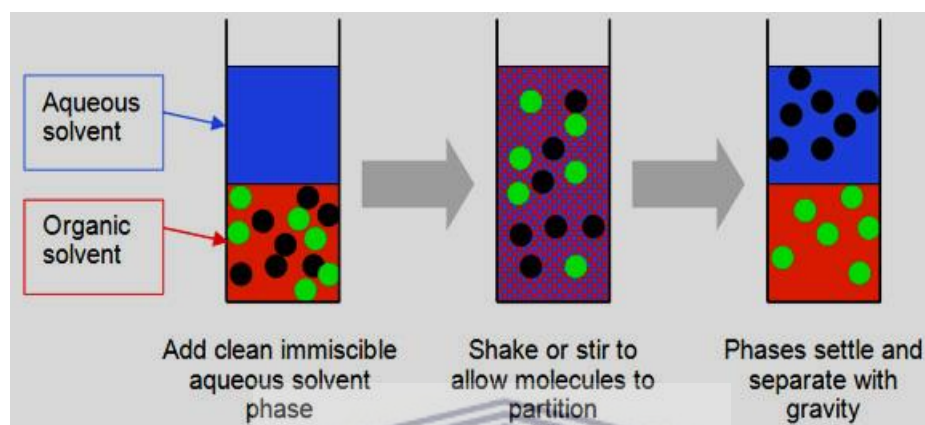
Figure 2.7: Schematic diagram of a solvent extraction technique
(SOURCE: https://slideplayer.com/slide/6246629/)

2.2.2.3 Ion-exchange chromatography

This technique exploits the interaction between charged molecules in a sample and oppositely charged moieties in the stationery phase of the chromatography matrix. This type of separation is difficult using other techniques as charge is easily manipulated by the pH of buffer used.

Two types of ion exchange separation are possible - cation exchange and anion exchange. In anion exchange the stationary phase is positively charged whilst in cation exchange it is negatively charged. Ion exchange chromatography is used in the separation of charged biomolecules. The crude sample containing charged molecules is used as the liquid phase. When it passes through the chromatographic column, molecules bind to oppositely charged sites in the stationary phase, as shown in Figure 2.8.

The molecules are separated on the basis of their charge are eluted using a solution of varying ionic strength. By passing such a solution through the column, highly selective separation of molecules

according to their different charges takes place (Sheehan & FitzGerald, 1996, Cummins et al., 2017; Acikara, 2013).
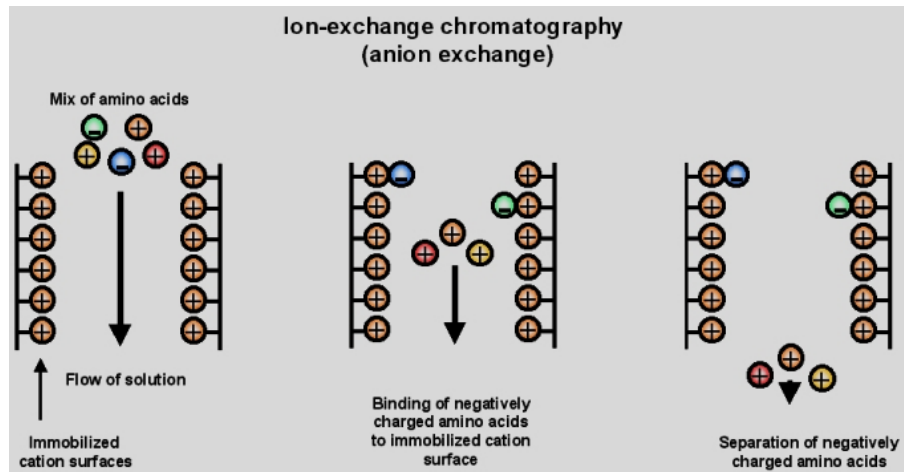
Figure 2.8: Schematic diagram of Ion-Exchange Chromatography
(SOURCE: Knudsen et al., 2001)

2.2.2.4 Non-ionic resin technique

Non-ionic resin focuses on providing an alternative to using liquid organic solvents by employing a porous resin that has a functional group similar to that of the liquid solvent (Zhang et al., 2020).
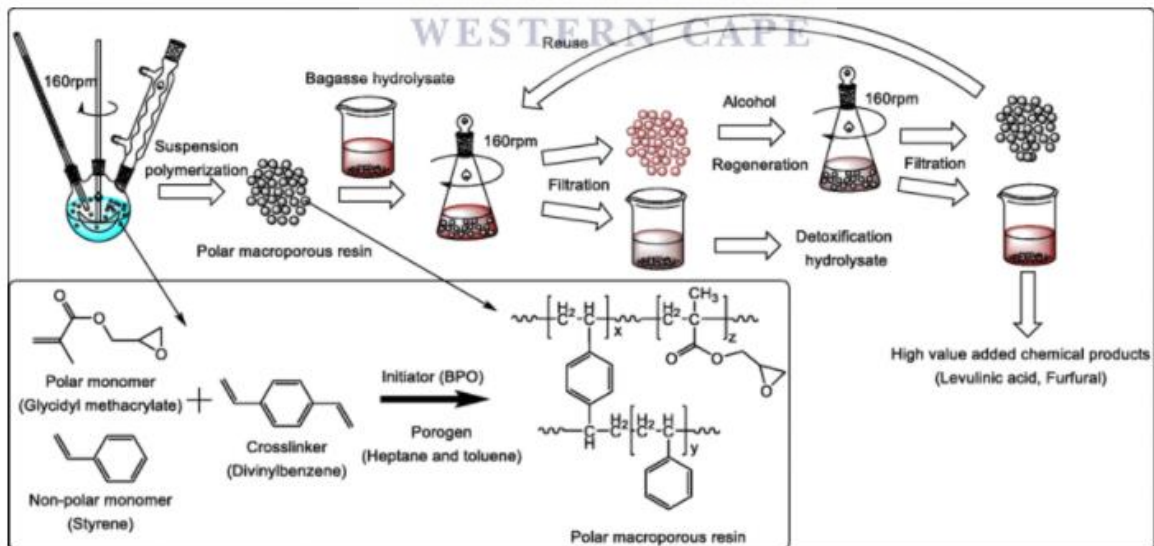
Figure 2.9: The synthesis of polar macroporous resin and adsorption process
(SOURCE: Zhang et al., 2020)

Although all these methods could achieve separation, the task and indeed the challenge is to pursue a comprehensive understanding of these separation techniques, which would typically encompass understanding all aspects of separation technology to all aspects involving ^{68}Ge generators. According to Chen and colleagues (2016), column chromatography and solvent extraction separations can be time-consuming, labour intensive and environmentally polluting. On the other hand, the ion exchange resins and macroporous resins possess some advantages including high adsorption capacity, easy elution, low operation expense, less solvent consumption and easy regeneration (Chen et al., 2016).

However, it is important to have a choice that takes the future into a more beneficial direction, thereby creating a path by which separation of ^{68}Ge from ^{68}Ga unfolds to its full potential. Of the discussed separation methods, the ion exchange chromatography appeared as the most likely candidate. Not only is there enough evidence to show that this separation technique has the capacity to benefit the study, but also there is evidence that the technique is relevant to the separation goals and can serve as the basis for testing the surface modification theory in practice.

2.2.3 ^{68}Ga^{3+} Chemistry

Focusing on the nature of gallium chemistry itself, Berry and colleagues (2011) described coordination chemistry as the main tool driving the ongoing developments of the ^{68}Ge/^{68}Ga generators. He pointed out how the growth of ^{68}Ga coordination chemistry allowed developments of chelators resistant to in vivo transchelation of ^{68}Ga^{+3}. The author highlighted the fact that these developments, i.e. bifunctional chelators that present a functionality that is able to covalently couple to a target vector besides binding to the metal cation, would ultimately manifest in what is today known as gallium labelling. Based on the periodic table and the classification groups (third element of Group 13 of the Periodic Table), as explained by Mäecke and Andre' (2007), Ga, when in aqueous solution, assumes the +3 oxidation state. More importantly, the coordination chemistry of Ga^{3+} is quite similar to that of the high spin Fe^{3+} ion. Not only have the two elements to contend with the same charge, but also with the same major coordination number of six and almost similar ionic radii (62 pm for Ga^{3+}and 65 pm for Fe^{3+}). On the contrary, Ga^{3+}ions are stable only under acidic conditions; while within a pH range of 3-7, hydrolysis of insoluble tri-hydroxide occurs if its

concentration exceeds nanomolar level. This was confirmed by Waterstram-Rich and Gilmore (2016), who stated that at physiological pH the solubility of gallium is high due to the almost exclusive formation of $[Ga(OH)_4]^-$ ions.

Maecke and Andre' et al., (2007); and Green et al., (1993), including many other researchers (Cusnir et al., 2017; Kilian 2014; Baum and Rösch, 2013) all agree that Ga^{3+} ions are classified as hard Lewis acids, forming thermodynamically stable complexes with ligands that are hard Lewis bases. For researchers this debate has remained topical, because ligands with oxygen and/or nitrogen donor atoms (such as carboxylate, phosphonate, phenolate, hydroxamate and amine groups) constitute good chelating agents for Ga^{3+}. Considering these chelating agents, several suitable chelators have been proposed, developed and coupled to biomolecules for gallium labelling (Asti et al., 2014; Berry et al., 2011; Notni et al., 2010). ^{68}Ga-labeled 1,4,7,10-tetraazacyclododecane-tetraacetic acid (DOTA)-peptides, most widely used as a class of ^{68}Ga radiotracers for PET, 1,4,7-triazacyclononane-triacetic acid (NOTA) and triazacyclononane-phosphinate (TRAP) chelators are but a few examples to mention, as shown in Figure 2.10.

(a)   *(b)*
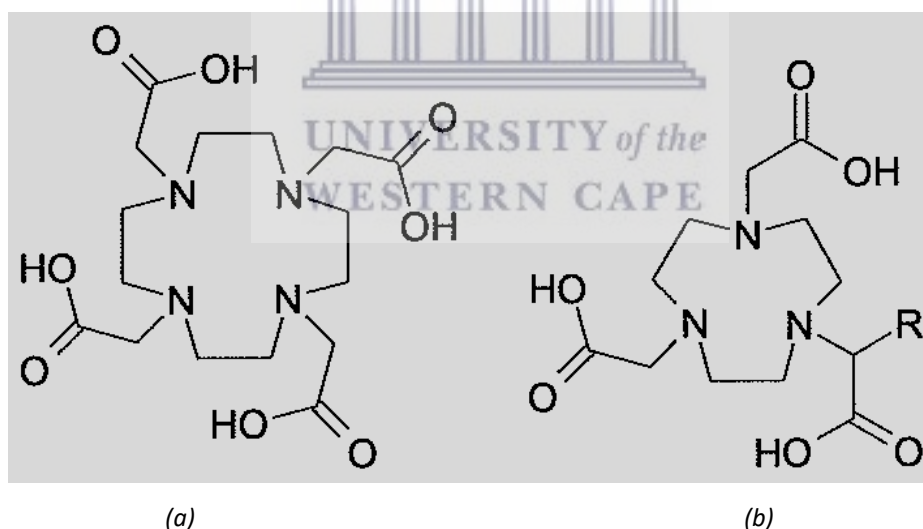
Figure 2.10:   Structure of (a) 1,4,7,10-tetraazacyclododecane-1,4,7,10-tetraacetic acid (DOTA)
and (b) 1,4,7-triazacyclononane-triacetic acid (NOTA)
(SOURCE: Viola-Villegas and Doyle., 2009)

Chelators usually have to be introduced into precursor molecules by bio conjugation, wherein they readily determine the labelling chemistry. For more details on surface chelators, literature surveys

by Liu and Edwards (2001) and Zhernosekov et al., (2007) may be consulted. In order to avoid commercial failure, a Ga^{3+} chelate has to be thermodynamically stable towards hydrolysis at physiological pH or to be kinetically stable during the period of clinical use. Also the presence of other metal ions in the Ga eluate should be avoided at all cost, since these can compete with the Ga chelators and in the process reduce the labelling yield.

2.2.4 Reaction Rate

Many different types of ^{68}Ge production routes are in use in different places. This multitude evolved over a long time and many of these research ideas fulfill a certain need. Similarly, here too, a long tradition exists for creating and designing bombardment station context, ranging from irradiation parameters to manufacturing processes. For deriving design implications for irradiation parameters, understanding practices and the rationale behind these is very valuable. In particular, there is a vested interest in the choice of irradiation parameters and potential radionuclidic impurities. An overview of the irradiation parameters can be found in Appendix D.

In general, Gallium (Ga) occurs in nature as a stable gallium-69. In order to produce Germanium 68, a prolonged beam is required on a Ga target for irradiation at a beam current >200 µA. Research has shown that any beam current greater than this value leads to target rupture and a loss of beam time. Protons with energies of approximately 40 MeV irradiate gallium metal and produces germanium-68 by proton capture and double neutron knockout, from the gallium 69. This reaction is: ^{69}Ga(p,2n)^{68}Ge.
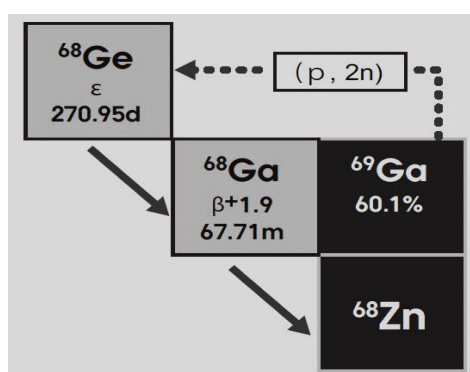
Figure 2.11:   Schematic diagram of a decay mechanism of ^{68}Ge to ^{68}Ga
and finally to a stable Zn isotope
(SOURCE: Velikyan, 2015)

A simplified scheme for the decay of ^{68}Ge and its ^{68}Ga daughter is shown in Figure 2.11.The unstable ^{68}Ge radioisotope produced, in turn, decays by pure electron capture (EC) to the ground state of ^{68}Ga with a half-life of 270.95 days. Gallium-68 in turn decays with a half-life of 67.71 minutes by a combination of EC and positron emission to the ground state of ^{68}Zn, and interestingly with a branch to an excited state at 1077 keV with a probability of about 3% and a number of higher excited states with a combined probability of under 0.4%. Depending on how much energy this electron has, it can travel shorter or longer distances. When it releases its energy, it can damage genetic material DNA of the cancer cell or form radicals that have further destructive effects on cancer cells.

2.2.5   TiO$_2$ as ^{68}Ge/^{68}Ga Generator adsorbents

The ^{68}Ga radioisotope contained within a generator system is a product of a decay process of a ^{68}Ge radioisotope (Figure 2.5). The quality of the ^{68}Ga is a function of its interaction with adsorbents such as SnO$_2$, TiO$_2$, Al$_2$O$_3$ etc. According to the literature, adsorption and desorption are the main drivers of the generator system (Mirzadeh & Lambrecht, 1996; Roesh & Riss, 2010; Fani et al., 2008). There are a number of types of inorganic matrices used as ^{68}Ge/^{68}Ga generator adsorbents: Al$_2$O$_3$ or ZrO$_2$ (Chakravarty et al., 2010); TiO$_2$ (Loc'h et al., 1982); SnO$_2$, (Aardaneh & Van der Walt, 2006), Sb$_2$O$_5$ (Loc'h et al., 1982). These adsorbents differ from each other by their characteristics (Chakravarty et al., 2011). Literature reports that price competitiveness and better accessibility are key factors for adoption of an adsorbent. Besides this, other ways of making the adsorbent more attractive to the research community and industry comprise of developing useful properties that are compatible with the demands and technical specifications of the ^{68}Ge/^{68}Ga generator.

In recent years there has been considerable discussion about whether TiO$_2$ has the capability of producing ^{68}Ga^{+3} radionuclides which are suitable for medical applications. With this in mind, detailed studies of TiO$_2$ as an adsorbent have been performed (Loc'h et al., 1982; Razbash et al., 2005). Even with this information available, ^{68}Ga^{+3} radionuclide are still plagued by unwanted contamination. TiO$_2$ is known to regularly fail critical labelling and quality control parameters. It is in this context that there is a high potential for tapping into surface modification chemistry. In 1986, Cox and his colleagues wrote a book titled "Progress in Radiopharmacy", in which the authors give selection criteria of the separation systems, studying direct consequences for the separation

chemistry and selection of materials for the generator construction. This book specifically addressed the role of inorganic sorbents in chromatographic techniques and the reasons behind the limited choice of inorganic sorbents meeting the requirements. Nonetheless, the authors highlighted the fact that perhaps *"sometimes the solution can be found in so called modified sorbents, consisting of inorganic matrix, chemically or physically coated with the active sorbent or provided with chemically bonded organic chelating ligands"*.

Traditional elution steps, such as adjusting the eluent volumes, are insufficient for producing optimum efficiencies together with low metallic impurities. High levels of metal contaminants in the product can lead to severe health impacts (Meyer et al., 2005; Velikyan et al., 2004). Among other metal contaminants like the long lived ^{68}Ge radionuclide, iron and zinc are also found in the product as a result of decay processes (Zhernosekov et al., 2007). Bad adsorption properties contribute excessively to contamination levels in the final product. Estimations reveal that one in every five generators is bound to fail when in use, adding to the many concerns of production worldwide (Vaquero and Kinahan (2015); Riemann et al., 2008; Jung et al., 2016).

So, despite the benefits of a TiO$_2$ based ^{68}Ge/^{68}Ga generator, the search for reliable methods of modifying the TiO$_2$ metal oxide has intensified in recent years. From the literature, it is clear that what is studied till now is not enough, and stringent operational, toxicological and environmental concerns need to be addressed for a better understanding of the advantages being sought, namely high ^{68}Ga efficiencies and low ^{68}Ge breakthroughs.

Rösch and Baum (2011) presented an interpretation of ^{68}Ge/^{68}Ga generators for PET imaging as a state of the art clinical diagnosis for PET/CT, which again depended upon research learning and complete understanding of the way radiochemistry evolved through these so-called radiopharmaceuticals revolutions. For example, ^{68}Ga, a positron emitter, allowed dramatic improvements of tomographic detection systems and imaging of the human brain. Representing Bhabha Atomic Research Centre, Mumbai, Chakravarty et al., (2010) maintained however that the unavailability of a suitable sorbent material is hindering progress to generate scientific and technological knowledge of ^{68}Ga labelled radiopharmaceuticals. When Rösch and Baum (2011) observed that sweeping changes in developments towards the optimisation of ^{68}Ge/^{68}Ga generators over the past 50 years did not lead to fundamentally transformed chemical and

regulatory points of view, a lack of reliable adsorbent for the design for radiochemical systems was claimed as the most significant variable towards the explanation of this setback.

Inspired by Kozlova's ideas (Kozlova et al., 1970), it was early in 2012 when, through the University of the Western Cape (S. Buwa, 2015), work commenced where several examples of TiO_2 adsorbents illustrated how different particle sizes could be embedded into a working environment to help in solving the clinical relevance of the ^{68}Ga radiopharmaceuticals. From the results, a number of lessons were learned including important guidelines, and lastly recommendations. The most important contributions were:

- By characterization of the various TiO_2 sources with XRD and XRF, techniques, the study allowed identification of phase and particle size as well as level of purities that helped to fulfil the research goals. XRD allowed the researcher to choose the appropriate TiO_2 metal oxide phase.
- When SEM and TEM of the of the TiO_2 metal oxide were performed, information covering particle size, crystallinity and morphology was obtained.
- Consequently, insight into the finer details about the behaviour of the TiO_2 sources during [68]Ge loading, ^{68}Ga elution, breakthrough analysis and metal impurity analysis were deduced.
- Understanding of the factors affecting phase stability and phase transformation was important to design and controllably manipulate phase types and percentage purity for more efficient use.

It was also at that time that the idea to research titanium dioxide based on promising nanoscale developments was born. To help do so, Buwa (2014) proposed using the anatase with nano size particles as a model on which critical information would be gathered to give direction to the design process. The existing modalities are often not understood (at least not easily) at first glance, especially when it comes to modification of adsorbents. Many studies (Rösch & Riss, 2010; Rösch & Baum 2011; Velikyan et al., 2004) deliberately leave out key modification processes as a leverage to avoid any duplication for commercial purposes. In Russia (Obsnick), a similar model was produced with modification as the only leading clue to the adsorbent used for their model of the [68]Ge/^{68}Ga generator. These generators are eluted with 0.1N HCl and show initial ^{68}Ga elution yields

of about 80%, with ^{68}Ge breakthrough of about 1×10^{-3}%. Sadly, there is no mention of information about the surface modification performed. Examples of inorganic oxides with potential application in the preparation of $^{68}Ge/^{68}Ga$ generator systems are SnO_2, ZrO_2, TiO_2, $Al(OH)_3$ and $Fe(OH)_3$, Fe_2O_3 and CeO_2 (Romero and Morcillo, 2017). All systems support the concept of surface modification based on information about that particular inorganic oxide.

The strength of the surface modification model can be seen that: (1) it supports a number of commonly accepted quality control measures, and (2) findings such as stabilisation or functionalisation of nanoparticles are based on a comprehensive literature review. As a result, the central research question of this study is:

Is it possible to modify adsorption properties of the TiO_2 to such an extent that the TiO_2 could be used to enhance the capacity of a $^{68}Ge/^{68}Ga$ generator?

2.3   The Benefits of Surface Modification

After decades of development in the laboratories, PET radionuclides produced by generator systems technologies are finally in a position to reshape the imaging industry. With column support material at the centre of the selective separation of parent and daughter radionuclides, it is believed that surface modification will be the production model that drives optimisation of $^{68}Ge/^{68}Ga$ generators. The goal of surface modification is to stabilise nanoparticles against agglomeration, render nanoparticle compatible with another phase, and lastly functionalise nanoparticles with the use of organic groups. Surface modification of metal oxides nanoparticles by means of organic compounds (silane coupling agents, alkoxy derivatives or metalloid chloro) make it a powerful tool for achieving these goals. In the end, these properties have the potential to change production of radionuclides in three main ways: improve low sorption capacity, improve limited selectivity, and improve poor radiation and chemical stability on prolonged use.

Since the adsorption occurs on the surface of the metal oxide, modification of the surface can be altered while keeping the intrinsic properties of the material (Yates (Jr) and Campbell, 2011; Somorjai and Li, 2011). Such surface modifications can be evaluated with surface characterisation techniques. Metal oxide surfaces are terminated by hydroxyl groups under atmospheric conditions,

enabling the attachment of molecules via condensation reactions. While this is not an exhaustive exploration of this complex topic, the issues described by researchers will assist in terms of understanding the variety of problems one may anticipate and identify which ones are of greatest importance emerging from the range of approaches highlighted in the literature.

Shen and colleagues (2008) says the surface modification can be used to prevent aggregation, improve stability, and enhance the compatibility of nanoparticles with solid matrices or biological environments. A critical look at the strategy for modification or functionalisation of nanoparticles depends on the specific atomic structures of the surfaces and their interactions with ligands. Nanoparticles with capped groups on their surfaces can be modified with organic or inorganic molecules, regardless of whether they are synthesised in aqueous or non-hydrolytic solutions. The hydroxyl reacts with carboxyl groups via its oxygen atom or with various silane groups through -O-Si bond (Shen et al., 2008).

The essential functions of the metal oxide in the $^{68}Ge/^{68}Ga$ generator system are three fold (Decristoforo, 2012). Firstly, it is responsible for the establishment of chemical, radiochemical and radionuclidic purity of the eluate. Secondly, in keeping with the code relating to medicinal products for human use, it is necessary to ensure the sterility of the ^{68}Ga product over a prolonged period of time (a year or even longer). Thirdly, full responsibility for the quality of the final radiopharmaceutical is required, by entailing minimal risk of toxicity or side effects. Under the operating conditions in the $^{68}Ge/^{68}Ga$ generator system, impurities such as ^{68}Ge, Fe and Zn do find their way into the final product, and the accidental breakthrough of ^{68}Ge (the parent radionuclide) in much higher amounts can never be ruled out with certainty. While the adoption of the various metal oxides is increasing, a lack of information on the metal oxide surface properties is often a big factor leading to minimal use of metal oxides as carriers of radiotracers. This aspect makes the adoption of these metal oxides less attractive.

Advances have been made on the topic of metal oxide technology during the past three decades (Chakravarty et al., 2010; Niculae and Niculae, 2015; Barahona et al., 2018; Velikyan, 2015), through various column matrices, elution yields, and strength of hydrochloric acid used in the eluent, assisted by research, to provide a better understanding of the physical and chemical workings of the metal oxide. The fields of research have included factors affecting the spread of peptide-based

radiopharmaceuticals in clinical implementation for PET imaging, particularly in Europe. Yet despite these advances, metal oxides remain unappealing as generator adsorbent due to challenges such as low ^{68}Ga yield and high ^{68}Ge breakthrough. For this reason, a clear understanding of how ultrathin coatings could be used to change surface characteristics of nanoparticles is needed.

On the other hand, ^{68}Ge/^{68}Ga generators are expensive. Even though the European market has been affording generators, the price of generators remains high, especially for the South African market, due to production and distribution retail costs. When compared to other radionuclides the cost of a generator is 80 times higher than that of other radionuclide sources. Besides being costly, generators provide very poor elution yields after a short period of time, usually 2-3 months, which averages at 30% of the life span supposedly guaranteed by the supplier. This means users could save up to 3/4 on their total budget, if surface modification could overcome the barriers associated with the limited use. A summary of worldwide distribution of ^{68}Ge/^{68}Ga generators by iThemba LABS can be viewed on Appendix F.

2.4 Surface Modification Methods

In order to improve or change the dispersion of the nanoparticles, and the compatibility between the nanoparticles and other materials, physical or chemical methods are needed to alter the physical, chemical, mechanical properties, and the surface structure of nanoparticles (Shen et al., 2008; Selegard, 2013; Campbell and Sauer, 2013; Parkinson and Diebold, 2016). More specifically, research shows that in order to control the surface of nanoparticles and to apply nanoparticles in industry and biomedicine in particular, an in-depth understanding of the fundamental properties of the nanoparticles is needed. According to the principles of surface modification, the surface modification of nanoparticles can be divided into partial chemical modification, mechanical and chemical modification, external membrane modification (i.e. capsule), high-energy surface modification, and surface modification using precipitation, esterification, coupling and grafting reactions (Williams, 2011).

Surface modification in general is through physical adsorption, coating or grafting, and depends on the properties of the particle surface. The use of ultraviolet rays for the plasma surface modification

of particles is a form of physical modification. By the chemical reactions between the nanoparticle surface and modifier, the surface structure and state of nanoparticles are changed. Shen and colleagues (2008) writes that surface chemical modification of nanoparticles plays a very important role to reduce the agglomeration. Due to modifier adsorption or bonding on the particle surface, which reduces the surface force of hydroxyl groups, the hydrogen bonds between particles are eliminated to prevent the formation of oxygen bridge bonds when nanoparticles are drying, thereby preventing the occurrence of agglomeration (Shen et al., 2008). A total of six general approaches to surface modification of nanostructures are considered (Shen et al., 2008). In the following sections, each of these methods is briefly described.

Given the fundamental role of the surface modification in the treatment of nanoparticle surfaces and the understanding of a theory behind this technology, and the additional contribution this may make a concept of solid-phase chromatographic ^{68}Ge/^{68}Ga radionuclide, the core aspects of these contributions will be dealt with in more detail below.

2.4.1   Surface Modification based on Self-Assembled Monolayers (SAMs)

The surfaces of a support can be modified by its reaction with various organic compounds. In order to obtain strong adhesion to the support covalent bonds between the surface molecules and the organic species are highly desirable. Usually compounds which contain Si-Cl or SI-OR (R = methyl, ethyl) are used for such reactions. These groups react with surface silanol groups to form covalent bonds. The reaction proceeds at room temperature and the organic molecules assemble themselves to form a dense monolayer within a few hours. The drawbacks of this approach is that when a monodentate ligand is exchanged by an equally charged bi or tri-dentate ligand, the metal oxide surface has to rearrange to accommodate the additional ligand centres, a scenario that is not favourable, moreover there are few examples to compare. This is particularly so because ligand exchange at a metal oxide nanoparticle surface is only possible without rearrangement of the particle or particle surface, when the incoming and outgoing ligands have the same charges and occupy the same number of coordination sites (Neouze & Schubert, 2008).

Unlike post treatment approaches that involve physical deformation, self-assembly represents a method that is able to produce particles with complex structures (Chaki et al., 2001). Self-

assembled monolayers (SAMs) provide a unique and controllable system. According to Chaki and colleagues (2001), self-assembly methods can start with pre-synthesised uniform particles and then use templates as physical confinement to assemble a limited number of particles into the desired geometric structures.

In general, Self-Assembled Monolayers on surfaces find use in a number of applications such as wetting and micro/nanofabrication, use simple tail groups (-CH_3, -COOH, -OH) and rely on the structure and function of SAMS that are already well-characterised and accepted (Shen, 2009). Further, other applications such as inorganic/molecular electronics require SAMS that contain a diverse range of chemical structures; including organometallic complexes, aromatic hydrocarbons, biomolecules and ligands for proteins. The structures of these SAMS are more complex than those simple alkane thiolates and most of these SAMS have not been characterised rigorously.

Surface modification with self-assembled monolayers appeared to be straightforward for good stability and hydrophilicity, however, the method was found by Hasan and Pandey (2017) to under physical adsorption processes on the solid surface without specific interactions. Such a process usually results in a loss of functionality of the interface and ultimately to unwanted biofouling. Also, most importantly, organic SAMS are chemically unstable, and when exposed to air, oxidation within a day can be observed (Watson et al., 2015)

2.4.2   Surface Modification Based on Organic Reactions

An approach based on organic reactions came up within the discourse of sustainable surface modification, which promotes an integrated approach to problems such as electrostatic interactions, surface tension, capillary forces, hydrophobic interactions and bio-specific recognition (De Campos, et al., 2003). The organic reactions approach mainly focuses upon outer most layer surface modifications. Under this approach hydrolysis and polycondensation of -Si-$(C_xH_y)_3$ were identified as powerful options when creating new coating layers. The surface modification based on organic reactions has gained ground, and is increasingly being mainstreamed in surface modification of nanoparticles. Silanisation has also been identified as a type of surface modification method where the silanol group of silane coupling agents (SCAs) reacts with surface species. Evidence of new coating layers have been documented in the past and its relevance has been

discussed (Brzoska et al., 1994; Garcia-Gonzalez et al., 2009; Hashim et al., 2015 and Hayichelaeh et al., 2018).

As the covalent bonding of silane coupling agents (SCA) with surface species on the support can ensure strong linkage, silanisation can be used to create an ultra-thin or single molecular layer on the surfaces of nanoparticles. Thus SCAs are regularly used as primers to activate the surfaces of nanoparticles. (3-Aminopropyl) triethoxysilane (APS) and (3-mercaptopropyl) trimethoxysilane (3-MPTMS) are the primers most often used for this purpose (Ozcan et al., 2011; Rebholz-Zaribaf & Ozcan, 2016; Kimura et al., 2018). Poly ethylene glycol (PEG) (Kralevich & Koenig, 2012), amino (Kim et al., 2003), vinyl (Marini et al., 2008) and phenyl (Yoshino et al., 1995) are some of the popular functional groups at the other end of these SCA ligands.

2.4.3   Surface Modification Based on Polymerisation

Modification of particles by the adsorption of polymers or surfactants is a simple way to alter particle surface characteristics (Vengate & Mittal, 2015; Toth, 2002; Gao et al., 2006). A polymer layer on the particle surface can generate steric repulsion between the modified particles, and consequently, enhance stability. The adsorption of polymers on surfaces is, among others, affected by the adsorption energy and the polymer-solution interactions. In the case of polyelectrolytes, that is, charged polymers, adsorption in aqueous solutions is also affected by the polyelectrolyte charge, the surface charge density and the ionic strength (Delcorte et al., 1997). The adsorption of a polyelectrolyte onto an uncharged substrate is weak if no chemical affinity exists. On a substrate with a charge of the same sign, adsorption is negligible at low ionic strength, but increases with increasing salt concentration due to decreased repulsion between the polyelectrolyte segments and the surface.

Increased usage of polymers is due to the desirable physical and chemical bulk properties of polymers, such as high strength-to-weight ratio and moisture resistance. Unfortunately, these excellent bulk properties extend to surface regions, resulting in an inert, hydrophobic, very low energy surface. This leads to problems with adhesion for applications that require binding of two different polymer systems, or the binding of polymer and metal surfaces. It also creates wetting problems for paints, inks, and other surface coatings.

2.4.4   Surface Modification with Layer by Layers Assembly

The Layer by Layer (LbL) approach appeals to the research community because it is environmentally friendly, easy and versatile, i.e. no special or complicated instruments are needed. The basic layer by layer (LbL) can be performed using only a beaker and tweezers (Ariga et al., 2007). Another advantage to the approach is the variety of the applicable multilayer materials and templating substrates. A further advantage of LbL is that LbL-films often display close to identical properties after deposition of the first few layers, even if films are deposited on very different surfaces. The LbL technique can be applied to solvent accessible surfaces of almost any kind and shape, the more exotic ones being colloids, fruit, textile, paper or even biological cells (Decher, 2012).

A dissenting view came from Rotello (2004), who submitted that true layer by layer growth was not fully established when the work by Nalwa (2000) showed oppositely charged silica and alumina particles could be electrostatically self-assembled in multilayer structures. Since this argument by Rotello (2004), researchers have been very active in this field and have demonstrated layer by layer electrostatic self-assembly of cationic and anionic polyelectrolytes and multi-layer structures containing combinations of charged colloidal particles for DNA purposes. Many researchers, worldwide, used electrostatically driven layer by layer assembly to realise structures containing polyelectrolyte/inorganic nanoparticle sandwich structures with nanomagnetite, TiO_2/CdS, SiO_2, TiO_2 and CeO_2, Au or alternating layers of positively charged gold and negatively charged silver particles (Atta & Galal, 2018; Şahan et al., 2015; Kang et al., 2017)

From a research point of view, where the method is based on non-covalent interactions of oppositely charged species, the problem of leaching out during application still exists. On the other hand, while LbL technique generally works well due to the fact that the processing window is rather large, it is highly recommended to keep the deposition conditions as constant as possible in order to get highly reproducible results. According to Gero Decher (2012) there is a general agreement in the research community that when comparing data, one should not overlook that one must not only maintain the deposition conditions exactly, but the conditions under which the measurements were taken. In spite of its simplicity and appeal, and the progress made with its practical application, determination of the film thickness by x-ray reflectometry remains an unmet challenge until now to researchers. Not only have researchers to contend with these challenges per se, but

also with coating of very small particles. This scenario is confirmed by Keller and his colleagues (1994) who suggested the introduction of oppositely charged macromolecules in the same solution containing very small particles.

2.4.5   Surface Modification using Stöber Method

The Stöber method is mainly used for the surface modification of nanoparticles with silica coatings. Since its invention, it has been modified and improved for use on nanoparticles with different compositions, sizes, shapes and surface chemistry (Shen, et al., 2008; LizMarzan, et al., 1996). The Stöber method has several advantages. First, the synthesis can take place in solvents with a wide range of hydrophilicity or hydrophobicity. A primer can be introduced if necessary to activate the surfaces of nanoparticles synthesised in highly hydrophobic solvents. Second, the formation of silica shells not only prevents the nanoparticles from merging but can also generate functional surfaces for further modification. Silica coated nanoparticles are often dispersed readily in aqueous solutions. Third, a silica coating can improve the biocompatibility of nanoparticles due to its low toxicity (LizMarzan, et al., 1996). These researchers (LizMarzan, et al., 1996) reported that the silica coating of gold nanoparticles was achieved using the Stöber method. Silica precursors-(3-aminopropyl)-trimethoxysilane can easily react at the surface region of the nanoparticles in an aqueous phase. For nanoparticles synthesised from hydrophobic solvents, the Stöber method cannot always be applied directly and usually a primer is required to activate the surface (Shen, et al., 2008). Mostly these primers used for the Stöber method are silane-based agents such as (3-aminopropyl) trimethoxysilane (APTMS) or 3-mercaptopropyl trimethoxysilane (MPTMS), which can make the surfaces of nanoparticles hydrophilic. Metal (Shen, et al., 2008; LizMarzan, et al., 1996; Yin, et al., 2007), metal oxide (Shen, et al., 2008) and alloy nanostructures (Tsang, et al., 2008; Yu, et al., 2006) have been modified with silica shells using this method. The capping agents used for the synthesis of these nanoparticles can affect the efficiency of the surface modification. Commonly used capping agents in non-hydrolytic systems such as acryl amine, oleic acid and long carbon chain thiol groups need to be at least partly replaced before the proper deposition of silanol groups.

While the Stöber method is widely used in modifying spherical nanoparticles, achieving uniformity in coated layers for nanowires, nanocubes, nanorods, and nanobars is also feasible. There have been reports on the silica coating of quantum dots of CdSe/ZnS, nanobars and rods of $L_n(BDC)_{1.5}(H_2O)_2$, (where $L_n=Eu^{3+}$, Gd^{3+}, or Tb^{3+} and BDC=1,4-benzenedicarboxylate), and silver nano wires, using the Stöber method (Caruso, et al., 2001; Yin, et al., 2002; Rieter, et al., 2007; Lee, et al., 2006; Bakalova, et al., 2008). These silica layers can be as thin as a few nanometers, and still maintain their uniformity indicating an excellent level of control of deposition.

However, the synthesis methods have become increasingly complex with no clear benefits. The process's high sensitivity to the effects of temperature, pH and reactant concentrations have affected reproducibility, and consistent trends have not always been observed. Whilst there have been attempts to demonstrate how each of these variables affects the final particle properties, most papers use different concentrations and processing methods, making comparison difficult.

2.4.6 Surface Modification using Sol-Gel Methods

Wei et al., (2002) presented an interpretation of the sol-gel technique as a process for producing nanoparticles for the preparation and application of thin layers or coatings, based on either inorganic materials or inorganic-organic hybrids. In another book titled *Surface Modification of Textiles* (Wei, 2009), it is explained how the sol-gel technique allows one to tailor certain properties and combine different properties in a single coating step. The sol gel method has found its application in textile materials due to far-reaching possibilities for developing improved and new products, especially with regard to the growing market of textile technology. The principle of the sol gel process can be summarised by three main steps: hydrolysis, application and curing. The first step is the hydrolysis of the precursors, for example, tetraethoxy silane (TEOS). Sols are small colloidal nanoparticles in solution and can form interconnected networks of metal oxides, which are called gels, upon further polycondensation in the presence of acid or base catalysts (Brinker, 2013). The common inorganic oxides such as silica, zirconia and titania are frequently made from the precursors of alkoxides. The widely used silica precursors are short carbon chain alkoxylsilanes, particularly tetraethoxy silane (Chen, et al., 2008; Chen, et al., 2005; LizMarzan et al., 1996). Ammonia and sodium hydroxide (NaOH) are the typical base catalysts, while hydrochloric acid (HCl)

and nitric acid (HNO_3) can be used as acid catalysts for the hydrolysis and condensation of TEOS in water and alcohol mixtures.

$$Si(OC_2H_5)_4 + H_2O \xrightarrow{\quad NH_4OH \quad} Si(OH)_4 + C_2H_5OH \qquad (2.1)$$

$$Si(OC_2H_5)_4 + C_2H_5OH + H_2O \xrightarrow{\quad\quad\quad} [Si(OH)_4]_n \cdot xC_2H_5OH \cdot xH_2O \qquad (2.2)$$

$$[Si(OH)_4]_n \cdot xC_2H_5OH \cdot xH_2O \xrightarrow{\quad\quad\quad} SiO_2 + C_2H_5OH + H_2O \qquad (2.3)$$
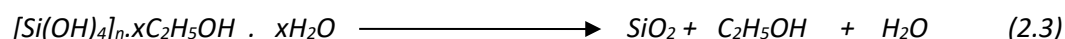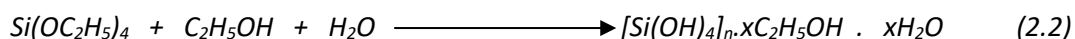
When TEOS is used as the precursor, hydrolysis leads to the formation of silanol and ethanol in the solvent mixture during the first step. These silanol groups cross link to form oligomers which further condense catalytically through –OH interactions on the surfaces of nanoparticles and form silica networks. The second and third steps are the polycondensations, during which reactions dense silica networks are formed. Other silane and halide precursors have also been studied for the formation of silica sol-gel for surface modification of nanoparticles. 3-aminopropyltrimethoxysilane (APTMS) and methacryloxypropyltri-methoxysilane (MPTMS) are among the most widely used precursors (Liu et al., 2005).

In an endeavour to sum up the debate of sol-gel techniques, Wei (2009) argued that an appropriate choice of precursor makes it possible to change the properties of the matrix/network itself, for example by introducing precursors such as organically modified silanes, either into the initial mixture (before hydrolysis) or to the readily prepared sols, which is a contention supported in earlier work by Que (2001). As a result, new materials are available on the market, for the advancement of this cause, and are known as inorganic – organic hybrid polymers.

The concept of the sol gel technique presents a wide range of possibilities for the modification of inorganic metal oxide materials as elaborated above. This concept allows, for example, a readily prepared nanosol to be mixed with an apparently unlimited number of compounds – polymers, pigments, drugs, fragrances, dyestuffs, or nanopowders, to name but a few.   To do so, however, the compounds must be: (1) miscible with the sol (2) be dissolved in the sol (3) may be dispersed in the sol. One disadvantage is that the compound must not initiate the gelation process, which would impair further processing of the sol. One of the main drawbacks of using the sol gel route is

the fact that it is more suitable for the synthesis of glassy or amorphous and crystalline materials than conventional methods. Also, it turns out that the method does not have universal experimental conditions for the synthesis of various types of metal oxide coatings.

2.5   Surfactants and Surface Modification

Farn (2008) defines surfactants as organic compounds with at least one lyophilic, loosely translated as solvent-loving, group and one lyophobic, loosely translated as solvent-fearing, group in the molecule. Two phenomena result from these opposing forces within the same molecules: adsorption and aggregation (Shen, 2009). For the purpose of this research, it follows that in aqueous media, surfactant molecules will migrate to water and solid interfaces and orientate in such a fashion as to minimise, as much as possible, the contact between their hydrophobic groups and water. This process is referred to as adsorption and results in a change in the properties at the interface. Conversely, the surfactant molecule is able to aggregate the contact angle between the hydrophobic group and the water by orientating the hydrophilic head groups towards the aqueous phase. As such, their selection for a specific use is not only governed by their intrinsic surface active properties but must also considered in terms of toxicological, environmental, regulatory and application-specific requirements which may dictate their suitability for purpose. Physical modification of nanomaterials is usually performed with the help of surfactants or macromolecules. The polar groups in the surfactants are selectively adsorbed on nanoparticles surfaces as a result of electrostatic interactions. The surfactants reduce the physical forces between the nanomaterials which decrease the inter particle interactions and control the agglomeration. Surface-adsorbed surfactants not only influence toxicity of nanoparticles, but also lower the accessibility of the nanoparticle surface (Farn, 2008).

A fine and precise control of the surface chemistry plays a key role in the choice of various surface modification methods. The choice of a surface modification method is very important in order to create nanoparticles for clinical application that are able to disperse in water and other hydrophilic media that are biocompatible and selective toward specific targets. According to Manuela Killian (Killian, 2013) silanes with reactive groups, i.e., chloro-, methoxy- and ethoxysilanes, are converted to hydroxysilanes when in contact with water. This indicates that the maximum coverage is limited by the amount of available adsorption sites, i.e., the density of -OH groups determines the

maximum amount of adsorbates. Barry Arkles (Arkles, 1977) writes that silanes with three alkoxy groups are the usual starting point for substrate modification. In his work, it is further explained that experimentally, in the conceptual framework and along the case study, the amount of silane required to obtain minimum uniform multilayer coverage on a substrate is given by the following equation:

$$\text{Amount of silane (g)} \; = \; \frac{\text{amount of substrate (g) x surface area of filler (m}^2\text{/g)}}{\text{Specific wetting surface}}$$

Specific Surface areas of common substrates are found on Appendix G.

Today, methoxy and ethoxysilanes are the most widely used organofunctional silanes for surface modification. It is reported by Barry Arkles (Arkles, 1977) that the reason relies on the fact that they are easily handled and the alcohol by-products are non-corrosive and volatile. With this in mind, one method, surface modifications based on organic reactions, was identified as worthy of exploring for this work. One major drawback of this method is the possibility of polymerization, which can occur if the reaction conditions are not carefully controlled. Literally one or two studies have examined factor that show close relation to the ^{68}Ge/^{68}Ga generators. Consequently, there is a large body of research on how to modify TiO_2 nanoparticles and at the same time highlight necessary factors to be considered when the nanoparticles are modified.

2.6   Molecular Imprinted Polymers

Molecular Imprinted Polymers can be shortly defined as a 'manual locking' technique for identifying 'molecular bonds (Jo et al., 2013). Based on this explanation, the concept implies that a template molecule interacts with a selected functional monomer to form main host-guest complex. Then, a certain amount of cross-linking agent and initiator is added together into the complex to obtain a macromolecule polymer. Upon removing the template molecule, a recognition cavity which is complementary with the template molecule in shape, size and chemical functionality is formed in the highly cross-linked polymer matrix, so that the obtained MIP has a higher recognition ability and can selectively separate the specific template molecule (Jo et al., 2013; Alexander et al., 2006). This definition is overly simplified and refers mainly to the historic aspect of the technique, but it is nevertheless descriptive enough.

The earliest version of the MIP was invented by the Russian researcher Polyakov in 1931, writes Alexander and colleagues (2006). From there on, the technique continued to be developed and improved by the research community. A lot of the articles on MIP studies (Jo et al., 2013; Yang et al., 2016; Mosbach and Ramstrom, 1996) build on the classical study by Polyakov (1931). One important milestone was the invention of separating antipodes of camphor sulfonic acid and mandelic acid using highly specific silica gel as chromatographic adsorbents by Curtis in 1951. The versatility of MIPs has led to a number of significant applications, for example, separation sciences and purification, chemical sensors, catalysis drug delivery, biological antibodies and receptors systems (Gui et al., 2018; Yáñez-Sedeño et al., 2017; Chen et al., 2011; Zhang et al., 2018; Bossi et al., 2001). Today MIPs can be used to obtain information on both biological and chemical molecules including amino acids and proteins, nucleotide derivatives, pollutants, drug and foods (Ng et al., 2017; Wu et al., 2016; Jian et al., 2017; Vicario et al., 2018; Goalker et al., 2017). Approaches often vary slightly in design depending on the different types of contexts but the principle remains the same.

Molecular imprinting technology (MIT) offers the opportunity to bestow TiO_2 based $^{68}Ge/^{68}Ga$ generators good selectivity because they may form composite tailor-made receptors which can selectively recognize and bind target molecules with high affinity. The major lesson to take from this is to consider how one may develop the composite and how this would affect the perception of the $^{68}Ge/^{68}Ga$ generators in the research community.

Based on the concepts explained so far, the MIP prototype was aimed at being applicable to the scenarios introduced in Section 1.2. This prototype will be functional, hence enabling the realization of the presented approach. At the same time, it is based on conceptual considerations that are assumed to be applicable for the $^{68}Ge/^{68}Ga$ generators as proposed by the approach in Figure 3.1. In the next section (Chapter 3), the study introduces the design architecture and implementation. The system, thus, must provide an insight that can result in efficient separation of the ^{68}Ge by the principle of the imprinting phenomenon. Vasapollo and colleagues (2011) defined MIP as a technique able to design artificial receptors with a predetermined selectivity and specificity for a given analyte. The adoption of MIP is aimed to have a great potential to promote separation of

complicated samples such as bio macromolecules and proteins (Vasapollo et al, 2011; Ertüka and Matiasson, 2016). What is exceedingly relevant to the successful adoption of MIP is the compatibility of the technique with researchers' functional preferences (Marty and Mauzac, 2005).

2.6.1. Components of MIPs

2.6.1.1. Template

In all molecular imprinting processes the template plays a fundamental role, the molecular structure determines the type of functional monomer to be used in the synthesis, since the chemical bonds between both substantiates the molecular recognition. The template should ideally be chemically inert under the polymerization conditions and stable under the synthesis conditions (e.g. temperature).

2.6.1.2. Functional Monomers

Functional monomers are substances responsible for binding sites on the imprinted polymer resulting from their interaction with the template. Generally, the type and concentration of the functional monomers used in non-covalent imprinting are chosen from experience or from published reviews. The choice of functional monomers will determine the structure of the recognition site and the concentration will influence the number of binding sites (Arshady, 2006).

2.6.1.3. Cross-linkers

According to Cormack and Elorza (2004), the cross-linker used to obtain a MIP has three main roles: (i) the cross-linker is important in controlling the morphology of the polymer matrix (gel-type, macroporous or a microgel), (ii) it serves to stabilize the imprinted binding site and (iii) it imparts mechanical stability to the polymer matrix. Generally high cross-link ratios are preferable from polymerization perspective, in order to access permanently porous (macroporous) materials and to be able to generate materials with adequate mechanical stability.

2.6.1.4. Solvent (Porogen)

The solvent is part of the medium where the polymerization is carried out. It serves to drive the formation of monomers and template complexes forward or in reverse depending on the strength and the form of interactions. Because of the creation of pores in macroporous polymers, it is common to refer to the solvent as the "porogen".

2.6.1.5. Initiator

Initiators have been extensively used in conventional free radical polymerization. The initiator generates the first radical through its decomposition by thermolysis or photolysis, and initiates the first molecule polymerization of cross-linking agent to the last molecule, getting the chain lock with all monomers and forming a polymer. Initiator such as 2,2'-Azobis(2-methylpropionitrile) (AIBN) can be decomposed by both temperature and by photolysis (Panagiotopoulou et al., 2015).

2.6.2. Preparative Approach of MIPs

Molecular Imprinting technologies have been the subject of research for many years (Mosbach and Ramstrom, 1996; Wang et al., 2003). Many research approaches have been studied, in terms of the synthesis and application of MIPs. There have been several studies of this kind that looked at the strengths and weaknesses of the MIP approaches in order to increase research interest in this area. Some of their findings, e.g., low cost, excellent stability and continuously advancing performance, support the perspective that these polymers promise to be the most useful materials for molecular recognition in different scientific fields.

Vasapollo and colleagues (2011) described how molecular imprinting processes interact between monomer and template during polymerisation. Molecular imprinted polymers are prepared by co-polymerisation of cross-linking monomer and complex which is pre-formed between template molecule and functional monomers using covalent, non-covalent or semi covalent interactions. When the template molecule is removed from the imprinted material after polymerisation, it leaves behind specific cavities that are complementary to the template in size, shape and chemical functionality. In the end this means the resultant polymer recognises and binds selectively only the template molecules. For example Figure 2.12 further clarifies this topic.
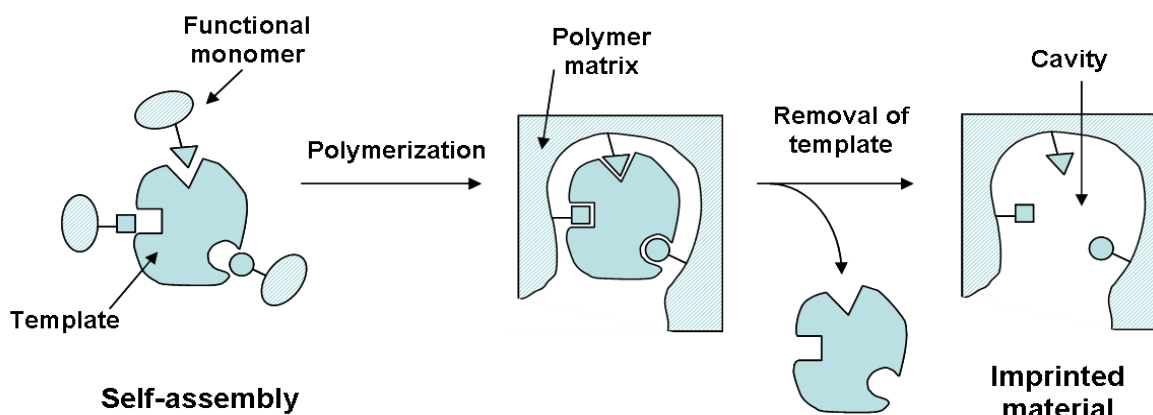
Figure 2.12: Schematic diagram of a basic principle of molecular imprinting polymers

(SOURCE: Sarafraz-Yadi and Razavi, 2015)

The findings in the literature show the great potential that MIPs possess together with the capability to achieve selective molecular recognition, depending on the application. No single approach may serve for all the current uses of MIPs. The literature offers a starting point for researchers to note when evaluating theoretical and experimental parameters for MIPs design; researchers should pay attention to interaction between template and polymer functionalities. The design should capitalise on the fact that the application of the molecular imprinting polymers will be in diverse fields (Vasapollo et al., 2011).

Apart from the nature of the interactions between the monomer and template during polymerisation, further spaces exist in the MIP that could be shared for selectivity and affinity for the ^{68}Ge target molecule used in the production of ^{68}Ga generator system. For example, in this context this research was particularly interested in: (1) higher physical robustness possessed by MIP's, (2) strength and resistance to elevated temperatures and pressures and (3) inertness towards acids, bases and organic solvents. The literature survey shows that molecular imprinted polymers are less expensive with long storage life at room temperature. A final and interesting finding was with regard to the selectivity results that showed good retention of a certain molecule over the other is due to its particular physicochemical properties rather than to the specific imprinted sites. With advances in generator technologies, it can be anticipated that there will be new ways for ^{68}Ge binding capacity by MIP's. In turn, this would create new opportunities for

suitable chromatography models for ^{68}Ge separation technique. This research will argue that the context will play a major role for efficiency and acceptance of MIP's into the generator systems.

The design housing molecular imprinted polymers (MIPs) needed to take into account several operating parameters in order to be successful in the wide spread production of the ^{68}Ge/^{68}Ga generators: foremost, the design must function at the required acid strength (0.1 M) in order to make significant amounts of ^{68}Ga radionuclide, while ^{68}Ge radionuclide is being retained optimally by the system. Secondly, the design must physically fit inside the 40 mm thick lead shielding enclosure used for operating and transporting the ^{68}Ge/^{68}Ga generators. Thirdly, the design needs to fit within the existing operating space in order to reduce radiation exposure to personnel.

2.7   Characterisation

To achieve a thorough analysis of the surface science of metal oxides and the potential that TiO$_2$ nanoparticles may provide, characterisation of various surface dimensions was useful to assess their synthesis and functionalisation. Several of the articles reviewed refer to characterisation in their research, recognising how a knowledge of well characterised metal oxide surfaces creates an understanding of the numerous applications where oxide surfaces play a role. The surface characterisation techniques used have varied with different authors, but the most recent studies were found to include the following techniques: X-ray diffraction, high resolution transmission electron microscopy, high resolution scanning electron microscopy, BET and FTIR to better understand the relationship between atomic surface structure and other physical and chemical properties (Kamiya et al., 2006; Ranjan, 2008; Radoman et al., 2015).

2.7.1   X-Ray photoelectron spectroscopy

X-ray photoelectron spectroscopy (XPS) is a standard tool for the investigation of surfaces. It is surface sensitive, provides information about the elemental composition and allows the determination of oxidation states and quantitative investigations. Samples are required to be stable under ultra-high vacuum (UHV) conditions and X-ray irradiation. They should be conductive as charging of the sample leads to spectral shifts. The detection limit of XPS for lab instrument typically is 0.1 – 1.0 at %. The fundamental principle of photoelectron spectroscopy (e.g., XPS and

ultra-violet photoelectron spectroscopy (UPS)) is the photoelectric effect. The sample is irradiated with photons of known energy hv, which leads to the emission of photoelectrons. These can escape into the vacuum if generated in the near surface region.

2.7.2   X-ray Diffraction Technique

The only comprehensive journal found on the topic about the TiO_2 at a crystallinity level is the one written by Ulrike Diebold (2002). Others, like Zhang and colleagues (2002) and Bagheri and colleagues (2013), have conducted research on TiO_2 X-ray diffraction analysis, which is covered in their articles. They defined X-ray diffraction analysis, through study of the crystal structure, as "identification of the crystalline phases present in a material and thereby revealing its chemical composition information".

Using XRD analysis for TiO_2 nanoparticles phase identification is a useful tool to assess structures, phases and crystal orientation (texture). XRD highlights some important features that TiO_2 nanoparticles can contribute to during the study such as grain size, crystallinity, strain and crystal defects, to help provide the study with information to help establish processes and procedures to implement.

2.7.3   High Resolution Transmission Electron Microscope Technique

Another tool that can prove useful during an investigation of nanoparticles for their sizes, grain size, size distribution and morphology, is the use of a High Resolution Transmission Electron Microscopy (Muneesawang and Sirisathitkul, 2015). HRTEM is often also a topic when assessment of dispersed nanoparticles are examined from the use of images of higher magnifications. TEM can prove to be powerful, with some research showing the importance of particle size, size distribution, shape and surface features (Williams, 2011). Williams (2011) defines HRTEM as an electron microscopy that works by bombarding a sample with a stream of electrons and monitoring either the resulting transmission (TEM) or scattering (SEM) effects. He further adds to this description that the electrons are detected and converted into magnified images of particles in the sample dispersion. This information is used by image analysis software to generate particle size data for
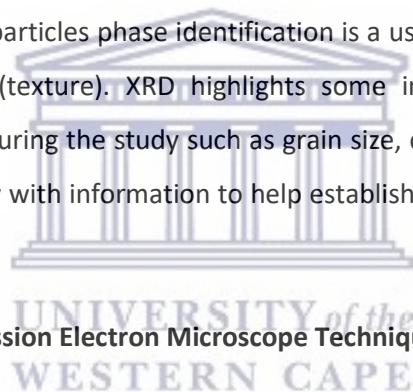
individual particles, as well as size distribution for the entire particle size distribution including shape and morphology.

2.7.4   High Resolution Scanning Electron Microscope Technique

Another element that adds importance to the investigation of physical properties of nanoparticles at nanoscale level is the use of High Resolution Scanning Electron Microscopy (Nanakoudis (2019). According to Nanakoudis (2019), obtaining images of particles is somewhat challenging and the use of automated statistical analysis to understand the outcome of the measurements is vital. Williams (2011), wrote that HRSEM produces 3D images of particles in the dispersion while HRTEM produces 2D images that require further interpretation. This view is supported by Ersen and colleagues (Ersen et al., 2015), who did a review on recent developments in the field of 3D imaging at the nanoscale using nanomaterials. In the field of investigation of physical properties of nanoparticles the use of HRSEM technique appear to be suitable as it enables one to view pores on the surface materials if there are any.

2.7.5   *Brunauer–Emmett–Teller* (*BET) and* Barrett-Joyner-Halenda (BJH) Pore Size and Volume Analysis

One of the methods considered to measure the surface area of the TiO_2 nanoparticles was the use of Brunauer–Emmett–Teller (*BET) and* Barrett-Joyner Halenda (BJH) Pore Size and Volume Analysis, defined as "the physical adsorption of gas molecules on solid surface and serve as the basis for the measurement of the specific surface area of materials" (Brame and Griggs, 2016). BET and BJH provide information on the physical structure as the area of a material's surface affects how that solid will interact with its environment. Anton Paar (Paar, 2018) also emphasises that surface area analysis is one of the mostly widely used methods in materials characterisation.

These analytical techniques are in line with the purposes of exploratory research described by Roesch and Riss (Roesch and Riss, 2010) as first to diagnose a situation (the literature review), then to screen alternatives (compared to the literature) with the purpose to discover new ideas (improvement areas) based on the previous findings.
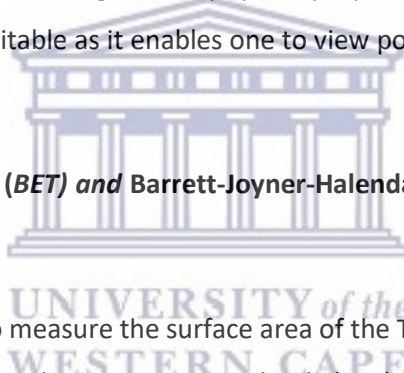
2.7.6   Thermogravimetric Analysis

Thermogravimetric analysis (TGA) is a thermal analysis that monitors the sample mass against time or temperature on a controlled environmental furnace. The sample can be analysed in an increasing or decreasing temperature at a constant rate or an isothermal temperature. Mueller and colleagues (2003) write that thermogravimetric analysis can provide information about chemical phenomena including chemisorption, desolvation and solid gas reactions. Furthermore, common applications of thermogravimetric analysis are (a) materials characterisation through analysis of characteristic decomposition patterns, (b) studies of degradation mechanism and reaction kinetics, (c) determination of organic content in a sample and (d) determination of inorganic content in a sample (Suyanya et al., 2018; Yodyingyong et al., 2011).

Thermogravimetric analysis (TGA) comprises the radiant heating chamber, a microbalance, a temperature controller, gas feeding system and a data acquisition system. The mass sample is measured on the microbalance, while it is heated or cooled in the furnace, according to the predetermined program. While TGA provides characteristic information about the composition kinetic analysis of thermal decomposition, it does not give a direct identification of the gases produced from the sample during heating. Instead the gases are transferred from the TGA instrument through a heated transfer-line to avoid the possibility of condensation. Additionally, TGA is a destructive analysis and a presence of volatile components in the sample often compromises the analysis.

2.7.7   Fourier Transform Infrared Spectrometry

Fourier Transform Infrared Spectroscopy (FTIR) is a technique that is used for the identification of organic, inorganic, and polymeric materials utilising infrared light for scanning the samples. For this reason FTIR is useful in identifying and characterising unknown materials, detecting contaminants in a material and identifying decomposition and oxidation. This is achieved by alterations in the characteristic pattern of absorption bands which implies a change in the material composition. Faix (1992) writes that FTIR can be used to collect high spectral resolution data over a wide range, usually between 5000 and 400 cm-1 for mid-IR region wavelength and between 10 000 and 4000 cm-1 for near-IR region IR wavelength (Faix, 1992; Smith, 2011).

A typical FTIR spectrometer includes a source, sample cell, detector, amplifier, A/D convertor and a computer. Radiation from the source reaches the detector after it passes through the interferometer. The signal is amplified and converted to a digital signal by the amplifier and the A/D convertor. Thereafter, the signal is transferred to the computer where the Fourier transform is carried out (Ami et al., 2014).

2.8   Experimental Approach

One very recent study (Sun et al., 2018), utilizes the knowledge from Lai et al. (2018) and compares it with Mosbach & Ramstrom approaches (Mosbach & Ramstrom, 1996) in an attempt to figure out how Molecular Imprinted Polymer accounts for successful selectivity towards the analyte. The suggested categories to include has varied with different authors (Niu et al., 2016; Gui et al., 2018; Yáñez-Sedeño et al., 2017; Dai et al., 2015), but the most recent study found on the topic includes the following categories: solid phase extraction, sensor construction, membranes, catalysts and drug delivery. As many other studies (Lei et al., 2016; Feinle et al., 2016; Daghrir et al., 2013; Gupta and Tripathi, 2011) reviewed during this thesis, seem to rarely include application in the preparation of $^{68}Ge/^{68}Ga$ generators systems and provided limited evidence of practical applicability. In this specific case, their research is also based on the review of others' research whereby one could expect the term to have been applied somewhat differently in the different research projects. Even though this is not the major topic of the research, it stands as a question of the comparability between the studies used in the project.

2.9   Summary

The literature review starts off with a short overview of the origin, properties and applications of the TiO_2. The literature review provided theoretical and practical tools in terms of generally accepted research doctrines of surface modification. Though a number of methods have already been reported for the production of solid phase chromatographic generators, the development of methods bridging several aspects such as design, performance, labelling chemistry and clinical applications etc. is still a challenge. The development of a generator that can fulfil all these requirements and which can be utilised for large scale production is a promising area of research. Building up on this knowledge was the investigation into the use of titanium dioxide (TiO_2) as an

adsorbent for $^{68}Ge/^{68}Ga$ generators, otherwise termed the positron cow. This is a theme that has been made popular by solid phase chromatographic generators for nuclear medicine technologies and the formation of associated radiotracers. With the ^{68}Ga generator research now having reached maturity, the focus of the literature review shifted to a new approach of optimising inorganic matrices, i.e. that of so called surface modification.

Bertho et al., (2009) mentioned several authors (Linsebigler et al., 1995; Makarova et al., 2000; Ulrike Diebold, 2002) who sowed the seeds for altering the properties of a TiO_2 surface. These researchers have been recognised for putting onto the agenda some of the ingredients of surface modification for the TiO_2 nanoparticles. Notwithstanding such recognition, the said theory still lacks key issues for a successful assimilation of the surface modification model. This is described as one of the reasons for the slow development of practical procedures for TiO_2 based surface modifications.

Harnessing of surface modification knowledge when dealing with fundamental problems of TiO_2 as an adsorbent was the focal point of the review, referring to the ability of the surface modification technique to resolve challenges such as the low efficiencies and high breakthroughs. The choice of titanium dioxide as a material for ^{68}Ge adsorbent was due to its anticorrosion, thermal, mechanical and antibacterial properties which are extremely important for research in areas of diagnostics and drug delivery. Surface modification of nanomaterials was important because of its potential influence on particle behaviour, including agglomeration and aggregation which may affect nanoparticle reactivity. In the review, many sources were used, including Science Direct Topics, Wikipedia, Sigma-Aldrich just to name a few, and many major journals, including Journal of Material Sciences and Chemistry etc., have been utilized for the literature exploration. As shown, a lot of the topics that were found to be relevant are under the Surface Modification of Silica Nanoparticles category. During the exploration of the literature, one of the main topics believed to be key was the fact that Silane Coupling Agents (SCA) involve an irreversible covalent cross-linking step. This process was found to be the most fitting description to the study. Other authors have in recent articles called for more research on surfaces of inorganic materials by functionalizing with polymer chains, either chemically (through covalent bonding) or physically (by physisorption). In the case of physisorption, a drawback of physisorbed polymer is that they are thermally and solvolytically

unstable due to the relatively weak van der Waals forces or hydrogen bonding that anchors them to the surface (Advincula et al., 2006). *"Rather than relying on the weak physisorption of a polymer onto a surface, much effort has been expended to attach the polymers covalently"* *(Rigoberto et al., 2006).*

The basic principles of TiO_2 as the $^{68}Ge/^{68}Ga$ generator adsorbent were discussed under section 2.2.1, whereby the material was studied for successful production of the ^{68}Ga radionuclide. Practically, the ^{68}Ge and ^{68}Ga radionuclide must be separated in the generator system to avoid the contamination of one (^{68}Ge) by the other (^{68}Ga) in the final product. A typical means of ensuring successful separation is the use of an ion exchange adsorbent, such as TiO_2, in which the separation of ^{68}Ga from the ^{68}Ge occurs by the decay and elution processes. Further details on the principle of the $^{68}Ge/^{68}Ga$ generator may be found in section 2.2.2 of this chapter.

The use of Positron Emission Tomography (PET) and Positron Emission Computed Tomography (PECT) is one possible approach to using radiotracers to alleviate tumour diseases. Currently, most positron emitting radiotracers are produced by generator systems and the benefit is that they can be transported to remote areas without cyclotron facilities. To assess the suitability of materials for possible capacity to produce the ^{68}Ga radionuclide in these generators, it is necessary that eluent volumes, low metallic impurities and environmental concerns, which may be summarised in scientific terms as: ^{68}Ga efficiencies and ^{68}Ge breakthroughs, be addressed. Against a background of increased search for reliable methods coupled by excess contamination levels in the current productions, the role that inorganic sorbents play is a significant global challenge. As a result, chromatographic techniques and the low number of inorganic adsorbents meeting requirements are under the spotlight. Surface modification of the titanium dioxide (TiO_2) nanoparticles to improve challenges associated with generator adsorbents is one possible approach to mitigate the challenges encountered when the generator systems are in operation. The potential benefit is the altered chemistry of the nanoparticle while keeping the inherent properties. Another potential advantage for using surface modification is the prevention of aggregation, improved stability and enhancement of compatibility to help the several situations highlighted in the literature.

In order to assess the detailed surface structures of the TiO$_2$ nanoparticles, surface characterisation techniques used to quantitatively analyse the information presented by the modification procedures were reviewed. These techniques have been shown to be particularly effective when studying surface compositions of nanoparticles, in addition to information that can be deduced regarding elemental composition and relative positions of atoms in a surface lattice. The advantage of characterisation of the surface chemistry of nanomaterials is that it is not only limited to the surface elementary composition, but also gives information on coating thickness, identification of additives, contaminants, defects, phase separation, crystalline state hydrophilicity, charge and topology/surface roughness may be obtained.

A key construct in this research was to measure the value of surface modification as a model for testing of the research hypothesis by meeting the requirements as set out by the organs of radiation chemistry. To do so, systematically selected surface modification methods had to be found in the literature related to this kind of research. Using surface chemistry, the methods were identified for creation, validation and testing of a ^{68}Ga generator for optimal productivity. According to Shen and colleagues (2008) at least six different models reflect a theory of surface modification, i.e. the (1) surface modification based on Self-Assembled Monolayers (SAMs) (2) surface modification based on Organic Reactions (3) Surface modification based on Polymerisation (4) surface modification with Layer by Layer (LbL) (5) surface modification using Stöber Method (6) surface modification using Sol-Gel method. Of these, the surface modification based on organic reactions appeared as the most likely option to help form a coherent and unified theoretical structure, and it is this model which will consequently serve as the primary theme of this dissertation.

The core indicators of a successful surface modification procedure are: to comply with clinical applications, comply with stability requirements and comply with compatibility of biological environments. To eliminate obstacles that may impede particle interactions from a successful modification procedure, it was important to pay attention to some of the setbacks experienced by researchers to some of the listed surface modification procedures.

Research conducted with the goal of understanding of surfaces of nanoparticle behaviour must take into account factors that control structural properties such as the capping agents through

either kinetic stabilisation or chemical bonding. The six different research methods proposed by Shen (2009) are all important, but they lead to various applications and may not necessarily be relevant to the approach required by this work. One aspect of studying the different surface modification methods was to investigate the drawbacks between the various procedures, which gave insight in the determining features of the choices presented by the literature.

Reviewing the literature, it became clear that despite the promising surface modification techniques, only one study could be found in the literature that has been able to merge the technique of surface modification context with that of the ^{68}Ge/^{68}Ga generator. An interesting approach was the functionalisation of TiO$_2$ nanoparticles by making use of concepts based on organic reactions. The silanisation method has potential for creating surface modification of TiO$_2$ and can be applied with comparatively low technical efforts and at moderate temperatures. Particularly, the use of organosilanes, as one of the most frequent ways of modifying surfaces of nanoparticles in order to achieve a coupling with the polymer matrix, can be applied to yield excellent durability results.

After decades of developments in the laboratories, molecular imprinting polymer technologies are finally in a position to reshape ^{68}Ge generator systems. Similar to developments on the adsorbents, it is believed that MIP's will be the separation model that drives ^{68}Ga radiopharmaceutical chemistry. As illustrated above, the goal of MIP's is to create artificial recognition sites in polymeric matrices which are complimentary to the template in their size, shape and spatial arrangement of the functional groups. The properties of MIP's (robustness, strength, resistance to elevated temperatures and pressures) make it a powerful tool for achieving these goals. These properties have the potential to change ^{68}Ge generator system in two main ways: radionuclidic impurities and non-radioactive metallic impurities.

In conclusion, titanium dioxide (TiO$_2$) remains a unique metal oxide with many desirable properties for ^{68}Ge/^{68}Ga generators. A review of the literature reveals that there are hundreds of studies that assist not only to the clinical acceptance but also to the realisation of the great potential of the ^{68}Ge/^{68}Ga generator for modern nuclear medicine. Despite the increasing interest in this area, little attention has been focused on: (i) determining the exact radiochemical separation design, which is essential for both chemical and regulatory point of views, and (ii) developing a valid and

comprehensive ^{68}Ga generator that is able to meet the range of clinical requirements that may be relevant across a variety of routine clinical uses.

This thesis aims to make two main contributions to the field of radionuclide production with a focus on TiO$_2$ adsorbents and ^{68}Ge/^{68}Ga generators: first, different modification treatments of the TiO$_2$ adsorbent will be used in order to construct desirable characteristics of high exchange capacity; second, in order to remove ^{68}Ge impurities from the ^{68}Ga radionuclide product, molecular imprinting polymers technique will be used, a method that is known for receiving much attention to alter surface properties so that it is appropriate for the envisaged application and use. The argument for the functionalisation of metal oxides by surface modification is a response to the need for a better understanding of today's radionuclide generator systems. As such this is supported by sentiments by Rösch and Baum (2011) who predicted that it may be a dream, or in another decade from now onwards, whereby ^{68}Ge/^{68}Ga generators may approach rank 3 or 4 of clinical impact after that of ^{99m}Tc and ^{18}F. Apart from the outcome of modifying TiO$_2$ nanoparticles, another outcome pursued here is to formulate propositions for further research and refinement of the surface modification method for the benefit of the research community.
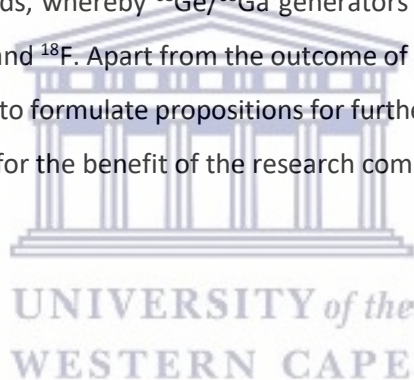
CHAPTER III

METHODOLOGY

3.1 Overview

The literature review revealed a broad set of study types and methods of $^{68}Ge/^{68}Ga$ generators been that have been used by researchers during their evaluations. This review was used to identify fundamental challenges of the $^{68}Ge/^{68}Ga$ generators. The challenges are strongly tied to different research disciplines, most importantly pharmaceutical, but also research and science. Consequently, there is the need to bridge a substantial knowledge gap between the disciplines involved. In an attempt to address this challenge, this study put considerable effort into assembling a titanium dioxide (TiO_2) based $^{68}Ge/^{68}Ga$ generator and following commonly accepted guidelines with regard to modification of nanoparticles and evaluation in the field from different angles. Evaluation of different stages was rigorously conducted and helped to identify shortcomings and to improve the developed prototypes.

3.1.1 Working Environment

The setting up of experimental work with radionuclides required a highly controlled environment in the production of ^{68}Ge, thus many experiments were conducted in a hotcell chamber. Other experiments required a lab environment in order to obtain valid data, for example the investigation of modified TiO_2 nanoparticles behaviour, elution of ^{68}Ga or synthesis of the Molecular Imprinted Polymers (MIPs). During the course of experiments, a broad set of materials, equipment, methods and analytical protocols were used for evaluation, including chemical stability of the column material, eluate sterility and pyrogenecity, **^{68}Ge** breakthrough and elution profile. The appropriate working environment for each aspect is described in the following sections. The schematic of the hotcell is presented in Figure 3.1.
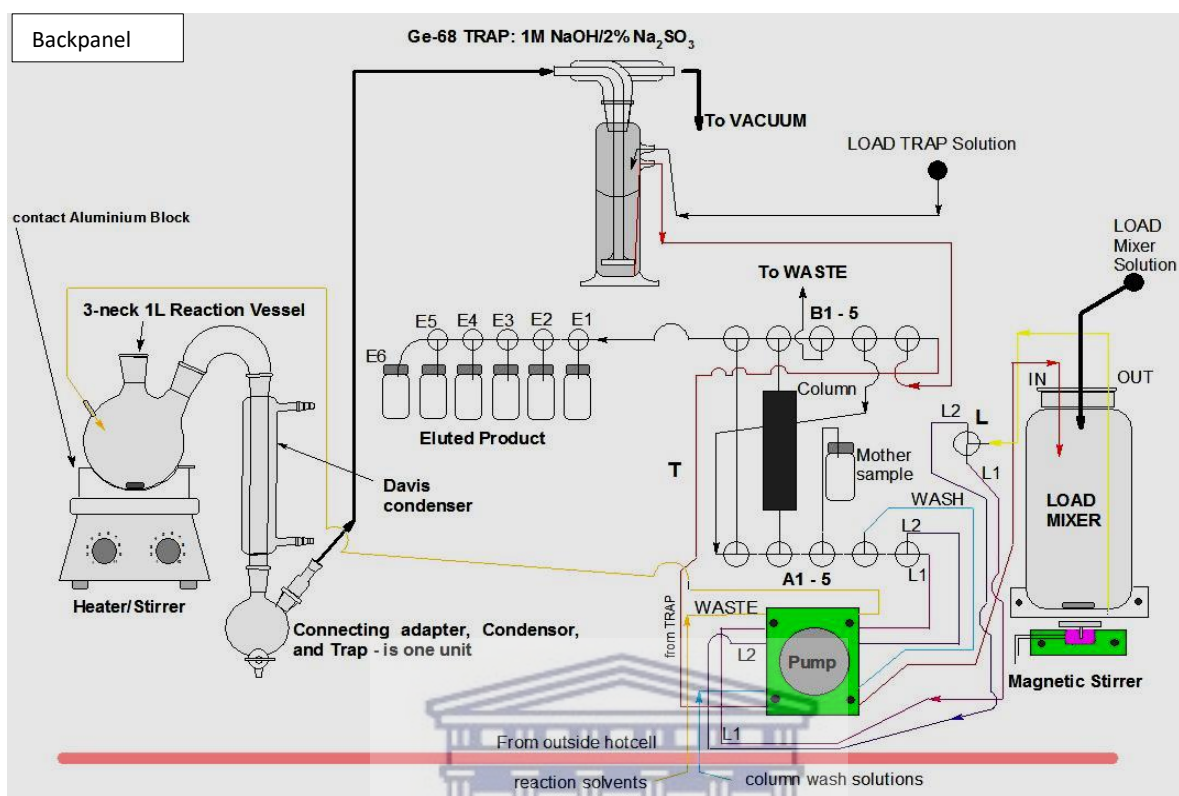
Figure 3.1:   Schematic diagram of the hot-cell used for the ^{68}Ge production
(SOURCE: iThemba LABS Radionuclide Department Archives)

Developing the ^{68}Ge/^{68}Ga generators rely upon creating a workable hotcell environment that goes beyond the mere adjustments such as door openings for production means. For example, the hotcell environment was designed and equipped to anticipate the fact that ^{68}Ge productions were performed every week for the period this study was conducted. This was achieved by designing two back panels that are easily removable each week a production was performed. The hotcell design was explored in two major steps. In the first step, the back panel (see Figure 3.1) was able to distribute control among key production areas. For example, the reaction vessel was designed such that heat was applied directly underneath, while a chemical reaction is taking place. This was achieved by placing the reaction vessel in contact with the heater, with aluminium foil only separating the two. On the other hand, vacuum was able to direct the resulting gas through the condenser to the trapping solution. Furthermore, methods were developed to direct the ^{68}Ge trapped solution to the hydrofluoric acid solution using tubes, peristaltic pump and stop taps. In order to achieve this, automated peristaltic pumps were used and tongs as manipulators for taps

and on and off switches when the production was complete. In the second step, legal agreements between safety health environmental officers and production staff regulated that hotcell during ^{68}Ge production were operated from the outside front area only using tongs as manipulators. Conducting ^{68}Ge production from the back of the hotcell chamber while the reaction is taking place contravenes safety protocols from the ionising radiation emitted from the ^{68}Ge. Heavy leaded filled doors are able to close off the hotcell chamber while at the same time providing safety to other researchers. The following flowchart depicts the research approach:
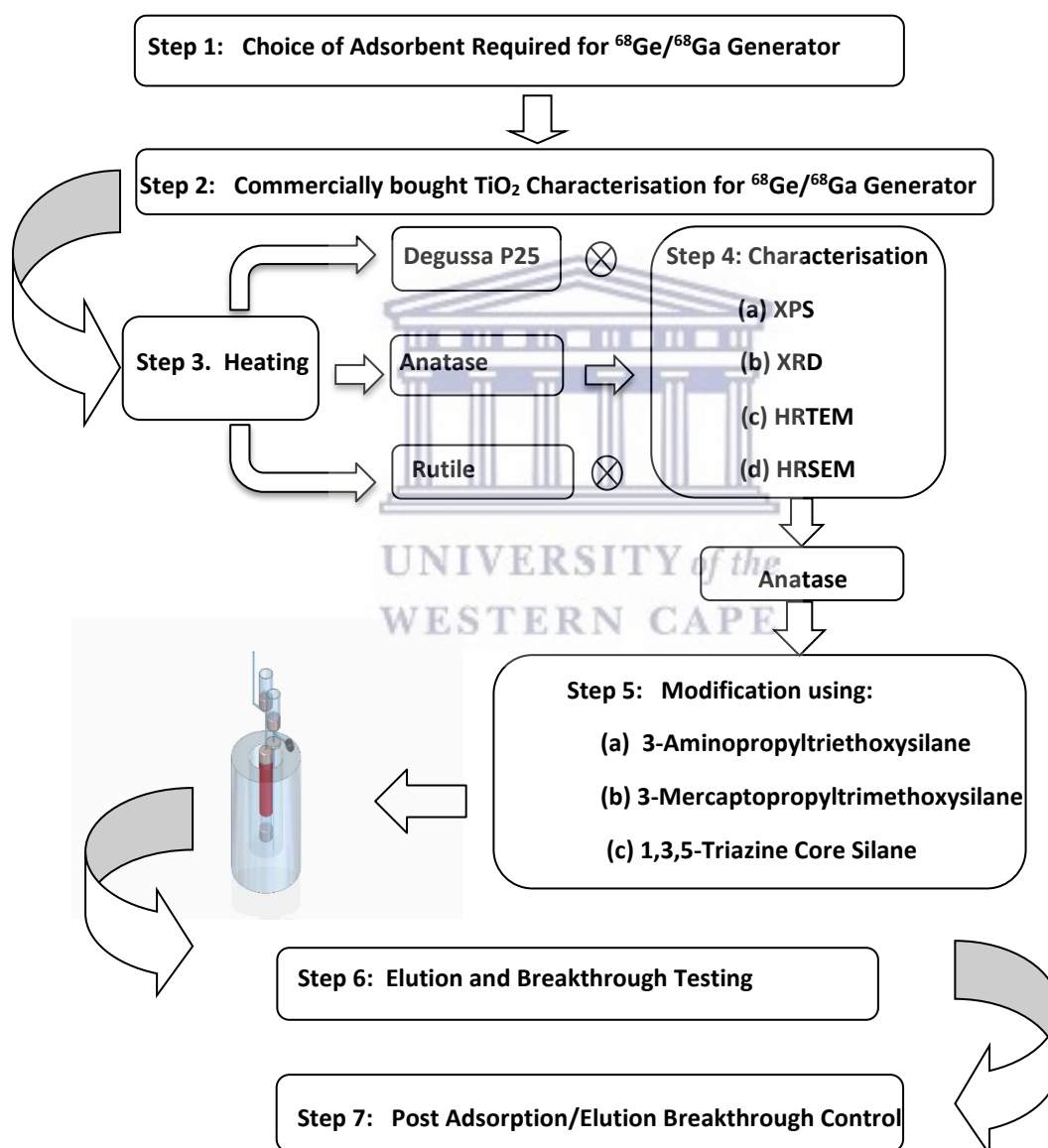
Figure 3.2: A schematic overview of the research approach

3.2 Materials, Chemicals and Equipment

3.2.1 Materials

The following table (Table 3.1) provides an overview of the materials used when the ^{68}Ge production was conducted:

Table 3.1: ^{68}Ge Production Materials

Materials	Brand	Catalogue Number	Supplier
Terumo luerlock syringe, 3 mL	Terumo	SS+03L	Ysterplaat Medical Supplies
Terumo luerlock syringe, 10 mL	Terumo	SS+10L	Ysterplaat Medical Supplies
Magnetic stirring bar, PTFE	Brand	Z328812	Sigma-Aldrich/Merck
Polyethylene frits, 20 μm porosity	N/A	57183	Sigma-Aldrich/Merck
Pyrogen free vials 10 mL, stoppered	N/A	62121S	International Vial Packaging and Sterilisation
Vygon Lector Cath tube, 50 cm	Vygon	1155.05	Vygon Value Life
Vygon Lector Cath tube, 100 cm	Vygon	1155.10	Vygon Value Life
Vygon Lector Cath tube, 150 cm	Vygon	1155.15	Vygon Value Life
Vygon 4-way lockable stopcock	B Braun	458001	Vygon Value Life
Silicone double segment tube, green/green	Watson Marlow	983.0205.000	Watson and Marlow
Micro cassettes	Watson Marlow	MNA 0286A	Watson and Marlow
Discofix manifold, 5 way	B Braun	513552	SSEM Thembu Medical
Crucible	Coors	Z247138	Sigma Aldrich
3-necked round bottom flask, 1000 mL	N/A	CLS49501L	Sigma Aldrich
Pipette, 200 μL	Eppendorf	4689927	Merck
Pipette, 1000 μL	Eppendorf	4728817	Merck
Pipette, 5000 μL	Eppendorf	3679567	Merck
GV 2.00 μm Filter, syringe driven	Millex	SLGV033RS	Merck
Plungers, 10 mL	Teflon	N/A	iThemba LABS
Plungers, 3 mL	Teflon	N/A	iThemba LABS

3.2.2 Chemicals

The Table below (Table 3.2) presents chemicals that were used in all the experiments conducted.

Table 3.2: Chemicals used when the $^{68}Ge/^{68}Ga$ Generator was prepared

Type of Chemical/Reagent	Formula	Molecular Weight (g/mol)	Catalogue Number	Supplier
1,1-Azobis(cyclohexanecarbonitrile), ACHN, 98%	$C_7H_{11}N$	244.34	380210	Sigma Aldrich
2-Chloro-4,6-dimethoxy-1,3,5- triazine (CDMT)	$C_3H_3N_3$	81.08	T46051	Sigma Aldrich
3-Aminopropyltriethoxysilane,3- APTES	$C_9H_{23}NO_3Si$	221.37	440140	Sigma-Aldrich
3-Mercaptopropyltrimethoxysilane, 3-MPTMS	$C_{16}O_3SSi$	196.34	175617	Sigma-Aldrich
Acetic Acid, pure, glacial	CH_3COOH	60.05	71251	Sigma Aldrich
Acetonitrile, 99,9%	CH_3CN	41.05	34998	Sigma-Aldrich
Aerolyst® Titanium Dioxide, anatase	TiO_2	79.87	48.7870.100	Evonik Indusries
Anion Exchange Resin, AG® MP-1M, 100-200 mesh, chloride form;	$CH_2N^+(CH_3)_3$	~2700 MW limit	1401241	BIORAD
Bis(3-Aminopropyl)amine (BAPA)	$NH_2CH_2CH_2CH_2)_2NH$	131.22	I1006	Sigma Aldrich
Chloroform, 99.4%	$CHCl_3$	119.38	32211	Sigma Aldrich
Degussa P25 Titanium Dioxide Nanopowder, rutile 85%/anatase15%	TiO_2	79.87	NS6130-03-351	Evonik Industies
Ethanol, absolute grade, 99,9%	EtOH	46.07	32205	Sigma-Aldrich
Hydrochloric Acid, suprapur, 30%	HCl	36.46	1.09060	Merck
Hydrofluoric Acid,40%	HF	20.04	30103	Merck
Methacrylic Acid, MAA, 99%	$C_4H_6O_2$	86.09	155721	Sigma Aldrich
Methanol, 99,9%	MeOH	32.04	34860	Sigma Aldrich
Nitric Acid, 65%	HNO_3	63.01	84380	Sigma Aldrich
Sodium Hydroxide, pearl	NaOH	40.00	221465	Sigma Aldrich
Sodium Sulfite, extra pure	Na_2SO_3	126.04	239321	Merck
Titanium Dioxide, rutile	TiO_2	79.87	44375	Alfa-Aesar
Triethylamine, 99,9%	$(C_2H_5)_3N$	101.19	90340	Sigma Aldrich

3.2.3 Equipment

In Table 3.3, the equipment used when the experiments were conducted is presented.

Table 3.3: The Table of Equipment used when the $^{68}Ge/^{68}Ga$ Generator System was Prepared

Equipment	Model	Company
Hot-cell, with panel of 1,2 x 0,9 m dimensions	n/a	iThemba LABS
Analytical Balance	MS204S /01	Mettler Toledo
Heater/Stirrer	HC502	Bibby Sterilin (Pty)
Vacuum Pump	n/a	iThemba LABS
Muffle Furnace	CWF	Carbolite
Target Holder Cutting Tool & Press	n/a	iThemba LABS
Deionised water dispenser	F7HA13136 A	Merck
Condenser System	n/a	iThemba LABS
Ionisation Chamber	CRC-15	Capintec, Inc.
Peristaltic Pump,	030.7022.0	Watson Marlow
Microcassettes Pumphead	308MC	Watson Marlow
Gamma Spectrometer	HPGe	Canberra
Microplate Reader	Multiskan Sky	Thermo Fischer Scientific
Accuspec Multichannel Analyser (Genie 2000)	2030 SCA	Canberra
Inductively Couple Plasma	Optima 3300XL	Perkin Elmer
Soxhlet Extractor, 50 mL	Z556165	Sigma Aldrich
Isomantle Electric Heater	45-5580	ELE (USA)

3.2.4 $^{68}Ge/^{68}Ga$ Generator Construction

The generator required a lead shielding of 40 mm thickness, as shown in Figure 3.3. A TiO_2 inorganic sorbent was housed in a 3 mL syringe and placed in the centre of the lead shielding, supported for vertical positioning using silver wool. Two polyethylene tubes were connected to the column, one at the top and the other at the bottom. These tubes were fitted into two empty vials, while one vial was fitted with a 2 µm filter for final purification of the eluate before collection. The other vial was used for the 0.1 M HCl eluent delivery to the column. In order to control and analyse the ^{68}Ge

breakthrough, a molecular Imprinted polymer trap was fitted on the bottom section of the column. For this practical reason, the decision was to design the fitment the same size as the area of the column first and leave the improvements for future work.
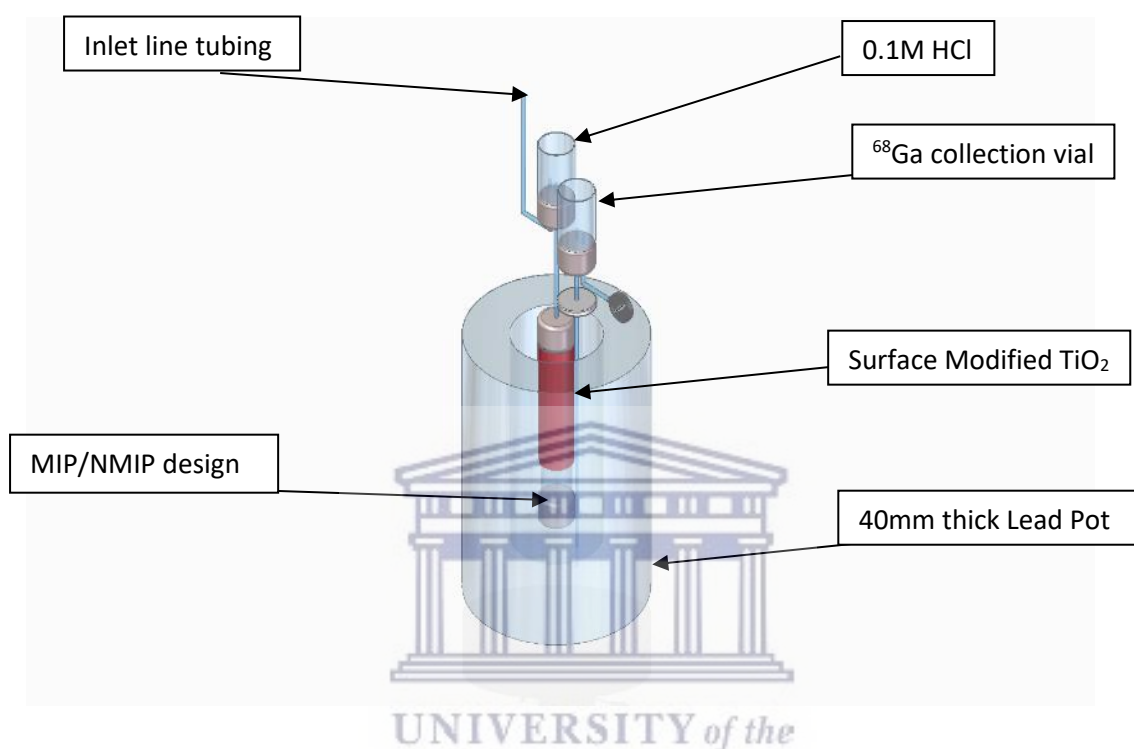
Figure 3.3:   A schematic diagram of the $^{68}Ge/^{68}Ga$ Generator system

3.2.5 Production of $^{68}Ge/^{68}Ga$ Generator

The iThemba LABS Separated Sector Cyclotron beam time has a dedicated beam time slot allocated to the radioisotope productions. The facility has two vaults consisting of a high current bombardment station (up to 250 µA) in vault 1 and a medium current bombardment station (up to 80 µA) in vault 2, two rows of hot cells (each row containing 7 hot cell chambers), quality control and microLAB laboratories. The production plan is achieved by a modern beam delivery system capable of providing protons with a precise control over the beam properties. In general, the metal niobium (Nb) gets used as the encapsulating material of the Ga metal target. In this case, The Nb capsule, which has a diameter of 40 mm and wall thickness of 0.5 mm, typically contained 20 ± 0.3 g of Ga metal inside the capsule. The advantage of this method is that niobium has a high

resistance to chemical attack by molten gallium, making water-cooling of the target much more possible. The excitation function for the ^{nat}Ga(p, x)^{68}Ge general process estimates a maximum of 330 MBq at 20 MeV[2].

Irradiation parameters perform a vital function in the production of the ^{68}Ge yield by conveying information about physical integrity of the target, which benefits both cyclotron operators and production staff. Duration and integrated current of the irradiation are dictated by the ^{68}Ge yield required. For production purposes, the aim is 800-1000 mCi ^{68}Ge per month. A summary of the irradiation parameters can be seen in Table 3.4.

Table 3.4: A summary of the Ga(Nb) Metal Target Irradiation Parameters

Parameter	Units
Target	Ga metal in a niobium capsule
Beam Current	190-200 µA
Duration of irradiation	50-100 hours
Integrated Current	10-20K µA/h
Proton Beam Energy	34 MeV (entrance energy)

The next step is the separation of germanium radionuclides from the gallium target by selective volatilisation as GeCl$_4$. In order to allow the ^{69}Ge to decay away, the Ga metal was allowed to cool down for four weeks. Based on the order of irradiation, Ga targets were stored in their respective target holders in a shielded area to allow decaying of the ^{69}Ge. In this context, usually there is <0.1% ^{69}Ge left after four weeks of decay. To access the Ga metal after irradiation, the Nb back encapsulation is cut off using a remotely controlled cutting press equipment. Removal of the Ga (m. p. 29.8 °C) is accomplished by liquefying it in boiled water and resolidifying it in cold water to provide a solid gallium target for chemical processing. In order to remove the co-produced ^{69}Ge ($T_{1/2}$ = 39.05 h) impurity, separation of the germanium radionuclide as GeCl$_4$ from the gallium target was performed using a selective volatilisation method as set out in section 3.2.5.1. In addition, this step immediately eliminated any Nb present as impurities. Gallium on the other hand together with ^{65}Zn ($T_{1/2}$ = 244.5 d) remains in the HCl dissolution medium. In the end the production process leads to volatisation and an overview is found under section 3.2.5.1.

3.2.5.1 Volatisation of Impurities

In this section, a unique, selective, volatilisation separation method of [68]Ge from the gallium metal was developed. In the reaction flask (1000 mL), connected to a mechanical stirrer, a tubing inlet, a contact thermometer and a condenser for vacuum distillation, 20 g of the metal target was placed into a 100 mL solution of 30% suprapur HCl. The flask was gently heated to 60 °C and the reaction was controlled by addition of nitric acid (65%) in small volumes (5 mL). [68]Ge in the target was volatilised as GeCl$_4$ into a NaOH trap solution. Germanium (IV) chloride reacts with sodium hydroxide to produce germanium (IV) oxide, sodium chloride and water as follows:

$$GeCl_4 \quad + \quad 4NaOH \quad \xrightarrow{\hspace{1cm}} \quad GeO_2 \quad + \quad 4NaCl \quad + \quad 2H_2O \quad …………………3.1$$
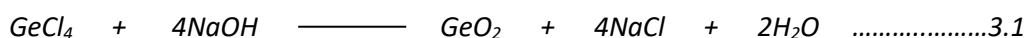
The course of the reaction was controlled by the amount of the formed GeO$_2$. At the end of the dissolution of the Ga metal target, the NaOH solution was transferred into another container (1000 mL), already containing 800 mL 0.2 M HF solution and equipped with a stirrer option. Germanium (IV) oxide reacts with hydrogen fluoride to produce germanium (IV) fluoride and water as follows:

$$GeO_2 \quad + \quad 4HF \quad \xrightarrow{\hspace{1cm}} \quad GeF_4 \quad + \quad 2H_2O \quad ……………………………3.2$$

The 1000 mL GeF$_4$ reaction mixture of 0.2 M HF and NaOH (9:1, v/v) was stirred with a magnetic stirrer at room temperature for 30 mins. Next, the BioRad AG MP 1M anion exchange resin was rinsed several times until the solution remained colourless. A slurry that was made up of the resin and water was prepared, then transferred into a 10 mL graduated Terumo syringe casing, closed off on one end with a sinter filtering mechanism cut to size. When the column was filled to the 10 mL mark, another sinter was used to keep the resin in position and a plunger was inserted to secure the column setup. Next, the GeF$_4$ solution was loaded onto the column, previously activated by passing 100 mL of a 0.2 M HF solution through the column. Thereafter, the column was washed with 50 mL 0.05 M HF followed by 20 mL 0.1 M CH$_3$COOH. After that, the [68]Ge was eluted with 0.1 M Suprapur HCl.

Based on the concepts explained so far, the following is a diagram (Figure 3.4) which aims to provide an explanation to the scenarios introduced in Section 3.2.5.1.
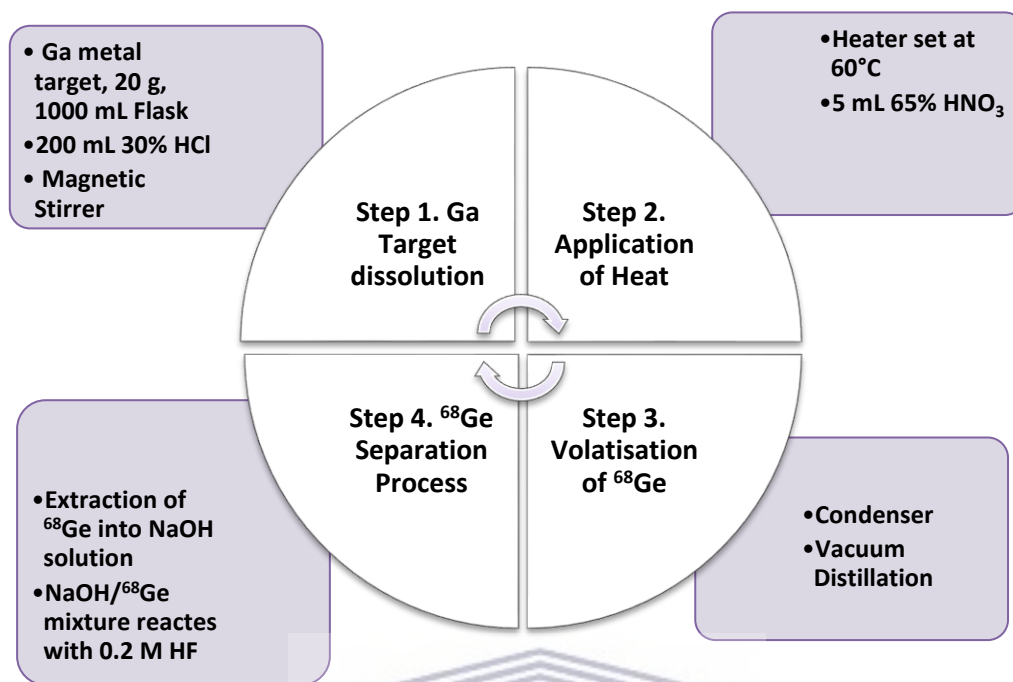
Figure 3.4:   A diagram based on the volatisation steps of the ^{68}Ge Production

3.2.6   Preparation of Degussa P25, Anatase, Rutile TiO₂ Column

Commercially available Degussa P25 (Evonik, Germany), P25, Rutile (Alfa Aesar), R1 and Aerolyst (Evonik, Germany) (anatase), A1, TiO_2 metals oxide were used as supplied. Ion-exchange columns were prepared using the commercially obtained P25, A1 and the R1 by sifting the adsorbents through a 212 μm stainless steel sieve. A 5 g portion of the sieved oxide (with particle size of 100–212 μm) was used for the generator column preparation. The commercially available Degussa P25, Anatase, Rutile TiO_2 were first washed several times with deionised water until the rinse solution remained colourless. Each sample was then packed while wet into a 3 mL syringe (O.D. 9.2 mm and I.D. 5 mm) and was fitted with a sintered polypropylene frit at the bottom and a Luer-lock cap at the top. A plunger (made from Teflon and fitted with a Luer-lock fitting) was pushed into the column syringe. In this arrangement, the titanium dioxide in the 3 mL syringe was tightly held between the sinters.

3.2.6.1 Calcination of the Degussa P25, Anatase, Rutile TiO₂ in preparation for the columns

In a typical calcination process, about 5.0 g of the commercial TiO_2 powders were transferred into a 30 mL crucible, followed by calcination at 850 °C in a furnace for 3 h. After the thermal treatment, the crucible was cooled to room temperature to obtain the TiO_2 powders. The annealed and untreated TiO_2 powder samples were characterised as controls for evaluating the changes in properties before and after modification. Table 3.5 shows TiO_2 materials and their corresponding codes.

Table 3.5: TiO₂ Materials and Corresponding Codes

Code	Materials	Formula	Molecular Weight (g/mol)	Treatment
TiO₂unhP25	Degussa P25	TiO_2	79.867	none
TiO₂heaP25	Degussa P25	TiO_2	79.867	heated to 850 °C
TiO₂unhA	Anatase	TiO_2	79.938	none
TiO₂heaA	Anatase	TiO_2	79.938	heated to 850 °C
TiO₂unhR	Rutile	TiO_2	79.866	none
TiO₂heaR	Rutile	TiO_2	79.866	heated to 850 °C

The column preparation involved four steps:

- **Conditioning -** the practice requires the TiO_2 in the column to be properly wetted to remove trapped gasses and ensure uniform flow. In this step, the TiO_2 in the column was equilibrated by passing through 100 mL of 0.1 M HCl using a peristatic pump at a flowrate of 0.5 mL/min.

- **Loading -** in this step, the column was loaded with the parent radionuclide ^{68}Ge by passing through 100 mL solution containing ^{68}Ge in 0.1 M HCl using a peristatic pump under the same flowrate as the conditioning step.

- **Washing –** in this step, the column was washed by passing through 100 mL 0.1 M HCl; the same flowrate was used.

- **Eluting –** 24 hours later, the ^{68}Ge on the column of TiO_2 was eluted by passing through 5 mL 0.1 M HCl by means of a syringe, into a 10 mL collection vial. The 24-hour decay period

is essential for the generator system to sufficiently provide ^{68}Ga in a pure form for labelling and other research methods.

Table 3.6 provides a list of various anion exchange columns loaded with various forms of TiO$_2$ metal oxide for the ^{68}Ge/^{68}Ga generator study. In all these experimental setups, ^{68}Ga elutions were conducted using 0.1 M HCl since it is widely used in pharmaceutical applications.

Table 3.6: A list of TiO$_2$ metal oxide Columns Prepared for the ^{68}Ge /^{68}Ga Generator Investigation

Code	Titanium Dioxide	Conditions
TiO$_2$unhA	anatase	column packed with unheated TiO$_2$
TiO$_2$heaA	anatase	column packed with heated TiO$_2$
TiO$_2$unhR	rutile	column packed with unheated TiO$_2$
TiO$_2$heaA	rutile	column packed with heated TiO$_2$
TiO$_2$unhP25	P-25 Degussa	column packed with unheated TiO$_2$
TiO$_2$heaP25	P-25 Degussa	column packed with heated TiO$_2$
3-APTES (MIP)	anatase	column packed with modified TiO$_2$ coupled to an MIP design
3-APTES (NMIP)	anatase	column packed with modified TiO$_2$ coupled to an NMIP design
3-MPTMS (MIP)	anatase	column packed with modified TiO$_2$ coupled to an MIP design
3-MPTMS (NMIP)	anatase	column packed with modified TiO$_2$ coupled to an NMIP design
BAPA (MIP)	anatase	column packed with modified TiO$_2$ coupled to an MIP design
BAPA (NMIP)	anatase	column packed with modified TiO$_2$ coupled to an NMIP design
CDMT (MIP)	anatase	column packed with modified TiO$_2$ coupled to an MIP design
CDMT (NMIP)	anatase	column packed with modified TiO$_2$ coupled to an NMIP design

3.2.7 Quality Control

The evaluation of ^{68}Ge/^{68}Ga generators needs to meet criteria of high standards; not only for the functionality of the separation of the daughter and parent elements, but also to comply with requirements that would assure product quality, reliability, robustness and lastly traceability. All these requirements are to be fulfilled within the rules of analytical protocols. In order to exploit different techniques and be able to draw meaningful conclusions, an understanding of the current

^{68}Ge/^{68}Ga generator processes was required to help fulfil the study goals. This understanding consist of four steps: activity measurements using ionisation chamber to gain information about the radionuclidic identity, conducting gamma ray spectrometry to gain knowledge of radionuclidic purity, quality control of the ^{68}Ga eluate for sterility and pyrogenecity purposes and, finally, producing an elution profile to monitor aspects such as ^{68}Ga eluate volume, ^{68}Ga radioactivity concentration and metal cationic impurities. Consequently, methods were proposed (Figure 3.3) based on a set of principles, and validated equipment were used for the study to investigate the TiO$_2$ nanoparticles for their potential as generator adsorbents.
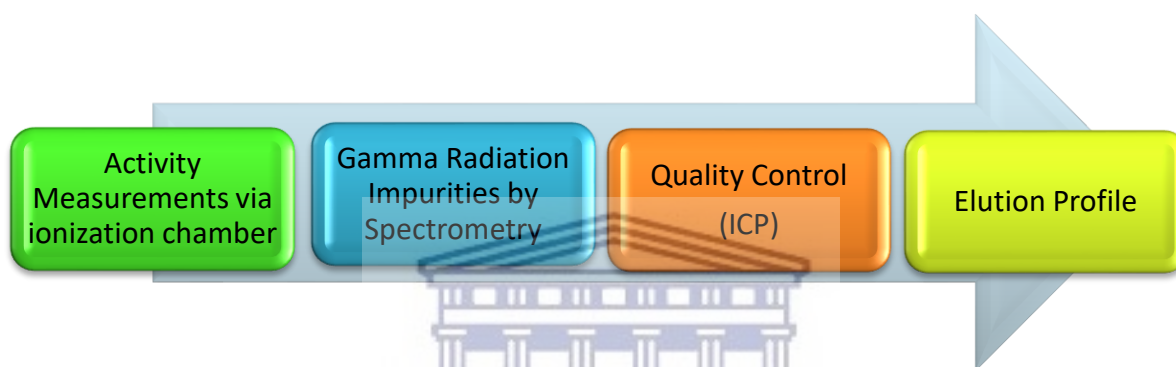
Figure 3.5:   A schematic overview of the Quality Control methodology approach

3.2.7.1 Activity Measurements

The eluted ^{68}Ga was collected and immediately measured by inserting the vial in an ionisation chamber (Capintec CRC 15R, USA), which provided activity readings at milli Curie (mCi) level.

3.2.7.2 Gamma Measurements

Impurities were measured by using Gamma-ray spectrometry (High-Purity Germanium gamma spectrometric), which has to be calibrated before each ^{68}Ga elution, by running a standard of known activity and known volume. The spectrum was recorded with an Accuspec multichannel analyser and Genie 2000 software (Canberra). The gamma lines used to quantify the ^{68}Ga yield and radionuclidic impurities such as ^{66}Ge and ^{69}Ge were 511 and 1077 keV, respectively. The European Pharmacopeia states that peaks in the gamma-ray spectra that do not belong either to ^{68}Ga or to annihilation radiation, or a possible sum of a peak at 1,022 keV shall 'represent not more than 0.1 per cent of the total radioactivity'.

3.2.7.3 Quality Control

The chemical purity of the eluate was determined using an ICP optical emission spectrometer (Optima 3300XL, Perkin Elmer), with special consideration given to the presence of iron, zinc and germanium. Sterility and bacterial endotoxins were also examined once every 2 months. Samples taken for sterility and bacterial endotoxins analysis were treated as follows: 0.5 mL samples were pipetted out of the ^{68}Ga eluate and each transferred into two sterilised 10 mL vials. One vial was tested for sterility by adding Soy Broth medium and incubated at 37 °C for seven days. The other vial was analysed using LAL (limulus amebocyte lysate) testing and its bacterial endotoxin content recorded for quality control purposes. This reaction is widely used for the detection and quantification of bacterial endotoxins.

3.2.7.4 Elution Profile

The collected ^{68}Ga eluate readings were recorded on an excel spreadsheet and the results were used to plot a graph over a period of two years.

3.2.8 Quality Control Parameters of the TiO$_2$ Columns

The most appropriate avenues to pursue for an undertaking like this was to align the quality control process to a recognised framework such as the one found in Table 3.7.

Table 3.7: Summary of the Quality Control Parameters used when the ^{68}Ge/^{68}Ga Generator was evaluated

Parameter	Quality and Characteristic of the ^{68}Ge/^{68}Ga Generator
Chemical separation specificity	Be able to produce ^{68}Ga in cationic chemical form, allowing subsequent versatile and direct labelling chemistry as well as reproducible and robust performance.
Radiation resistance and chemical stability	Use of nanocrystalline ceramic material is recommended due to their stability. Inorganic column sorbents are used more widely as they are less sensitive to radiolysis.
Eluate sterility and pyrogenecity	Be able to keep up with proven cGMP standards such as sterility and pyrogene tests.
^{68}Ge breakthrough	The generator should be able to display low ^{68}Ge breakthrough of <10^{-3}%, also diminish cationic impurities.
Eluent Type	Use of acidic eluent is highly recommended since it provides cationic Ga(III) for the further direct chemistry.
Elution profile	Elution profile that is able to provide 95% of ^{68}Ga in the smallest volume possible.

3.3 Surface Modification of the TiO$_2$ Metal Oxides

To answer the study research questions under section 1.3.3, the method in this section was to address drawbacks such as measurable eluent activities of the parent radionuclide ^{68}Ge (^{68}Ge breakthrough) high eluate volume and the high HCl concentration (0.1 – 1.0 M). In addition, metallic impurities such as Zn^{+2}, generated from the decay of ^{68}Ga, Ti^{+4} impurities from the column material, and lastly Fe^{+3}. Hence, the TiO$_2$ was modified with 3–Aminopropyltriethoxysilane (3-APTES), 3–Mercaptopropyltrimethoxysilane (3-MPTMS), Bis(3-Aminopropyl)amine (BAPA) and 2-chloro-4,6-dimethoxy-1,3,5-triazine (CDMT) and preparations protocols are presented in the following subsections.

3.3.1   Material (Reagents) and Equipment

The following commercial reagents were used without any further purification: TiO$_2$ – anatase, TiO$_2$ - rutile; ethanol (absolute grade, 99.9%), anhydrous toluene (purity 99.9%), trimethylamine (purity 99.9%), 3-aminopropyl triethoxysilane (3-APTES), 3-mercaptopropyl triethoxysilane (3-MPTMS), Bis(3-aminopropyl)amine (BAPA) and 2-Chloro-4,6-dimethoxy-1,3,5-triazine (CDMT). In Table 3.8, the surface modifiers including their properties are presented.

Table 3.8: Chemical Properties of the Alkoxysilanes used

Silane Coupling Agents	Chemical Formula	Molecular Weight (g/mol)	Boiling Point (°C)	Flash Point (°C)	Density (g/ml)	Appearance	Reactivity
3-APTES	C$_9$H$_{23}$NO$_3$Si	221.37	217	93	0.946	liquid	soluble in H$_2$0
3-MPTMS	C$_6$H$_{16}$O$_3$SSi	196.34	213-215	96	1.057	liquid	soluble in H$_2$O
BAPA	(NH$_2$CH$_2$CH$_2$CH$_2$)$_2$NH	131.22	151	117	0.938	liquid	soluble in H$_2$O
CDMT	C$_5$H$_6$ClN$_3$O$_2$	175.57	114	71-74	N/A	crystalline	soluble in Toluene

3.3.2 Preparation of modified TiO₂ nanoparticles using 3-Aminopropyltriethoxysilane (3-APTES), 3–Mercaptopropyl trimethoxysilane (3-MPTMS), Bis(3-aminopropyl)amine (BAPA) and 2-Chloro-4,6-dimethoxy-1,3,5-triazine (CDMT)

The reaction conditions were chosen according to literature and reaction conditions were kept constant (concentration, time, temperature, solvent).

3-APTES ($C_9H_{23}NO_3Si$) - 1 g of the TiO_2 nanoparticles was suspended in an ethanol/water mixture in a volume ratio of 95:5, and was acidified with acetic acid until pH = 5 into a two-neck round bottom flask (100 mL) equipped with a magnetic stir bar. The dispersion was sonicated for 30 min at room temperature in an ultrasonic bath (Elmasonic S30, 280 W) to enhance particle dispersion. Then, 10 mL of 3-APTES (Aldrich) was added to the dispersion, and the mixture was maintained for 24 h under continuous flowing nitrogen and stirring. Then, the surface modified TiO_2 nanoparticles were recovered from the reaction medium by vacuum filtering and washed twice with ethanol. Finally, the surface modified TiO_2 nanoparticles were dried in a vacuum oven for 24 h at 40°C.

In the second and third modification steps, the above method was followed but 3–mercaptopropyl trimethoxysilane (3-MPTMS), bis(3-aminopropyl)amine (BAPA) and 2-Chloro-4,6-dimethoxy-1,3,5-triazine (CDMT) were used as silane coupling agents. All experiments were conducted in triplicate (n=3) and the average results were computed.

3.4 The Molecular Imprinted Polymer

[68]Ge breakthrough analysis was done by using a molecular imprinted polymers (MIP) technique sourced from various previous studies discussed under section 2.8, in order to establish a method where complete removal of the Ge radionuclide is attained. Additionally the study investigated how the Ge template can be introduced and removed from the polymer, thereby allowing complete control over the method. Once a method was identified, suitability and preparedness to contribute in the study were investigated through ^{68}Ga elutions and results were captured on a database and the process was repeated. Three experimental routes were identified and used to initiate the hypothesised relationship in the conceptual method. The first experiment consisted of three replicas relating to Ge-MAA synthesis. The second experiment consisted of three replicas relating

to Ge template removal and the last experiment was about three replicas used for control (NIP synthesis). In addition to serving as Ge absorbers, structural and physical characteristics of the MIP particles were examined by using a TGA, BET, FTIR characterisation analysis and results thereof are discussed in section 4.4.

3.4.1 Material (reagents) and Equipment

The chemicals used for the synthesis of molecular imprinted polymers (MIPs) were all purchased from Sigma Aldrich (Johannesburg, SA). The names, abbreviations and the chemical structures of the different reagents (monomer, cross-linker, initiator, solvent, surfactant and template) used in synthesis are detailed in Tables 3.9.

Table 3.9: Reagents used when MIPs were synthesised

Chemical name	Reagent name	Symbol	Chemical Formula	M. W. (g/mol)
Methacrylic Acid	Monomer	MAA	$C_4H_6O_2$	86.09
Ethylene Glycol Dimethacrylate	Cross-linker	EGDMA	$C_{10}H_{14}O_4$	198.22
1,1 azobis (cyclohexanecarbonitrile)	Initiator	ABCHC	$C_7H_{11}N$	109.17
Acetonitrile	Solvent	ACT	C_2H_3N	58.08
Chloroform	Solvent	ACT	$CHCl_3$	119.38
Germanium	Template	Ge	Ge	54.0

3.4.2 Experimental Procedure for Molecular Imprinted Polymers

The Ge–MAA polymerization was prepared from a reagent mixture obtained by mixing 300.0 µL (3.52 mmol) of methacrylic acid, 525.0 µL (2.78 mmol) of ethylene glycol dimethacrylate, 25.1 mg (239 mmol) of Germanium (IV) oxide, 99,99% and 70.0 mg (0.42 mmol) of AIBN in 2.01 mL chloroform. The mixture was uniformly dispersed by sonication for 30 min. After sonication, it was purged with N_2 for 10 min and the Erlenmeyer flask was sealed under this atmosphere. It was, then, stirred in a water bath maintained at 60 °C for 20 h. The produced polymer was filtered using a

Whatman filter paper and washed with acetone and methanol before the template removal. All experiments were conducted in triplicate (n=3) and the average results were computed.

3.4.3 Removal of the Imprinting Molecule

The obtained MIPs were immersed in acetonitrile for 24 h, followed by filtering to remove Ge template molecules. The Ge template removal was further achieved by successive washes the polymers in 25 mL of a methanol/acetic acid solution (10:1, v/v, of 99.99% methanol and pure acetic acid) for three times, each time for 1 h, and then twice with 15 mL of pure water for 1 h. The template-free polymer (MIP) particles were collected and dried in vacuum.

3.4.4 Non-Imprinted Polymers (NIPs)

Parallel with MIP synthesis, non-imprinted polymers (NIPs) were prepared by following the same synthesis protocol without the use of a template Ge molecule. NIPs acted as a "control" to evaluate the strength of the interactions between the synthesized MIPs and the germanium template that were specific in the case of MIPs, and nonspecific for NIPs. For this reason, MIPs and NIPs were tested in terms of particle size, shape, porosity, and surface composition and information was provided about the number of the imprinted cavities, and their selectivity between the template and similar molecules.

3.4.5. ^{68}Ge Breakthrough Analysis using Molecular Imprinted Polymers (MIPs)

This case study can be treated under three headings: ^{68}Ga efficiency, eluate medium and ^{68}Ge breakthrough. In the first, the amount of ^{68}Ga achieved in the end as a product was measured against the ^{68}Ge loaded onto the TiO$_2$ column. The next section was about the elution medium which had to be kept under a well-established approach in the imaging studies. Lastly, a case study approach that was adopted to present the assumptions underpinning this research, as well as to introduce the molecular imprinted polymer research strategy technique in the control of the ^{68}Ge breakthrough.

Data collection was done through a day to day elution consisting of a column containing surface modified TiO$_2$ and MIP and NMIPs. Two polypropylene frits with pore size of 10 μm from Biotage

(Uppsala, Sweden) were fitted at the top and bottom of a 3 mL syringe and this used to house the TiO$_2$ material before being loaded with a ^{68}Ge radioisotope. Just below this design was unit that was modified to be able to house the MIPs. Elution of the ^{68}Ga was achieved by transferring about 5 mL of 0.1 M HCl into the column and the unit resting the MIPs. The eluted ^{68}Ga solution was collected into a 10 mL vial that was shielded by a 40 mm lead and used for ^{68}Ga efficiency, ^{68}Ge breakthrough analysis, sterility and endotoxins test, pH and statistical analysis. The use of the equations below for collection and analysis of data has been applied in this study.

$$^{68}Ge\ elution\ efficiency\ = \frac{^{68}Ga\ activity\ at\ time\ of\ elution}{^{68}Ge\ activity\ on\ the\ column\ at\ time\ of\ elution}\ x\ 100\% ..3.3$$

$$^{68}Ge\ Breakthrough\ (\%)\ = \frac{^{68}Ge\ activity}{^{68}Ga\ activity\ at\ time\ of\ elution}\ x\ 100\%\ …………..….3.4$$

3.5 TiO$_2$ Preparation and Characterisation

The following steps were followed during the characterisation procedure. The experimental details and parameters (*e.g.* sample identity, size, mass and annealing details) are reported here.

Sample Preparation: The samples were prepared by weighing TiO$_2$ nanomaterials (anatase, rutile and Degussa P25) in replicates using a total sample weight of $\sim$30 g. The samples were then heated in a vacuum oven at 120 °C overnight (10-12 hours) in order to remove all volatile components (water and hydrocarbons).

Dry Sample measurement: The weight of the dried samples (*DryWt*) was then measured in a Mettler Toledo HB43™ (with a readability 0.1 mg) and the dry weight was recorded down. Care was taken as to not allow re-adsorption of moisture from the air during the dry weight measurement.

Annealing of the samples: After the dry weight measurement, a $\sim$10 g sample from each nanomaterial was weighed and annealed by heating at 10°C/min rate to 850 °C, using a Muffle furnace from Horiba and held at this temperature for a period of 3 hours. Thereafter, the TiO$_2$ samples were cooled at 10°C/min rate in the furnace to room temperature, for another 3 hours. The samples were then transferred to a vacuum system of less than 1.33 Pa (10 μmHg) overnight.

Characterisation: The samples were taken out of the vacuum system and were ready for the X-ray diffraction (XRD), X-ray fluorescence (XRF),   XRD, HRSEM, HRTEM and the BET analysis.

TiO_2 was characterized using different techniques in order to investigate its structure and properties. The chosen TiO_2 samples that were suitable for [68]Ge adsorption were characterized using X-ray Powder Diffraction (XRD), X-Ray Fluorescence (XRF), Scanning Electron Microscopy, High Resolution Transmission Emission Microscopy Inductively Coupled Plasma-Optical Emission Spectroscopy (ICP-OES).

3.5.1   X-ray Fluorescent (XRF) Analysis

The chemical composition of the TiO_2 nanomaterial samples was carried out using a PANalytical PW2400 WD XRF (Wavelength Dispersive X-Ray Fluorescence spectrometer). Determination of loss on ignition (LOI) of each sample was performed using approximately 1 g of TiO_2 powdered sample weighed in ceramic beakers.

XRF Instrument Calibration

The seven standards used for calibration are listed in Table 3.10. Samples were analysed in triplicate to assess accuracy of elemental composition. Precision of the XRF data were examined through analysis of duplicate measures. Triplicate measurements were taken in succession, without moving the sample between screenings.

Table 3.10: XRF Calibration Standards

Standard #	Analyte	Formula
1	Vanadium Oxide	V_2O_5
2	Titanium Oxide	TiO_2
3	Potassium Oxide	K_2O
4	Phosphorus Pentoxide	P_2O_5
5	Aluminium Oxide	Al_2O_3
6	Magnesium Oxide	MgO
7	Sodium Oxide	Na_2O

3.5.2 X-ray Diffraction (XRD) Analysis

Approximately 0.5 g sample of the annealed and unannealed TiO_2 nanomaterial samples were deposited onto a Plexiglas sample holder and the XRD patterns were recorded at angles between 20° and 80°, with a scan rate of 1.5 °/min. The recording parameters were:

Table 3.11: XRD Experimental Parameters

Parameter	Condition
Mass of sample	0.5 g
Diameter of sample	35 mm
2 theta range	20 - 80°, 2θ
Step size	0.04°, 2θ
Dwell time for one step	2 s
λ (Cu Kα)	1.54Å
Fixed slit opening	0.6°
Sample rotation	yes

3.5.3   High Resolution Scanning Electron Microscope (HRSEM) Analysis

Annealed and unannealed TiO_2 nanomaterial samples were examined using a Hitachi X-650 Scanning Electron Microscopy (SEM) equipped with a CDU- lead detector at 25 kV. High Resolution Scanning electron microscopy was performed by putting a small amount of the TiO_2 nanomaterial samples on aluminium stubs coated with a thin carbon film to make the surface conductive and also to enhance the sample images. The coating process was done by EMITECH K950X carbon coater.

3.5.4   High Resolution Transmission Electron Microscopy (HRTEM) Analysis

A small amount of the annealed and unannealed TiO_2 nanomaterials were put in ethanol separately, and the suspensions were left for 15 minutes in an ultrasonic bath to avoid agglomerations of particles. Two drops of the suspension were placed on a 3 mm diameter carbon-coated copper grid (S147 - 4 Holey carbon film 400 mesh Cu grids) and the alcohol evaporated completely in air. The images were captured using a Field Emission gun, lens 1 was used with spot size 3, at 200 kV using HTEM-EDS Tecnai G2 F20 XT winMAT.

3.5.5 Brunauer-Emmett-Teller (BET) Analysis

The BET surface areas and pore size distributions were determined by nitrogen adsorption at -196 °C using Quantachrome Autosorb 1 sorption analyzer (Quantachrome Instruments, USA). The samples were degassed at 90 °C for 4 hours prior to nitrogen measurements. The experimental details were:

Table 3.12: BET Experimental Parameters

Parameter	Condition
Adsorbed Gases	Nitrogen
Test Method	TriStar II 3020 Version 2.00
Temperature Correction	No
Warm Free Space	14.9400 cm³ Measured
Equilibration Interval	10 s
Sample Density	1.000 g/cm³
Sample Mass	0.5662 g
Cold Free Space	46.4707 cm³
Low Pressure Dose	None
Automatic Degas	No

The N_2 isotherms obtained were used to determine the surface area using the following equation:

$$\frac{1}{X[\left(\frac{Po}{P}\right)-1]} \; = \; \frac{1}{XmC} + \frac{C-1}{XmC} + \frac{P}{Po} \quad\text{.............................}3.5$$

3.5.6 Inductively Coupled Plasma-Optical Emission Spectroscopy (ICP-OES) Analysis

All ICP-OES analyses were carried out on a Perkin Elmer Optima® 3300XL ICP-OES. The ICP-OES operating parameters are shown in Table 3.13. To avoid contamination from the lab environment, samples were prepared in a clean hood, and the auto-sampler was covered. All sample preparation was done in PFA bottles which were pre-soaked in 5% (v/v) nitric acid for 24 hours, then rinsed several times with milli-Q water before use. All measurements were made against calibration curves using the Method of Additions Calibrations, with 5 ppm, 10 ppm and 20 ppm standards. The standards were prepared by serial volume/volume dilution in vials (International Vial Packaging and

Sterilisation). Micropipettes with disposable tips (Merck, South Africa) were used for pipetting all solutions. Reference standard solutions of Zn, Ti, Al, Fe, Cu, Ge, Ga and Sn were used to prepare standard stock solutions in 0.1 M suprapur HCl to generate the calibration curves. The sample eluates were analysed directly without any dilutions necessary.

Table 3.13:   ICP-OES Instrument Conditions

Parameter	Conditions
RF Power	1500 W
Plasma view	Axial
Processing peak	Area
Auxiliary gas flow rate	0.4 (L/min)
Nebulizer gas flow	0.6 (L/min)
Plasma gas flow	8.0 (L/min)
Viewing height	15.0 (mm)
Spray chamber	Cyclonic
Read parameter	Auto (1-5 (min-max))
Calibration	Linear calculated intercept
Quartz torch	1-slot
Injector i.d	2.0 (mm, alumina)
Nebulizer	Meinhard concentric (high solid)
Wash time	e-ionized water
Peristaltic pump flowrate	1.5 (mL/min)

3.5.7   Thermogravimetric Analysis and differential scanning calorimetry (TGA/DSC)

The thermal properties of the modified TiO_2 materials were analyzed using a Discovery STD 650 Simultaneous Analyzer instruments, Chemical Engineering unit, UCT, RSA. For the measurements, the following technical specification were used:

- Temperature: ambient to 800 °C
- Inert – Nitrogen, 25 mL/min
- Oxidative – O_2, Air
- Reductive – Hydrogen/Argon mixture
- Sample: 10 mg
- Heating Rate: 10 °C/minute

3.5.8 Fourier Transform Infrared Spectrometry

The Fourier Transform Infrared Spectrometry (FTIR) measurements were taken on a Perkin-Elmer FTIR Spectrum Two instrument, a Singapore design, for data collection over a spectral range of 6,000 to 350 cm^{-1}. The FTIR measurements were obtained by making use of a 15 tonne press to make Potassium bromide (KBr) discs (2 mm discs), and a mortar and pestle was used to make Nujol mulls. For the measurements, a mass of about 0.5 to 1 grams of the samples was required.

CHAPTER IV

Results and Discussion

4.1 Introduction

In this chapter the commercially available TiO_2 nanoparticles were assessed first by adsorbent performance then using the five characterisation techniques in accordance with the methods described in chapter three. The chemical analysis of the commercially obtained TiO_2 samples was conducted using the XRF technique in order to assess the elemental composition of the materials. Subsequently, XRD analysis was able to provide information regarding the crystalline structure, nature of the mineral phase and crystalline grain size. The use of both high resolution scanning electron microscopy and transmission electron microscopy was able to provide information on the size, morphology and crystal structure of the TiO_2 nanomaterials. Lastly, the surface area of the TiO_2 nanomaterials was measured using BET method. Given the significance of TiO_2 nanoparticles in the application of $^{68}Ge/^{68}Ga$ generators, a combinatorial characterization approach was needed. The characterisation was thus used as a yardstick to measure properties that may alter the surface chemistry, hydrophilic properties and general reactivity of the TiO_2 nanomaterials.

4.1.1 $^{68}Ge/^{68}Ga$ Generator Results of the commercially obtained TiO_2 nanomaterials

To identify the impact of the commercially obtained TiO_2 nanomaterials on the preparation of a $^{68}Ge/^{68}Ga$ generator system, a comprehensive approach was required, combining techniques in a complementary way. In this context, it was desirable to know the limitations and strengths of the different TiO_2 nanomaterials, in order to provide information that could be useful to the production of the TiO_2 based $^{68}Ge/^{68}Ga$ generator. Since the adsorbent choice was directed at its potential application in the preparation of a $^{68}Ge/^{68}Ga$ generator system, the study was based on selective separation of the parent (^{68}Ge) and daughter (^{68}Ga) radionuclides. In all three adsorbents, annealed

and unannealed data performances were gathered. During the study, ^{68}Ge loading and ^{68}Ga elution were performed using 0.1M HCl medium. The experimental protocol is detailed under section 3.2.6.1. This was consistent with most clinical practices in the functional and metabolic imaging field. Table 4.1 presents the comparison between the TiO_2 nanomaterials performances.

Table 4.1: Evaluation of adsorbent performance between the P25, rutile and anatase samples

	$TiO_2unhP25$	$TiO_2heaP25$	TiO_2unhA	TiO_2heaA	TiO_2unhR	TiO_2heaR
^{68}Ge Retention (%)	100	0	100	53	41	44
^{68}Ga Elution (%)	38	-	57	54	21	26
^{68}Ge Breakthrough	0.002	-	0.018	3.65	0.022	0.034

Table 4.1 shows that there was a stark difference between heated and unheated Degussa P25 samples when evaluated for the ^{68}Ge retention. As a result, the heating of Degussa P25 was immediately abandoned. In heated samples of anatase, the ^{68}Ge retention was not sufficient either and no heating was considered for further analysis. On the other hand, in both rutile samples, the ^{68}Ge retention was less than 30% and this was enough to disqualify rutile as the ^{68}Ge adsorbent. The collected data indicated that TiO_2unhA was the better adsorbent when compared to the Degussa P25 and rutile, with comparable ^{68}Ga elution figures of 57 and 54% for heated and unheated samples, respectively. The ^{68}Ge breakthrough analysis of the TiO_2 nanomaterials was found to be 0.002 for the Degussa P25, 0.018 and 3.65 for the heated and unheated anatase, and 0.022 and 0.034 for rutile, respectively. Heating Degussa P25 was considered worthwhile but obtaining only 38% elution was deemed unsatisfactory. Furthermore, heating anatase was not a good idea according to the results, and no heating was considered for further testing.

Without additional effort, loading of the ^{68}Ge using Anatase was achieved successfully (100%) when no heating was applied. At the same time, the above 50% elution results show that the approach has the potential to be considered an attractive candidate in the development of ^{68}Ge/^{68}Ga generator systems. There was no significant correlation between the mineral phase of the inorganic oxides and the metal analysis in the ^{68}Ga product (see Table 4.1). Possible options were to further subject the anatase nanomaterial to surface modification for its optimisation. Further research was needed to find the most efficient modification method that is able to overcome aspects such as the

[68]Ga elution and the [68]Ge breakthrough. So far, the research mainly focused on ion exchange properties affecting developments of [68]Ge/^{68}Ga generator system. The results in table 4.1 show that adopting TiO_2 inorganic oxide based on selective separation of [68]Ge and ^{68}Ga radionuclide behaviour is feasible and effective. The results in Table 4.1 demonstrated the most crucial weaknesses that needed to be overcome to improve the performance relating to ^{68}Ga elution and [68]Ge loading. Hence, further research was needed to provide modification methods, taking into account the results at hand. It was envisioned that, a modified [68]Ge/^{68}Ga generator system may eventually lead to a more positive separation and retention based on chromatographic column design using TiO_2 as an adsorbent.

Literature reports the effect of the annealing temperature using a graphite furnace on the TiO_2 nanomaterials. In general, with annealing temperature the phase transition from anatase to rutile occurs. According to Sahbeni and colleagues (2017), annealing temperatures influence the structural properties of the TiO_2 nanomaterial; and this was discovered when they performed work to understand the physical properties of the TiO_2.

4.2 Characterisation Techniques

This study used a characterisation approach to examine the differences between the commercially available TiO_2 nanoparticles. Furthermore, the relationship between important variables and key quality control measures was investigated. The use of characterisation methods such as X-Ray Fluorescence (XRF), X-Ray Diffraction (XRD), High Resolution Scanning Electron Microscopy (HRSEM), High Resolution Transmission Electron Microscopy (HRTEM) and Brunauer-Emmett-Teller (BET), provided insight of aspects such as the size, crystal structure, elemental composition and a variety of other physical properties of the TiO_2 nanomaterials.

Furthermore, characterisation techniques such as XRF and XRD were applied in order to gain knowledge about the mass content, structural analysis and crystallinity of the TiO_2 nanomaterials. One of the concerns was the composition of impurities on the titanium dioxide (TiO_2) samples. This is partly due to the need for compliance of the [68]Ge/^{68}Ga generators to Good Manufacturing Practice and partly due to the stipulated quality control measures necessary for the ^{68}Ga product.

One limitation was that due to the disappointing adsorption results obtained using Degussa P25, BET analysis for this particular sample was omitted due to cost implications.

4.2.1 ICP-OES Measurements

A summary of the metal analysis is shown in Table 4.2. The process of metal analysis was explained earlier (refer to section 3.5.6). The ICP-OES operating parameters are shown in Table 3.13. The ICP-OES instrument was chosen for this investigation because for most of the elements, the detection limits are very low and a wide range of concentrations varying from ultra-trace (10 ng/g) to high concentrations (ppm) can be determined.

Table 4.2: Evaluation of metal ion impurities between the P25, rutile and anatase samples (n=3)

	TiO$_2$unhP25	TiO$_2$heaP25	TiO$_2$unhA	TiO$_2$heaA	TiO$_2$unhR	TiO$_2$heaR
ICP Analysis (ppm)	Zn = <2	Zn = <2	Zn = <1	Zn = <1	Zn = <1	Zn = <1
	Fe = <1	Fe = <1	Fe = <1	Fe = <1	Fe = <2	Fe = <2
	Ga = <1	Ga = <1	Ga = <1	Ga = <1	Ga = <1	Ga = <1
	Ge = <1	Ge = <1	Ge = <1	Ge = <1	Ge = <2	Ge = <1

It can be observed that TiO$_2$unhP25 and TiO$_2$heaP25 had higher Zn content (Zn = <2) when compared to the rutile and anatase nanomaterials. It should be pointed out that the total impurities content should be <1 ppm for each metal, as any deviation will lead to interference in the complexation of ^{68}Ga with the various ligands and biomolecules. Therefore, TiO$_2$unhA and TiO$_2$heaA from the summary in Table 4.2 were comparable with the best ^{68}Ga adsorbents. Thus, they show less contamination of the eluate with other metal cations, which means that they have a potential to be suitable for use ^{68}Ge/^{68}Ga generator systems.

4.2.2 XRF measurements

In order to verify ICP-OES results and determine major oxide content XRF was used to investigate the chemical content of the TiO$_2$ samples; the results obtained are shown in Table 4.3. Using this approach, refer to section 3.5.1, certified reference material (CRM) standards were used to create calibration curves. This method involves measuring several samples of known elemental

concentration and finding the relationship between the intensity of the measured element's fluorescent X-rays and the concentration. Thus, this relationship is then used to obtain the element concentration of an unknown sample from its fluorescent X-ray intensity. Only the unheated samples were analysed in triplicate.

Table 4.3: XRF analysis of TiO$_2$ nanoparticles, weight %, (n=3)

Sample Code	Fe$_2$O %	MnO %	Cr$_2$O$_3$ %	V$_2$O$_5$ %	TiO$_2$ %	K$_2$O %	P$_2$O$_5$ %	Al$_2$O$_3$ %	MgO %	Na$_2$O %	Total
*CRM 61	0.69	0.01	0.13	0.45	93.38	0.06	0.05	1.18	0.17	0.10	93.38
TiO$_2$unhP25	0.01	0.00	0.00	0.27	95.09	0.06	0.01	0.00	0.10	0.65	99.44
TiO$_2$unhP25	0.01	0.00	0.00	0.28	95.34	0.06	0.01	0.00	0.10	0.67	99.53
TiO$_2$unhP25	0.01	0.00	0.00	0.27	95.28	0.06	0.01	0.00	0.10	0.66	99.45
TiO$_2$unhR	0.01	0.00	0.00	0.27	98.91	0.00	0.01	0.00	0.05	0.00	99.63
TiO$_2$unhR	0.01	0.00	0.00	0.27	99.20	0.00	0.01	0.00	0.06	0.00	99.75
TiO$_2$unhR	0.01	0.00	0.00	0.28	99.18	0.00	0.01	0.00	0.07	0.00	99.76
TiO$_2$unhA	0.01	0.00	0.00	0.28	97.38	0.00	0.01	0.00	0.07	0.03	99.04
TiO$_2$unhA	0.01	0.00	0.00	0.28	97.41	0.00	0.01	0.00	0.07	0.05	99.09
TiO$_2$unhA	0.01	0.00	0.00	0.27	97.56	0.00	0.00	0.00	0.07	0.03	99.21

*Certified Reference Material

Samples were analysed against a known certified reference material. In all samples that were investigated, the TiO$_2$ content as dry weight (mass %) in the samples was found to be above 95% by mass. Also, in all the TiO$_2$ samples, the content of the other impurities made up less than 1% by mass. Adopting TiO$_2$ with a high trace metal impurity content could result in a compromised quality of the ^{68}Ga product as these metals may inadvertently co-elute with the daughter nuclide. Both rutile and anatase samples showed low elemental impurities thus were considered for later research studies. It was recommended that loss on ignition (LOI) be performed to determine the loss in weight that results from heating a sample of the TiO$_2$ material to a high temperature. Thus, more insight was gained into the weight change of a sample after it has been heated to high temperature causing some of its content to burn or to volatilise. This information was crucial since the loss in weight that results should be taken into consideration when XRF

analysis is conducted. The percent weight loss during the ignition step was reported as LOI (% wt. loss). Table 4.4 presents the LOI separately.

Table 4.4: Loss on Ignition analysis of TiO$_2$ nanoparticles, weight %

Degussa P25		Rutile		Anatase	
TiO$_2$unhP25	3.05	TiO$_2$unhR	0.00	TiO$_2$unhA	0.03
TiO$_2$unhP25	3.05	TiO$_2$unhR	0.00	TiO$_2$unhA	0.03
TiO$_2$unhP25	3.05	TiO$_2$unhR	0.00	TiO$_2$unhA	0.03

When an unheated P25 was used, the Loss on Ignition (LOI) value was found to be 3.05 mass %. This value was considered high when compared to other TiO$_2$ samples. This finding indicated a volatile loss in Degussa P25 TiO$_2$, signalling a high moisture content. It also had a high content of Na$_2$O (0.65-067 %) when compared to rutile and anatase, with 0.00 and 0.03, respectively. A trace amount of elements such as Na or Mg, other than the TiO$_2$ compound could mean higher impurity content. These results seem to suggest that all samples were mainly composed of TiO$_2$. During the data analysis, an observation of high content of V$_2$O$_5$ was found. This was attributed to a reaction between metallic V atoms in the air moisture and the TiO$_2$ nanomaterials, which takes place naturally at room temperatures. Based on the literature (Diebold, 2002) it was reported that deposition of vanadium in an oxygen ambient facilitates a reaction between vanadium oxide and that particular support, in this case the TiO$_2$ nanomaterials.

4.2.3   Analysis by X-Ray Diffraction

To identify the phase purity of TiO$_2$ crystals and aspects such as average grain size, crystallinity and crystal defects, XRD analysis was used due to its non-destructive nature for characterising crystalline materials. The crystallite size (D) was calculated by the Scherrer formula as expressed in equation 4.1:

$$D = \ k\,\lambda/\beta cos\,\vartheta \qquad\qquad (4.1)$$

where D is the mean size of crystallite, k is crystallite shape factor (0.9), λ is the x-ray wavelength (1.5406Å), β is the full width at half the maximum (FWHM) in radians and θ is the diffraction angle in degrees (Diebold, 2002; Zhang et al, 2002).

In Figure 4.1, XRD patterns of TiO_2unheaA, TiO_2unheaR and the TiO_2unhP25 samples are presented.
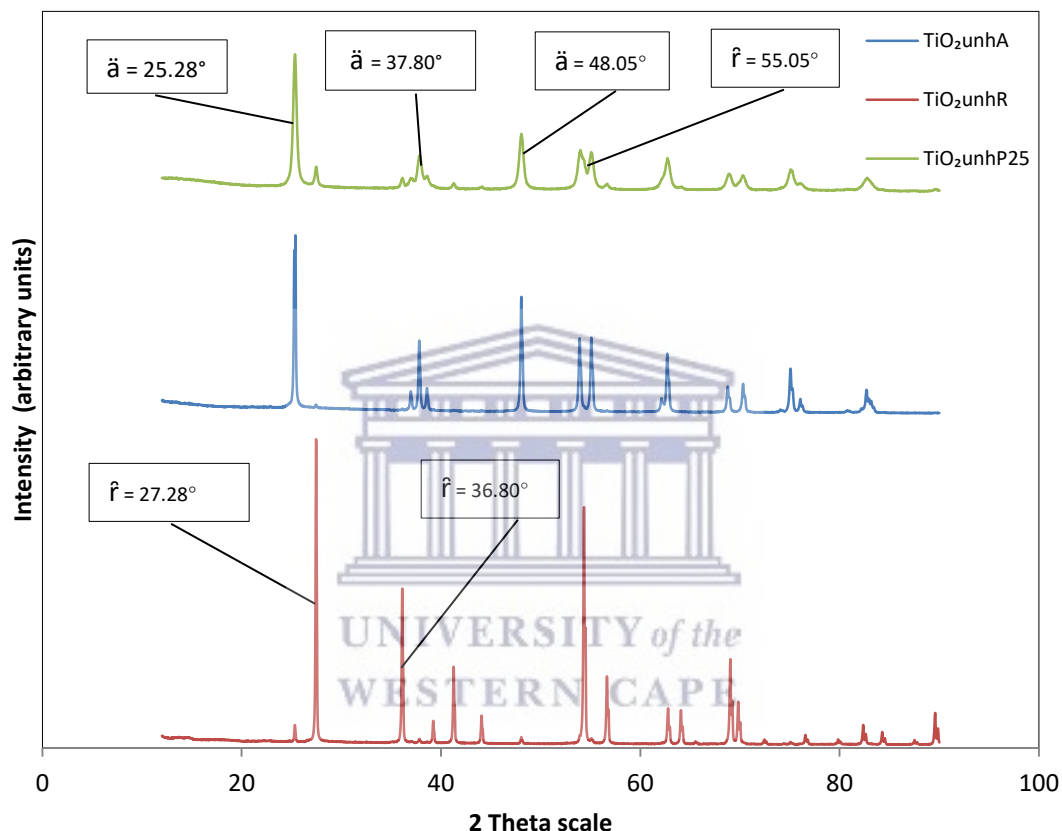
ä = anatase; r̂ = rutile

Figure 4.1: XRD Patterns of TiO_2unhA, TiO_2unhR and the TiO_2unhP25 samples

The XRD spectra revealed peaks at 25.28°, 37.80° and 48.05° that were consistent with the (101), (004) and (200) peaks of anatase TiO_2 (Pattern No. 00-21-1272, Appendix H). The peak at 2θ = 37.80° is usually 0.2 times that of 2θ = 25.28°, as shown in correlation between (004) and (101) diffraction intensities in JCPSD data (No. 00-21-1272). However, the peak at 2θ = 37.80° was found to be 0.4 times that of that of 2θ = 25.28° when Degussa P25 was studied, 0.5 times for rutile and 0.3 for

anatase. Next, the crystallite sizes relative to the main diffraction peaks were estimated from the in full-width-half maximum and sizes were found to be anatase (101) 12 nm, rutile (110) 11 nm and Degussa P25 (101) 28 nm (see Table 4.5)

In Figure 4.2, on the other hand, XRD patterns of the TiO_2heaA, TiO_2heaR and the $TiO_2heaP25$ are presented.
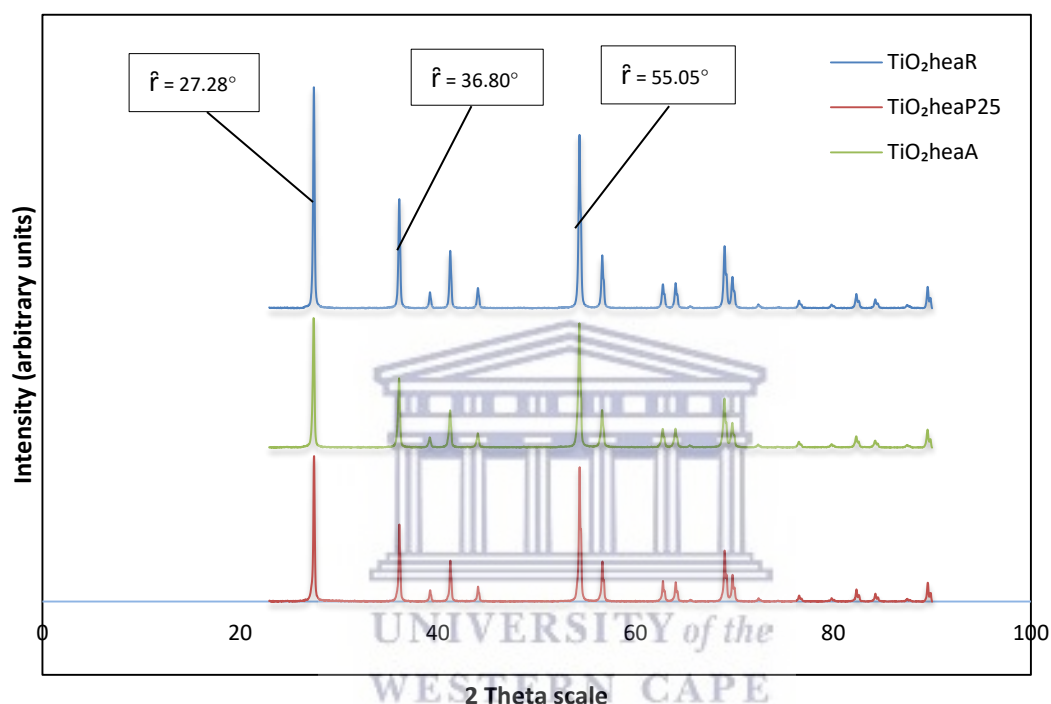
$\hat{r}$ = rutile

Figure 4.2: XRD Patterns of the TiO₂heaA, TiO₂heaR and the TiO₂heaP25 samples

.

Figure 4.2 revealed peaks at 27.28°, 36.80° and 55.05° consistent with the (110), (101) and (211) peaks of rutile TiO_2 (Pattern No. 00-21-1276, Appendix I). Next, the crystallite sizes relative to the main diffraction peaks were estimated from the in full-width-half maximum and sizes were found to be anatase (101) 24 nm, rutile (110) 21 nm, and Degussa P25 (101) 91 nm (see Table 4.5)

As was expected, Figure 4.2 shows the calcination at 850 °C transformed anatase to the rutile phase. Ulricke Diebold (2002) writes that heating TiO_2 nanomaterial to a high temperature produced the (110) peaks consistent with rutile content in the samples. Thus, considering that TiO_2

95

nanomaterial in anatase phase reconstructs when heated to elevated temperatures, this means that calcination temperatures should be lower to prevent this phase change. What should be added to this is that in Table 4.2, when the anatase in heated phase was analysed for ^{68}Ge breakthrough, the results were unsatisfactory and as a result this experiment was abandoned. A possible explanation might be related to the phase change upon very high temperature or annealing of the TiO_2 nanomaterial. To illustrate the effects of temperature on the crystallite size, a measure of the peak position (2θ) and the full width at half height (FWHM were used. In this way, particles sizes of the TiO_2 nanomaterials were identified and presented in Table 4.5.

Table 4.5: XRD Data of the TiO₂ Materials

Material	2θ	θ	Cos θ	Sin θ	FWHM (°)	FWHM (radians)	Size (nm)
TiO₂unhP25	25.4	12.7	0.9755	0.2198	0.70	0.0122	12.16
TiO₂heaP25	27.7	13.9	0.9707	0.2402	0.77	0.0134	25.10
TiO₂unhR	25.1	12.6	0.9759	0.2174	0.70	0.0122	12.15
TiO₂heaR	27.7	13.9	0.9707	0.2402	0.35	0.0134	24.43
TiO₂unhA	25.4	12.7	0.9755	0.2198	0.77	0.0134	11.05
TiO₂heaA	27.6	13.8	0.9711	0.2385	0.20	0.0126	21.37

Table 4.5 shows that when particle size became smaller, the peaks became broad and the width larger. The broadening occurs due to micro strains of the crystal structure arising from defects like dislocation and twinning (Zhang et al., 2002). From the XRD data, it was evident that the crystallite size increased with temperature due to annealing and thus the diffraction peaks became more intense and their FWHM gradually became narrower suggesting an increase in particles size and increase in the crystallinity of the relevant phase. In addition, the Debye-Scherrer formula was used to estimate the crystallite size of the anatase (101) and rutile (110) peaks.

A valuable benefit related to the XRD research method is that it generated an insights into the phase identification of the crystalline material, thereby helping to clarify heat induced mineral phase transformation. It was concluded that the phase structure and the particle size could play an important role in the ^{68}Ge loading of the titanium dioxide based $^{68}Ge/^{68}Ga$ generator system.

4.2.4 Analysis by Scanning Electron Microscopy (SEM)

As [68]Ge/^{68}Ga generator systems are being widely deployed there is an emergent need to understand how the calcination processes can affect morphologies of the adsorbent. A comparison of the anatase, rutile and the Degussa P25 TiO_2 powders before and after calcination was made using the scanning electron microscope technique, which is given in Figure 4.3 and Table 4.6.

(a) TiO$_2$unhA

| 200 nm | EHT = 5.00 kV | Signal A = InLens |
| WD = 4.5 mm | Mag = 50.00 K X |

(b) TiO$_2$heaA

| 300 nm | EHT = 5.00 kV | Signal A = InLens |
| WD = 4.3 mm | Mag = 100.00 K X |

(c) TiO$_2$unhR

| 200 nm | EHT = 5.00 kV | Signal A = InLens |
| WD = 4.4 mm | Mag = 50.00 K X |

(d) TiO$_2$heaR

| 200 nm | EHT = 5.00 kV | Signal A = InLens |
| WD = 4.4 mm | Mag = 100.00 K X |
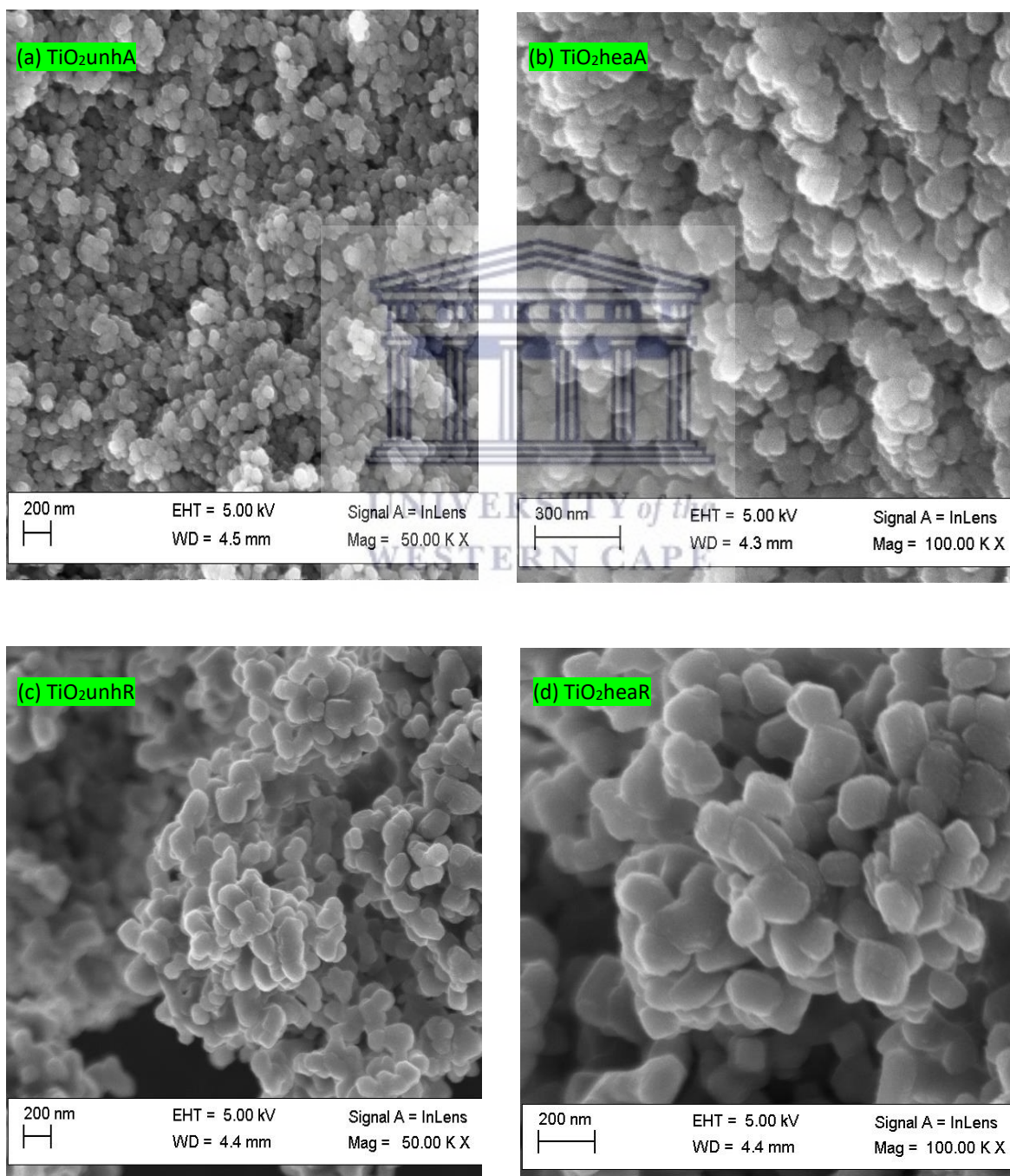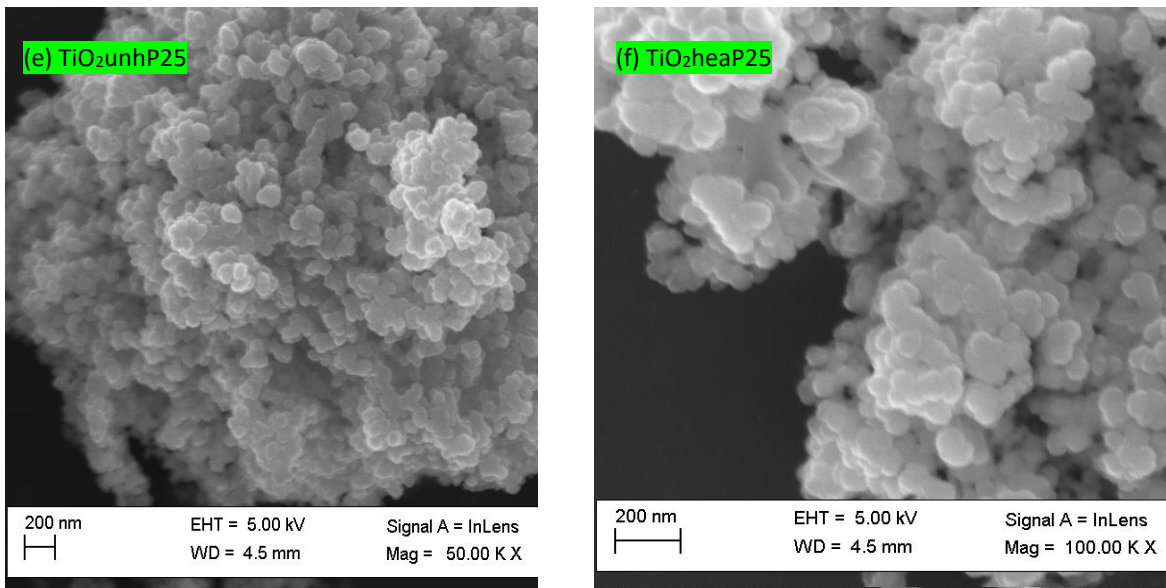
Figure 4.3: High Resolution Scanning Electron Microscopy micrographs of the uncalcinated (left) and calcinated (right) anatase, rutile and Degussa P25 TiO$_2$ samples

According to the scanning electron microscope (SEM) technique, micrograph A (TiO$_2$unhA) revealed particles in the form of spherical morphology with clumped distribution. Upon heating at 850 °C, there was evidence of particle growth in the TiO$_2$heaA sample (micrograph B). The micrographs of the rutile TiO$_2$ sample before calcination showed randomly packed flat-like morphology with less-clumped distribution. Upon heating, also at 850 °C, the micrograph showed that the particle size became larger with temperature. A comparison of micrograph E and F revealed the difference caused by the calcination at 850 °C. Micrograph E showed nanoparticles that were of courser in nature with agglomeration and clustering visible in the TiO$_2$unhP25 sample. Micrograph F, on the other hand, was able to show growth of the nanoparticles as a result of the calcination at 850 °C for 3 hours. From the above, it is obvious that the calcination of the TiO$_2$ nanoparticles at 850 °C for 3 hours cased swelling. The further influence of calcination temperature on the TiO$_2$ nanoparticles was to be determined by the High Resolution Transmission Electron Microscopy (HRTEM).

4.2.5   Analysis by High Resolution Transmission Electron Microscopy (HRTEM)

The HRTEM images of the TiO_2 nanoparticle samples ($TiO_2unhP25$, $TiO_2heaP25$, TiO_2unhR, TiO_2heaR, TiO_2unhA and TiO_2heaA) are shown in Figures 4.4.

Instrument	Accelerating	Field	Magnification
Field Emission	**Voltage**	**Width**	50.00 kx
Transmission	30 kV		
Electron Microscope			
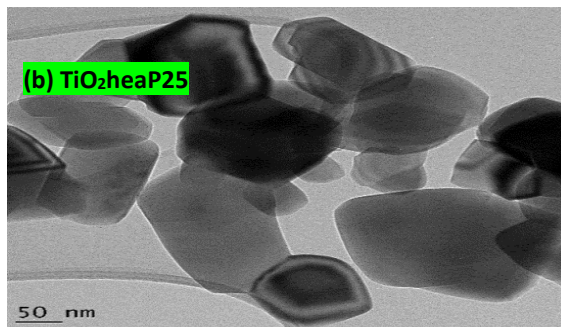
Instrument	Accelerating	Field	Magnification
Field Emission	**Voltage**	**Width**	50.00 kx
Transmission	30 kV		
Electron Microscope			

Instrument	Accelerating	Field	Magnification
Field Emission	**Voltage**	**Width**	25.00 kx
Transmission	30 kV		
Electron Microscope			
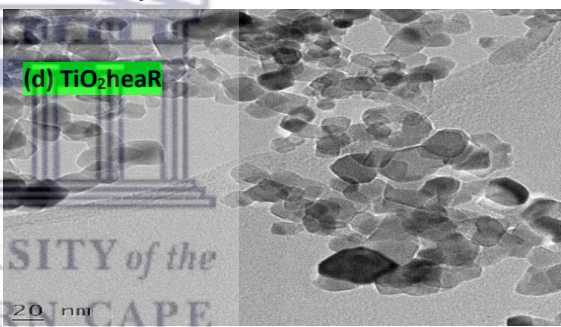
Instrument	Accelerating	Field	Magnification
Field Emission	**Voltage**	**Width**	30.00 kx
Transmission	30 kV		
Electron Microscope			

Instrument	Accelerating	Field	Magnification	Instrument	Accelerating	Field	Magnification
Field Emission	**Voltage**	**Width**	25.00 kx	Field Emission	**Voltage**	**Width**	50.00 kx
Transmission	30 kV			Transmission	30 kV		
Electron Microscope				Electron Microscope			

Figure 4.4: High Resolution Transmission Electron Microscopy micrographs of the unannealed (left) and annealed (right) Degussa P25, rutile, and anatase TiO₂ samples

HRTEM measurements showed bigger annealed particles of average sizes of 52, 38 and 35 nm for the TiO_2heaP25, TiO_2heaR and TiO_2heaA, respectively. With the unheated TiO_2 samples, the following sizes were evident, 11, 14 and 21 nm for the TiO_2unhP25, TiO_2unhR and TiO_2unhA, respectively. In most cases, the nanoparticles are angular sided crystals in shape and mono-dispersed. After heating the nanoparticles have generally increased in particle size. Images of the TiO_2unhP25 and TiO_2heaP25 samples revealed that particles were less mono-disperse when compared to the TiO_2unhR, TiO_2heaR, TiO_2unhA and TiO_2heaA nanoparticles. These results indicate that the particles exhibited a relatively uniform particle size distribution and this was also confirmed by the particles size distribution obtained from HRSEM micrographs (Figures 4.3). In addition, annealed samples (TiO_2heaR and TiO_2heaA) were packed randomly and interparticular voids were formed from the particle packing. The results indicate that calcination treatment influenced the microstructure of the TiO_2 powders.

In Table 4.6, particle size from the XRD, HRSEM and HRTEM results were summarised and compared.

Table 4.6: Comparison between XRD, HRSEM and HRTEM of TiO₂ nanoparticle size

TiO₂ nanomaterials	Sample Code	XRD Particle size Analysis (nm)	HRSEM Particle size Analysis (nm)	HRTEM Particle size Analysis (nm)
Degussa P25	TiO₂unhP25	12	13	11
	TiO₂heaP25	28	41	52
Anatase	TiO₂unhA	11	12	21
	TiO₂heaA	21	29	35
Rutile	TiO₂unhR	12	14	14
	TiO₂heaR	26	32	38

In most cases, the TiO₂ nanomaterials when heated revealed particles that were larger in size due to the annealing. The particle size results confirmed that high annealing temperature did not promote the nano structure. Considering that XRD analysis uses bulk measurements, it was decided that it was the most reliable method for TiO₂ investigation.

4.2.6   Analysis by Brunnauer-Emmett-Teller (BET)

As mentioned earlier, XRF results revealed that Degusssa P25 TiO₂ had a high content of Na₂O, and 38% of ^{68}Ga yield was eluted when ^{68}Ge/^{68}Ga generator analysis was performed. Thus, only the annealed and un-annealed TiO₂ in anatase phase and rutile phase were further studied in this work. The data from analysis of BET observations provided pore texture of the TiO₂ nanoparticles. For simplicity, BET results were classified into (1) surface area (2) pore volume and (3) pore size subsections.

4.2.6.1   Nitrogen Adsorption at -196 °C (surface area, pore volume and size distribution)

Two different curves (nitrogen adsorption and desorption) were plotted for each TiO₂ nanomaterial sample and showed the effect of annealing on the surface area, pore volume and size distribution. The curves (Figure 4.5), which were plotted as the quantity adsorbed/desorbed in square cubic metre per gram versus the relative pressure (P/Po), could be fitted adequately for the full range of relative pressures (P/Po). The interpretation of the hysteresis was made from this information. Also, it was part of the BET investigation to reveal y axis intercepts using the N₂ adsorption-

desorption isotherms. The goal of using y intercept of the curves is that at this point microporosity is revealed while the tail end gives insight of the surface area. The isotherms reveal a type I profile similar to microporous solids.
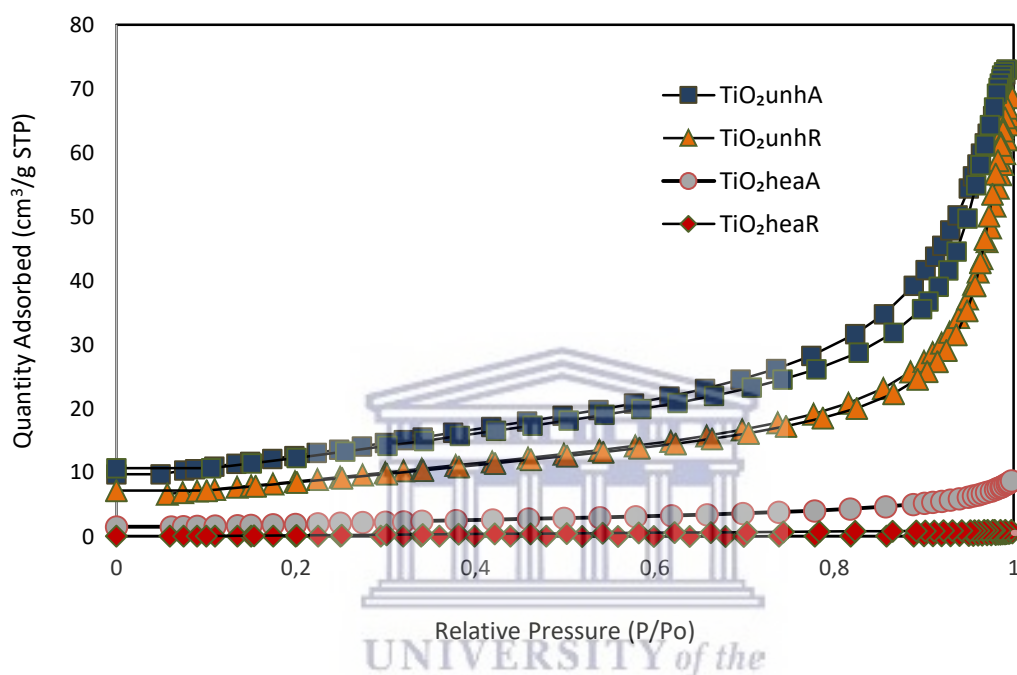
Figure 4.5: N$_2$ Isotherms of the TiO$_2$unhA, TiO$_2$heaA, TiO$_2$unhR and TiO$_2$heaR samples

The N$_2$ BET revealed total surface areas of 72.99 and 68.64 m^2/g for the TiO$_2$unhA and TiO$_2$unhR, respectively. Thus, more surface area was available for the [68]Ge adsorption, thereby increasing loading capacity of the TiO$_2$ nanomaterial. This could give the [68]Ge/^{68}Ga generator better efficiency, which could not be sacrificed by annealing of the TiO$_2$ nanomaterials. The curves also revealed y-intercepts of 9.77 and 6.64 m^2/g for the TiO$_2$unhA and TiO$_2$unhR, respectively. The unheated samples without annealing had higher microporosity. These findings were in good agreement with the observations from the XRD, HRSEM and HRTEM analysis.

On the other hand, N$_2$ BET revealed total surface areas of 8.73 and 0.60 m^2/g for the TiO$_2$heaA and TiO$_2$heaR, respectively. Thus, heat annealing should be avoided since it did not contribute to

improve the microporosity or textural properties of the TiO$_2$ nanomaterials. On the basis of these results, it was concluded that un-annealed TiO$_2$ nanomaterials were preferred for the [68]Ge loading.

On further BET data scrutiny, adsorbate desorption after saturation was also obtained. More importantly, this highlighted that hysteresis provided information about pore shapes. Table 4.7 summarises microporosity and surface area data of the TiO$_2$unhA, TiO$_2$heaA, TiO$_2$unhR and TiO$_2$heaR samples.

Table 4.7: Comparison between Microporosity and Surface Area sizes of TiO$_2$ nanomaterials

	TiO$_2$unhR	TiO$_2$heaR	TiO$_2$unhA	TiO$_2$heaA
Microporosity (y-intercept) (m^2/g)	6.64	0.07	9.77	1.53
Total BET Surface Area (m^2/g)	68.64	0.60	72.99	8.73

Both unheated TiO$_2$ nanomaterials samples in anatase and rutile phases exhibited type IV adsorption-desoprtion isotherms showing signs of being mesoporous materials given to nanoporous materials containing pores with diameters between 2 and 50 nm, according to IUPAC nomenclature. Leofanti and colleagues (1998) explain that the formation of monolayer of adsorbed N$_2$ molecules is the prevailing process at low relative pressure, while at high relative pressure multilayer adsorption occurs. On the other hand, both unheated TiO$_2$ nanomaterials samples in anatase and rutile phases exhibited type I adsorption-desorption isotherms showing characteristics of microporous solids. This is shown in Figure 4.5. Again, Leofanti and colleagues (1998) interpret this phenomenon as one where pore filling takes place without capillary condensation in the low relative pressure region. The pore–size distribution was obtained by application of the BJH (Barret, Joyner, and Halenda) technique, which assumes cylindrical, non-connecting pore geometry.

4.2.6.2 A Barrett, Joiner and Halenda (BJH) Adsorption Report (mesopore volume and mesopore size distribution)

In this technique, the assumption is that a geometric model exists (usually cylindrical or slit shaped) that allows calculation of the contribution of the thickness of the adsorbed N_2 film to the total adsorption and then the core volume. The following equation was used:

$$ln\ (p/p_s) = -(2\Upsilon w_m\ cos\ \vartheta)\ /\ (RTr_c) \qquad (4.2)$$

Where, r_c represents the radius for cylindrical pores, the distance between walls for slit shaped pores, Υ, the surface tension, w_m the molar volume and θ the contact angle. Figure 4.6 presents average pore size distribution of the TiO_2unhA, TiO_2heaA, TiO_2unhR and the TiO_2heaR samples obtained when applying the BJH method.
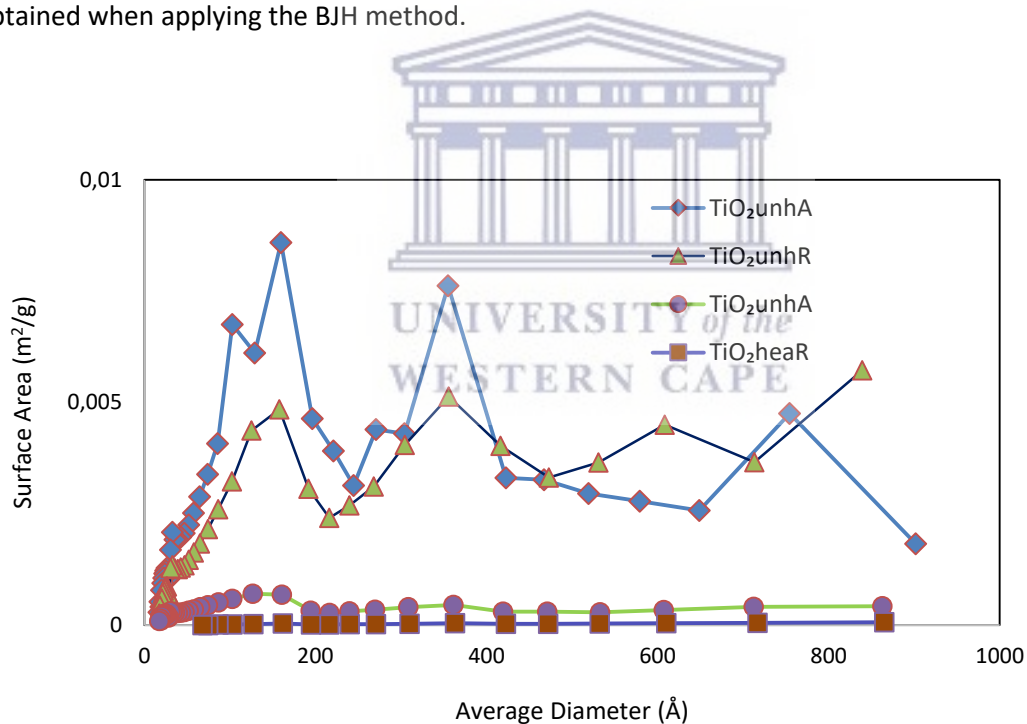
Figure 4.6. Comparison of the Pore size distributions of the TiO₂unhA, TiO₂heaA, TiO₂unhR and TiO₂heaR samples

First, curves did not show plateaus, an indication that nitrogen physisorption occurred between agglomerates, thus showing interparticular void spaces. Secondly, the pore size distribution curves

had multiple semi uniform peaks, thus indicating a rather non-uniformity of the pore pore size distribution in the mesoporous textures. In this case, the analysis of the meso pore size distribution indicated that for the heated and thus annealed TiO_2 samples, pore volumes were destroyed (curves had no meaningful Gaussian peaks). Samples TiO_2unhA and TiO_2unhR showed pore size distributions of similar curve arrangement. Both curves contained three Gaussian peaks (trimodal distribution), which were used to estimate symmetry of the distribution. Sample TiO_2unhA showed a higher pore size distribution when compared with the TiO_2unhR sample. The average pore diameter was approximately 390 Å for the TiO_2unhA sample. For the TiO_2unhR sample, the average mesopore diameter was approximately 210 Å. Table 4.8 summarises BET surface areas and the mesopore measurements obtained by the BJH method of the different TiO_2 nanoparticles analysed.

Table 4.8: BET Characteristics of the TiO₂ nanomaterials

TiO_2 nanomaterials	Sample Code	BET Surface Area (m^2/g)	Pore Volume (cm^3/g)	Pore Size (Å)
Anatase	TiO_2unhA	97	0.1	210
	TiO_2heaA	7	0.001	72
Rutile	TiO_2unhR	45	0.1	98
	TiO_2heaR	0.2	0.003	43

The surface area of the TiO_2unhA sample was 97 m^2/g, compared to 7 m^2/g for the TiO_2heaA. In addition, surface area of the TiO_2unhR sample was 45 m^2/g, compared to 0.2 m^2/g for the TiO_2heaR.

It was found that calcination, which is the only parameters between these samples, changes the properties of the nanoparticles significantly. From the above results, it is obvious that the calcination of TiO_2heaA and TiO_2heaR samples caused some shrinkage in the total surface area of the TiO_2 nanomaterial samples. This phenomena was confirmed by the pore volume and pore size analyses. These observations were in good agreement with the XRD, HRSEM and HRTEM results produced earlier on which indicated that effect of temperature increased the size of the nanoparticles. This behaviour was of particular importance in the production of the [68]Ge /^{68}Ga generator, where surface areas mark the overall success by allowing [68]Ge adsorption to the surface of the TiO_2 nanomaterial.

Overall, it can be concluded that the textural properties of the TiO$_2$ nanoparticles with Brunauer-Emmett-Teller (BET) gave important information which supported findings from the other characterisation techniques. The information was able to demonstrate that though more needs to be done in terms of surface modification to improve functionality by the anatase TiO$_2$, there is considerable potential for using the metal oxide as an adsorbent in the development of the [68]Ge/^{68}Ga generators.

4.3 Surface Modification of TiO$_2$ Metal Oxide Nanoparticles

In this section the four surface modification methods were assessed on the TiO$_2$ materials in accordance with the method described in chapter three (section 3.5). First, TiO$_2$ materials were assessed for their thermal stability using thermogravimetric analysis technique. Subsequently, infrared spectra of the TiO$_2$ materials were used to gain insight on their functional groups. Third, the HRSEM and HRTEM spectroscopic analysis were conducted for morphological insight on the TiO$_2$ materials. Next, XRD patterns of the TiO$_2$ material samples provided insight on the interrelationship of the particle size and specific surface area. Lastly, since surface area and adsorption by nanoparticles goes hand in hand, the specific surface areas of the surface modified TiO$_2$ nanoparticles were measured using Brunauer, Emmett and Teller (BET) method. The effectiveness of the surface modification of the TiO$_2$ nanoparticles in the end was assessed by comparing all properties of modified with non-modified nanoparticles.

4.3.1 Thermogravimetric / Differential Thermal Analysis

To understand the thermal stability of the surface modified TiO$_2$ materials, thermogravimetric/differential under an inert and oxygen atmosphere of up to 700 °C from an analysis was undertaken. The heating at the prescribed temperatures was to ensure the TiO$_2$ materials do not transform into rutile phase, which occurs at temperatures above 800 °C (Wu et al., 2016). Figure 4.7 shows TGA/DTA curves of the TiO$_2$ nanoparticles prepared by the different surface modification methods.
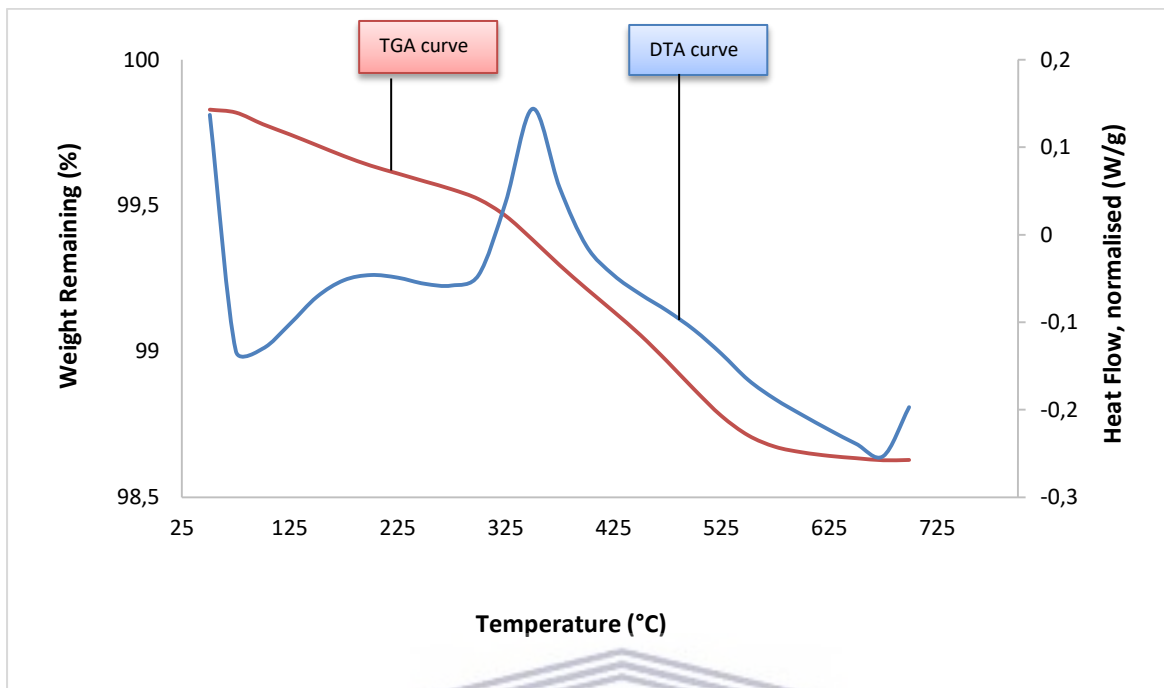
(a) TG/DT analysis of the unannealed anatase phase TiO₂ modified with 3-APTES (a-TiO₂unhA)
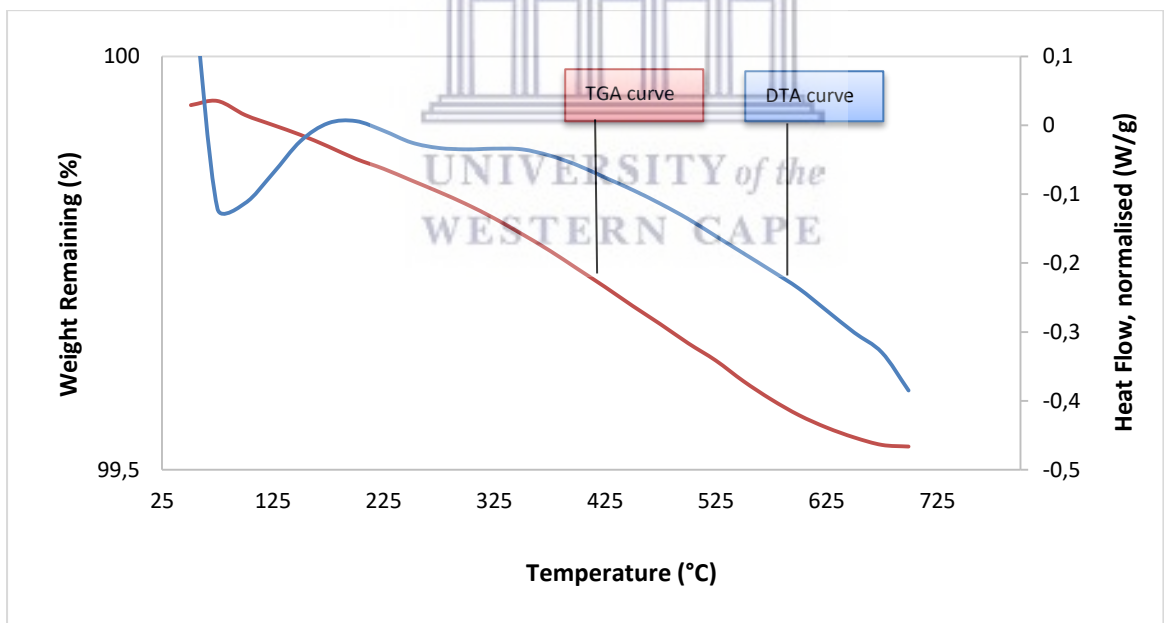
(b) TG/DT analysis of the annealed anatase phase TiO₂ modified with 3-APTES (a-TiO₂heaA)
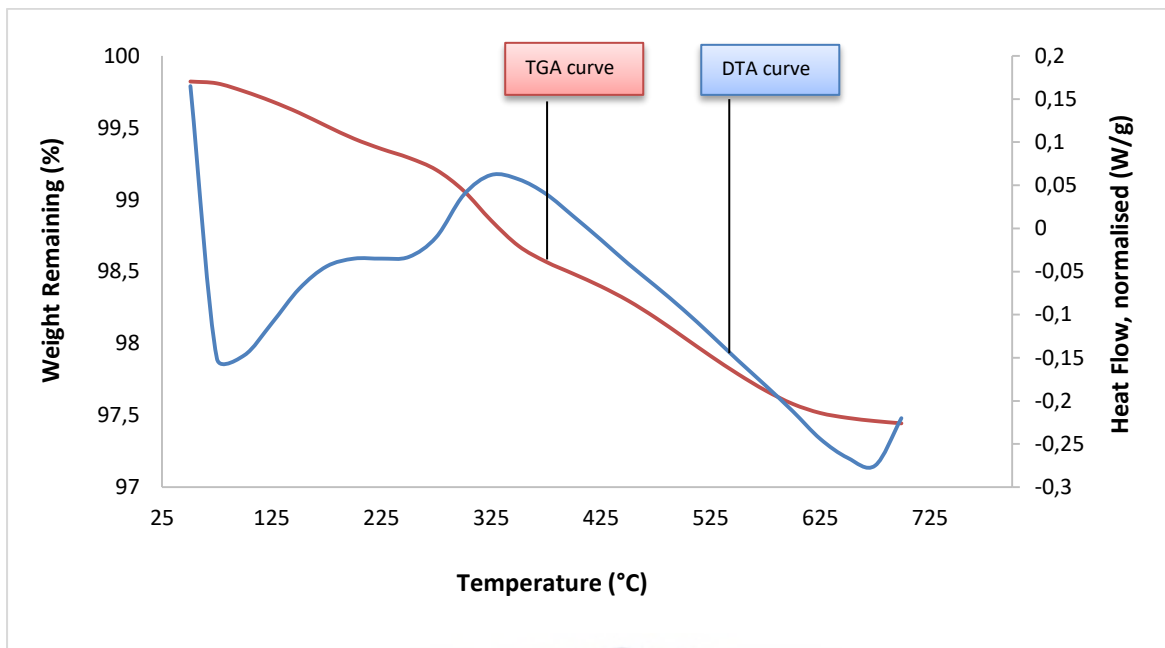
(c) TG/DT analysis of the unannealed anatase phase TiO₂ modified with 3-MPTMS (m-TiO₂unhA)
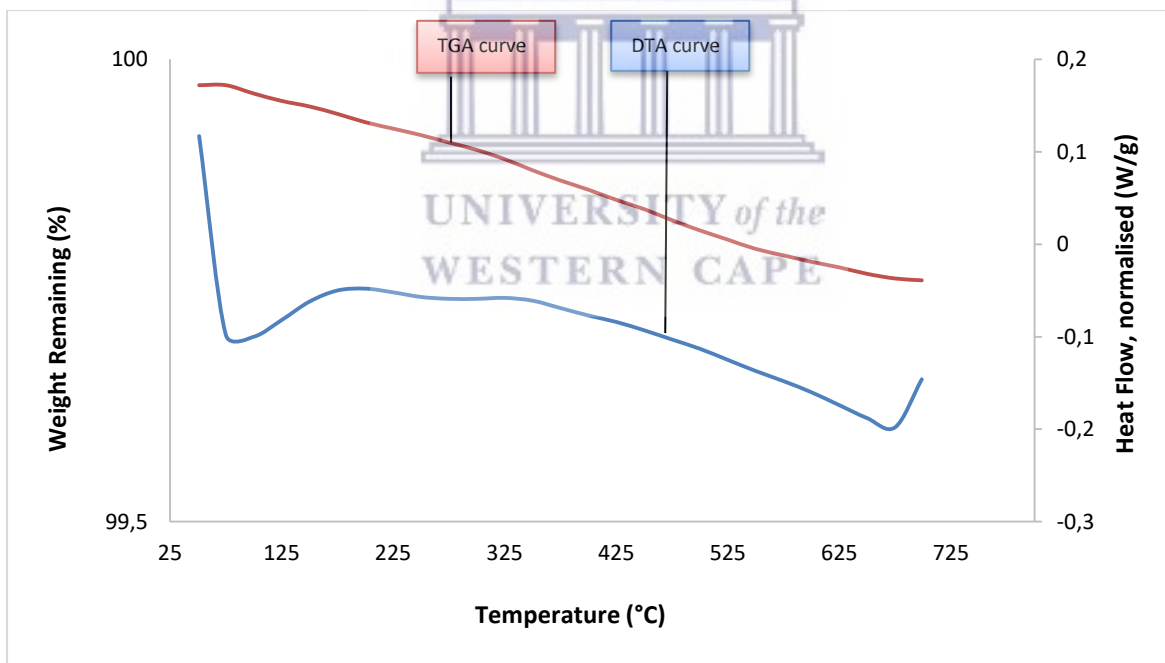
(d) TG/DT analysis of the annealed anatase phase TiO₂ modified with 3-MPTMS (m-TiO₂heaA)
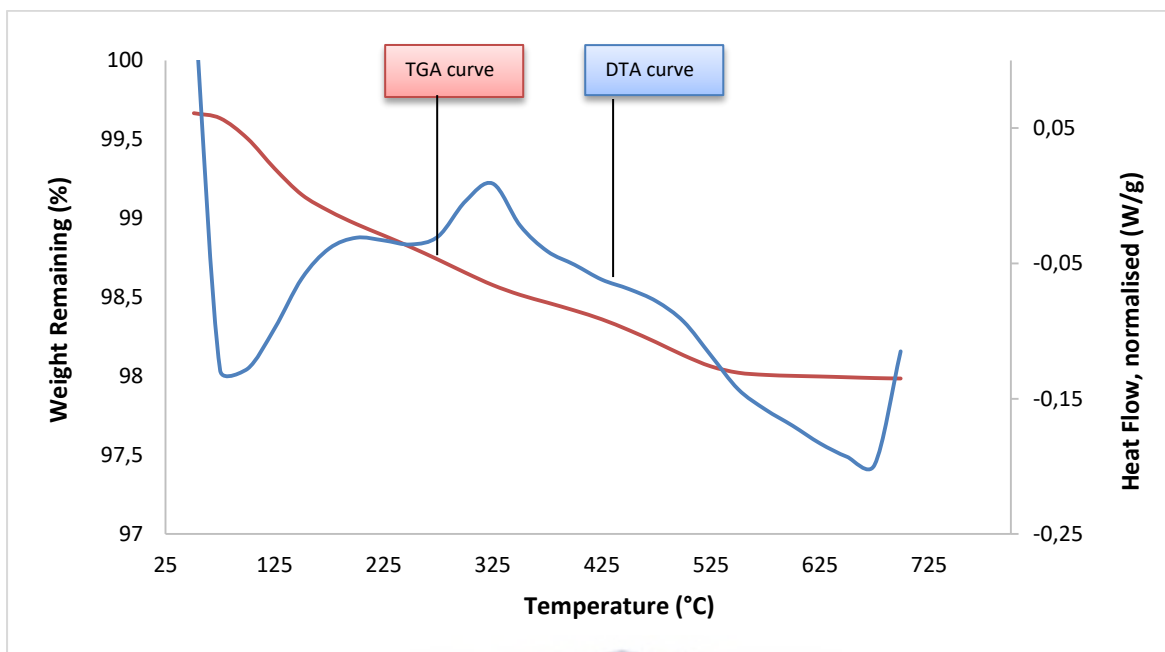
(e) TG/DT analysis of the unannealed anatase phase TiO₂ modified with BAPA (b-TiO₂unhA)
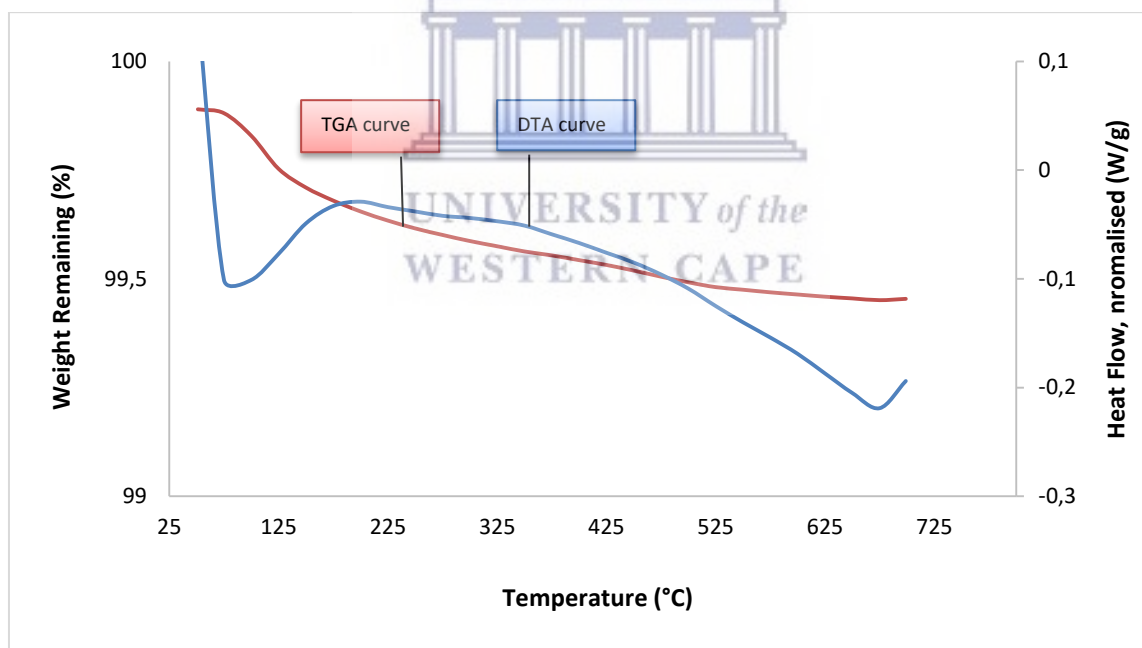
(f) TG/DT analysis of the annealed anatase phase TiO₂ modified with BAPA (b-TiO₂heaA)
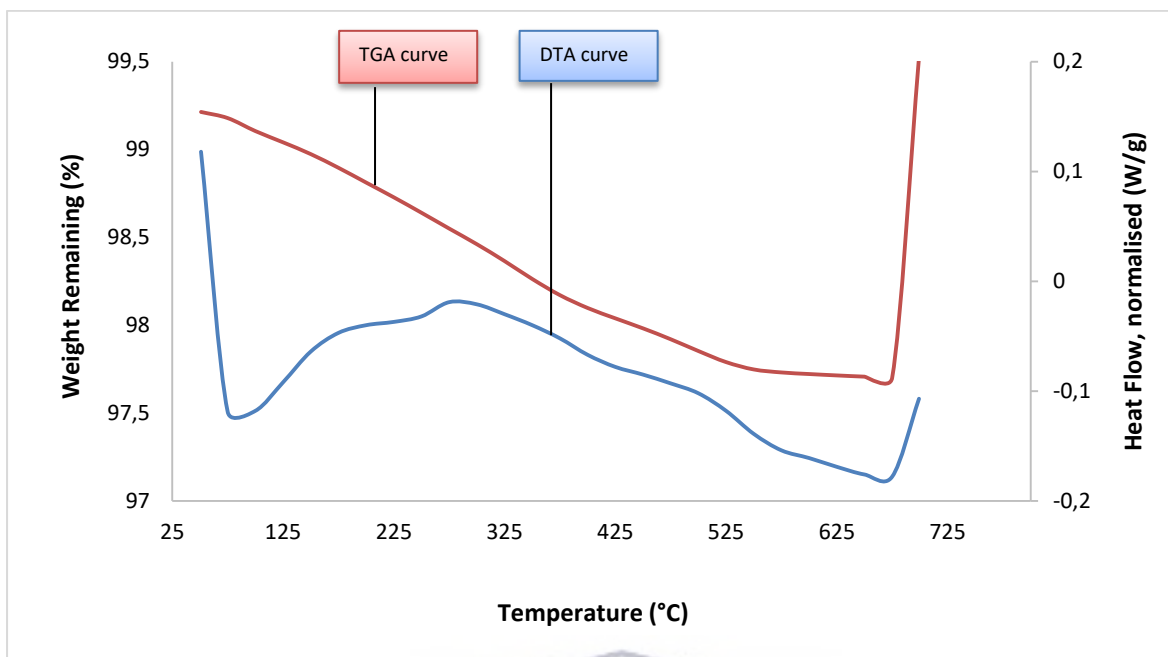
(g) TG/DT analysis of the unannealed anatase phase TiO₂ modified with CDMT (c-TiO₂unhA)
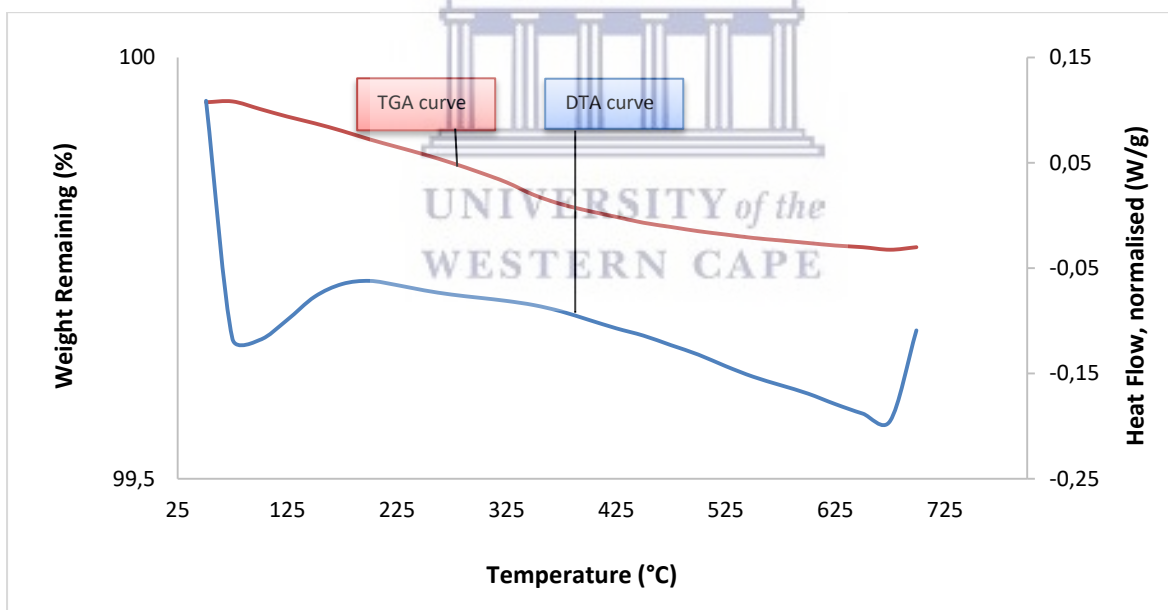
(h) TG/DT analysis of the annealed anatase phase TiO₂ modified with CDMT (c-TiO₂heaA)

Figure 4.7. TGA/DTA micrographs of the surface modified TiO₂ nanoparticles

From the obtained thermal decomposition spectral studies of the modified TiO_2 samples, quantification constituents such as reverse engineering and comparison of the material were determined. In addition, thermal stability, for example, decomposition behaviour and degradation, were also assessed.

For the *a-TiO₂unhA* sample, an endothermic reaction with a mass loss of approximately 0.3% was registered in the first region. This was due to dehydration of the m-TiO₂unhA sample and this shows up on DTA curve as an endotherm. Next, an exothermic reaction with a mass loss of approximately 0.7% was registered in the second region. The decrease in mass comes from the decomposition of the hydrocarbon material in the sample. Noticeably, both regions required long temperature ranges (100 to 320 °C, 325 to 525 °C), and this was associated with less impurities in the samples. Thereafter, sample degradation followed at a temperature of approximately 650 °C.

For the *a-TiO₂heaA* sample, similarly, two regions of mass loss were notices as before. As before, an endothermic reaction with a mass loss of approximately 0.2% was registered in the temperature range 100 to 250 °C. This was attributed to dehydration of the annealed TiO₂ sample. While on the other hand, an exothermic reaction with a mass loss of approximately 0.3% was registered in the second region. No changes were noticed in the temperature ranges, an indication that heating the sample did not bring about change in the sample stability.

For the *m-TiO₂unhA* sample, at the temperature range 100 to 250 °C there is a change in mass that occurred on the TGA curve, which corresponds to dehydration of the m-TiO₂unhA sample and this shows up on DTA curve as an endotherm. At 250 to 400 °C, a second change in mass is visible which corresponds to the decomposition of the hydrocarbon material in the sample. This showed up on the DTA curve as an exothermic reaction. A third DTA effect occurred at the temperature range 650 to 725 °C but was not registered on the TGA curve, because this event corresponds to phase changing of the dehydrated TiO₂ material. This phase change process was exothermic.

For the *m-TiO₂heaA* sample, the thermal degradation of the material demonstrated two changes in mass regions. The first weight loss stage occurred at about 100 to 200 °C, and was associated with evaporation of the adsorbed moisture in the sample. In this region, very little change in mass was observed on the DTA curve indicating there was little moisture in the material. Unlike the

unheated m-*TiO₂heaA* sample, at 250 to 400 °C, a minor second change in mass is visible which corresponds to the decomposition of the hydrocarbon material in the sample. This difference in weight loss was attributed thermal stability caused by the heat applied to prepare the sample.

For the b-TiO_2unhA sample, at the temperature range 90 to 250 °C there is a change in mass that occurred on the TGA curve, which corresponds to dehydration of the b-TiO_2unhA sample and this shows up on DTA curve as an endothermic reaction. At 250 to 400 °C, a second change in mass is visible which corresponds to the decomposition of the hydrocarbon material in the sample. This showed up on the DTA curve as an exothermic reaction. A third exothermic DTA effect occurred at the temperature range 400 to 530 °C, and was attributed to further degradation of aminosilane chains residues to yield the carbon and hydrocarbons. A fourth DTA effect was registered on the sample at the temperature range 530 to 700 °C but was not registered on the TGA curve, because this event corresponds to phase changing of the dehydrated TiO_2 material from anatase to rutile crystal phase. This phase change process was exothermic.

For the b-TiO_2heaA sample, the thermal degradation of the material demonstrated two change in mass regions. The first weight loss stage occurred at about 100 to 300 °C, and was associated with evaporation of the adsorbed moisture in the sample. Additionally, in this region, very little change in mass was observed on the DTA curve indicating there was little moisture in the material. However, unlike the unheated b-*TiO₂heaA* sample, at 250 to 400 °C, a very minor second change in mass was visible which corresponds to the decomposition of the hydrocarbon material in the sample. As stated earlier, this difference is weight loss this time was attributed thermal stability caused by the heat applied to prepare the sample. This change process was exothermic.

For the c-TiO_2unhA sample, Figure 4.7 (g) revealed that at the temperature range 90 to 250 °C there is a minor change in mass that occurred on the TGA curve, which corresponds to dehydration of the c-TiO_2unhA sample and this shows up on DTA curve as an endotherm. At 225 to 400 °C, a second change in mass is visible which corresponds to the decomposition of the hydrocarbon material in the sample. This showed up on the DTA curve as an exothermic reaction. A third exothermic DTA effect occurred at the temperature range 400 to 530 °C, and was attributed to further degradation of aminosilane chains residues to yield the carbon and hydrocarbons.

Finally, for the annealed c-TiO$_2$heaA sample, the thermal degradation of the material demonstrated two minor change in mass regions. The first weight loss stage occurred at about 100 to 250 °C, and was associated with evaporation of the adsorbed moisture in the sample. As before when heat was applied to the samples, very little change in mass was observed on the DTA curve indicating there was little moisture in the material. As before, the c-*TiO$_2$heaA* sample, at 250 to 400 °C, a minor second change in mass is visible which corresponds to the decomposition of the hydrocarbon material in the sample. Decomposition temperature was registered at 700 °C, indicating that at this region there is not much capping agent in annealed c-TiO$_2$heaA sample (Figure 4.7 (h)). Table 4.9, summarises weight changes of each sample at a given time and temperature.

Table 4.9: Thermogravimetric analysis (TGA) results obtained for the modified TiO$_2$ samples

Sample	Initial degradation Temperature (°C) range and weight loss (%)			Second degradation Temperature (°C) range and weight loss (%)			Comments
	T (°C)	W (%)	Endothermic/ Exothermic	T (°C)	W (%)	Endothermic/ Exothermic	
a-TiO$_2$unhA	100 - 320	0.3	Endothermic	325 - 525	0.75	Exothermic	2 x regions of mass loss
a-TiO$_2$heaA	100 - 320	0.2	Endothermic	325 - 600	0.3	Exothermic	2 x regions of mass loss
m-TiO$_2$unhA	100 - 225	1	Endothermic	225 – 400 400 - 650	0.5 1.5	Exothermic Exothermic	3 x regions of mass loss
m-TiO$_2$heaA	100 - 225	0.02	Endothermic	225 - 650	0.05	Exothermic	2 x regions of mass loss
b-TiO$_2$unhA	100 - 250	1.2	Endothermic	255 – 400 400 – 550 550 - 650	0.5 1 1	Exothermic Exothermic Exothermic	4 x regions of mass loss
b-TiO$_2$heaA	100 - 250	0.7	Endothermic	250 - 625	0.3	Exothermic	2 x regions of mass loss
c-TiO$_2$unhA	100 - 225	1.2	Endothermic	225 – 425 425 - 550 550 - 650	0.1 0.7 0.2	Exothermic Exothermic Exothermic	4 x regions of mass loss
c-TiO$_2$heaA	100 - 225	0.025	Endothermic	225 – 425 425 - 650	0.07 0.025	Exothermic Exothermic	3 x regions of mass loss

Each of the thermal decomposition processes from each modified TiO$_2$ material resulted in different qualitative and quantitative information about physical changes in the sample. A careful description of the responses to the prescribed temperature, heating rate and the inert atmosphere (N$_2$-rich) from these interactions were needed to predict the resulting spectra. By combining major

constituents of the modified TiO_2 material, one can use the obtained spectra to study decomposition and thermal stability, which have the largest contribution when identifying the best TiO_2 material.

The findings from these studies suggest an indication that incorporation of TiO_2 to these surface modifiers had no influence on the beginning of its thermal degradation. These results are in good agreement with the work of Zoccal and his colleagues (2009), where they applied the TGA characterization techniques for assessing nanosized TiO_2. Overall, the stability of the chemical adsorption was evident in the TGA/DTA results of the surface modified TiO_2 samples. In all samples prepared, the maximum weight loss was less than 2 %.

4.3.2 Fourier Transform Infrared Spectroscopy

The surface modified TiO_2 nanoparticles were then investigated using Fourier transform infrared spectroscopy (FTIR) for their absorption over a wide spectral range (400 – 4000 cm^{-1}). A detailed overview of an FTIR spectrometer was presented in section 2.7.7. The results of the FTIR assessment are shown in Table 4.10.

Table 4.10   Identification of functional groups present in the surface modified TiO_2 nanoparticles

Wavenumber (cm^{-1})	Functional Group
3350	-OH stretch
2883	-CH stretching vibration
2162	-CH stretching vibration
1541	$-NH_2$ stretch
1098	Si-O-C stretching mode
1001	C-O stretch
689	Ti-O-Ti bonding

The table (Table 4.10) assigned the peaks obtained to their respective functional groups. Thus, in Figures 4.8 and 4.9 the functional groups and the respective wavenumbers are depicted.
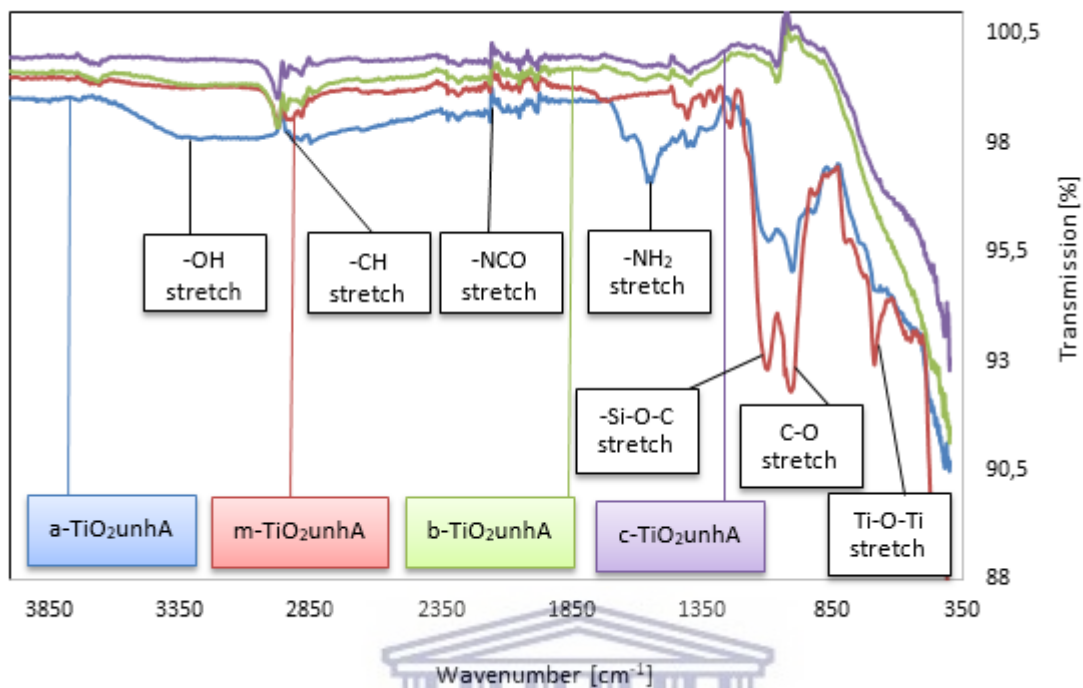
Figure 4.8. FTIR spectra of the modified unannealed TiO$_2$ nanoparticles

The analysis of the FTIR spectra from the surface modified TiO$_2$ nanoparticles before heat treatment indicated the following: a weak absorption peak at 3350 cm^{-1} indicating the presence of the hydroxyl groups –OH of the TiO$_2$ nanoparticles. This region was depicted as a measure of hydrophobicity and hydrophilicity of the surface modified TiO$_2$ materials. A weak peak in this case resulted in high hydrophobic behaviour by the TiO$_2$ material and vice versa. Strong absorption peaks in this area (3000-3400 cm^{-1}) would have indicated high hydrophilicity and were a preferable outcome. With further analysis, a peak at 2883 cm^{-1} was observed and ascribed to a -CH$_2$ stretch, resulting from the asymmetric stretching vibrations. Upon further analysis, there are small zigzag peaks at 2162 cm^{-1} corresponding to a disappearing peak of -NCO groups. Next, peaks were observed at the wavenumber of 1541 cm^{-1}, depicting the characteristic peak of the -NH$_2$ groups, due to the bending vibrations from the primary amines. Strong peaks were also observed between 1098 and 1001 cm^{-1}, which were attributed to Si-O-C and C-O stretch modes, respectively. The overlapping of the peaks was attributed to condensation reactions between the silanol groups. Surprisingly, in the 1098 - 1001 cm^{-1} region, assigned to Si-O-C and C-O stretch modes, the strong peaks were only observed for the a-TiO$_2$unhA and m-TiO$_2$unhA samples, while the two other

samples (b-TiO$_2$unhA and c-TiO$_2$unhA) had one small peak in the 1001 cm^{-1} region. In addition, a peak related to TiO$_2$ nanoparticles that represents Ti–O–Ti could be seen at the low wavenumber region of 689 cm^{-1}. Again, this peak could only be observed in the case of samples (a-TiO$_2$unhA and m-TiO$_2$unhA).
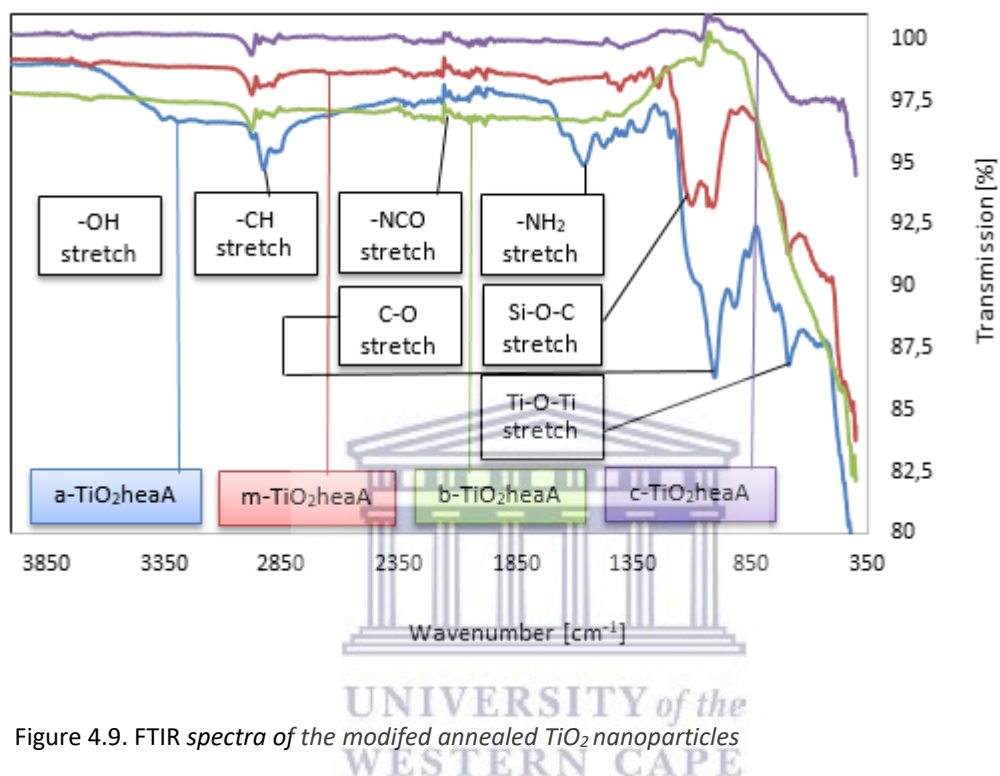
Figure 4.9. FTIR *spectra of the modifed annealed TiO$_2$ nanoparticles*

For the annealed TiO$_2$ nanoparticle samples, the following peaks were observed: a weak absorption peak at 3350 cm^{-1} indicating the presence of the hydroxyl groups –OH absorbed by the TiO$_2$ nanoparticles. Again, the peak at 2883 cm^{-1} was observed and ascribed to a -CH$_2$ stretch, resulting from asymmetric stretching vibrations. As before, small zigzag peaks at 2162 cm^{-1} were observed corresponding to a disappearing peak of -NCO groups. As before, peaks were observed at the wavenumber of 1541 cm^{-1}, depicting the presence of characteristic peaks of the -NH$_2$ groups, due to the bending vibrations from the primary amines. Strong peaks were also observed at 1098 and 1001 cm^{-1}, which were attributed to Si-O-C and C-O stretch modes, respectively. Again, the overlapping of the peaks was attributed to condensation reactions between the silanol groups. Finally, peaks of TiO$_2$ nanoparticles were observed that represents Ti–O–Ti bonds in the samples at the low wavenumber region of 689 cm^{-1}. Similar observations were also documented by Zhao and

colleagues (2012) when they studied the surface modification of TiO₂ nanoparticles with silane coupling agents.

4.3.3 High Resolution Scanning Electron Microscopy Observation of the modified TiO₂ nanoparticles

The High Resolution Scanning Electron Microscopy (HRSEM), reviewed in section 2.7.4, can resolve properties such as crystal structures, thermal stability, morphology and mechanical properties. The HRSEM technique helped to understand how the various surface modifiers impacted on the morphology and crystal structures of the TiO₂ nanoparticle samples. Figure 4.10 HRSEM micrographs images of the TiO₂ nanoparticle samples prepared from the different surface modifiers.

(a)   (b)   (c)

(d)   (e)   (f)

(g)　　　　　　　　　　　　　　　(h)
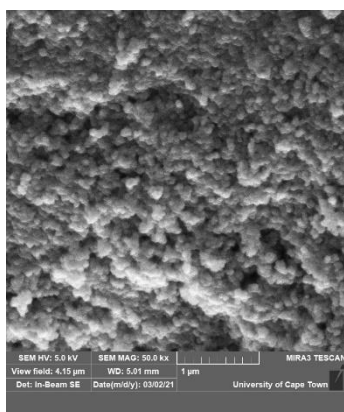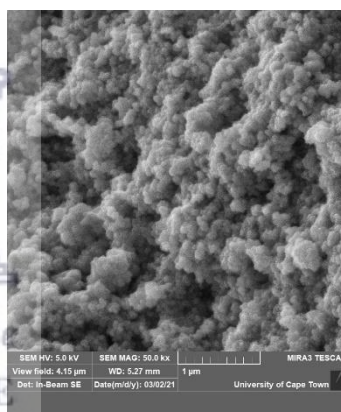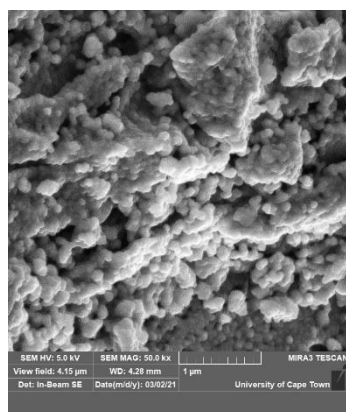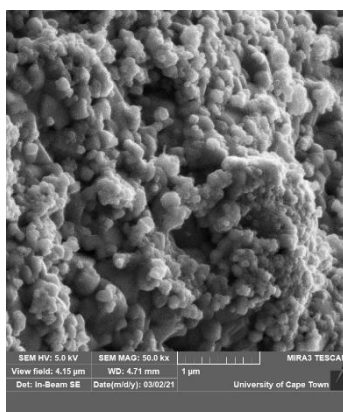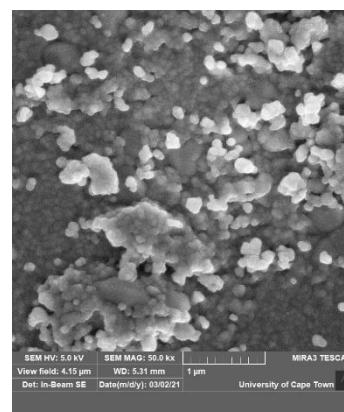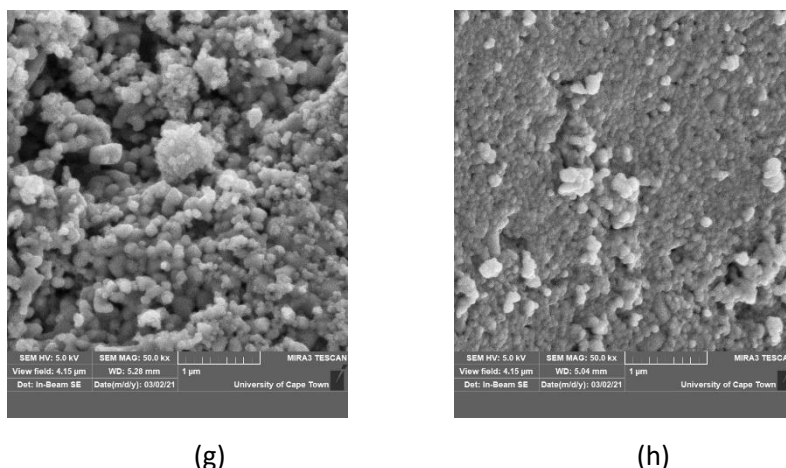
Figure 4.10: High Resolution Scanning Electron Microscopy micrographs of the surface modified TiO₂ nanoparticles. From left to right: (a) a-TiO₂unhA, (b) a-TiO₂heaA, (c) m-TiO₂unhA, (d) m-TiO₂heaA, (e) b-TiO₂unhA (f) b-TiO₂heaA, (g) c-TiO₂unhA and (h) c-TiO₂heaA

Based on the HRSEM images for the annealed TiO_2 samples (b, d, f and h), their surface morphology appeared less defined when compared to the unheated samples. It should also be noted that there was a visible increase in grain size which was attributed to annealing during heating when the TiO_2 samples were prepared. In addition, the annealed TiO_2 sample images revealed non-uniformity and which resulted in difficulty of estimating the nanoparticle sizes. The HRSEM images indicated caution when applying heat after surface modification of TiO_2 nanoparticles for the use in the $^{68}Ge/^{68}Ga$ generator systems. The unannealed TiO_2 samples (a, c, e and g), revealed spherical and agglomerated particles. Upon further analysis, it was revealed that nanoparticles of the unannealed TiO_2 samples were not well dispersed and thus meant that a medium that was able to disperse nanoparticles was required. Taken together, these results suggested nanoparticle size between 25 and 75 nm, at which size the TiO_2 nanoparticles in the production of a $^{68}Ge/^{68}Ga$ generator system was maximum.

To simplify the results in order to gain knowledge of the elemental composition of the TiO_2 materials at the time of SEM analysis, five energy Dispersive X-Ray Analysis (EDS) spectrums from each analysis were taken and a summary of their respective results can be found in Figure 4.11.
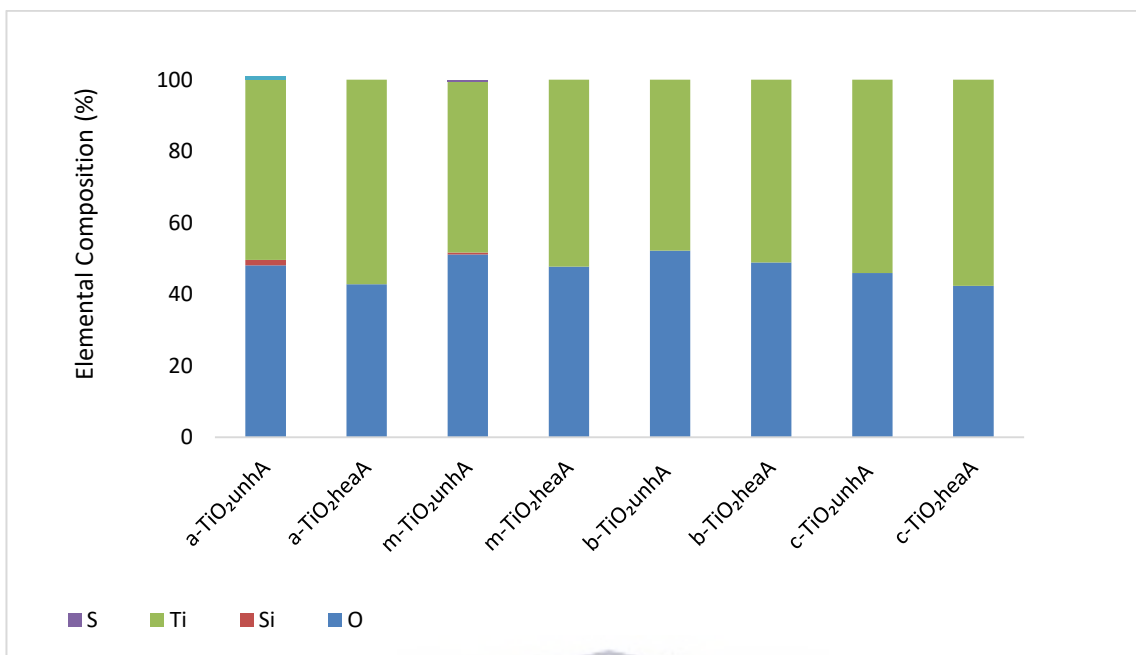
Figure 4.11: Energy Dispersive X-Ray Analysis (EDS) elemental bar graphs of the surface modified TiO₂ nanoparticles

It was useful here to analyse the energy spectrums of the surface modified TiO$_2$ nanoparticles in order to determine the abundance of the specific elements in the samples. The process commenced with identification of the unknown elements prior to quantitative analysis. During the investigation into the elemental analysis using the 3-APTES surface modifier, there were irregularities in the elemental composition, due presumably to the heating applied on one of the TiO$_2$ samples. It was observed that the unheated TiO$_2$ sample contained small but significant amounts of Si elements. Further investigation indicated that this unevenness clearly related to the surface modifier used during the preparation stages was removed upon heating. A 50:48 ratio (Ti and O, respectively) was achieved for the a-TiO$_2$unhA. On the other hand, the a-TiO$_2$heaA sample has a 57:42 ratio for the Ti and O elements, respectively.

Similarly, irregularities were observed in the elemental composition when the TiO$_2$ samples were surface modified using the 3-MPTMS. Like before, when the 3-APTES was used, an additional slightly smaller Si element was identified. Again, the Si elements suggested that the modifier was being incorporated into the TiO$_2$ nanoparticle. As before, upon heating, the Di element was removed and the annealed TiO$_2$ sample able revealed a spectrum without this contaminant. A

47:51 ratio (Ti and O, respectively) was achieved for the a-TiO$_2$unhA. On the other hand, the a-TiO$_2$heaA sample had a 52:47 ratio for the Ti and O elements, respectively.

Next, the investigation using the bis(3-aminopropyl) amine revealed no additional changes in the content of each sample after each functionalisation step. A 48:52 ratio (Ti and O, respectively) was achieved for the b-TiO$_2$unhA. On the other hand, the b-TiO$_2$heaA sample has a 51:49 ratio for the Ti and O elements, respectively.

Finally, the investigation into the elemental analysis of the modified TiO$_2$ samples using the 2-chloro-4,6 dimethoxy-1,3,5 triazine silane, also revealed no additional changes in the content of each sample after each functionalisation step. A 51:49 ratio (Ti and O, respectively) was achieved for the c-TiO$_2$unhA. On the other hand, the c-TiO$_2$heaA sample has a 54:46 ratio for the Ti and O elements, respectively.

The introduction of the Si contaminant by the surface modifiers is of concern in light of the surface modification experiments, but the significance here is too small to be able to constrain the TiO$_2$ adsorbent. Therefore, the focus of the analysis in this chapter was on the surface modification method. To better understand the impact caused by the Si contaminant, quality control measurements of the eluted ^{68}Ga will be performed. The quality control methods of the eluted ^{68}Ga has been discussed in detail in section 3.2.7.

4.3.4 Crystal phase of the modified TiO$_2$ nanoparticles

Characterisation by an XRD instrument was applied in order to gain insight into the structure of crystalline material, as detailed in Section 2.7.2. Figure 4.12 and 4.13 show the X-ray diffraction patterns of TiO$_2$ nanoparticle samples prepared from different surface modifiers. The unannealed surface modified TiO$_2$ materials were compared to the annealed surface modified TiO$_2$ materials.
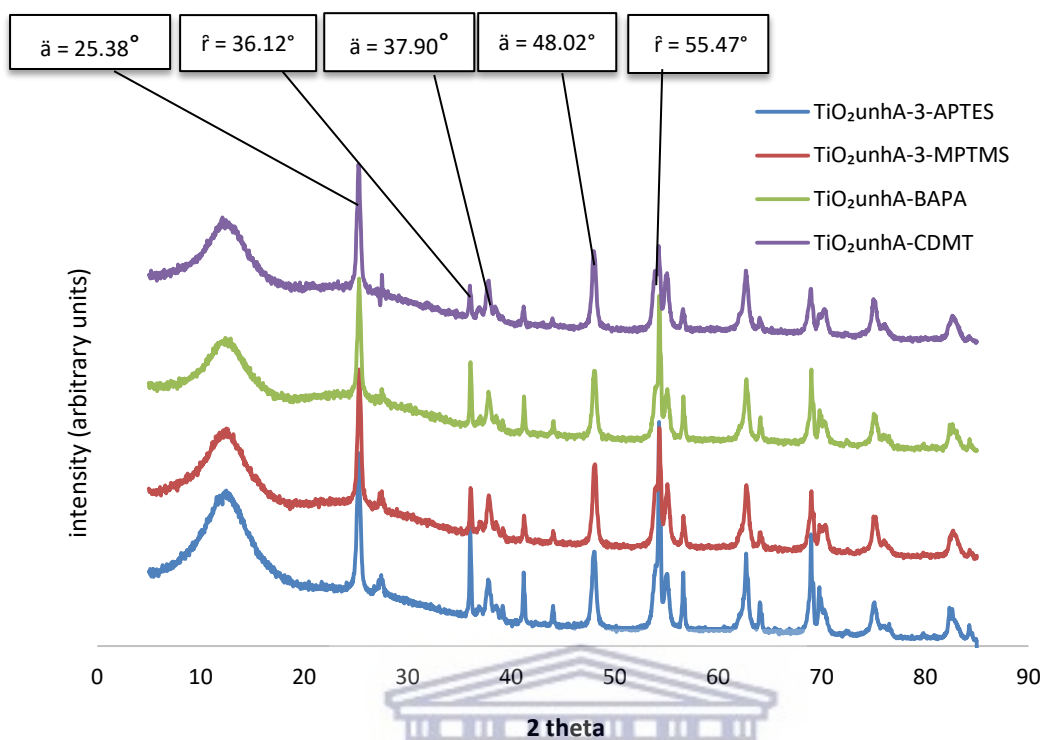
Figure 4.12: XRD patterns of the modified unannealed TiO₂ nanoparticles

The XRD analysis revealed peaks that were consistent with the standard XRD data of the anatase TiO₂ phase (diffraction peaks at 25° and 48°, Appendix H, Pattern No. 00-21-1272). Figure 4.12 illustrates that the surface modified TiO₂ samples did not undergo phase transformation as a result of the modification methods applied, indicating their structure remains unchanged. The broadening of the peaks indicated very small size crystals. The calculated crystallite size of the TiO₂unhA nanoparticles after modification with the 3-APTES, 3-MPTMS, BAPA and CDMT by the Scherrer formula (equation 4.1) were about 24-38 nm.
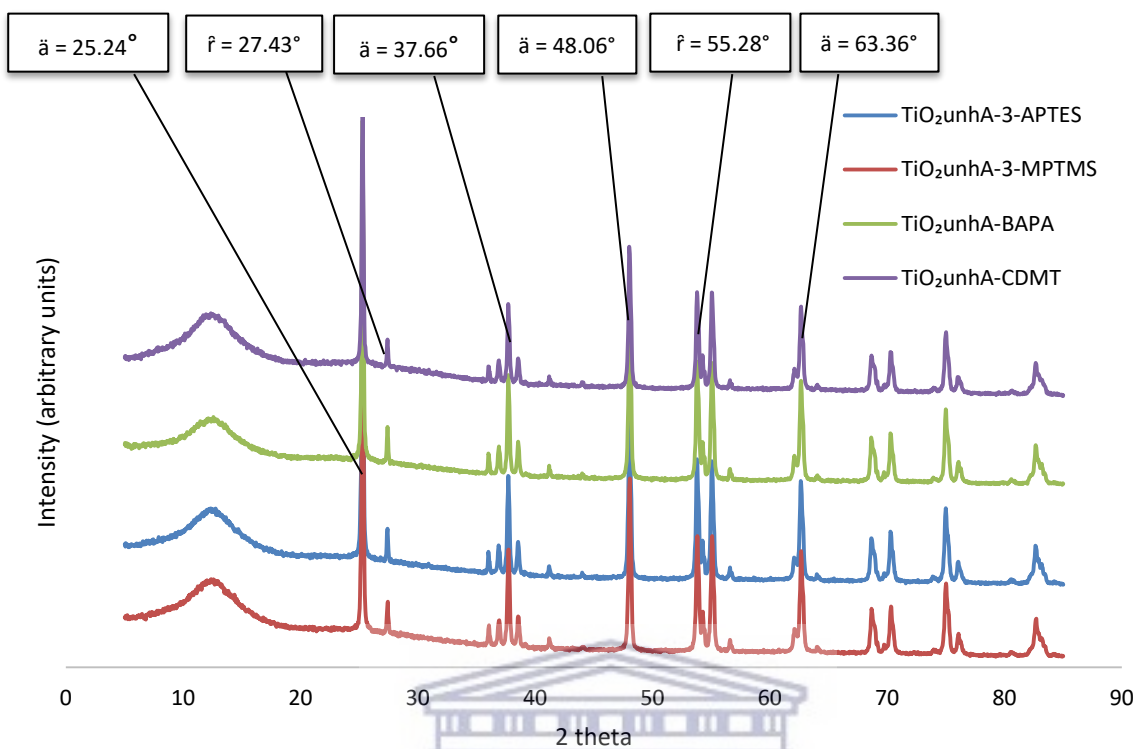
Figure 4.13: XRD patterns of the modified annealed TiO_2 nanoparticles

ä = anatase; r̂ = rutile

Based on the XRD spectra, analysis of the annealed TiO_2heaA nanoparticles revealed XRD peaks of higher intensity, thus an increased degree of crystallinity, as shown in Figure 4.13. As can be seen in Figure 4.13, sharp and well-defined diffraction peaks in the 2θ range of 20–90° were also revealed by the spectra. The results of the XRD patterns of the annealed sample further reveal presence of weak peaks in the regions 27°, 36° and 55° (diffraction peaks of rutile at 27°, 36° and 48°, Appendix I, Pattern No. 00-21-1276). Such a phase transformation resulted from the heat applied and appeared as phase contaminants in the TiO_2 samples. As such, annealed surface modified TiO_2 samples were of limited practical value to the study. The result had also been verified in Table 4.1, where an evaluation of the TiO_2 adsorbents was performed. Table 4.1 illustrate that when anatase and rutile nanoparticles were used under similar conditions, anatase showed much higher performance than the rutile. The calculated crystallite size of the TiO_2heaA nanoparticles after modification with the 3-APTES, 3-MPTMS, BAPA and CDMT by Scherrer formula in equation 4.1 was between 33-67 nm.

The results of this investigation did not show which surface modification method had the most impact within the context of the ^{68}Ge/^{68}Ga generators. The findings imply that the various surface modification methods could not be determined by the use of the XRD technique and further characterisation was needed.

4.3.5 Nitrogen (N$_2$) adsorption characteristics of the modified TiO$_2$ nanoparticles

The benefit of this approach is that morphological characteristics of interest such as surface area, pore volume and pore size distribution were studied. N$_2$ adsorption isotherms were conducted on all the surface modified TiO$_2$ nanoparticles to measure their surface areas which may influence their effectiveness. Thereafter, pore textures of the eight surface modified TiO$_2$ samples were identified by means of plotting of the N$_2$ isotherms. Finally, taken together, the results for each sample were tabulated in order to simplify data for interpretation purposes. N$_2$ isotherms analyses of the modified TiO$_2$ samples are shown in Figure 4.14 and 4.15. The approach was such that samples prepared without annealing are shown together and those annealed are also grouped together.

(a)   (b)

(c)   (d)
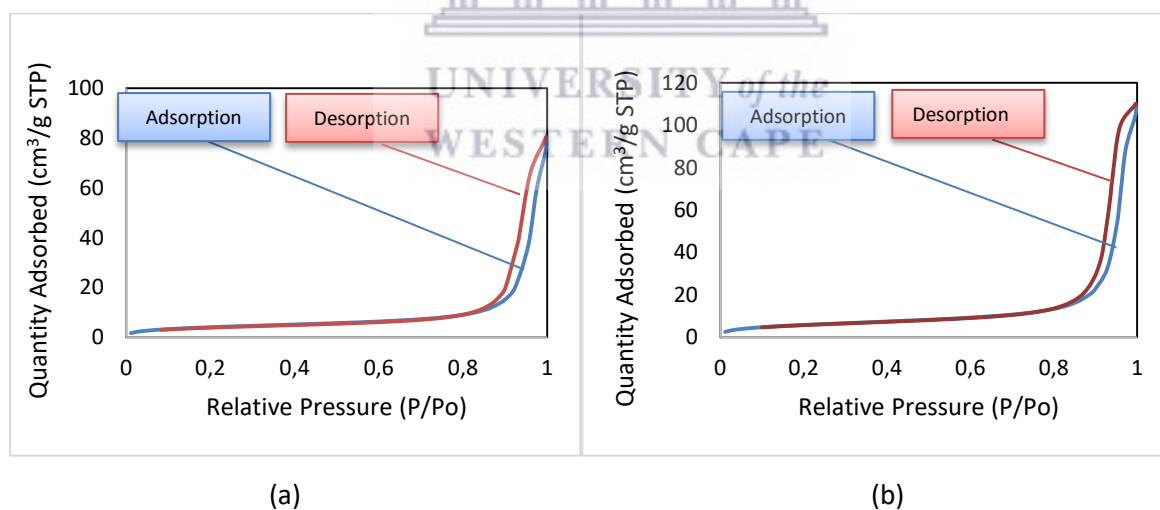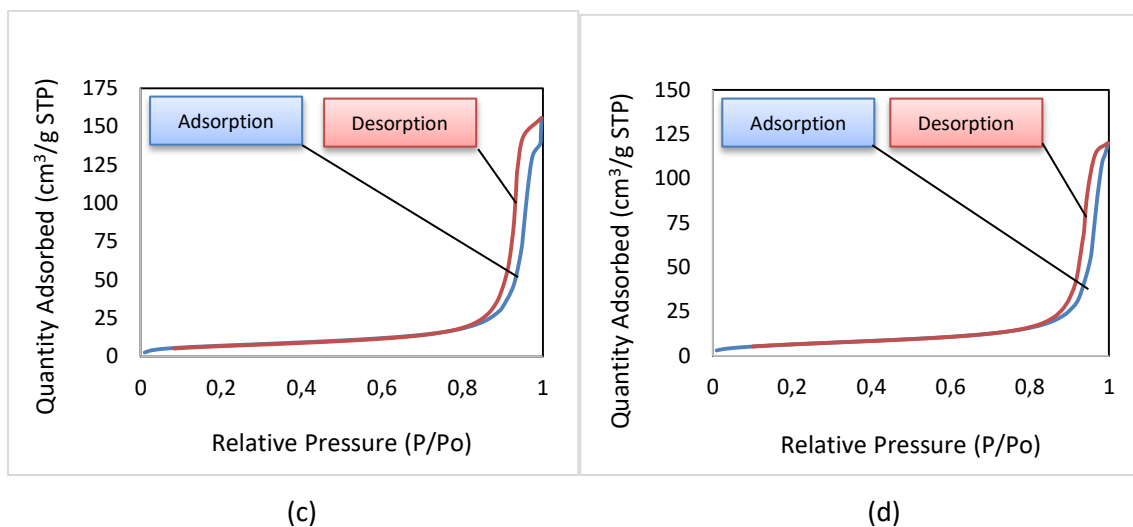
Figure 4.14. Sorption isotherms of N$_2$ on (a) a-TiO$_2$unhA, (b) m-TiO$_2$unhA, (c) b-TiO$_2$unh and (d) c-TiO$_2$unh

Figure 4.14 shows that the un-annealed surface modified TiO$_2$ nanoparticles exhibited a type II adsorption isotherm with a type H1 hysteresis loop in the relative pressure of 0.8 – 1.0 according to the IUPAC classification. Type II curves are an indication of macroporous solids characterised by stronger adsorbate and adsorbent interactions. In addition, the presence of H1 hysteresis loop was an indication of pores of uniform size and shape.

(a)   (b)
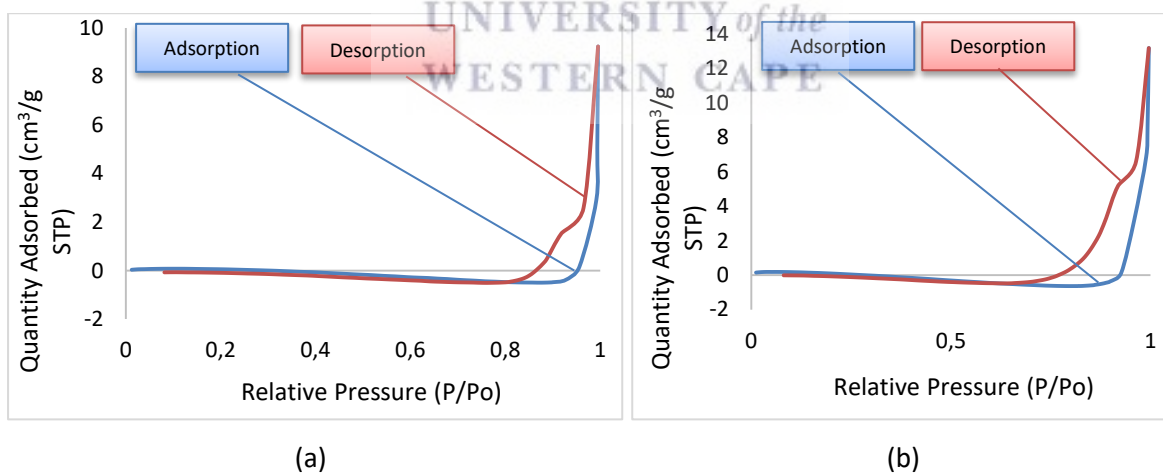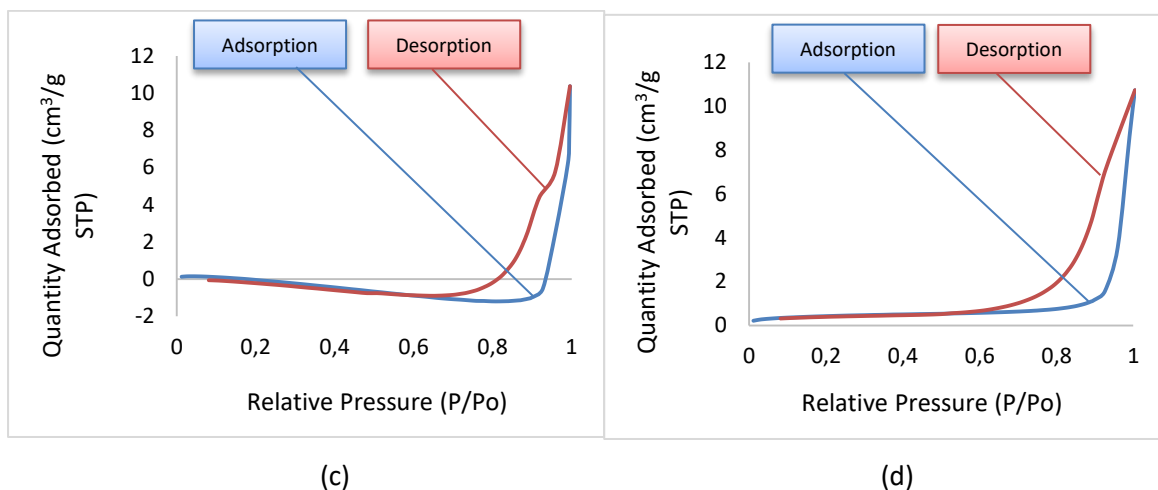
Figure 4.15. Sorption isotherms of N$_2$ on (a) a-TiO$_2$heaA, (b) m-TiO$_2$heaA, (c) b-TiO$_2$heaA and (d) c-TiO$_2$heaA

In contrast, N$_2$ isotherm shapes from the annealed surface modified TiO$_2$ nanoparticles exhibited type I adsorption isotherm with a type H1, H2 and H3 hysteresis loop in the relative pressure of 0.6 – 1.0 according to the IUPAC classification. In this case, type I curves are an indication of microporous solids. Unlike macroporous solids, interaction is between pore walls and adsorbate. This type of interaction is unfavourable since more pressure is required for the filling of the pores by the adsorbed molecules. As before, presence of both H1, H2 and H3 hysteresis loops was associated with solids consisting of non-uniform size or shape particles. In addition, H3 hysteresis loop are found on solids containing agglomeration. The most striking thing about Figure 4.15 was the shape of the isotherms under investigation with the exception of the *c*-TiO$_2$heaA.

A negative slope could be noticed when the curves resulting from the *a*-TiO$_2$heaA, *m*-TiO$_2$heaA and *b*-TiO$_2$heaA samples were analysed. This condition was unfavourable and was attributed to incomplete degassing of the TiO$_2$ material. Another fundamental difference between the annealed samples and c-TiO$_2$heaA sample was that no H2 or H3 characteristics were observed. The findings imply that the annealed surface modified TiO$_2$ samples provided no improvement envisaged by annealing. Their characteristics was deemed as unsatisfactory and not beneficial being less likely to work as [68]Ge adsorbents and as such no further BET analysis was performed on these annealed samples.

4.3.5.1 Surface Area Analysis of the TiO$_2$ nanomaterials

In addition to the N$_2$ sorption isotherms characteristics, Figure 4.16 shows the pore width of the modified unheated TiO$_2$ materials plotted against the cumulative pore area, while in Figure 4.17, the heated materials are shown. In a number of publications (Ren et al., 2009 and Hirano et al., 2004) it has been reported that the addition of surface modifiers to titanium dioxide not only improves the mechanical properties, but gives the TiO$_2$ particles highly developed specific surface areas. In turn, all authors agree that a parameters such as the specific surface area of inorganic oxide system play an important role in the adsorption and functionalisation of the TiO$_2$ surface and its effectiveness. Firstly, the four surface modifiers (see section 3.4.1) were examined for their degree of enhancement of surface area on the TiO$_2$ material when heat was not applied. Secondly, the investigation was carried out using TiO$_2$ materials that were subjected to preheat treatment (see section 3.4.1 for experimental details) and then analysed for their surface area alterations. This is shown with the curves in Figure 4.16 and Figure 4.17, respectively.
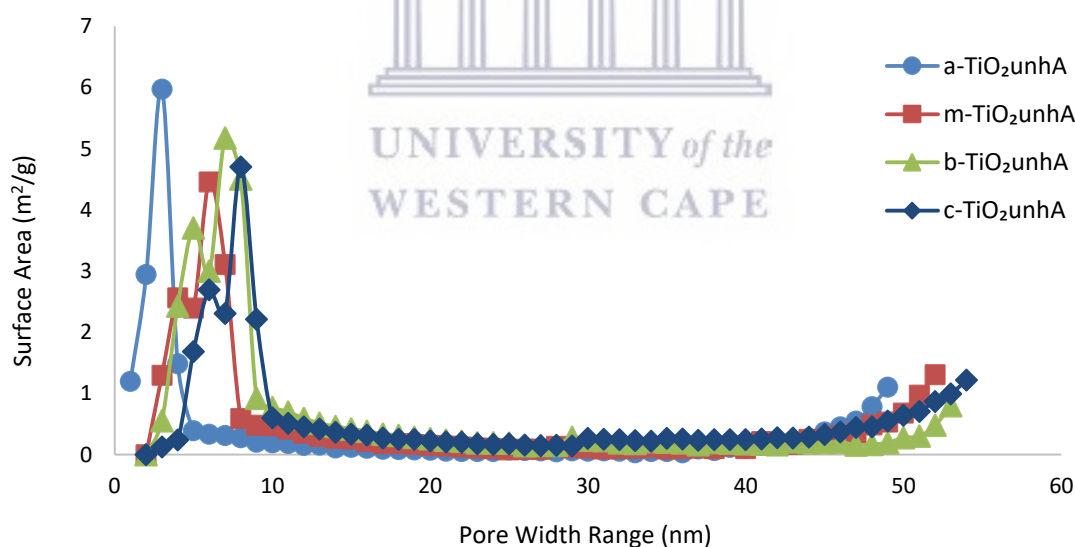
Figure 4.16. Comparison of pore width versus cumulative pore area for the different unannealed surface modified TiO$_2$ materials

The analysis of the surface areas using and pore widths gave a more realistic assessment of the pore size distribution and ultimately effectiveness of the use of the un-annealed TiO_2 materials. Significant differences in the pore width analysis using the BJH technique were present (Figure 4.16). The pore size distribution, as interpreted by BJH theory (Figure 4.16) show TiO_2 samples which comprises of macro and meso porous nanoparticles. The synthesized TiO_2 and showed high meso porosities with different pore sizes ranging from 17 to 46 nm. Remarkably, the surface areas of all the modified TiO_2 samples were significantly improved when compared with finding where no modification was performed (Figure 4.6). It was clear that the surface areas of the TiO_2 samples were enhanced by the silane coupling agents applied. Lastly, the findings in Figure 4.16 revealed the following order of results: a-TiO_2unhA > m-TiO_2unhA > b-TiO_2unhA > c-TiO_2unhA.

Because of the practical importance of the findings, it was decided to examine the effect of temperature on surface area on surface area.
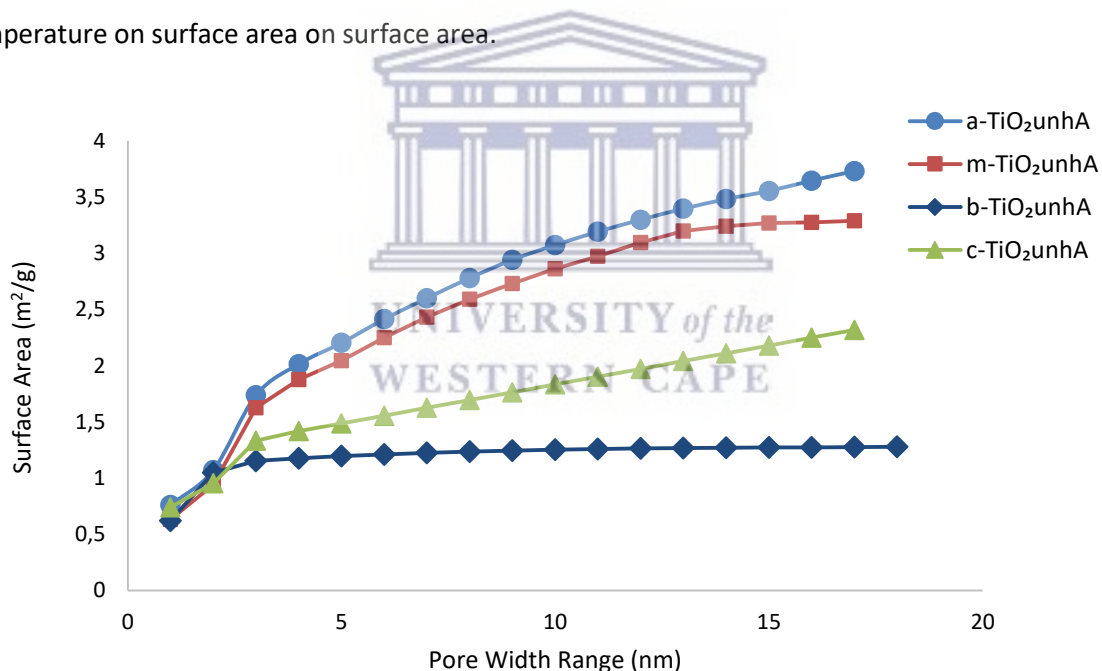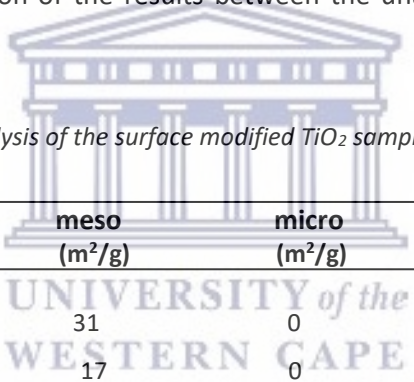
Figure 4.17. Comparison of pore width versus pore area for the different annealed surface modified TiO_2 materials

Samples a-TiO_2heaA, m-TiO_2heaA, b-TiO_2heaA and c-TiO_2heaA produced similar curve shapes, which agrees very well with the N_2 isotherms obtained in section 4.3.5. While sufficiently high calcination temperatures are needed in order to completely remove the organic matter, surface

modified TiO$_2$ materials had a strong tendency to sinterize at high temperatures and the TiO$_2$ structure collapsed at temperatures ≥700 °C. This, did compromise the surface area of the anatase phase, which might be due to the collapsed pores being constituted by the large crystallites in the samples. Thus, the calcination method caused a collapse of the mesoporous microstructure since signs of hydrophilic blockage were visible. The above findings were in good agreement with the work by Chen and colleagues (2016), which indicated that that both pore volume and surface area decreased as the temperature increased. The authors proposed that as the annealing temperature increases, the total surface area decreases. Similar observations were also reported by Raj and Viswanath in the year 2009. These authors investigated effects of surface area, pore volume and particle size on the phase transformation of anatase to rutile. Using XRD and BET analysis, the authors proved that conversion of anatase to rutile leads to lowered surface area and pore volume.

Finally, in Table 4.11, a comparison of the results between the unannealed and annealed TiO$_2$ samples is presented.

Table 4.11. Summary of the BET Analysis of the surface modified TiO$_2$ samples

Sample	macro (m^2/g)	meso (m^2/g)	micro (m^2/g)	BET Surface Area (m^2/g)
a-TiO$_2$unhA	15	31	0	46
m-TiO$_2$unhA	6	17	0	26
b-TiO$_2$unhA	4	15	0	22
c-TiO$_2$unhA	3	12	1	17
a-TiO$_2$heaA	0.7	2,3	0	3,6
m-TiO$_2$heaA	0,7	3,6	0	3,1
b-TiO$_2$unhA	0,6	3,2	0	2,2
c-TiO$_2$unhA	0,6	1,2	0	3,6

When the prepared TiO$_2$ samples were compared, as included in Table 4.11, it was shown how the unannealed samples annealed possessed higher surface area and pore areas. The results were able to confirm that large pore size of the mesoporous TiO$_2$ samples was favourable for the adsorption of inorganic nanoparticles. The data for the annealed TiO$_2$ materials are shown for comparison

purposes. BET surface area decreased from ~ 46 m^2/g (samples a-TiO$_2$unhA, m-TiO$_2$unhA, b-TiO$_2$unhA and c-TiO$_2$unhA to 1.4 m^2/g (sample a-TiO$_2$heaA, m-TiO$_2$heaA, b-TiO$_2$heaA and c-TiO$_2$heaA). In addition meso porous nature is known for consisting of well-ordered mono layered mesoporous TiO$_2$, leading to highly accessible surface area for effective access, enabling excellent rate capability. Thus to summarize, the observed experimental results of the present work highlighted the significant impact of unannealing in modifying TiO$_2$ nanomaterials for ability to perform as ^{68}Ge/^{68}Ga generator adsorbents.

4.3.6 BET analysis summary of the surface modified TiO$_2$ nanomaterials

The characterisation analyses of the surface modified TiO$_2$ samples using TGA, FTIR, XRD, SEM, and BET techniques provided information about the role that surface modification is able to play in the development of TiO$_2$ based ^{68}Ge/^{68}Ga generators. From the data obtained, it is readily apparent that surface modification is economically possible provided several intermediate steps are considered. In addition, qualification of the characteristics of the porous TiO$_2$ materials yielded the following results:

(a) From the TGA graphs (Figure 4.7), it was revealed that the a-TiO$_2$unhA revealed less mass change over the entire spectrum of the temperature. It was concluded that this sample was able to maintain its properties as nearly as unchanged as possible on heating.

(b) From the FTIR spectra in Figures 4.8 and 4.9 and Table 4.10, information was provided by the study about the number of peaks present in the surface modified TiO$_2$ samples and their respective functional groups that were observed.

(c) From the scanning electron micrographs, in Figure 4.10, it is apparent that the particle size becomes coarser when the temperature is applied.

(d) The XRD analysis (Figure 4.12 and 4.13), showed the rutile and anatase phases were present through the peak positions obtained, which were essentially in the same positions as before surface modification. Therefore, the surface modification methods did not significantly change the phases of the TiO$_2$ materials. Also XRD analysis was able to confirm that heat treatment was responsible for larger crystallite sizes of the TiO$_2$ materials.

(e) From the N_2 adsorption and desorption isotherms (Figure 4.14 and 4.15), information on porosity and surface areas under a given set of circumstances of the surface modified TiO_2 materials was obtained. The formation of micropores and mesopores was enhanced by the surface modification. When no annealing was applied, micropores and mesopores were the dominating features and when a temperature of >700 °C was applied macropores were dominant so that the surface area attributable the material's pores decreased. This phenomena is confirmed by the present porosity measurements.

These results were consistent with the HRSEM images shown in Figure 4.10, which show extensive degradation of the sample annealed at >700 °C. As pointed out several times in this study, the combination of heat and surface modification did not yield favourable results, for instance, lowered surface area and decreased pore volume. The advantages of BET analysis has been presented in detail previously in section 2.8 with regard to parameters such as pore size and surface area essential for optimisation of adsorbents. Those that are relevant to the aspects discussed in this study are summarized in Table 4.11.

In short, a comparison of the results obtained reveal that when an annealing temperature was applied a worse N_2 adsorption performance was obtained. On the other hand, the opposite was true when un-annealed TiO_2 samples were used. On the basis of these results it is concluded that heat treatment is not preferred as the enhancing factor. From the above considerations it may be concluded that a-TiO_2unhA is probably the most reliable adsorbent and was able to keep the intrinsic TiO_2 properties. In contrast as discussed earlier, when the other surface modifiers were used, clusters and agglomerations were experienced. The presence of agglomeration and clusters eventually decreases the performance of the TiO_2 material.

4.4 Molecular Imprinted Polymer

In this investigation molecular imprinted polymers (MIPs) and non-molecular imprinted polymers (NMIPs) were synthesised for their suitability in the [68]Ge breakthrough control. A typical synthesis procedure is given in section 3.4.2. When the polymers were synthesised, analysis of the particles formed was made as follows: (a) thermogravimetric analysis (TGA) of the samples to determine thermal stability, (b) high resolution scanning electron microscopy (HRSEM) to determine the

structure of the particles and (c) Fourier Transform Infra-red spectroscopy (FTIR) to determine the functional groups of the polymer molecules.

4.4.1. TGA Analysis of the Molecular and Non-Molecular Imprinted Polymers

Thermogravimetric analysis was conducted to determine thermal stability of the MIPs together with their fraction of volatile components by monitoring the weight change that occurs as a sample is heated at a constant rate. The molecular polymer synthesis work was firmly grounded on a comprehensive literature survey by Vasapollo and colleagues (2011). Also, samples before the [68]Ge template imprinting were analysed by TGA to identify thermal stability at this stage. The result were separated accordingly into curves before and after template removal. For both samples, two similar curves were found for each series of runs which showed the effect of temperature variation on the percentage reduction of the sample weight. The curves, (Figure 4.18 and 4.19) were plotted as the temperature in degree centigrade versus the percentage of the mass reduction.
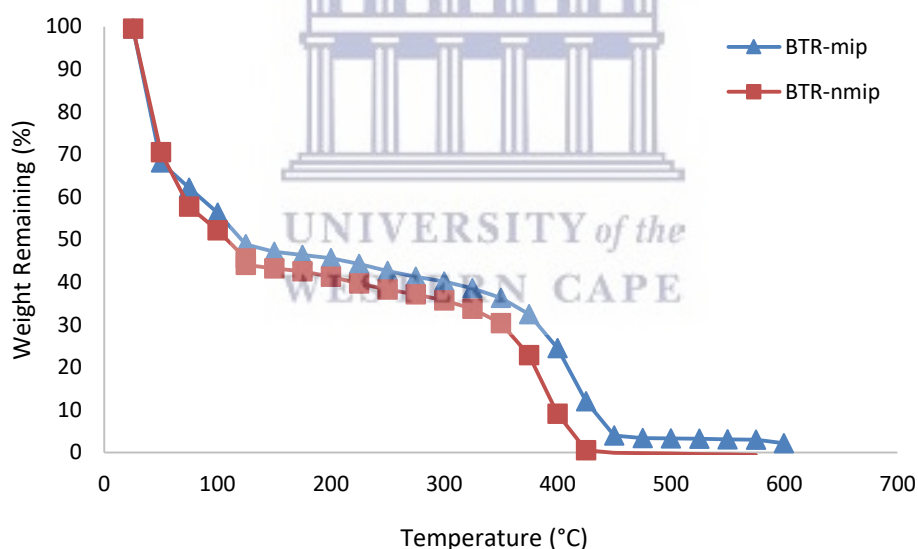
BTR stands for before template removal; ATR stands for after template removal

Figure 4.18. Thermogravimetric analysis of the molecular imprinted polymers (MIPs) and non-molecular imprinted polymers (NMIPs) before [68]Ge template removal
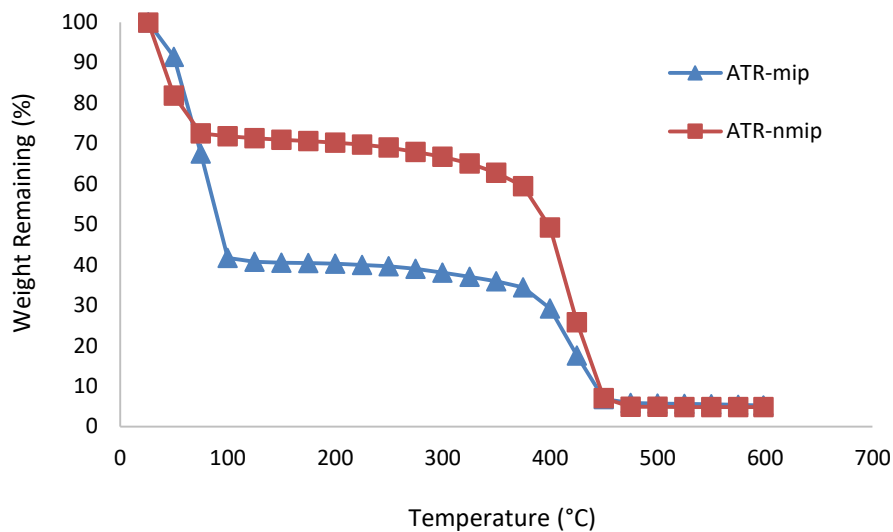
BTR stands for before template removal; ATR stands for after template removal

Figure 4.19. Thermogravimetric analysis of the molecular imprinted polymers (MIPs) and non-molecular imprinted polymers (NMIPs) after ^{68}Ge template removal

The thermograms of the BTR-mip and BTR-nmip samples showed similar kind of degradation patterns. Both samples started decomposition at about 110 °C and displayed final decomposition at a temperature range of 420 to 450 °C. On the final decomposition temperature figures, the BTR-nmip and BTR-mip sample were at 420 and 450 C°, respectively. This discrepancy indicated that BTR-nmip sample had a lower thermal stability compared to the BTR-mip sample. This was confirmation that the BTR-nmip sample has lower molecular weight compared to BTR-mip matrix.

For the BTR-nmip sample, the TGA analysis initially presented a peak corresponding to an endothermic dehydration at a temperature range 50 to 150 °C, corresponding to a weight loss of approximately 50%. With increasing temperature, the material initiated a second minor loss of mass, which was attributed to endothermic dehydration at a temperature range 350 to 450 °C, corresponding to a weight loss of approximately 10%. Next, melting of the BTR-nmip sample was observed at temperatures beyond 450 °C.

For the BTR-nmip sample, similarly, the TGA analysis initially presented a peak corresponding to an endothermic dehydration at a temperature range 50 to 150 °C, associated with a weight loss of approximately 55%. As before, when the temperature was increased, the material initiated a

second minor loss of mass, which was attributed to endothermic dehydration at a temperature range 350 to 450 °C, corresponding to a weight loss of approximately 25%. Next, melting of the BTR-nmip sample was observed at temperatures beyond 450 °C.

In the follow up phase of the study, comparison between presence and absence of the template (Ge) molecule were made using same method as above, except that the Ge template was removed.

Figure 4.19 shows two stages of weight loss for the ATR-mip sample. Almost 60% weight loss was observed at first stage, with temperature range at 50 to 110 °C, which showed the dehydration of water residues from the non-imprinted polymer. The second stage of weight loss occurred in the range of 350 - 450 °C, with a weight loss of 30%. Both peaks were endothermic.

Lastly, the sample containing ATR-nmip showed a first endothermic peak at a temperature of less than 100 °C. A 30% weight loss was observed in this region, corresponding to the dehydration of water residues in the sample. Thereafter, a second weight loss was observed in the entire temperature range used, associated with decomposition of organic matter and loss of water. Since this difference has not been found elsewhere, this behaviour could be attributed with loss of water still present in the sample. A summary of the results obtained is shown in Table 4.12.

Table 4.12: Thermogravimetric analysis (TGA) results obtained for the MIPs and NMIPS

Sample	Initial degradation Temperature (°C) range and weight loss (%)			Second degradation Temperature (°C) range and weight loss (%)			Comments
	T (°C)	W (%)	Endothermic/ Exothermic	T (°C)	W (%)	Endothermic/ Exothermic	
BTr-mip	50 - 150	50	Endothermic	350 - 450	10	Endothermic	2 x regions of mass loss
BTr-nmip	50 - 150	55	Endothermic	350 - 450	10	Endothermic	2 x regions of mass loss
ATr-mip	50 - 110	60	Endothermic	350 - 450	30	Endothermic	2 x regions of mass loss
ATr-nmip	20 - 50	30	Endothermic	50 – 450	55	Endothermic	2 x regions of mass loss

This weight loss between 50 and 60% might be owing to the decomposition of the polychain backbone (Methacrylic acid). The literature was able to reveal a complete degradation of pure Methacrylic acid around 100 °C, as reported by Azhgozhinova et al., 2004. On the other hand, the obtained thermograms revealed a degradation of ethylene glycol diacetate (EGDA) cross linked

with the polychain in the range of 350–450 °C, with the exception of the ATr-nmip sample, which had a range between 50 and 450 °C. A possible explanation for these results may be that higher thermal stability was shown by the samples. In 2019, Maria Guc´ and Grzegorz Schroeder reported similar findings when they successfully prepared molecularly imprinted polymer (MIP) and magnetic molecularly imprinted polymer (mag-MIP) for solid extraction and pre-concentration of quercetin by thermal polymerization method. Though their work was based on Quercetin, a flavonoid most commonly met in plants, they were able to synthesise polymers that are chemically stable, thermally stable and water insoluble, which permits their multiple uses in chemical analysis, and their synthesis process is relatively simple, reproducible and cheap.

4.4.2 High Resolution Scanning Electron Microscopic Characterisation of MIPs and NMIPs

Figure 4.20 is illustrating scanning electron microscopic images of the molecular imprinted polymers (MIPs) and non-molecular imprinted polymers (NMIPs) prepared under the procedure found in section 3.4. In addition, a table was created next to each molecule in order to list elements making up the molecule at the time of measurements.
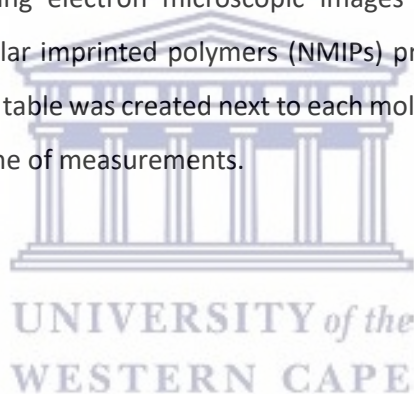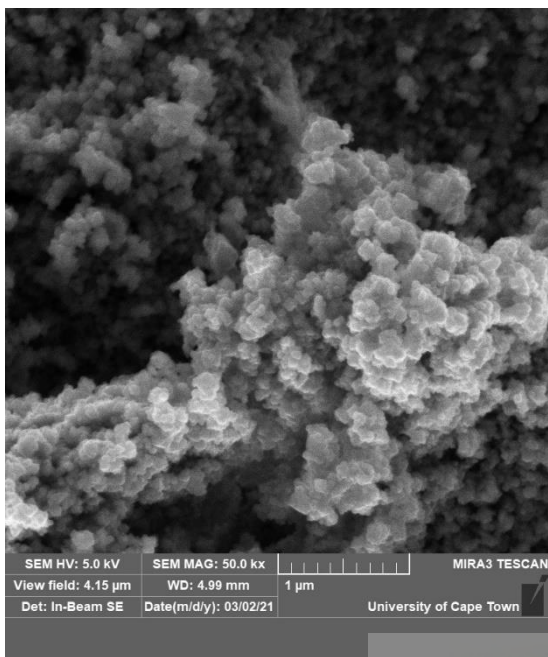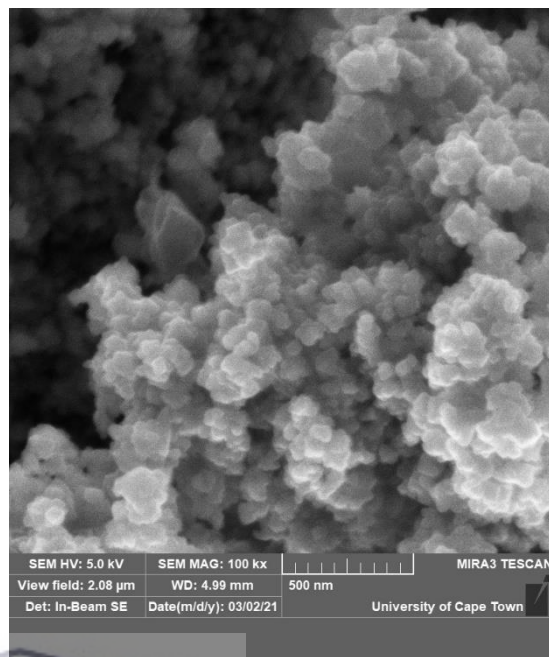
(a) MIP polymers before Ge template removal   *(b) MIP polymers after the Ge template removal*
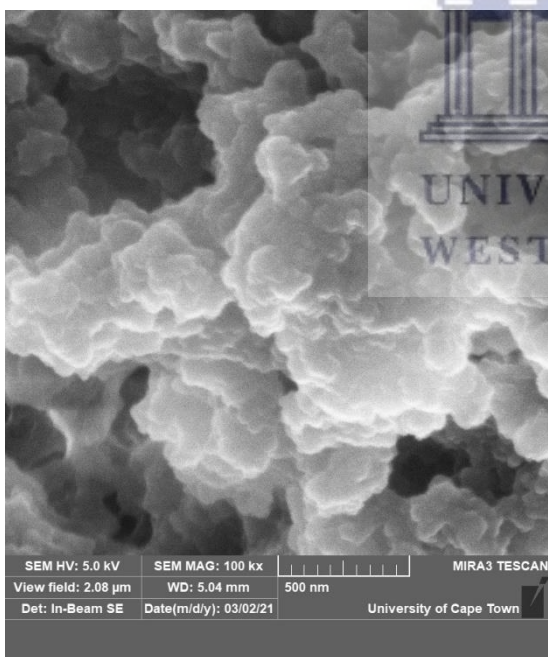
(c) NMIP polymers before Ge template removal   *(d) polymers after the Ge template removal*
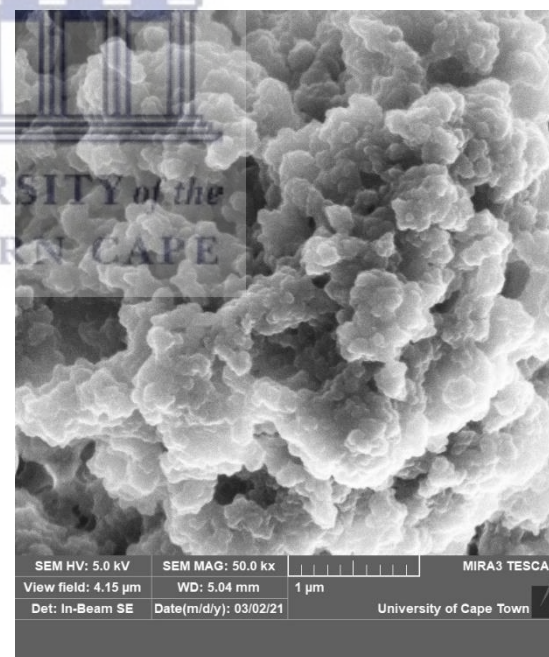
Figure 4.20. SEM images of molecular imprinted and non-imprinted polymers.

As can be seen, the molecular imprinted and non-imprinted polymers had fine pore structures. It was apparent from the micrographs that before the template was removed, agglomeration of the MIP grains was noticeable. On the other hand, the removal of the template provided polymers of less agglomeration. From an elution point of view, when agglomeration is high, this usually leads to back pressuring by the eluent media used for elution. Thus some extra volumes would be provided and this makes it difficult to remain within the prescribed elution volume. Therefore, less agglomeration was favourable. Visual inspection also highlighted uniform shape and size of polymer particles were achieved when the template was removed for the MIPs molecules. The phenomenon explains well that the experimental results confirms that the MIP have high adsorption capacity to germanium.

In contrast to MIPs before and after template removal, a similar image (Figure 4.20, c-d) was observed when non-imprinted molecular polymers were analysed. As can be seen, the nature of the particles obtained after preparation of NMIPs was found to be more irregular. The images also show that the size of the polymer particles increased. It was expected that for the MIPs and NMIPs a similar size was to be found due to similar applied conditions, with one difference being the added Ge template which was later removed. Because of the practical importance of these findings, it was decided to subject the polymers to further investigations such as Fourier Transform infra-red spectroscopy. In Figure 4.21, a quantitative energy dispersive X-ray (EDS) analysis was performed to observe the amount of main chemical constituents such as carbon (C) and oxygen (O) present in the non-imprinted and imprinted polymers.
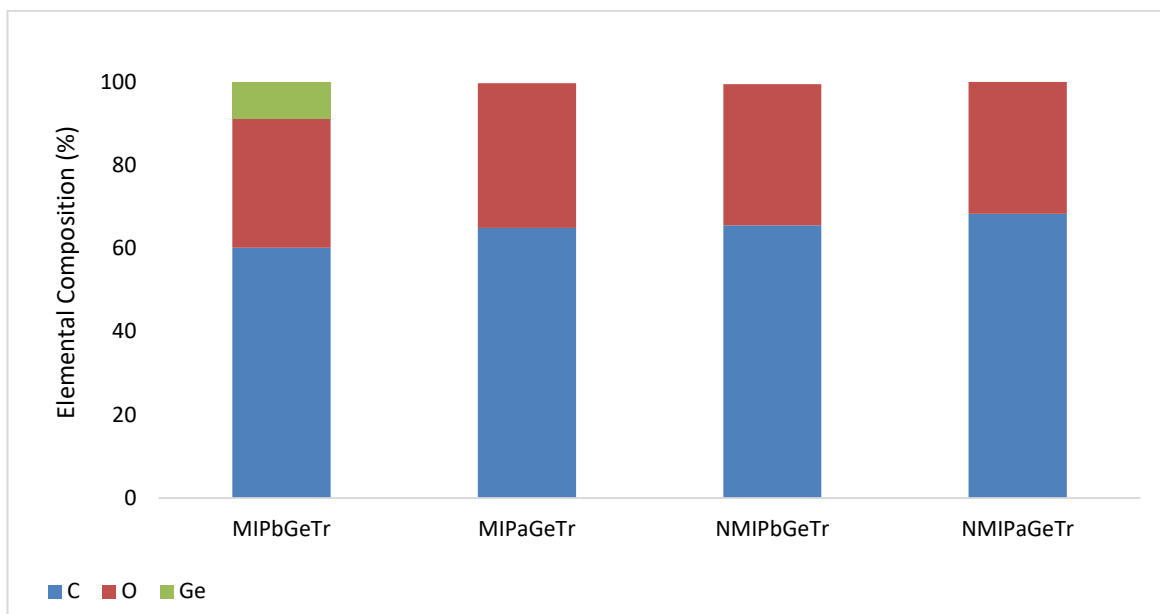
bGeTr stands for before germanium template removal; aGeTr stands for after germanium template removal

Figure 4.21: Energy Dispersive X-Ray Analysis (EDS) elemental bar graphs of the molecular and non-molecular imprinted polymers

It was observed that between 60 to 70% amount of carbon was present in the MIPs and NMIPs sample. This indicated the polymer back bone was mainly composed of carbon with substituent elements present in the chain. Further analysis of the Energy Dispersive X-Ray Analysis (EDS) spectrums showed the presence of germanium, as expected, in the MIP sample before template removal. Elemental analysis was able to reveal that this amount of Ge was completely removed by the method applied for the template removal. The percentage of carbon resulted 60, 65, 66 and 70% for the MIPGeTr, MIPaGeTr, NMIPbGeTr and NMIPaGeTr samples, respectively. Both blanks (NMIPbGeTr and NMIPaGeTr) were able to show similar results (7:3 ratio, C and O, respectively) and a small difference in these values was observed for the MIPaGeTr sample (6:4 ratio, C and O, respectively). Thus, Fourier Transform Infrared Spectrometry (FTIR) was recommended for the analysis of the functional groups of these elements.

4.4.3 FTIR Analysis of Molecular and Non-Molecular Imprinted Polymers

The MIP and NMIP were analysed for their functional groups in the polymer matrix using Fourier transform infrared analysis over the range 400 – 4000 cm^{-1}. To confirm the template removal, FTIR

spectra of the polymers were taken before and after the template removal process. The analyses are given in Table No. 4.13 and are shown in Figure 4.22 and 4.23.

Table 4.13   Identification of molecular imprinted and non-imprinted polymers

Wavenumber (cm^{-1})	Functional Group
3310	O-H stretch
2992	C-H stretching vibration
1740	C=O bending absorption
1450	asymmetric deformation of C-H
1295	C-O stretching vibration
1150	CH$_2$ stretch
1022	C-O-C asymmetrical stretching
755	para substitution
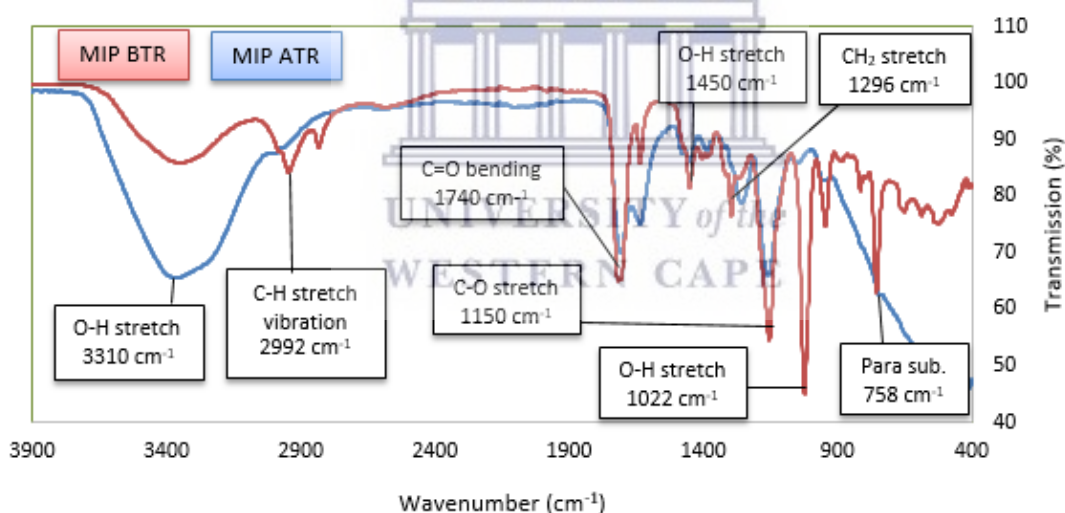
Figure 4.22. FTIR spectra of the molecular imprinted polymers (MIPs) before and after Ge template removal
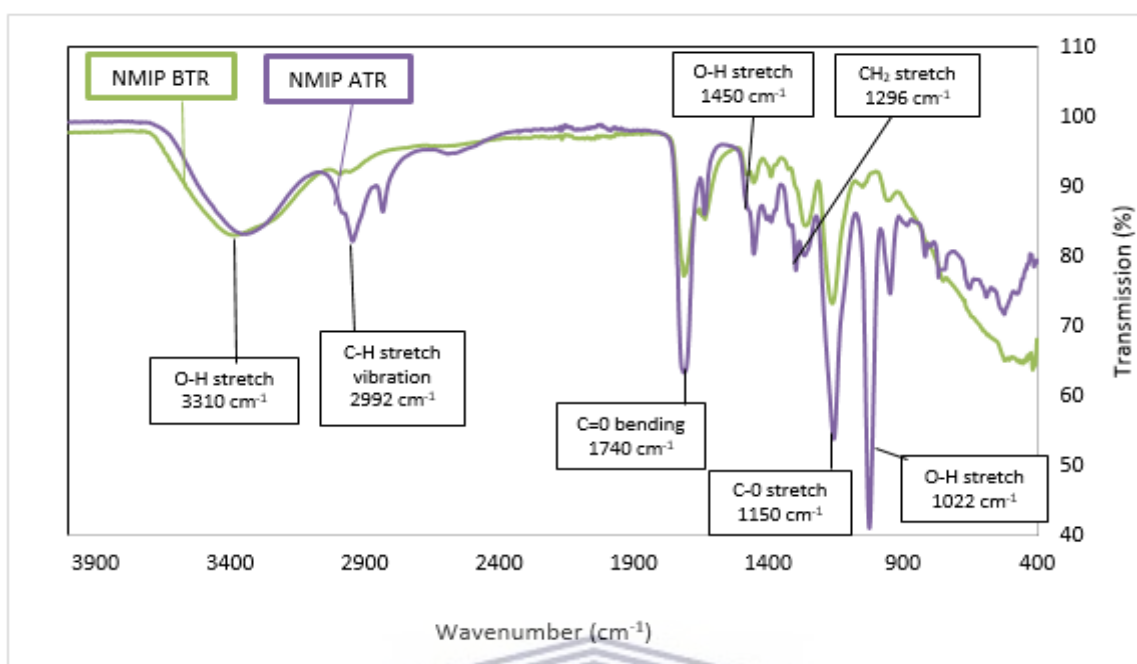
Figure 4.23. FTIR spectra of the non-imprinted polymers (NMIPs) before and after Ge template removal

In Figure 4.23, the spectra for MIPs before and after the Ge template was removed are compared. Both spectra possess broad and strong peaks at approximately $3210 - 3500 \text{ cm}^{-1}$ that corresponded to O-H stretching vibrations. The most obvious differences between the two spectra is the presence of weak peaks for the C–H vibrations at 2992 cm^{-1} for the MIP BTR sample, in contrast to a much lower signal for the MIP ATR particles. This can be attributed to a C_{10} linear alkane chain which is not present in the MIP ATR particles. Both spectra possesses strong peaks at 1740 cm^{-1} corresponded to a carbonyl group C=O double bond bend and originated from the methacrylic acid (MAA) and ethylene glycol dimethacrylate EDMA. The peak at 1450 cm^{-1} corresponded to the C-H bending of amine and carboxylic acid groups in the samples. The peaks at 1296 cm^{-1} and 1150 cm^{-1} belong to the C-N stretching of primary and secondary aromatic amines, respectively. Furthermore, for the molecular imprinted polymer (before the Ge template was removed), a clearly visible peak at the region 1022 cm^{-1} is observed which is not appearing on the MIP ATR spectra. This is attributed to the absorption of C-O-C vibrations in the MIP BTR and is attributed to the overlap with the bending vibration of C–O–Si peak. According to that peak, it could be concluded that the germanium has reacted with MIP molecules and the reaction products contains Ge–O–Ge bonds. The biggest difference between the spectra is the appearance of the Ge-O vibration in the

region 758 cm^{-1} of the MIP BTR particles. This peak implies the presence of the Ge template in the molecule before it was removed. Similarly, in 2016, Yanti and colleagues discussed synthesis and characterization of MAA-based molecularly imprinted polymer (MIP) with D-glucose template. They were able to claim, through the use of FTIR spectroscopy, how their method was able to successfully synthesise molecularly imprinted polymer (MIP) using D-glucose as the template and MAA as the functional monomer.

To assess successful binding and removal of the germanium template onto the MIPs, the second non-imprinted polymer step was conducted (as experimentally illustrated in section 3.4.4). A similar spectra to Figure 4.22 was observed for the NMIPs except the disappearance of the peak in the region 758 cm^{-1}, corresponding to the Ge template. By comparing the FTIR spectra of the MIP before the Ge template removal and MIP after it was removed, it was concluded that the removal process was successful due to the absence of significant peaks. Another attempt at synthesising of molecularly imprinted polymers for the selective extraction and removal of 2,4,6-trichlorophenol was performed by Bhawani and colleagues (2019). The authors considered MIPs could be used as a potential material for the solid-phase extraction and as a stationary phase material for chromatographic separations, after successfully producing MIPs and NMIPs for the selectivity of MIPs towards the template 2,4,6-trichlorophenol.

4.4.4 ^{68}Ga Efficiency and the ^{68}Ge Breakthrough Analysis

The basics of gamma-ray detection measurements, of which detection of the ^{68}Ge is an example, are introduced in Section 3.2.7.2. Also, details and an overview about the Accuspec multichannel analyser and Genie 2000 software (Canberra) instrument were given in section 3.2.7.2. The major advantage about the study of the 511 and 1077 keV emissions is that information about the ^{68}Ga efficiency and the ^{68}Ge breakthrough is gathered and used to define the ^{68}Ge/^{68}Ga generator performance, respectively. After decades of technological advancements, the 511 keV gamma-ray detection, also, allows for the suppression of the atmospheric background through mathematical models. To ensure an uninterrupted data set, a program was developed to elute the surface modified TiO$_2$ based columns on a daily basis for a period of up to six months. Thereafter, the data was loaded on an Excel spreadsheet in order to develop a pattern of the performance of the TiO$_2$ columns for interrogation, comparison and interpretation purposes. Figure 4.24 illustrate an

example of the 511 and 1077 keV from the gamma ray emissions when the ^{68}Ga elutions were conducted using the surface modified TiO$_2$ based column together with the molecular imprinted polymers (MIPs).
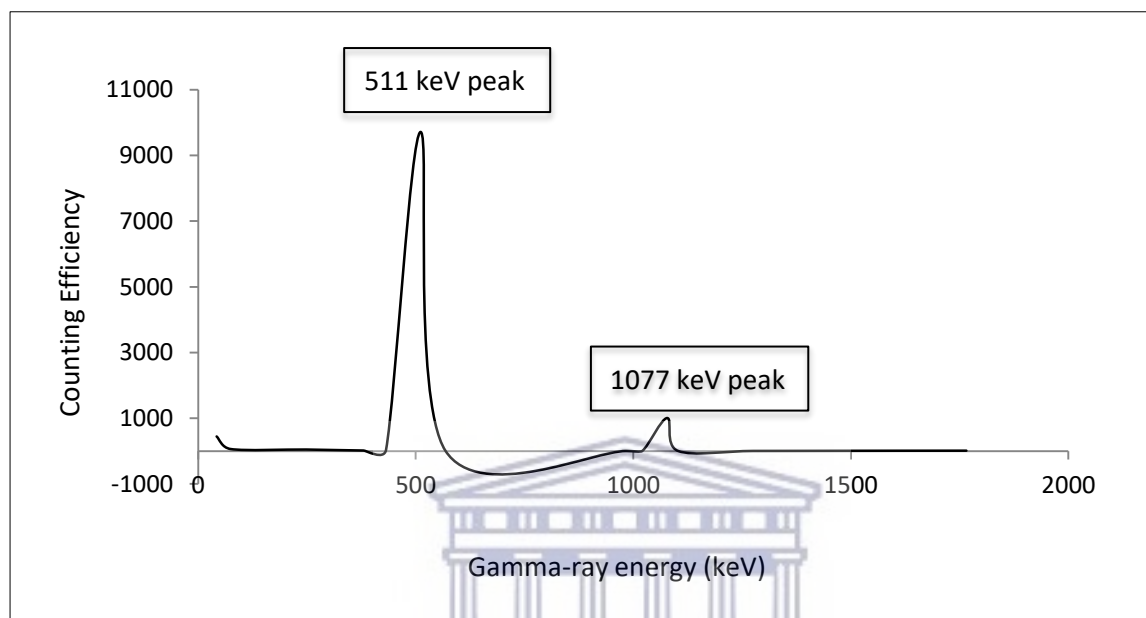
Figure 4.24. The 511 and 1077 keV gamma ray emission of the ^{68}Ga elution when MIPs and NMIPs were used

The 511 and 1077 keV emissions reveal two Gaussian peaks with useful point source distributions to compare the ^{68}Ga and ^{68}Ge radionuclides, respectively. For the ^{68}Ge breakthrough discussions presented in the following section, the examination will only consider the 1077 in relation to the 511 keV distribution since both MIPs and NMIPs were subjected to the same examinations. Lastly, smaller γ-rays were also present but their contributions were very small compared to the 511 and 1077 keV peaks, and were later simply eliminated as background noise.

4.4.5 ^{68}Ge breakthrough analysis using molecular imprinted polymers and non-molecular imprinted polymers

The ^{68}Ge breakthrough measured in this investigation using the surface modified TiO$_2$ nanoparticles was measured under conditions similar to those applied in section 4.1. In this series of experiments, ^{68}Ga efficiencies and ^{68}Ge breakthroughs were studied using the four surface modifiers (3-APTES,

3-MPTMS, BAPA and CDMT, see section 3.3) onto the TiO$_2$ nanoparticles. In a similar manner as in section 4.1, it was possible to modify TiO$_2$ nanoparticles and design an attachment for the molecular imprinted polymers housing for the [68]Ge breakthrough analysis. In the same manner ^{68}Ga efficiency and [68]Ge breakthrough can be calculated using questions 3.3 and 3.4. This way ^{68}Ga elutions were performed and immediately followed by measurements of the spectral shapes and positions as explained in section 3.2.7. It was part of the task of the present work to develop an understanding of the changes, if any existed, within the pH context. Table 4.14 summarises the resulting ^{68}Ga efficiency and [68]Ge breakthrough from the study when the MIPs and NMIPS were used.

Table 4.14. Summary of results obtained by analysis of ^{68}Ga elution on MIPs and non-MIPs with the modified TiO$_2$ based [68]Ge/^{68}Ga generators, (n=3)

Material	[68]Ge Retention (%)	[68]Ga Elution (%)	[68]Ge Breakthrough (%)	pH
3-APTES (MIP)	77	90	0.001	1.0
3-APTES (NMIP)	70	67	0.01	1.0
3-MPTMS (MIP)	71	84	0.007	1.0
3-MPTMS (NMIP)	68	80	0.01	1.0
BAPA (MIP)	69	77	0.002	1.0
BAPA (NMIP)	67	72	0.06	1.0
CDMT (MIP)	66	33	0.05	1.0
CDMT (NMIP)	64	21	0.1	1.1

As mentioned earlier in section 4.1.1, an optimum [68]Ge retention is achieved when a retention of 100% is obtained with the respective surface modified TiO$_2$ nanoparticles. One problem common to all the surface modifier investigational techniques is that none of the TiO$_2$ columns was able to load [68]Ge up to 100%. Thus, the highest [68]Ge retention obtained was 77% (3-APTES), indicating a 23% loss due to the capacity of the column material. It was established in Section 4.1.1 that the [68]Ge retention is 100%, when the unmodified anatase phase was utilised. Thus, in this series the [68]Ge retention capability of the column material was reduced when surface modification of the TiO$_2$ nanoparticles was conducted. However, it is perhaps surprising that in contrast to less than 60% [68]Ga elution efficiencies obtained for the unmodified TiO$_2$ nanoparticles (section 4.1.1), 90% of the ^{68}Ga was eluted from the [68]Ge content adsorbed onto the 3-APTES column. This was a remarkable

improvement when compared to unmodified TiO_2 samples. A similar pattern was observed when the 3-MPTMS and the BAPA surface modifiers were utilised. In addition, it was not deemed useful to investigate the CDMT surface modifier further because an elution profile of only 33% [68]Ga in a 5 mL volume was achieved. Another possible area of future research would be to investigate why the CDMT surface modifier did not have an effect. If the process is to be economical, eligibility criteria requires column to achieve 60-100% [68]Ga elution efficiency.

In the follow-up phase of the study, [68]Ge breakthrough analysis is the most common procedure for determining the best surface modifier coupled to MIPs. In the runs with the 3-APTES, only 0.001% of [68]Ge breakthrough was obtained. Similarly, for the 3-MPTMS and the BAPA surface modifiers, 0.007 and 0.002% were achieved, respectively. As before, CDMT was problematic with figures of 0.05% [68]Ge breakthrough.

Furthermore, the various quality control parameters such as the pH and the metal contaminants were assessed for quality purposes of the [68]Ge/^{68}Ga generator, as discussed in detail in section 2.2.1. The ICP-OES graphs for these metal contaminants are presented in Appendix J. Table 4.15 summarises the comparison of ^{68}Ga efficiency and [68]Ge breakthrough as well as metal leaching between the MIPs and NMIPs.

Table 4.15. Summary of results obtained by analysis of MIPs and non-MIPs with the modified TiO_2 based [68]Ge/^{68}Ga generators, n=3

Material	Mass (mg)	pH	[68]Ga Efficiency (%)	[68]Ge Breakthrough (%)	Metal Analysis			
					Ga (ppm)	Ge (ppm)	Zn (ppm)	Ti (ppm)
MIP	20	1.0	91	0.0002	<0.1	<0.1	<0.2	<0.1
MIP	40	1.0	90	0.0001	<0.1	<0.1	<0.2	<0.1
MIP	80	1.0	88	0.0001	<0.1	<0.1	<0.2	<0.1
Non-MIP	20	0.9	65	0.004	<0.2	<0.1	<0.2	<0.1
Non-MIP	40	1.0	65	0.007	<0.2	<0.1	<0.1	<0.1
Non-MIP	80	0.9	66	0.005	<0.2	<0.1	<0.2	<0.1

The observations in Table 4.14 show a consistent pH data measurements. More significantly, there is no significant difference in the metal contaminants. For the zinc content, as expected, a slight increase in the percentage amount (0.2 ppm) was observed and could be due to the decaying of

the ^{68}Ga to ^{68}Zn in the end of the decay cycle. With respect to a 40 or 80 mg mass of the MIPs, there is no change in terms of the findings that were obtained (Table 4.15). The average of the ^{68}Ge breakthrough percentages is 0.001%, consistent when compared to the 20 mg samples. Furthermore, there was no significant difference when other quality control parameters were compared. With regard to the 80 mg samples, much improved ^{68}Ge breakthrough can be observed, 0.0001%. It seems that an increase in the amount of the MIPs is leading to a decrease in the amount of the ^{68}Ge breakthrough. As before, other parameters remain consistent between the 20 or 40 mg samples. Finally, also in Table 4.15, the results of the 511 and 1077 keV emission distribution are compared between the MIPs and NMIPs. The parameters of the quality control procedure, as well as the metal contaminants analysis, are included in Table 4.14 for comparison purposes. Figure 4.25 and 4.26 summarise the differences between the ^{68}Ga efficiencies and the ^{68}Ge breakthrough of the surface modified TiO$_2$ nanoparticles combined with the MIP and NMIP.
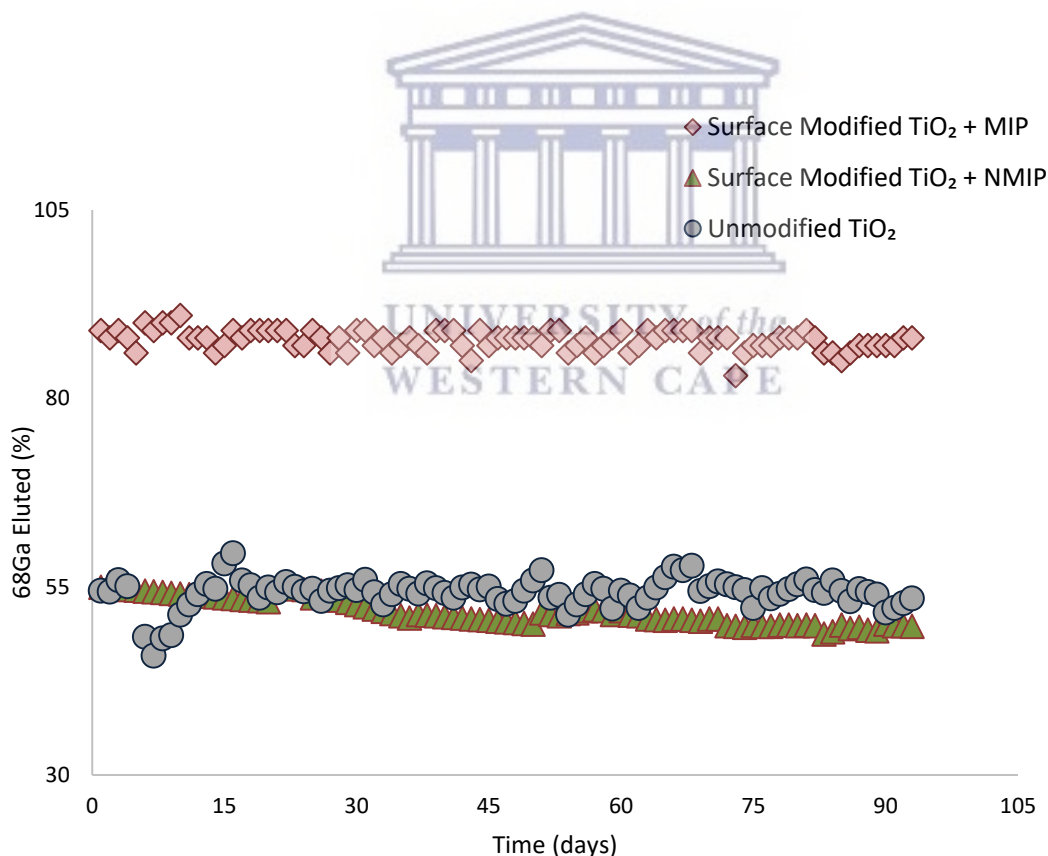
Figure 4.25. Comparison of the ^{68}Ga efficiencies between surface modified TiO$_2$ nanoparticles combined with the MIP and NMIP
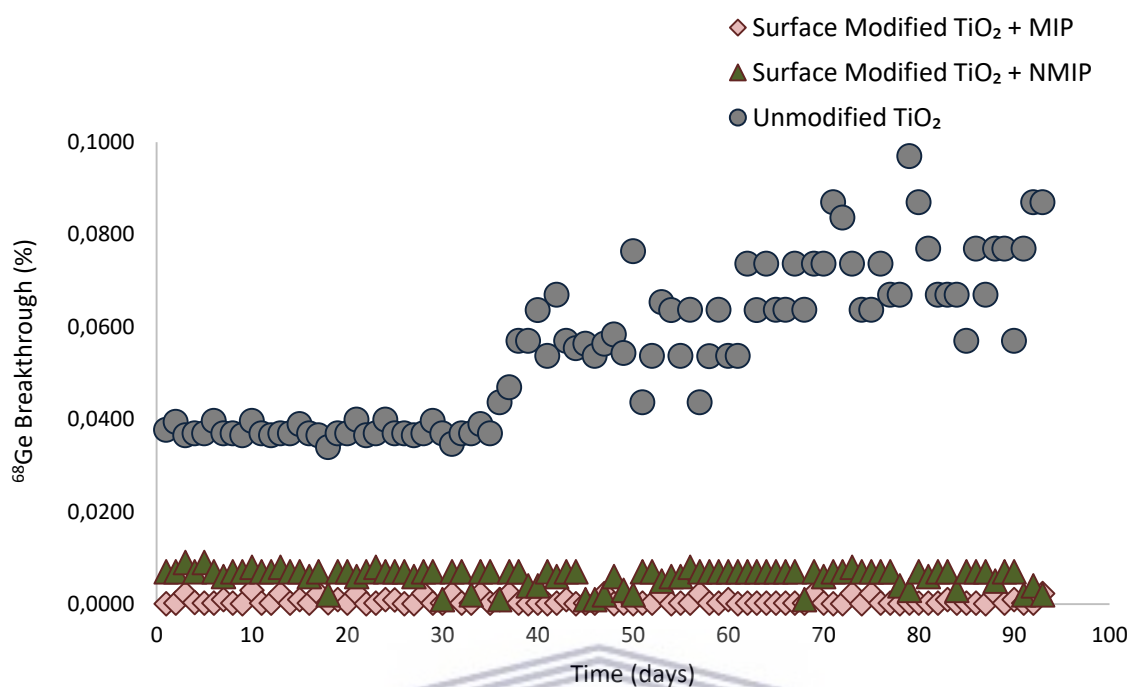
Figure 4.26. Comparison of the ^{68}Ge breakthroughs between surface modified TiO_2 nanoparticles combined with the MIP and NMIP

The analysis of the surface modified TiO_2 combined with MIPs has a trend that averages at 90% over time for the ^{68}Ga elution. In contrast, the surface modified TiO_2 combined with NMIPs has a spectra that averages at 50% and declines with time for the ^{68}Ga elution. This observation and the relationship with MIPs reveal a strong systematic correlation which has important implications for the $^{68}Ge/^{68}Ga$ generator production capacity in nuclear chemistry. This is consistent with the previous reported surface modified TiO_2 nanoparticles (Baum and Rösch, 2013). Next, comparison of the ^{68}Ge breakthroughs between the surface modified TiO_2 was undertaken to reveal how best minimization of the ^{68}Ge breakthrough can be achieved using the MIPs technique. There is no reported evidence of MIPs in the production capacity of the $^{68}Ge/^{68}Ga$ generator systems. After looking at Figure 4.26, one major observation is the significant difference between the trends over time when the MIPs or NMIPs were used for the ^{68}Ge breakthrough minimization. In detail, the MIPs were able to reduce ^{68}Ge breakthrough from 0.01 % to a significant 0.0001%, which was due to the contribution of the MIP technique (Figure 4.26). Therefore, a conclusion could be drawn that the MIPS technique allows for accurate and almost complete removal of any ^{68}Ge eluting from the column, one of the biggest challenges that $^{68}Ge/^{68}Ga$ generators face.

4.4.6   Summary of the ^{68}Ge Breakthrough Analysis using Molecular Imprinted Polymers

The basic architecture of the MIP design is depicted in Figure 2.12. Based on the design specifications discussed in section 2.6, the elution of the ^{68}Ga radionuclide and the resulting ^{68}Ge breakthrough were assessed to understand whether the design was able to withstand existing conditions in order to address performance related challenges highlighted in section 2.2.2. Thereafter, ^{68}Ge breakthrough analysis followed in order to assess the MIPs design functionality adopted for its feasibility to operate within the existing quality control parameters, as explained in section 3.2.8. Thus, the design was able to demonstrate strong ^{68}Ge retention capabilities, without sacrificing existing production parameters. When the amount of MIPs was increased (Table 4.15), a decrease in the ^{68}Ge breakthrough was observed and was an indication of more Ge sites available in the substrate. On the other hand, as expected, the amount of non-MIP did not account for the ^{68}Ge retained since the ^{68}Ge breakthrough level remained consistent at 0.01%. The observations during the study and the analysis of demonstrate that MIPs design is a powerful modality for ^{68}Ge breakthrough control.

CHAPTER V

CONCLUSION AND

RECOMMENDATIONS

5.1 Conclusions

New imaging procedures in the nuclear medicine industry are on the rise, and ^{68}Ge/^{68}Ga generators are set to fulfil a larger percentage of this need. Of these generators, titanium dioxide based generators have shown the promise of functioning effectively, exhibiting interesting material properties and the ability to fulfil three basic requirements: optimum ^{68}Ga elution efficiency, stability and removal of the ^{68}Ge breakthrough. Traditional methods have made little progress over many years and big challenges still exist in addressing the performance of the metal oxides. The purpose of this research was to optimize both ^{68}Ga efficacies and the ^{68}Ge breakthroughs, and related quality control parameters for generator performance in the period under review. As a result, two models were proposed in order to develop an appropriate shape, size and surface area of the TiO$_2$ nanoparticles, namely; surface modification and molecular imprinted polymer.

The two phases that TiO$_2$ exist under, anatase and rutile, were tested and the former was successful in loading the ^{68}Ge successfully. It was found that both ^{68}Ga efficacies and the ^{68}Ge breakthroughs did not yield satisfactory results. The surface modifications were carried out using 3-aminopolypropyltriethoxy silane (3-APTES), 3-mercaptopropyltrimethoxy silane (3-MPTMS), bis(3-aminopropyl)amine (BAPA) and 2-chloro-4,6-dimethoxy-1,3,5-triazine silane (CDMT). The variables examined in surface modifiers were based on stability, dispersibility and hydrophilicity concentration. These variables work hand in hand with the requirements specified above, and reaction conditions were chosen so as to improve efficiency of performance of the ^{68}Ge/^{68}Ga

generators. Once the TiO₂ nanoparticles were modified, they were used as adsorbents in the preparation of the ^{68}Ge/^{68}Ga generators. Of these surface modifiers, it was found that 3-aminopolypropyltriethoxy silane (3-APTES) was optimal under the prescribed conditions. ^{68}Ge breakthroughs were also investigated, and it was determined that molecular imprinted polymers were ideal.

Surface modification was able to yield significant benefits, and the ideal condition for the ^{68}Ge efficacy were revealed through the characterization techniques performed on the modified TiO₂ materials. Different modification strategies were used in order to obtain TiO₂ materials with distinct properties, namely i) be stable against radiation, ii.) be insoluble and non-toxic, iii) have good mechanical properties and iv.) possess very strong binding of the parent radionuclide. Analysis by the thermal gravimetric technique (TGA) technique was able to reveal that the surface modifiers had no influence on the thermal degradation of the modified TiO₂ materials. Next, Fourier Transform Infrared (FTIR) was able to detect different functional groups of the surface modifiers. This information was later used for characterisation of the covalent bonds found in the modified TiO₂ materials. Next, the High Resolution Scanning Electron Microscopy (HRSEM) was able to reveal information about the morphology and crystal structures of the surface modified TiO₂ materials. It was found that the size of the TiO₂ grains increased when heat was applied, causing the surface area to decrease affecting performance. Next, XRD patterns of the modified TiO₂ materials gave insight into the structure of the crystalline material. As before, the X-Ray diffraction (XRD) results were able to confirm that annealed modified TiO₂ materials were of limited practical value to the study. Next, Brunauer-Emmett-Teller (BET) analysis, through study of the morphological characteristics of interest such as surface area, pore volume and pore size distribution, was able to reveal how calcining TiO₂ materials led to lowered surface areas.

In comparison with the first attempts using more traditional techniques (Section 4.1), the results are a significant improvement. It was found that the ^{68}Ga efficacy was increased from 50 to above 80% region, and a ^{68}Ge % breakthrough improvement from 0.01 to 0.001 was achieved. By performing surface modification of the TiO₂ materials while using molecular imprinted polymers for the ^{68}Ge breakthrough control, and validating the nanoparticles using routine models of the production processes, it was shown that mechanical and surface properties could be improved

through surface modification methods. The results presented showed how the recommend steps helped to improve the TiO_2 nanoparticles in their performance as generator adsorbents.

One major uncertainty is the housing design of the molecular imprinted polymers such that when saturation takes place, releasing can take place without compromising the structure of the $^{68}Ge/^{68}Ga$ generator. Until this is better understood from a design perspective, either through more sophisticated simulations of a design software or from a mechanical design, it will be difficult to understand the difficulties relative to the proposed ^{68}Ge breakthrough control. Another area of concern is the introduction of impurities into the ^{68}Ga final product. It was shown in during metal analysis assessment that contaminants were kept at not more than 0.2 ppm for the Ga, Ge, Zn and Ti metals. This was in accord with the experimental results when the TiO_2 was used in Chapter 4 without surface modification, where there was no rapid increase in metal contaminants content during traditional elution stage. As already mentioned that high levels of metal contaminants in the product can lead to severe health impacts, and also leading to bad adsorption properties of the final ^{68}Ga product.

5.2 Research Recommendations

It is recommended that surface modification and the molecular imprinted polymer techniques be considered as important contextual parameters in the $^{68}Ge/^{68}Ga$ generator production. Such systematic chemical, radiochemical, and radiopharmaceutical efforts were implemented to guarantee reliability of the proposed $^{68}Ge/^{68}Ga$ generator system. For the surface modification technique, several silane coupling agents were examined against optimum production parameters for their contributions. On ^{68}Ge breakthrough, molecular imprinted polymers were applied to offer robust but technological solutions for the ^{68}Ge breakthrough control.

Both methods (surface modification and molecular imprinted polymer) highlighted effective and ineffective qualities in each method. Each method could reveal its flaws in order to get a more holistic adsorptive and selective capacity. Thus, columns and their content should be designed for a uniquely preferred surface modifier followed by data collection while conditions are slightly altered for improvements. A way to achieve this is to pick up where this work left off and continue with 3-APTES as a surface modifier and subject it to further experimental conditions such as eluent

strength and volume. Another good way of assessing is to determine the presence of metallic impurities in the ^{68}Ga eluate. The author proposes that surface modification and the molecular imprinted polymer techniques be further improved towards achieving approved ^{68}Ge/^{68}Ga generator systems.

Given the challenges associated with the ^{68}Ge/^{68}Ga generator models, the central goal of this thesis was to increase capacity of the TiO$_2$ inorganic oxide. As it currently stands, a single use of the ^{68}Ge/^{68}Ga generators may be expensive and inefficient. In addition, Roesch and Riss (2010) writes that while primary adsorption of ^{68}Ge occurs on the surface of these freshly prepared particles, diffusion and crystal growth processes may result in an increasing incorporation of ^{68}Ge inside the particles. They further allude that the ^{68}Ga generated inside the particles need to diffuse / migrate to the particles´ surface to be available for elution. To mitigate this, the study recommends surface modification in order to alter the chemistry behind the TiO$_2$ nanoparticles adsorption. In addition, the study also recommends that molecular imprinted polymer be introduced for the control of the ^{68}Ge breakthrough in the ^{68}Ga eluate product.
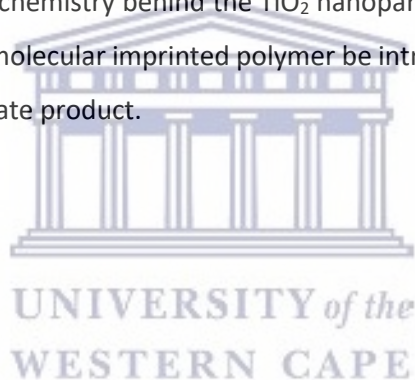
REFERENCES

1. Aardaneh K. and Van der Walt T.N. (2006). Ga_2O for target, solvent extraction for radiochemical separation and SnO_2 for the preparation of a $^{68}Ge/^{68}Ga$ generator, Journal of Radioanalytical Nuclear Chemistry, volume 268: 25-32.

2. Acikara Ö.B. (2013). Column Chromatography, Ankara University, Faculty of Pharmacy, Ankara, Turkey.

3. Advincula R.C., Brittain W.J., Caster K.C., Rühe J. (2006). Polymer Brushes: Synthesis, Characterisation and Applications, John Wiley and Sons, Copyright, pp. 331-335.

4. Albini A. and Fasani E. (2013). The Differences in Morphology, Surface Structures and Surface Chemistry, Photochemistry, volume 41: 182-265.

5. Alexander O., Andersson H., Andersson L.I., Ansell R. (2006). Molecular Imprinting Science and Technology - A survey of the Literature for the years up to and Including, Journal of Molecular Recognition, volume 19 (2): 106-180.

6. Ami D., Posteri R., Mereghetti P., Porro D., Doglia S.M., Branduardi P. (2014). Fourier Transform Infrared Spectroscopy as a Method to Study Lipid Accumulation in Oleaginous Yeast, Biotechnology for Biofuels, volume 7: 12.

7. Andersonn M., Österlund L., Ljungström S., Palmqvist A. (2002). Preparation of Nanosize Anatase and Rutile TiO_2 by Hydrothermal Treatment of Micro-emulsions and Their Activity for Photocatalytic Wet Oxidation of Phenol, Journal of Physical Chemistry, volume 106 (41): 10674-10679.

8. Ariga K., Hill J.P. and Ji Q. (2007). Layer by Layer Assembly as a Versatile Bottom-Up Nanofabrication Technique for Exploration Research and Realistic Application, Journal of Physical Chemistry Chemical Physics, volume 9: 2319-2340.

9. Arkles B. (1977). Tailoring Surfaces with Silanes. Surface Modification. Chemical Technology, volume 7(12): 766-778.

10. Atta N. and Galal A. (2018). Nano-Magnetite/Ionic Liquid Crystal Modifiers of Carbon Nanotubes Composites Electrode for Ultra-Sensitive Determination of a new Anti-Hepatitis Cr Drug in Human Serum, Journal of Electroanalytical Chemistry, volume 823: 296-306.

11.   Azhgozhinova G.S., Güven O., Pekel N., Dubolazov A.V., Mun G.A., Nurkeeva Z.S. (2004) Complex formation of linear poly (methacrylic acid) with uranyl ions in aqueous solutions. Journal of Colloid Interface Science, volume 278(1):155–159.

12.   Bagheri S., Shameli K., Hamid S.B.A. (2013). Synthesis and Characterisation of Anatase Titanium Dioxide Nanoparticles Using Egg White Solution via Sol-Gel Method, Journal of Chemistry, Centre for Research in Nanotechnology & Catalysis (NANOCEN), University of Malaysia .

13.   Bakalova R., Zhelev Z., Aoki I., Masamoto K., Mileva M., Obata T., Higuchi M., Gadjeva V., Kanno I. (2008). Multimodal silica-shelled quantum dots: Direct intracellular delivery, photosensitization, toxic, and microcirculation effects. Bioconjugate Chemistry, volume 19 (6): 1135-1142.

14.   Bandura A.V., Sykes D.G., Shapovalov V., Troung T.N., Kubicki J.D., Evarestov R.A. (2004). Adsoprtion of Water on the TiO2 (Rutile) (110) Surface: A Comparsion of Periodic and Clustered Calculations, The Journal of Physical Chemistry B, volume 108 (23): 7844-7853.

15.   Bao B. and Song M. (1996). A new ^{68}Ge/^{68}Ga generator based on CeO_2. Journal of Radioanalytical Nuclear Chemistry, volume 213: 233-238.

16.   Barahona I.F., Hernando M.M., Pellico J., Ruiz-Cabello J., Herranz F. (2018), Molecular Imaging with ^{68}Ga Radio-Nanometals: Shedding Light on Nanoparticles, Journal of Applied Sciences, volume 8: 1098.

17.   Barnejee S.R. and Pomper M.G. (2013). Clinical Applications of Gallium-68, Applied Radioanalytical Isotopes, volume 0: 2-13.

18.   Baum R. and Rösch F. (2013). Theranostics, Gallium-68 & other Radionuclides: A Pathway to Personalised Diagnostics & Treatment, Springer-Verlag Berlin Heidelberg (ISBN: 978-3-642-27993-5), Recent Results in Cancer research S194.

19.   Berry D.J., Ma Y., Ballinger J.R., Tavare' R., Koers A., Sunassee K., Zhou T., Nawaz S., Mullen G.E.D., Hider R.C., Blower P. (2011). Efficient bifunctional gallium-68 chelators for positron emission tomography: tris(hydroxypyridinone) ligands, Journal of Chemical Communication, volume 47: 7068-7070.

20.   Beyazit, S.; Bui, B.T.S.; Haupt, K.; Gonzato, C. (2016). molecularly Imprinted Polymer Nanomaterials and Nanocomposites by Controlled/living Radical Polymerization, Programme of Polymeric Science, volume 62: 1–21.

21.   Beyer T., Antoch G., Muller S., Egelhof T., Freudenberg L.S. Debatin J. (2005). Optimized Intravenous Contrast Administration for Diagnostic Wholebody ^{18}F-DFG PET-CT, Journal of Nuclear Medicine, volume 46: 429-435.

22. Bhawani S. A., Bakhtiar S., Shafqat S.R. (2019). Synthesis of Molecularly Imprinted Polymers for the Selective Extraction /Removal of 2,4,6-trichlorophenol, The Open Chemical Engineering Journal, volume 15: 122-133.

23. Bjørnstad T., Borroto-Portela J.I., Brisset P., Chankow N., Charlton J.S., Conejo-Solis M.A., Dagadu C.P.K., Dash A., Diaz-Vargas F., Ud-Din G., Jin J.H. and Jinfu L. (2013). Radiotracer generators for industrial applications, *International Atomic Energy Agency,* IAEA Radiation Technology Series No. 5 Book.

24. Bossi, A.; Piletsky, S.A.; Piletska, E.V.; Righetti, P.G.; Turner, A.P.F. (2001). Surface-grafted molecularly imprinted polymers for protein recognition, Analytical Chemistry, volume 73: 5281–5286.

25. Bourikas K., Kordulis C., Lycourghiotis A. (2014). Titanium Dioxide (Anatase and Rutile): Surface Chemistry, Liquid–Solid Interface Chemistry, and Scientific Synthesis of Supported Catalysts, Chemistry Revision, volume 114 (19): 9754-9823.

26. Brame J. and Griggs C. (2016). Surface Area Analysis Using the Brunauer-Emmett-Teller (BET) Method: Scientific Operation Procedure Series: SOP-C, Engineer Research and Development Centre, report 16-3.

27. Breeman W.A.P. and Verbruggen A.M. (2007). The ^{68}Ge/^{68}Ga generator has high potential, but when can we use ^{68}Ga-labelled tracer in clinical routine? European Journal of Nuclear Medicine, volume 34: 978-982.

28. Breeman WAP, de Jong M, de Blois E, Bernard BF, Konijnenberg M, Krenning EP. (2004). Radiolabelling DOTA-peptides with ^{68}Ga, European Journal of Nuclear Medicine, volume 32: 78–485.

29. Brinker J. C. and Scherer G. W. (2013). Sol-Gel Science: The Physics and Chemistry of Sol-Gel Processing. Elsevier Incorporation, pp. 908.

30. Brownell G.L. and Sweet W.H. (1953). Localization of brain tumors with positron emitters, Nucleonics, volume 11: 40-45.

31. Brucer M., Andrews G.A. Bruner H.D. (1953). A study of gallium, Radiology, volume 61: 534-600.

32. Brzoska J.B., Azouz I.B., Rondelez F. (1994). Silanization of Solid Substrates: A Step toward Reproducibility, Langmuir, volume 10(11): 4367 – 4373.

33. Campbell C.T and Sauer J. (2013). Introduction: Surface Chemistry of Oxides, Chemistry Revision, volume 6: 3859-3862.

34. Caruso F., Spasova M., Saigueirino-Maceira V., Liz-Marzan L. M. (2001). Multilayer assemblies of silica-encapsulated gold nanoparticles on decomposable colloid templates, Advanced Materials, volume 13(14): 1090-1094.

35. Chaki K.N., Aslam M., Sharma J., Vijayamohanan K. (2001). Application of Self-Assembled Monolayers in Materials Chemistry, Journal of Chemical Sciences, volume 113: 659-670.

36. Chakravarty R., Rakesh S., Ram R., Vekantesh M.V., Dash A. K., Tyagi (2010). Nanoceria-PAN Composite-Based Advanced Sorbent Material: A Major Step Forward in the Field of Clinical-Grade ^{68}Ge/^{68}Ga Generator, ACS Applied Material Interfaces, volume 2(7): 2069-2075.

37. Chakravarty R., Shukla R., Ram R., Tyagi A. K., Dash A., Venkatesh M. (2011). Development of a nano-zirconia based ^{68}Ge/^{68}Ga generator for biomedical application. Nuclear Medicinal Biology, volume 38(4): 575–583.

38. Chen D., Huang Y., Liang H., Xie Y. (2016). Column Chromatographic Extraction for quickly separating the volatiles, flavonoids and pectin from tangerine peel, Separation Science and Technology, volume 51 (3): 485-493.

39. Chen D., Jordan E. H., Gell M. (2008). Sol-Gel Combustion Synthesis of Nanocrystalline YAG Powder from Metal Organic Precursors, Journal of Ceramic Society, volume 91(8): 2759 – 2762.

40. Chen L., Xu S., Li J. (2011). Recent advances in molecular imprinting technology: Current status, challenges and highlighted applications, Chemistry Society, volume 40: 2922–2942.

41. Chen Z., Gu Z., Chen J., Yu J., Zhou L. (2016). Synthesis, characterization, and photocatalytic activity of porous La-N-co-doped TiO_2 nanotubes for gaseous chlorobenzene oxidation. Journal of Environmental Science, volume 46:203-213.

42. Chen Y., Zhang Z., Sui X., Brennan J. D., Brook M. A. (2005). Reduced Shrinkage of Sol-Gel derived Silica using Sugar based silsesquioxane precursors, Journal of Materials Chemistry, volume 15: 3132 – 3141.

43. Cho J.H. and Lee Y.W. (2015). Preparation of Composite Powder and Properties by Surface Modification of Inorganic Pigments for Papermaking, KONA Powder and Particle Journal volume 32: 270-278.

44. Christian P. and Waterstram-Rich K. (2007). Nuclear Medicine and PET-CT – Techniques and Technology, 6th Edition, St Louis: Mosby/Elsevier.

45. Cormack P. A. and Elorza A. Z. (2004). Molecular Imprinted Polymers: Synthesis and Characterisation, Journal of Chromatography, volume 804(1): 173 – 182.

46. Cozzoli P. D., Kornowski A., Weller H. (2003). Low-Temperature Synthesis of Soluble and Process able Oganic-capped Anatase TiO_2 nanorods, Journal of Am. Chemistry Society, volume 125: 14539 – 14548.

47. Creager A. N. H. (2013) Life Atomic: A History of Radioisotopes in Science and Medicine, Chicago: University of Chicago Press.

48. Crowe P. (2003) Making PET and PET-CT a Clinical Reality through Mobile PET Services, in: Von Schulthess G, editor. Clinical Molecular Anatomic Imaging, Philadelphia: Lippin-cott Williams and Wilkins.

49. Cummins P., Rochfort D.K. and Connor O. (2017) Ion-Exchange Chromatography: Basic Principles and Application, Methods Molecular Biology, volume 1485: 209-223.

50. Cusnir R., Imberti C., Hider R.C., Blower P.J., Ma M.T. (2017). Hydroxypyridinone Chelators: From Iron Scavenging to Radiopharmaceuticals for PET Imaging with Gallium-68, International Journal of Molecular Science, volume 18(1): 116.

51. Daghrir R., Drogui P., and Robert D. (2013). Modified TiO_2 for Environmental Photocatalytic Applications: A review, Industrial Engineering Chemistry, Res. Volume 52: 3581–3599.

52. Dai H., Xiao D.L., He H., Li H., Yuan D.H., Zhang C. (2015). Synthesis and Analytical Applications of Molecularly Imprinted Polymers on the Surface of Carbon Nanotubes: A Review, Microchimica Acta, volume 182: 893–908.

53. Dash A and Chakravarty R. (2017). Nanomaterial-Based Adsorbents: Promises, Opportunities and Challenges to develop Column Chromatography Radionuclide Generators for Nuclear Medicine, Journal of Separation and Purification Reviews, volume 46(2): 91 – 107.

54. Dash A and Chakravarty R. (2019). Radionuclide generators: the prospect of availing PET radiotracers to meet current clinical needs and future research demands, Journal of Nuclear Medicine for Molecular Imaging, volume 9(1): 30–66.

55. De Blois E. (2011) Radiopharmaceutical Aspects of Receptor Scintigraphy: labelling with Radiometals, Optimisation and Radiochemistry Purity, pp. 57 – 65.

56. De Campos, A. M.; Sanchez, A.; Gref, R.; Calvo, P.; Alonso, M. J. (2003). The effect of a PEG versus a chitosan coating on the interaction of drug colloidal carriers with the ocular mucosa, European Journal of Pharmaceutical Sciences, volume 20(1): 73-81.

57. Decher G. (2012). Multilayer Thin Films: Sequential Assembly of Nanocomposite Material, Second Edition, Wiley-VCH Verlag GmbH & Co. pp. 1-12.

58. Decristoforo C. (2012). A New Opportunity for PET Available From a Long Shelf-Life Generator – Automation and Applications, Current Radiopharmacy, volume 5(3): 212 -220.

59. Decristoforo C., Picket R.D., Verbruggen A. (2012). Feasibility and Availability of ^{68}Ga-labelled Peptides, European Journal of Nuclear Medicine for Molecular Imaging, volume 39 (1): S31–S40.

60. Decristoforo C., von Guggenberg E., Haubner R., Rupprich M., Scharz S., Virgolini I. (2005). Radiolabelling of DOTA-derivatised peptides with [68]Ga *via* a direct approach – optimization and routine clinical application [abstract]. 27th International Symposium, Radioactive Isotopes in Clinical Medicine and Research, Bad Gastein, Austria, Nuklearmedizin, 6: A191.

61. Delbeke D. and Martin W. (2004). PET and PET-CT for Evaluation of Colorectal Carcinoma, Semin Nuclear Medicine, volume 34:198-208.

62. Delcorte A., Bertrand P., Wischerhoff E., Laschewsky A. (1997). Adsorption of Polyelectrolyte Multilayer on Polymer Surfaces, Langmuir, volume 13(19): 5125-5136.

63. Deosorla F.A and Vallaurie D. (2009). Study of the process parameters in the synthesis of TiO_2 nanospheres through reactive micro-emulsion precipitation, Powder Technology, volume 190(3): 304-309.

64. Deutsch E. (1993). Clinical PET: its time has come? Journal of Nuclear Medicine, volume 34: 1132–1133.

65. Diebold U. (2002). The Surface Science of Titanium Dioxide, Journals of Surface Science Reports, volume 48: 53-229.

66. Dufton P.W. (1998). Functional Additives for the Plastic Industry: A Report from Rapra's Industry Analysis Group. Smithers Rapra Publishing. Shawbury.

67. Duncan K. (1998). Radiopharmaceuticals in PET Imaging, Journal of Nuclear Medicine and Technology, volume 26: 228-234.

68. Elgh B. and Palmqvist A.E.C. (2014). Controlling anatase and rutile polymorph selectivity during low-temperature synthesis of mesoporous TiO_2 films, Journal of Material Chemistry, Issue 9, volume 2: 3024-3030.

69. Eppard E., Loktionova N.S., Rösch F. (2014). [68]Ge Content Quality Control of [68]Ge/[68]Ga Generator Eluates and [68]Ga Radiopharmaceuticals – A Protocol for Determining the [68]Ge Content Using Thin Layer Chromatography, Applied Radioanalytical Isotopes, volume 91: 92-96.

70. Ertüka G. and Matiasson B. (2016). From Imprinting to Micro-Contact Imprinting – A New Tool to Increase Selectivity in Analytical Aevices, Journal of Chromatographic Biochemistry, volume 1021: 30-44.

71. Faix O. (1992). Fourier Transform Infrared Spectroscopy. In: Lin S.Y.., Dence C.W. (eds) Methods in Lignin Chemistry. Springer Series in Wood Science. Springer, Berlin, Heidelberg.

72. Fani M., Andre J.P., Maecke H.R. (2008). ^{68}Ga-PET: A Powerful Generator-based Alternative to Cyclotron-based PET Radiopharmaceuticals, Contrast Media Molecular Imaging, volume 3: 67-77.

73. Farn R.J. (2008). Chemistry and Technology of Surfactants, John Wiley and Sons. New York. Pp. 1-23.

74. Feinle A., Elsaesser M.S., Huesing N. (2016) Sol-Gel Synthesis of Monolithic Materials with Hierarchical Porosity, Chemistry Society Revision, volume 45: 3377–3399.

75. Fischer K., Gawel A., Rosen D., Krause M., Latif A.A., Griebel J., Prager A., Schulze A. (2017). Low-Temperature Synthesis of Anatase/Rutile/Brookite TiO_2 Nanoparticles on a Polymer Membrane

for Photocatalysis, Leibniz-Institute of Surface Modification, Permoserstr. 15, D-04318 Leipzig, Germany.

76. Gao J. C., Zou J., Tan X. W., Wang Y. (2006). Characteristics and properties of surface coated nano-TiO2. Transactions of Nonferrous Metals, Society of China, volume 16(6): 1252-1258.

77. Garcia-Gonzalez C.A., Saurina J., Ayllon J.A., Domingo C. (2009). Preparation and Characterisation of Surface Silanized TiO_2 Nanoparticles under Compressed CO_2: Reaction Kinetics, Journal of Physical Chemistry, volume 113(31): 13780 – 13786.

78. Green M.A., Mathias C.J., Neumann W.L., Janik F.M., Deutsch E.A. (1993). Potential Gallium-68 Tracers for Imaging the Heart with PET: Evaluation of Four Gallium Complexes with Functionalised Tripodal Tris(Salicylaldimine) Ligands, Journal of Nuclear Medicine, volume 34: 228-233.

79. Grosu A-L., Piert M., Weber W.A., Jeremic B., Pichhio M., Schratzenstaller U., Zimmerman F.B., Schwaiger M., Molls M. (2005) Positron Emission Tomography for Radiation Treatment Planning, volume 181 (18): 483-499.

80. Gründer G. and Wong D.F. (2003). Mechanism of New Antipsychotic Medications, Occupancy is not just Antagonism, Arch Gen Psychiatry, volume 60: 974–977.

81. Guc' M. and Schroeder G. (2019). Application of Molecular Imprinted Polymers (MIP) and Magnetic Molecular Imprinted Polymer (mag-MIP) to Selective Analysis of Quercetin in Flowing Atmospheric – Pressure Afterglow Mass Spectrometry (FAPA-MS) and Electrospray Ionization Mass Spectrometry (ESI-MS), Molecules, volume 24(13): 2364.

82. Gui R., Jin H., Guo H., Wang Z. (2018). Recent Advances and Future Prospects in Molecularly Imprinted Polymers-based Electrochemical Biosensors, Biosensors Bioelectrons, volume 100: 56–70.

83. Guillet B., Quentin P., Waultier S., Bourelly M., Pisano P., Mundler O. (2005). Technologist Radiation Exposure in Routine Clinical Practice with 18F-FDG, Journal of Nuclear Medical Technology, volume 33: 175-179.

84. Gupta S.M. and Tripathi M. (2011). A Review of TiO_2 Nanoparticles, Chinese Science Bulletin, volume 56: 1639–1657.

85. Hanaor D.A.H. and Sorrell C. (2011). Review of the Anatase to Rutile Phase Transformation, Journal of Materials Science, volume 46(4): 855-874.

86. Harkins W.D. and Jura G. (1944). Surface Solids. XIII. Vapour Adsorption Method for the Determination of the Area of a Solid without the Assumption of a Molecular Area, and the Areas Occupied by Nitrogen and Other Molecules on the Surface of a solid, Journal of American Chemistry Society, volume 66(8): 1366–1373.

87. Harvey D. Byerly S., Bowman A., Tomlin J. (1991). Optimisation of HPLC and GC Separations Using Response Surfaces, Journal of chemical Education, volume 68: 162 – 168.

88. Hasan A. and Pandey L.M. (2017). Self-Assembled Monolayers in Biomaterials, Woodhead Publishing, Elsevier.

89. Hashim U., Nadzirah S.H., Azizah N., Azmi M.S., Bala K. (2015). Silanization using 3-APTES in Different Solvents on Titanium Dioxide Nanoparticles, 2nd International Conference on Biomedical Engineering, 1-4.

90. Hayichelaeh C., Reuvekamp L.A.E.M., Dierkes W.K., Blume A., Noordermeer J.W.M., Sakaharo K. (2018). Enhancing the Silanization Reaction of the Silica-Silane System by Different Amines in Model and Practical Silica-Filled Natural Rubber Compounds, Journal of Polymers, volume 10: 584.

91. Herrmann J.M., Disdier J., Pichat P. (1986) Photo-assisted Platinum Deposition on TiO_2 using various Platinum Complexes, Journal of Physical Chemistry, volume 90(22): 6028-6934.

92. Hirano K., Ota M., Inagaki and Iwata H. (2004). Hydrothermal synthesis of TiO_2/SiO_2 composite nanoparticles and their photocatalytic performances. The Journal of the Ceramic Society of Japan, volume 112 (1303): 143–148.

93. International Atomic Energy Agency. (2001). Charged particle cross section database for medical radioisotope production: diagnostic radioisotopes and monitor reactions. IAEA-TECDOC-1211, IAEA, Vienna.

94. Isimjan T.T., Yan Z., Yang D.-Q., Rohani S., Ray A. K. (2012). A New Approach of Tailoring Wetting Properties of TiO2 Nanotubular Surfaces. Advanced Science Letters, volume 18(1): 158–163.

95. Jian J.-M., Guo Y., Zeng L., Liu L.-Y., Lu X., Wang F., Zeng E.Y. (2017). Global Distribution of Perfluorochemicals (PFCS) in Potential Human Exposure Source—A Review, Environmental International, volume 108: 51–62.

96. Jo C.W., Hee Y.S., Faiz A. (2013). Molecular Imprinted Polymers for Separation Science: A Review of Reviews, Journal of Separation Science, volume 36: 609–628.

97. Jung J.H., Choi Y., Im K.C. (2016). PET/MRI: Technical Challenges and Recent Advances, Journal of Nuclear Medicine and Molecular Imaging, volume 50(1): 3-12.

98. Kamiya H. and Iijima M. (2010). Surface Modification and Characterisation for Dispersion Stability of Inorganic nanometer-scaled Particles in Liquid Media, Science and Technology of Advanced Materials, volume 11(4).

99. Kamiya H., Suzuki M., Kikuchi M., Tsukada M. (2006). Analysis of Surface Interaction Between TiO_2 Fine Particles with Different Surface Modification In Isoparaffin by Using Colloid Probe AFM, Institute of Symbiotic Science and Technology, volume 2: 728-731.

100. Kang B.K., Lim B.S., Yoon Y., Kwag S.H., Park W.K., Song Y.H., Yang W.S., Ahn Y-T., Kang J-W., Yoon D.H. (2017). Efficient Removal of Arsenic by Strategically Designed and Layer-by-Layer Assembled PS@rGO@Go@Fe_3O_4 Composites, Journal of Environmental Management, volume 201: 286-293.

101. Karami A. (2010) Synthesis of TiO_2 nano powder by the sol-gel method and its use as a photocatalyst, Journal of the Iranian Chemical Society, volume 7, pages S154–S160.

102. Karp J.S., Surti S., Daube-Witherspoon M.E., Muehllehner G. (2008). Benefit of Time of Flight in PET: Experimental and Clinical Results, Journal of Nuclear Medicine, volume 49: 462-470.

103. Keller S.W., Kim H.N., Mallouk T.E. (1994). Layer by Layer Assembly of Intercalation Compounds and Heterostructures on Surfaces: Towards Molecular "Beaker" Epitaxy, Journal of Am Chemistry Association, volume 116: 8817 – 8818.

104. Khataee A. and Mansoori G.A., (2011). Nanostructured Titanium Dioxide Materials: Properties, Preparation and Applications, World Scientific Publishing Company, pp. 5-7.

105. Kilian K. (2014). ^{68}Ga-DOTA and Analogues: Current Status and Future Perspectives, Republican Practical Oncology Radiotherapy, volume 19: S13–S21.

106. Killian, M (2013). Organic Modification of TiO_2 and Other Metal Oxides with SAMs and Proteins – A Surface Analytical Investigation, Friedrich-Alexander-Universität Erlangen-Nürnberg (FAU).

107. Kim C.S., Byung K.M., Park J.H., Choi B.C., Seo H.J., (2003). Solvothermal Synthesis of Nanocrystalline TiO_2 in Toluene with Surfactant, Journal of Crystal Growth, volume 257: 309-315.

108. Kimura H., Sakamoto T., Yamada B. (2018). Novel Primer Composed of a Silane Coupling Agent and Multi Thiol for Adhesion of Versatile Dental Material, Journal of Applied Polymer Science, volume 135(46): 46763.

109. Knudsen H., Farner R.L., Xu Y., Norling L.A., Blank G.S. (2001). Membrane ion-exchange Chromatography for Process-sale Antibody Purification, Journal of Chromatography, volume 907 (1-2): 145-154.

110. Kopecký P. and Mudrová B. (1974). [68]Ge/^{68}Ga generator for the production of ^{68}Ga in an ionic form. International Journal of Applied Radioanalytical Isotopes, volume 25: 263-268.

111. Kopecky P., Mudrová B., Svoboda K. (1973). The Study of Conditions for the Preparation and Utilization of [68]Ge/[68]Ga Generator, International Journal of Applied Radiation Isotopes, volume 24: 73-80.

112. Kozlova M.D., Malinin A.B., Kodina G.E., Sevastyanova, A.S. (1970). Radiopharmaceutical Department, Institute of Biophysics, Ministry of Public Health, Moscow, Russia, volume 12: 505.

113. Kralevich M.L. and Koenig J.L. (2012). The Effect of Polyethylene Glycol and the Coupling Agent bis-(γ-triethoxysilylpropyl)-tetrasulfide (Si-69) on the Interactions of Silica-Filled Natural Rubber, Journal of Composite Interfaces, volume 5(2): 125-135.

114. Laskowski J.S. and Ralston J. (2015) Colloid Chemistry in Mineral Processing, Developments in Mineral Processing, volume 12: 37-90.

115. Legrini O., Oliveros E., Braun A.M. (1993). Photochemical Processes for Water Treatment, Chemistry Revision, volume 93 (2): 671-698.

116. Lei Y., Zhou T., Shen X. (2016). Molecular Imprinting in Particle-Stabilized Emulsions: Enlarging Template Size from Small Molecules to Proteins and Cells, Molecular Imprinted, volume 2: 8–16.

117. Leofanti G., Padovan M., Tozzola G., Venturelli B. (1998). Surface Area and Pore Texture of Catalysts, Catalysis Today, volume 41(1-3): 207-219.

118. Linsebigler A.L., Lu G. and Yates J.T. (1995) Photocatalysis on TiO$_2$ Surfaces: Principles, Mechanisms, and Selected Results, Chemistry Revision, volume 95(3): 735-758.

119. Liu S., and Edwards D. S. (2001). Bifunctional Chelators for Therapeutic Lanthanide Radiopharmaceuticals, Bioconjugate Chemistry, volume 12: 7 – 34.

120. LizMarzan, L. M.; Giersig, M.; Mulvaney, P. (1996). Synthesis of Nanosized Gold-Silica core-Shell Particles. Langmuir, volume 12(18): 4329-4335.

121. Loc´h C., Maziere B., Comar D. (1982). A New Generator for Ionic Gallium-68, Journal of Nuclear Medicine, volume 21: 171-173.

122. Loc´h C., Maziere B., Comar D., Knipper R. (1982). A New Preparation of Germanium 68. International Journal of Applied Radiation Isotopes, volume 33: 267-270.

123. Maecke H.R., Andre J.P., (2007). ^{68}Ga-PET Radiopharmacy: A Generator-based Alternative to ^{18}F-Radiopharmacy, Ernst Schering Res Found Workshop, Pages: 215-242.

124. Maecke H.R., Hofmann M., Haberkorn U. (2005). ^{68}Ga-labeled Peptides in Tumor Imaging, Journal of Nuclear Medicine, volume 46 (1):172S-178S.

125. Maecke H.R., Smith-Jones P., Maina T., Stolz B., Albert R., Bruns C.H., Reist H. (1993). New Octreotide Derivatives for *in vivo* Targeting of Somatostatin Receptor-Positive Tumours for Single Photon Emission Computed Tomography (SPECT) and Positron Emission Tomography (PET), Hormonal Metabolism Res. Supplies, volume 27: 12-17.

126. Makarova O.V., Rajh T., Thurnauer M.C., Martin A., Kemme P.A. Cropek D. (2000). Surface Modification of TiO$_2$ Nanoparticles for Photochemical Reduction of Nitrobenzene, Environmental Science Technology, volume 34 (22): 4797-4803.

127. Mandzy N., Grulke E., Druffel T., (2005) Breakage of TiO$_2$ Agglomerates in Electrostatically Stabilised Aqueous Dispersions, Powder Technology, volume 160: 121-126.

128. Marini M., Pourabbas B., Pilati F., Fabbri P. (2008). Functionally Modified Core-shell Silica Nanoparticle by One-Pot Synthesis, Journal of Colloids and Surfaces A: Physicochemical and Engineering Aspects, volume 317(3): 1-3.

129. Marty J.D. and Mauzac M. (2005). Molecular Imprinting: State of the Art and Perspective, Macromolecules, volume 172: 1-35.

130. Matsunaga K., Chang T.Y., Ishikawa R., Dong Q., Toyoura K., Nakamura A., Ikuhara Y., Shibata N. (2016) Adsorption Sites of Single Noble Metal Atoms on the Rutile TiO_2 (110) Surface Influenced by Different Surface Oxygen Vacancies, Journal of Physics: Condensed Matter, volume 28: 17.

131. McElvany, K.D.; Hopkins, K.T.; Welch, M.J. (1984). Comparison of ^{68}Ge/^{68}Ga generator system for radiopharmaceutical production, International Journal of Applied Radiation, volume 35: 521-524.

132. Meyer G.-J., Gielow P., Börner A.R., Hofmann M., Knapp W.H. (2005). Ga-67 and Ga-68 labelled DOTA-derivatised peptide-ligands [abstract]. 27th International Symposium, Radioactive Isotopes in Clinical Medicine and Research, Bad Gastein, Austria, Jan. 11-14, 2006. Products. Proceedings of the 5th International Conference on Isotopes 5ICI, Brussels, Belgium, April 25-29, 2005, Bologna, Italy, (Medimond), 147-151.

133. Meyer G-J., Gielow P., Börner A.R., Hofmann M., Knapp W.H. (2006). ^{67}Ga and ^{68}Ga labelled DOTA-derivatised Peptide-Ligands [abstract]. 27th International Symposium, Radioactive Isotopes in Clinical Medicine and Research, Bad Gastein, Austria, Nuclear Medicine, volume 6, A192.

134. Mirzadeh S. and Lambrecht R.M. (1996). Radiochemistry of Germanium, Journal of Radioanalytical Chemistry, volume 202: 7-102.

135. Mosbach K. and Ramstrom O. (1996). The Emerging Technique of Molecular Imprinting and its Future Impact on Biotechnology, Bio-Technology, volume, 14: 163–170.

136. Mueller R., Kammier H.K., Wegner K., Pratsinis S.E. (2003). OH Surface Density of SiO2 by Thermogravimetric Analysis, Langmuir, volume 1: 160-165.

137. Naidoo C., van der Walt T.N., Raubenheimer H.G. (2002). Cyclotron production of ^{68}Ge with a Ga_2O target. International Journal of Radioanalytical Nuclear Chemistry, volume 253: 221-225.

138. Nakayama M., Haöatake M., Ono M., Koiso T. Harada K., Nakayama H., Yahara S., Ohmomo Y., Arano Y, Ono M. (2003). A new ^{68}Ge/^{68}Ga Generator System using an Organic Polymer Containing N-methylglucamine Groups as Adsorbent for ^{68}Ge, Applied Radiation Isotopes, volume 58: 9–14.

139. Nalwa H.S. (2000). Handbook of Nanostructured Materials and Nanotechnology. Synthesis and Processing. Volume 1. Academic Press. Boston, New York, pp: 93-113.

140. Nam C.T., Wein-Duo Y., Le M.N. (2013). Solvothermal Synthesis of TiO_2 Photocatalysts in Ketone Solvents with Low Boiling Points, [1]Department of Chemical and Materials Engineering, National Kaohsiung University of Applied Sciences, 415 Chien-Kung Road, Kaohsiung 807, Taiwan, Volume Article ID 627385 | 11 pages.

141. Neirinckx R.D. and Davis M.A. (1980). Potential column chromatography for ionic Ga-68. II: Organic ion exchangers as chromatographic supports, Journal of Nuclear Medicine, volume 21: 81-83.

142. Neouze M.A. and Schubert U. (2008). Surface Modification and Functionalisation of Metal and Metal Oxide Nanoparticles by Organic Ligands, Institute of Material Science, volume 139: 183 – 195.

143. Ng H.K.M., Leo C.P., Abdullah A.Z. (2017). Selective Removal of Dyes by Molecular Imprinted TiO_2 Nanoparticles in Polysulfone Ultrafiltration Membrane, Journal of Environment and Chemical Engineering, volume 5: 3991–3998.

144. Ni H., Zhou X-H., Li H-H., Huang W-F. (2009). Column Chromatography Extraction and Preparation of Cordycepin from Cordyceps Militaris Waster Medium, Journal of Chromatography, volume 877: 2135-2141.

145. Niculae D. and Niculae A. (2015). Qualification of [68]Ge/[68]Ga Generators: A Comparison of Organic Matrix and Tin Oxide based Generators, Journal of Nuclear Medicine, volume 56(3): 1055.

146. Niu M., Pham-Huy C., He H. (2016). Core-Shell Nanoparticles Coated with Molecularly Imprinted Polymers: A Review, Microchimica Acta, volume 183: 2677–2695.

147. Nosaka Y. and Nosaka A. (2016). Introduction to Photocatalysis – From Basic Science to Applications, Royal Society of Chemistry, volume 1: 356–359.

148. Notni J., Hermann P., Havlíková J., Kotek J., Kubíek V., Plutnar J., Loktionova N., Riss, P.J., Rösch F. (2010). A Triazacyclononane based Bifunctional Phosphinate Ligand for Preparation of Pultimeric ^{68}Ga PET Tracers, Chemistry European Journal, volume 16: 7174-7785.

149. Ohno T., Sarukawa K., Tokieda K., Matsumara M. (2001). Morphology of TiO_2 Photocatalyst (Degussa P25) Consisting of Anatase and Rutile Crystalline Phases, Journal of Catalysis, volume 213, Issue 1, Pages 82 -86.

150. Ozcan M., Valandro L., Stomatol M. (2011). Effect of Silane Coupling Agents and Alloy Primers on Adhesion to Titanium, volume 60(9): 427-434.

151. Pan H., Wang X., Xiao S., Yu L., Zhang Z. (2013). Preparation and Characterisation of TiO_2 Nanoparticles Surface-modified by Octadecyltrimethoxysilane, Indian Journal of Engineering and Material Sciences, volume 20: 561-567.

152. Panagiotopoulou M., Beyzit S., Nestora S., Haupt K., Bui B.T.S. (2015). Initiator-Free Synthesis of Molecular Imprinted Polymers by Polymerization of Self-Initiated Monomers, Polymer, volume 66:43-51.

153. Park H. Park Y., Kim W., Choi W. (2013). Surface Modification of TiO_2 Photocatalyst for Environmental Applications, Journal of Photochemistry and Photobiology C: Photochemistry Reviews volume 15: 1-20.

154. Parkinson G.S. and Diebold U. (2016). Adsorption on Metal Oxide Surfaces, Surface and Interface Sciences: Solid-Gas Interfaces II, John Wiley and Sons, Chapter 44.

155. Polyakov M.V. (1931). Adsorption Properties and Structure of Silica Gel. Russian Journal of Physical Chemistry A, volume 2: 799–805.

156. Price P.M. and Green, M.M. (2011). Positron emission tomography imaging approaches for external beam radiation therapies: current status and future developments, British Journal of Radiology, volume 84 (Spec Iss 1): S019–S034.

157. Que W., Sun Z., Lam Y.L., Chan Y.C., Kam C.H. (2001). Sol-Gel silica-Titania Films via Organically Modified Silane Precursors. Journal of Physics, Applied Physics, volume 34 (4): 471.

158. Radoman T.S., Dźunuzović J.V., Trifković K.T., Palija T., Marinkovic A.D., Burgaski B., Dźunuzović E.S. (2015). Effect of Surface Modified TiO$_2$ Nanoparticles on Thermal, Barrier and Mechanical Properties of Long Oil Alkyd Resin-based Coatings, Innovation Centre, Faculty of Technology and Metallurgy.

159. Raj K.J.A. and Viwanathan B. (2009). Effect of Surface Area, Pore Volume and Particle Size of P25 Titania on the Phase Transformation of Anatase to Rutile. Indian Journal of Chemistry, Sect. A: Inorganic, physical, theoretical & analytical, volume 48A: 1378-1382.

160. Razbash A.A., Sevastianov Y.G., Krasnov N.N., Leonov A.I. and Pavlekhin V.E. (2005). Germanium-68 row of products. *Proceedings of the 5th International Conference on Isotopes 5ICI*, Brussels, Belgium, April 25-29, Bologna, Italy, (Medimond) 147-151.

161. Rebholz-Zaribaf N. and Ozcan M. (2016). Adhesion to Zirconia as a Function of Primer/Silane Coupling Agent, Luting Cement Types, Aging and Test Methods, Journal of Adhesion Science and Technology, volume 31(13): 1408-1421.

162. Ren J., Li Z., Liu S., Xing Y. and Xie K. (2008). Silica-titania mixed oxides: Si–O–Ti connectivity, coordination of titanium, and surface acidic properties, Catalysis Letters, volume 124(3-4): 185–194.

163. Ren S., Zhao X., Zhao L. (2009). Preparation of porous TiO$_2$/silica composites without any surfactants, Journal of Solid State Chemistry, volume 182(2): 312–316.

164. Reyes-Coronado D., Rodríguez-Gattorno G., Espinosa-Pesqueira M.E., Cab C., de Coss R., Oskam G. (2008). Phase-Pure TiO$_2$ Nanoparticles: Anatase, Brookite and Rutile, Nanotechnology, volume 19(14): 145605.

165. Richter B.E., John B.A. Ezell J.L. Porter N.L. Avdalovic N. and Pohl C. (1996). Accelerated Solvent Extraction: A Technique for Sample Preparation, Analytical Chemistry, volume 68(6): 1033-1039.

166. Riemann B., Schäfers K.P., Schober O., Schäfers M. (2008). Small Animal PET in Preclinical Studies: Opportunity and Challenges, The Journal of Nuclear Medicine and Molecular Imaging, volume 52(3): 215-221.

167. Rieter W. J., Taylor K. M. L., Lin W. B. (2007). Surface Modification and Functionalization of Nanoscale Metal-organic Frameworks for Controlled Release and Luminescence Sensing, Journal of the American Chemical Society, volume 129(32): 9852-9853.

168. Roesch F. (2012). Maturation of a Key Resource – The ^{68}Ge/^{68}Ga Generator: Development and New Insight, Current Radiopharmaceuticals, volume 5(3): 202-211.

169. Roesch F. and Riss P.J. (2010). The Renaissance of the Ge/Ga Radionuclide Generator Initiates New Developments in Ga Radiopharmaceutical Chemistry, Current Top Medicinal Chemistry, volume 10 (16): 1633 – 1668.

170. Roivainen A., Jalkanen S., Nanni C. (2012). Gallium-labelled Peptides for Imaging of Inflammation, European Journal of Nuclear Medicine in Molecular Imaging, volume 39 (1): S68–S77.

171. Romero E. and Morcillo M.A. (2017). Inorganic Oxides with Potential Application in the Preparation of a ^{68}Ge/^{68}Ga Generator System, Applied Radiation and Radioisotopes, volume 119: 28-35.

172. Rösch F. and Baum RP. (2011). Generator-based PET Radiopharmaceuticals for Molecular Imaging of Tumours: on the way to Theranostics. Dalton Trans.; volume 40(23): 6104-611.

173. Rotello V.M. (2004). Nanoparticles: Building Blocks for Nanotechnology, Springer Science and Business Media, pp. 241 – 246.

174. Rouquerol F., Rouquerol J., Sing K. S. W., Llewellyn P., Maurin G. (2014). Adsorption by Powders and Porous Solids: Principles, Methodology and Applications, 2nd ed.; Academic press.

175. Şahan N., Fois M. and Paksoy H. (2015). Improving ThermalConductivity Phase Change Materials – A Study of Paraffin Nanomagnetite Composites, Solar Energy Material and Solar Cells, volume 137:61-67.

176. Sahbeni K., Sta I., Jlassi M., Kandyla M., Hajji M., Kompitsas M., Dimassi W. (2017). Annealing Temperature Effect on the Physical Properties of Titanium Oxide Thin Films Prepared by the Sol-Gel Method, Journal of Physical Chemistry and Biophysics, volume 7:3.

177. Sathekge M., Warwick J.M., Doruyter A., Vorster M. (2015). Appropriate Indication for Positron Emission Tomography/Computed Tomography: College of Nuclear Physicians of the College of Medicine of South Africa, The South African Medical Journal, volume 105: 11.

178. Schöder H. and Yeung H. (2004). Positron Emission Imaging of Head and Neck Cancer Including Thyroid Carcinoma, Seminars in Nuclear Medicine, volume 34: 180-197.

179. Schubiger P.A. Zurich E. Lehmann L., Friebe M., and Yang D.J. (2007) PET Chemistry: The Driving Force in Molecular Imaging, Journal of Nuclear Medicine, volume 48(10): 1750-1750.

180. Schumacher J. and Maier-Borst W. (1981). A New ^{68}Ge/^{68}Ga Radioisotope Generator System for Production of ^{68}Ga in Dilute HCl, International Journal of Applied Radiation, volume 32: 31-36.

181. Seaman W.B., Ter-Pogossian M.M., Schwartz H.G. (1954). Localization of Intracranial Neoplasms with Radioactive Isotopes, Radiology, volume 62: 30-36.

182. Selegard L. (2013). Synthesis, Surface Modification and Characterisation of Metal Oxides Nanoparticles: Nanoprobes for Signal Enhancement in Biomedical Imaging, Linkoping University, Sweden.

183. Shealy C.N. Aronow S., Brownell G.L. (1964). Gallium-68 as a Scanning Agent for Intracranial lesions, Journal of Nuclear Medicine, volume 5: 161-167.

184. Sheehan D. and FitzGerald R. (1996). Ion-Exchange Chromatography, Methods Molecular Biology, volume 59: 145-150.

185. Shen R., Camargo P. H. C., Xia Y., Yang H. (2008). Silane-based Poly(ethylene Glycol) as a Primer for Surface Modification of Non-hydrolytically Synthesized Nanoparticles using the Stöber method. Langmuir, volume 24(19): 11189-11195.

186. Siwińska-Stefańska, K., Ciesielczyk, F., Nowacka, M., Jesionowski, T. (2012). Influence of Selected Alkoxysilanes on Dispersive Properties and Surface Chemistry of Titanium Dioxide and TiO_2–SiO_2 Composite Material. Journal of Nanomaterials, volume 2012:9.

187. Smith B.C. (2011). Fundamentals of Fourier Transform Infrared Spectroscopy, 2nd Edition, Taylor and Francis Group, CRC Press, pp. 1-17.

188. Smith-Jones P.M., Stolz B., Bruns C., Albert R., Reist H.W., Mäcke H.R. (1994). Gallium-67/Gallium-68 – [DFO]-octreotide: A Potential Radiopharmaceutical for PET imaging of somatostatin receptor-positive tumours: synthesis and radiolabelling in vitro studies, Journal of Nuclear Medicine, volume 35(2): 317-325.

189. Somorjai G.A. and Li Y. (2011). Impact of Surface Chemistry, National Academy of Sciences, volume 108(3): 917-924.

190. Strasheim A. and Steele T.W. (1978). Analytical Chemistry in the Exploration, Mining and Processing of Materials, National Institute for Metallurgy, Randburg.

191. Tachikawa T., Fujitsuka M., Majima T. (2007). Mechanistic Insight into the TiO_2 Photocatalytic Reactions: Design of New Photocatalysts, The Journal of Physical Chemistry, volume 111(14): 5259–5275.

192. Toth J. (2002). Adsorption: Theory, Modelling, and Analysis, Marcel Dekker, Inc. New York, pp. 175 – 198.

193. Tout D., Dickson J., Bradley A. (2016). Basic Priciple of PET-CT Imaging, PET/CT in Oesophageal and Gastric Cancer, Part of the Clinician's Guides to Radionuclide Hybrid Imaging, pp 21-42.

194. Townsend D.W (2004) Physical Principles and Technology of Clinical PET Imaging, Annals of Academic Medicine, Singapore, volume 33: 133-145.

195. Townsend D.W. (2008). Positron Emission Tomography/Computed Tomography, Seminars in Nuclear Medicine, volume 38: 152-166.

196. Tsang S. C., Yu C. H., Tang H. L., He H., Castelletto V., Hamley I. W., Narayanan T., Lo C.C. H., Tam K. (2008). Assembly of centimeter long silica coated FePt colloid crystals with tailored interstices by magnetic crystallization, Chemistry of Materials, volume 20(14): 4554-4556.

197. Vaquero J.J. and Kinahan P. (2015). Positron Emission Tomography: Current Challenges and Opportunities for Technological Advances in Clinical and Preclinical Imaging Systems, Annual Revised Biomedical Engineering, volume 17: 385-414.

198. Vasapollo G., Sole R.D., Lazzoi M.R. (2011) Molecular Imprinted Polymers: Present and Future Prospective, Journal of Molecular Science, volume 12(9): 5908-5945.

199. Velikyan I. (2015). ^{68}Ga-Based Radiopharmaceuticals: Production and Applied Relationship, Molecules, volume 20: 12913 – 12943.

200. Velikyan I. Beyer G.J., Bergstrom-Pettermann E., Johansen P., Bergstrom M., Langstrom B. (2008). The Importance of High Specific Radioactivity in the Performance of ^{68}Ga-Labeled Peptide, Nuclear Medical Biology, volume 35: 529-536.

201. Velikyan I., Beyer G.J., Langstrom, B. (2004). Microwave-supported Preparation of ^{68}Ga Bio-conjugates with high Specific Radioactivity, Bioconjugate Chemistry, volume 15: 554-560.

202. Velikyan I., Lendvai G., Vaelilae M., Roivainen A., Yngve U., Bergstrom M., Langstrom B. (2004). Microwave accelerated ^{68}Ga labelling of oligonucleotides, Journal of Labelled Compounds and Radiopharmacy, volume 47: 79-89.

203. Velikyan I., Maecke H.R., Langstrom B. (2008). Convenient preparation of ^{68}Ga-based PET radiopharmaceuticals at room temperature, Bioconjugate Chemistry, volume 19: 569-573.

204. Vengate M.R. and Mittal V. (2015). Surface Modification of Nanomaterials for Application in Polymer Nanocomposites: An Overview, pp. 1-28.

205. Vicario A., Aragón L., Wang C.C., Bertolino F., Gomez M.R. (2018). A simple and Highly Selective Molecular Imprinting Polymer-based Methodology for Propylparaben Monitoring in Personal Care Products and Industrial Waste Waters, Journal of Pharmacy and Biomedicine, volume 149: 225–233.

206. Viola-Villegas N. and Doyle R.P. (2009). "The co-ordination chemistry of 1,4,7,10-tetraazacyclododecane-N,N',N",N'"-tetraacetic acid (H$_4$DOTA): Structural Overview and Analyses on Structure–stability Relationships", Coordination Chemistry Reviews, volume 253 (13–14): 1906.

207. Vrancken K.C. (1995) Surface Modification of Silica Gels with Aminoorganosilanes, Colloids and Surfaces A: Physicochemical and Engineering Aspects, volume 98: 235-241.

208. Wang J.F., Cormack P.A.G., Sherrington D.C., Khoshdel E. (2003). Monodisperse, Molecularly Imprinted Polymer Microspheres Prepared by Precipitation Polymerization for Affinity Separation Applications, Angew. Chemistry, volume 42: 5336–5338.

209. L.S. Wang and R.Y. Hong (2011). Synthesis, Surface Modification and Characterisation of Nanoparticles, Advances in Nanocomposites - Synthesis, Characterization and Industrial Applications, Dr. Boreddy Reddy (Ed.), ISBN: 978-953-307-165-7.

210. Wang R., Sakai N., Fujishima A., Watanabe T., Hashimoto K. (1999). Studies of Wettability Conversion on TiO_2 Single-Crystal Surfaces, The Journal of Physical Chemistry B, volume 103 (12): 2188-2194.

211. Warson H. and Finch C.A. (2001). Application of Synthetic Resin Lattice, Lattice in Surface Coating, John Wiley and Sons, Inc. pp. 1529.

212. Waterstram-Rich K. and Gilmore D. (2016). Nuclear Medicine and PET/CT: Technology and Techniques, 8th Edition, Mosby Publishers, pp. 407 -490.

213. Watson C.C., Casey M.E., Bendriem B., Carney J.P., Townsend D.W. Eberl S. (2005). Optimizing Injected Dose in Clinical PET by Accurately Modelling the Counting-Rate Response Functions Specific to Individual Patient Scans, volume 46: 1825-1834.

214. Watson S., Nie M., Wang L. and Stokes K. (2015). Challenges and Developments of Self-Assembled Monolayers and Polymer Brushes as a green Lubrication Solution for Tribological Application, Journal of Royal Society Chemistry Advances, volume 5: 89698-89730.

215. Wechalekar K., Sharma B. and Cook G. (2005). PET-CT in Oncology – A major Advance, Clinical Radiology, volume 60: 1143-1155.

216. Wei Q. (2009). Surface Modification of Textiles, 1st Edition, Woodhead Publishing Series in Textiles, pp. 58 – 90.

217. Wei Z., Xu H., Noda M. Okuyama M. (2002). Preparation of BaxSr1-xTiO₃ thin films with Seeding Layer by a Sol-gel Method, Journal of Crystal Growth, volume 237: 443 – 447.

218. Williams R. (2011). Surface Modification of Biomaterials: Methods, Analysis and Applications, Woodhead Publishing Limited, pp. 102-142.

219. Wu Y., Dong Y., Xia X., Liu X., Li H. (2016). Facile Synthesis of n–f codoped and Molecularly Imprinted TiO_2 for Enhancing Photocatalytic Degradation of Target Contaminants, Application of Surface Science volume 364: 829–836.

220. Yáñez-Sedeño P., Campuzano S., Pingarrón J.M. (2017). Electrochemical Sensors based on Magnetic Molecularly Imprinted Polymers: A Review, Analytical Chemistry, volume 960: 1–17.

221. Yang S., Wang Y., Jiang Y., Li, S., Liu W. (2016) Molecularly Imprinted Polymers for the Identification and Separation of Chiral Drugs and Biomolecules, Polymers, volume 8: 216.

222. Yanti, Nurhayati T., Royani I., Widayani. Khairurrijal. (2016). Synthesis and characterization of MAA-based molecularly imprinted polymer (MIP) with D-glucose template, Journal of Physics: Conference Series, volume 739(1): 012143.

223. Yates (Jr) J.T. and Campbell C.T. (2011). Surface Chemistry: Key to Control and Advances Myriad Technologies, National Academy of Sciences, volume 108(3): 911-916.

224. Yazdi A.S. and Razavi N. (2015). Application of Moleculat Imprinted Polymers in Solid Phase Microextraction Technique. TrAC Trebds in Analytical Chemistry. Volume 73: 81-90.

225. Yoshino N., Sasaki A., Seto T. (1995). Synthesis of Silane Coupling Agent Contaning a 4-(perflouroalkyl)phenyl group and its Application to the Surface Modification of Glass, Journal of Fluorine Chemistry, volume 71(1): 21-29.

226. Zhang J.-Y., Boyd I.W., O'Sullivan B.J., Hurley P.K., Kelly P.V., Sénateur J.-P. (2002). Nanocrystalline TiO_2 films studied by Optical, XRD and FTIR Spectroscopy, Journal of Non-Crystalline Solids, volume 303 (1): 134 – 138.

227. Zhang W., Duan D., Liu S., Zhang Y., Leng L., Li X., Chen N., Zhang Y. (2018). Metal-organic Framework-based Molecularly Imprinted Polymer as a High Sensitive and Selective Hybrid for the Determination of Dopamine in Injections and Human Serum Samples, Biosensors and Bioelectrons, volume 118: 129–136.

228. Zhang L., Chen X.F., Zhang H., Guo H., Wang C., Yao S., Lin X., Chen X. (2020). Preparation of Polar-Modified Styrene-Divinylbenzene Copolymer and Its Adsorption Performance for Comprehensive Utilization of Sugarcane Bagasse Dilute-Acid Hydrolysate, Journal of Applied Biochemistry and Biotechnology, volume 190: 7206.

229. Zhao J., Wang Z., Yang H., Zhao M. (1998). The Synthesis and Characterisation of TiO_2/Wollastonite Composite, Material for Letters, volume 37: 149-155.

230. Zhao J., Milanova M., Warmoeskerkena M.M.C.G., Dutschk V. (2012). Colloids and Surfaces A: Physicochemical and Engineering Aspects. Journal of Biomedical Material Research Part A, volume 413 (2012) 273–279.

231. Zhernosekov K.P., Filosofov D.V., Baum R.P., Aschoff P., Bihl H., Razbash A.A., Jahn M., Jennewein M., Roesch F. (2007). Processing of Generator Produced ^{68}Ga for Medical Application, Journal of Nuclear Medicine, volume 48: 1741-1748.

232. Zimmerman B.E. (2013). Current Status and Future Needs for Standards of Radionuclides Used in Positron Emission Tomography, Applied Radiation and Isotopes, volume 76: 31-37.

233. Zoccal J.V.M, De Oliveira Arouca F., Goncales J.A.S. (2009). Synthesis and Characterization of TiO_2 Nanoparticles by the Method Pechini, Seventh International Latin American Conference on Powder Technology, Atibaia, SP (Brazil), 8-10.

Websites

1. https://www.simply.science/images/content/physics/modern_physics/nucleus/Concept_map/Isobars_Isotopes_Isotones.html.
2. https://slideplayer.com/slide/6246629/
3. http://www.intechopen.com/books/advances-innanocomposites-synthesis

APPENDICES

APPENDIX A - Radioisotopes Produced at iThemba LABS

Radionuclide	Target	Nuclear Reaction	Energy Needed (MeV)	Yield MBq/μAh
^{67}Ga	Zn	Zn(p,xn)	37 – 22	36
^{67}Ga	Ge	Ge(p, X)	62 – 39	75
^{123}I	NaI	I(p, 5n)	63 – 48	265
^{18}F-FDG	H_2^{18}O	^{18}O(p,n)	18 – 12	-
^{82}Sr/^{82}Rb	RbCl	Rb(p,xn)	63 - 40	5.4
^{68}Ge	Ga	^{69}Ga(p,2n)	34 - 0	75
^{22}Na	Mg	Mg(p,X)	62 - 40	0.6

APPENDIX B - Quality Control Parameters of A ^{68}Ge/^{68}Ga Generator

Parameter	Specification
Appearance	Clear and colourless
Radionuclidic Identity (half-life determination	62-74 min
Radionuclidic identity (gamma ray spectrometry)	511 + 1077 keV
Radionuclidic purity (gamma ray spectrometry)	>99.9%
^{68}Ge breakthrough	<0.001%
Radiochemical Purity (TLC)	>95%
Microbiological quality	sterile
Bacterial endotoxins	<175/V EU/ml
pH	<2
Iron	<10 μg/GBq
Zinc	<10 μg/GBq

APPENDIX C - ^{68}Ge/^{68}Ga Generator Properties (IAEA, 2001)

• The chemical and/or physical properties of the daughter must be different from those of the mother to permit efficient separation of daughter from mother.

• The separation of the daughter radionuclide should be easy and efficient using appropriate chemical or physical techniques.

• The daughter radionuclide separation should involve no violent chemical reactions.

• Human intervention in generator operation should be minimal to minimize radiation dose.

• The daughter radionuclide to be used as a tag on tracers for radiotracer investigations should be short lived and gamma emitting.

• In any case, a gamma emitter with a high gamma branching ratio is desirable.

• The elution yield and purity of the daughter radionuclide should be within the acceptable range.

• The physical half-life of the parent should be long enough for extending the shelf life of the generator.

• The generator constituents (i.e. eventual column packing material, liquids involved, tubings and fittings) should be radiation resistant.

• The daughter chemistry should be amenable to the preparation of a wide variety of compounds for radiotracer applications (such as water tracing, oil tracing, particle tracing, etc.).

• Shielding, handling and transportation of the generator, even across national borders, should be straightforward.

• The grand-daughter should be stable (or very long lived) to limit concern about site contamination, environmental persistence and waste disposal issues.

APPENDIX D – Gallium Metal Irradiation Parameters

▪ **Target:** Gallium metal in a niobium capsule

▪ **Beam Current:** 190 – 200 µA.

▪ **Duration of irradiation:** this depends on the 68Ge yield required and the beam current. In general this varies between 50-100 hours on average at 200 µA.

▪ **Integreated Current:** 10000 -20000 µAh.

▪ **Proton Beam Energy:** 34 MeV

APPENDIX E – Safe Human Quality Standards of Radiopharmaceuticals

(a) Readily available at a low cost.

(b) Be a pure gamma emitter, i.e. have no particle emission such as alphas and betas. These particles contribute radiation dose to the patient while not providing any diagnostic information.

(c) Have a short effective biological half-life so that it is eliminated from the body as quickly as possible.

(d) Have a high target to non-target ratio so that the resulting image has a high contrast (the object has much more activity than the background).

(e) Follow or be trapped by the metabolic process of interest.

Thus, in designing a realistic candidate for a radiopharmaceutical, the following three factors must be considered:

(i) Develop a radiotracer that binds preferentially to a specific site;

(ii) Determine the sensitivity of the radiotracer to a change in biochemistry;

(iii) Find a specific biochemical change as a function of a specific disease that matches that sensitivity.
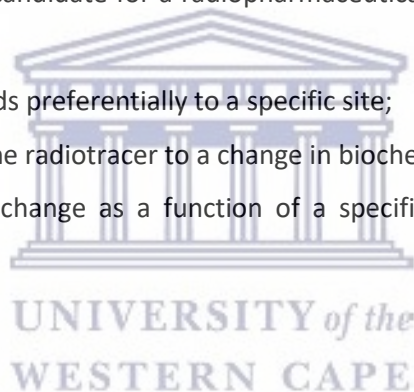
APPENDIX F – Location map of iThemba LABS Radionuclide Distribution Network
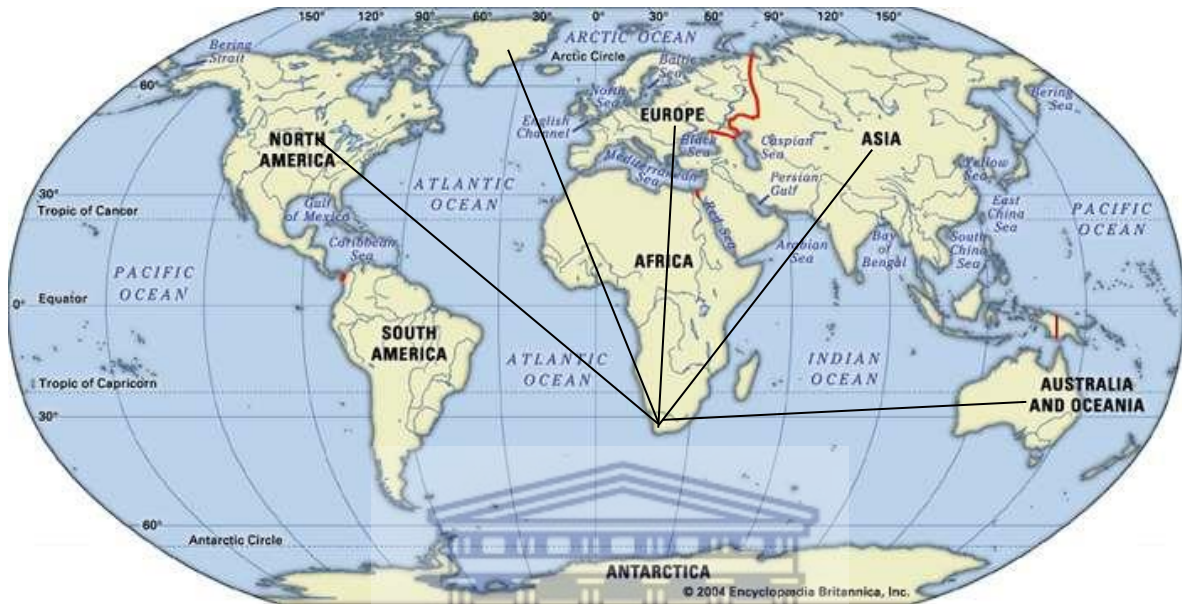
Countries: Africa, Australia, Asia, Canada, Europe and USA

APPENDIX G – Surface area of Common Substrate

Type of Substrate	Surface Area (m2/g)
E-Glass	0.10 – 0.12
Silica, ground	1-2
Silica, diatomaceous	1 – 3.5
Calcium silicate	2.6
Clay, kaolin	7
Talc	7
Silica, fumed	150 - 250

Pattern : 00-021-1272			Radiation = 1.540598			Quality : High		

TiO₂

Titanium Oxide
Anatase, syn

2th	i	h	k	l
25.281	100	1	0	1
36.947	10	1	0	3
37.801	20	0	0	4
38.576	10	1	1	2
48.050	35	2	0	0
53.891	20	1	0	5
55.062	20	2	1	1
62.121	4	2	1	3
62.690	14	2	0	4
68.762	6	1	1	6
70.311	6	2	2	0
74.031	2	1	0	7
75.032	10	2	1	5
76.020	4	3	0	1
80.727	2	0	0	8
82.139	2	3	0	3
82.662	6	2	2	4
83.149	4	3	1	2
93.220	2	2	1	7
94.181	4	3	0	5
95.143	4	3	2	1
98.318	2	1	0	9
99.804	2	2	0	8
101.221	2	3	2	3
107.448	4	3	1	6
108.963	4	4	0	0
112.840	2	3	0	7
113.861	2	3	2	5
114.909	2	4	1	1
118.439	4	2	1	9
120.104	2	2	2	8
121.725	2	4	1	3
122.336	2	4	0	4
131.035	2	4	2	0
135.998	2	3	2	7
137.391	4	4	1	5
143.887	2	3	1	9
150.039	4	4	2	4
152.633	2	0	0	12

Lattice : Body-centered tetragonal

S.G. : I41/amd (141)

a = 3.78520

c = 9.51390

Z = 4

Mol. weight = 79.90

Volume [CD] = 136.31

Dx = 3.893

I/Icor = 3.30

Color: Colorless
Temperature of data collection: Pattern taken at 25 C.
Sample source or locality: Sample obtained from National Lead Co., South Amboy, NJ, USA.
General comments: Anatase and another polymorph, brookite (orthorhombic), are converted to rutile (tetragonal) by heating above 700 C.
General comments: Pattern reviewed by Holzer, J., McCarthy, G., North Dakota State Univ, Fargo, ND, USA, ICDD Grant-in-Aid (1990). Agrees well with experimental and calculated patterns.
Additional pattern: Validated by calculated pattern.
Data collection flag: Ambient.

APPENDIX I – Pattern No. 00-21-1276 (TiO₂ – Rutile) Reference

| Pattern : 00-021-1276 | | Radiation = 1.540598 | | Quality : High |

TiO₂

Titanium Oxide
Rutile, syn
Also called: titania

2th	i	h	k	l
27.447	100	1	1	0
36.086	50	1	0	1
39.188	8	2	0	0
41.226	25	1	1	1
44.052	10	2	1	0
54.323	60	2	1	1
56.642	20	2	2	0
62.742	10	0	0	2
64.040	10	3	1	0
65.480	2	2	2	1
69.010	20	3	0	1
69.790	12	1	1	2
72.410	2	3	1	1
74.411	1	3	2	0
76.510	4	2	0	2
79.822	2	2	1	2
82.335	6	3	2	1
84.260	4	4	0	0
87.464	2	4	1	0
89.557	8	2	2	2
90.708	4	3	3	0
95.275	6	4	1	1
96.017	6	3	1	2
97.176	4	4	2	0
98.514	1	3	3	1
105.099	2	4	2	1
106.019	2	1	0	3
109.406	2	1	1	3
116.227	4	4	0	2
117.527	4	5	1	0
120.059	8	2	1	3
122.788	8	4	3	1
123.660	8	3	3	2
131.847	6	4	2	2
136.549	8	3	0	3
140.052	12	5	2	1
143.116	2	4	4	0
155.869	2	5	3	0

Lattice : Tetragonal

S.G. : P42/mnm (136)

a = 4.59330

c = 2.95920

Z = 2

Mol. weight = 79.90

Volume [CD] = 62.43

Dx = 4.250

Dm = 4.230

I/cor = 3.40

General comments: No impurity over 0.001%.
Sample source or locality: Sample obtained from National Lead Co., South Amboy, NJ, USA.
Temperature of data collection: Pattern taken at 25 C.
General comments: Two other polymorphs, anatase (tetragonal) and brookite (orthorhombic), converted to rutile on heating above 700 C.
Optical data: A=2.9467, B=2.6505, Sign=+
General comments: Optical data on specimen from *Dana's System of Mineralogy, 7th Ed.*, I 555.
General comments: Opaque mineral optical data on specimen from Sweden: R₃R%=20.3, Disp.=Std., VHN₁₀₀=1132-1187, Ref.: IMA Commission on Ore Microscopy QDF.
General comments: Pattern reviewed by Syvinski, W., McCarthy, G., North Dakota State Univ, Fargo, ND, USA, *ICDD Grant-in-Aid* (1990). Agrees well with experimental and calculated patterns.
General comments: Additional weak reflections [indicated by brackets] were observed.
Additional pattern: Validated by calculated pattern.

APPENDIX J – Inductively Coupled Plasma Analysis Graphs

Calibration curve of Ge — $y = 1012,1x$, $R^2 = 0,998$

Calibration curve of Zn — $y = 28973x$, $R^2 = 0,9999$

Calibration curve of Ti — $y = 32422x$, $R^2 = 1$

Calibration curve of Ga — $y = 4014,9x$, $R^2 = 1$
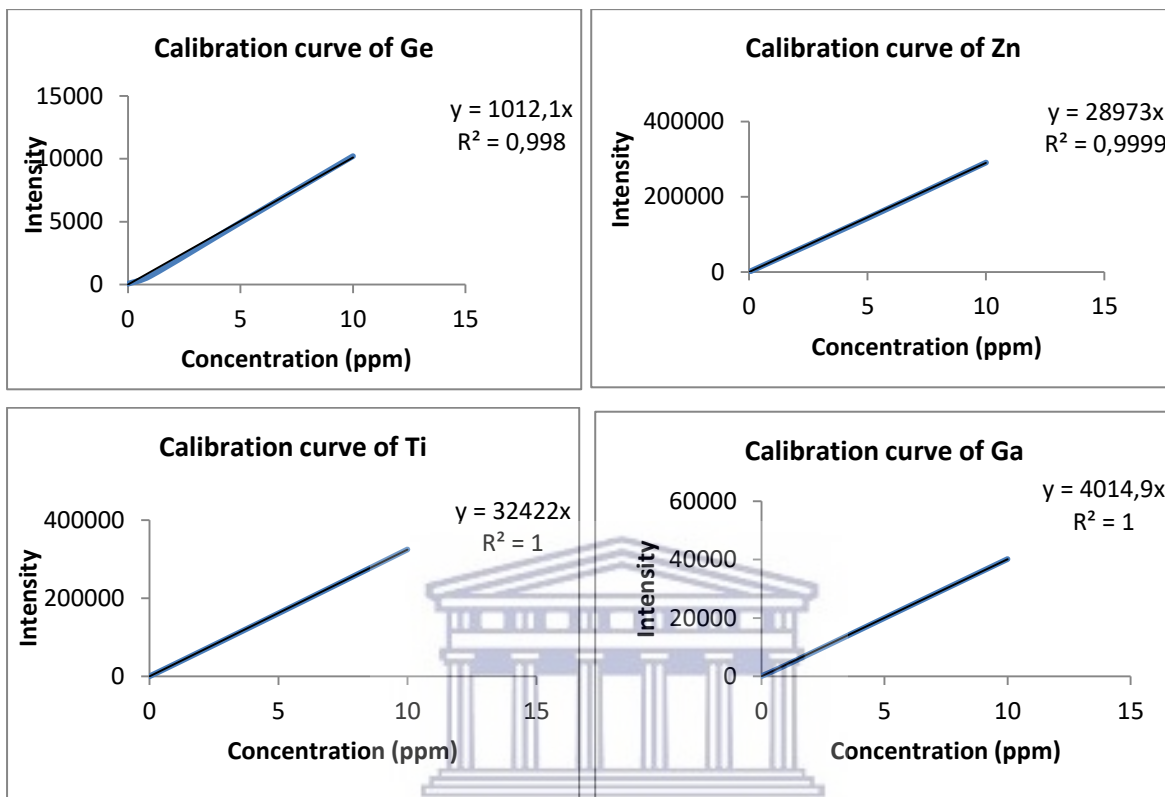
APPENDIX K – Energy Dispersive X-Ray Analysis (EDS) Data

(a) Modified TiO₂ nanoparticles

Spectrum	In stats.	O	Si	Ti	Total
Spectrum 1	Yes	55,21	1,28	43,51	100
Spectrum 2	Yes	34,93	1,35	63,71	100
Spectrum 3	Yes	47,31	1,48	51,21	100
Spectrum 4	Yes	48,39	1,73	49,88	100
Spectrum 5	Yes	54,76	1,86	43,38	100
Mean		48,12	1,54	50,34	100
Std. deviation		8,2	0,25	8,29	
Max.		55,21	1,86	63,71	
Min.		34,93	1,28	43,38	

Spectrum	In stats.	O	Ti		Total
Spectrum 1	Yes	57,75	42,25		100
Spectrum 2	Yes	48,63	51,37		100
Spectrum 3	Yes	60,78	39,22		100
Spectrum 4	Yes	25,98	74,02		100
Spectrum 5	Yes	21,18	78,82		100
Mean		42,86	57,14		100
Std. deviation		18,24	18,24		
Max.		60,78	78,82		
Min.		21,18	39,22		

Spectrum	In stats.	O	Si	S	Ti	Total
Spectrum 1	Yes	51,91	0,42	0,46	47,21	100
Spectrum 2	Yes	40,6	0,54	0,43	58,42	100
Spectrum 3	Yes	59,08	0,28	0,22	40,42	100
Spectrum 4	Yes	52,69	0,87	0,94	45,5	100
Spectrum 5	Yes	51,63	0,35	0,26	47,77	100
Mean		51,18	0,49	0,46	47,87	100
Std. deviation		6,66	0,23	0,29	6,58	
Max.		59,08	0,87	0,94	58,42	
Min.		40,6	0,28	0,22	40,42	

Spectrum	In stats.	O	Ti	Total
Spectrum 1	Yes	34,45	65,55	100
Spectrum 2	Yes	47,31	52,69	100
Spectrum 3	Yes	41,65	58,35	100
Spectrum 4	Yes	57,35	42,65	100
Spectrum 5	Yes	57,83	42,17	100
Mean		47,72	52,28	100
Std. deviation		10,1	10,1	
Max.		57,83	65,55	
Min.		34,45	42,17	

Spectrum	In stats.	O	Ti	Total
Spectrum 1	Yes	54,09	45,91	100
Spectrum 2	Yes	55,18	44,82	100
Spectrum 3	Yes	46,32	53,68	100
Spectrum 4	Yes	56,15	43,85	100
Spectrum 5	Yes	49,44	50,56	100
Mean		52,23	47,77	100
Std. deviation		4,19	4,19	
Max.		56,15	53,68	
Min.		46,32	43,85	

Spectrum	In stats.	O	Ti	Total
Spectrum 1	Yes	48,55	51,45	100
Spectrum 2	Yes	48,84	51,16	100
Spectrum 3	Yes	43,08	56,92	100
Spectrum 4	Yes	56,35	43,65	100
Spectrum 5	Yes	47,87	52,13	100
Mean		48,94	51,06	100
Std. deviation		4,76	4,76	
Max.		56,35	56,92	
Min.		43,08	43,65	

Spectrum	In stats.	O	Ti	Total
Spectrum 1	Yes	52,04	47,96	100
Spectrum 2	Yes	45,29	54,71	100
Spectrum 3	Yes	55,35	44,65	100
Spectrum 4	Yes	42,86	57,14	100
Spectrum 5	Yes	34,5	65,5	100
Mean		46,01	53,99	100
Std. deviation		8,16	8,16	
Max.		55,35	65,5	
Min.		34,5	44,65	

Spectrum	In stats.	O	Ti	Total
Spectrum 1	Yes	53,66	46,34	100
Spectrum 2	Yes	54,09	45,91	100
Spectrum 3	Yes	21,69	78,31	100
Spectrum 4	Yes	42,94	57,06	100
Spectrum 5	Yes	39,78	60,22	100
Mean		42,43	57,57	100
Std. deviation		13,22	13,22	
Max.		54,09	78,31	
Min.		21,69	45,91	

(b) Molecular Imprinted Polymers

Spectrum	In stats.	C	O	Na	S	Ge	Total
Spectrum 1	Yes	67,67	29,4	0,57	1,64	0,72	100
Spectrum 2	Yes	60,88	38,16	0,41	0,56	0	100
Spectrum 3	Yes	63,1	35,66	0,41	0,84	0	100
Spectrum 4	Yes	66,4	31,51	0,49	1,21	0,39	100
Spectrum 5	Yes	62,66	35,19	0,56	1,11	0,48	100
Mean		64,14	33,98	0,49	1,07	0,32	100
Std. deviation		2,81	3,49	0,08	0,41	0,31	
Max.		67,67	38,16	0,57	1,64	0,72	
Min.		60,88	29,4	0,41	0,56	0	

Spectrum	In stats.	C	O	S	Total
Spectrum 1	Yes	64,33	35,33	0,33	100
Spectrum 2	Yes	65,13	34,38	0,49	100
Spectrum 3	Yes	63,71	35,99	0,3	100
Spectrum 4	Yes	65,43	34,41	0,16	100
Spectrum 5	Yes	66,06	33,66	0,29	100
Mean		64,93	34,75	0,31	100
Std. deviation		0,92	0,91	0,12	
Max.		66,06	35,99	0,49	
Min.		63,71	33,66	0,16	

Spectrum	In stats.	C	O	Si	Total
Spectrum 1	Yes	61,9	37,81	0,3	100
Spectrum 2	Yes	66,85	32,88	0,26	100
Spectrum 3	Yes	64,38	35,24	0,39	100
Spectrum 4	Yes	67,02	32,6	0,38	100
Spectrum 5	Yes	67,5	31,18	1,32	100
Mean		65,53	33,94	0,53	100
Std. deviation		2,37	2,6	0,44	
Max.		67,5	37,81	1,32	
Min.		61,9	31,18	0,26	

Spectrum	In stats.	C	O	Total
Spectrum 1	Yes	67,87	32,13	100
Spectrum 2	Yes	69,96	30,04	100
Spectrum 3	Yes	69,1	30,9	100
Spectrum 4	Yes	66,31	33,69	100
Spectrum 5	Yes	68,26	31,74	100
Mean		68,3	31,7	100
Std. deviation		1,37	1,37	
Max.		69,96	33,69	
Min.		66,31	30,04	

°